



Uddin, Nazim (2022) Development Of Biodegradable Polymeric Nanoparticles: Repurposing Pimozide For Targeted Glioblastoma Chemotherapy. Doctoral thesis, The University of Sunderland.

Downloaded from: <http://sure.sunderland.ac.uk/id/eprint/17203/>

Usage guidelines

Please refer to the usage guidelines at <http://sure.sunderland.ac.uk/policies.html> or alternatively contact sure@sunderland.ac.uk.

DEVELOPMENT OF BIODEGRADABLE POLYMERIC NANOPARTICLES: REPURPOSING PIMOZIDE FOR TARGETED GLIOBLASTOMA CHEMOTHERAPY

Md Nazim Uddin

A thesis submitted in partial fulfilment of the requirements of the
University of Sunderland for the degree of Doctor of Philosophy (PhD)



February 2022

Abstract

Pimozide is a first-generation antipsychotic drug, which has also been reported as a potential chemotherapeutic candidate for glioblastoma, a fast-growing deadly brain cancer that is still quite difficult to treat with current clinical interventions. Repurposing pimozide for glioblastoma is not straightforward process since pimozide would induce its unwanted antipsychotic and related adverse side effects. Recently, nanomedicines are making outstanding progress in delivering new or existing therapeutics in targeted sites. However, there is a lack of studies that propose different approaches to repurpose pimozide in the form of nanomedicines. In fact, there is no study that has developed pimozide-nanomedicine targeting glioblastoma.

This thesis presents development of novel formulations of pimozide that could be applied as nanomedicine for glioblastoma targeted therapy. Formulations, in the form of nanoparticles, are composed of a biodegradable co-polymer, namely polylactide-co-glycolide (PLGA), which has been used as a safe drug delivery system for human. Nanoparticles were designed, prepared, and tuned to achieve desired physicochemical properties (particle size, size distribution, surface charge, and drug encapsulation efficiency) by exploring several process and formulation parameters, such as preparation methods (single emulsion-solvent evaporation and microfluidics), and formulation compositions (types and concentrations of excipients). In addition, an ultra-high-performance liquid chromatography method was developed and validated to analyse pimozide in the nanoparticles. Tuned PLGA nanoparticles were further functionalised (surface modified) with polyethylene glycol (PEG) and transferrin.

The key findings indicate that nanoparticles prepared by microfluidic method were significantly smaller and more efficient in entrapping pimozide than that of single emulsion-solvent evaporation method. Therefore, this study took the advantage of microfluidic method (and its tunable conditions) to further optimise the formulation. Tuned microfluidic conditions, based on the physicochemical properties of nanoparticles, were achieved at 12 mL/min (total flow rate) and 1:1 (flow rate ratio) of aqueous and organic phases. It was found that D- α -tocopherol polyethylene glycol 1000 succinate (TPGS)-stabilised nanoparticles were significantly smaller compared to the nanoparticles stabilised by other surfactants used in this study. In terms of PLGA concentration, results indicated that both particle size, anionic surface charge, and drug encapsulation efficiency were increased with the increase of PLGA concentration. It was also noticed that highly anionic PLGA nanoparticles became significantly less anionic after the surface modification with PEG and transferrin. Thus, this study achieved an optimised formulation with small particle size (<100 nm), narrow size distribution (polydispersity index of ≤ 0.3), anionic surface charge (zeta potential value of -10 to -18 mV), and high pimozide encapsulation efficiency (47-73%), which are ideal properties for drug delivery to the brain by intravenous administration. Furthermore, results suggested that targeted nanoparticles in suspension remained stable up to 4 months at 4°C of temperature. Western blot analysis confirmed the expressions of transferrin receptors on glioblastoma cell lines E2, G7, and R24, supporting other studies with different glioblastoma cell lines. Finally, by cell proliferation assay, an effective inhibition concentration of pure pimozide was found to be 5 μ M, which also supported previous studies. However, the effective concentration at which pimozide-loaded PLGA nanoparticles inhibited glioblastoma cell growth was achieved at 10 μ M. In addition, it was found that the targeted nanoparticles significantly inhibited the growth of glioblastoma cells than that of non-targeted nanoparticles. Therefore, this study suggests that pimozide, once encapsulated within biodegradable PLGA nanoparticles, could be repurposed for targeted glioblastoma treatment.

Declaration

I, Md Nazim Uddin, declare that this thesis is solely my own production. I also declare that no materials in this thesis have been submitted for any other academic award.

Signature: *Nazim*

Print name: Md Nazim Uddin

Date: 14th October 2021

Acknowledgements

I am honoured to acknowledge that this research has benefited from contributions of many people in many ways. Their kind supports have driven me all the way to this endeavour.

At first, undoubtedly, I would like to render my sincere gratitude to my director of studies, Dr. Ahmed Faheem, whose continuous guidance, commitment, professionalism, patience, and immense knowledge helped me shape this rewarding undertaking. I could not have imagined getting a better mentor for this study.

I would like to show my earnest appreciation to my co-supervisor Professor Amal Elkordy, who guided me every time when it was necessary, regardless I sought advice.

A special thank goes to Dr. John William Lough for his guidance and insightful comments in liquid chromatography. I would also like to thank Dr. Lewis Bingle and his PhD student Mayokun Ajeigbe for their support in microbiology.

I am grateful to Dr. Shafiq Ahmed, who generously provided me with glioblastoma cell lines, and advised me through and through during the immunoblotting and drug treatment experiments. I am also grateful to Dr. Shafiq's PhD students, Dr. Najla Moosa and Sara Azeem for their supports in cell culture.

I would like to thank my colleagues (especially, Li, Ijeoma, Anna, and Hardip), ex-colleagues (especially Dr. Samuel Girgis and Dr. Hassan Elsana), and all laboratory technicians (especially, Maria Barry, Kayleigh Ironside, Linda, Paul Stronach, Paul Neesam, Arun Mistry, Julie, and Mark Chapman) for their supports.

I am also grateful to Dr. Muhammad Irfan Alam, Dr. Muhammad Sheikh, and Shafqat Ullah for their positive influences that helped me undertake this journey.

Finally, I would like to thank my parents, my wife (Mymuna), parents-in-law, other family members, and friends, who always encouraged me throughout this journey. It would be ungrateful of me if I do not mention our beautiful infant baby girl (Marnia), who also, unknowingly, had to sacrifice many hours of father-daughter precious moments.

Contents

Abstract	ii
Declaration	iii
Acknowledgements.....	iv
Contents	v
List of Figures.....	ix
List of Tables.....	xiv
Abbreviations and Symbols	xvi
Chapter 1. Introduction (General)	2
1.1. Context of the Study	2
1.2. Background.....	5
1.2.1. Drug Repurposing.....	5
1.2.2. Pimozide	8
1.2.3. Cancer and its biology	13
1.2.4. Nanomedicines	23
1.3. General Aim and Objectives.....	45
1.3.1. General aim	45
1.3.2. Specific aims.....	45
1.3.3. Specific objectives	45
1.4. Structure of the Thesis.....	46
Chapter 2. Materials and Methods	48
2.1. Materials.....	48
2.1.1. Drug molecule.....	48
2.1.2. Carrier molecule	48
2.1.3. Surfactants and surface modifying agents.....	49
2.1.4. Reagents and solvents	50
2.1.5. Instruments and devices.....	52
2.2. Methods	54

2.2.1. Preparation of PLGA nanoparticles.....	54
2.2.2. Characterisation of nanoparticles.....	59
2.2.3. Detection microbial contamination in nanoparticles.....	80
2.2.4. Biological evaluation of targeted nanoparticles in glioblastoma cell lines	81
2.2.5. Statistical analysis	88
Chapter 3. Development and validation of an ultra-high-performance liquid chromatography method for pimozide analysis in PLGA nanoparticles.....	90
3.1. Introduction	90
3.1.1. Basic instrumentation	91
3.1.2. Separation principle	95
3.1.3. Modes of liquid chromatography	97
3.1.4. Ultra-high-performance liquid chromatography.....	99
3.2. Aims and Objectives	100
3.3. Results and Discussions	101
3.3.1. Development of the UHPLC method.....	101
3.3.2. Method validation.....	107
3.4. Conclusion	117
Chapter 4. Development of Pimozide-Loaded PLGA Nanoparticles: Exploration of Process and Formulation Parameters.....	119
4.1. Introduction	119
4.2. Aim and Objectives.....	120
4.3. Results and Discussions	121
4.3.1. Preliminary findings	121
4.3.2. Effect of preparation method	127
4.3.3. Effect of freeze-drying	132
4.3.4. Effect of surfactants on particle size, charge, drug encapsulation and drug release profile.....	135
4.3.5. Effect of PLGA terminal groups.....	146
4.3.6. Effect of PEGylation.....	154
4.4. Conclusion	158

Chapter 5. Development of Transferrin Receptors Targeted PLGA Nanoparticles: An Optimisation Study	160
5.1. Introduction	160
5.2. Aims and Objectives	161
5.3. Results and Discussions	162
5.3.1. Optimisation study	162
5.3.2. Active targeting with transferrin	183
5.3.3. Storage Stability Study	187
5.3.4. Detection of Microbial Contamination in Nanoparticles	190
5.4. Conclusion	194
Chapter 6. Cytotoxicity and Cellular Uptake Studies of Targeted Nanoparticles in Glioblastoma Cell Lines	196
6.1. Introduction	196
6.2. Aim and Objectives.....	204
6.3. Results and Discussions	205
6.3.1. Expression of potential receptor proteins.....	205
6.3.2. Cytotoxicity and cellular uptake of nanoparticles	208
6.4. Conclusion	221
Chapter 7. General Conclusions and Future Directions	223
7.1. General Conclusions	223
7.2. Future Directions	226
References	229
Appendices	250
Appendix 1: Preparation of surfactant solutions	250
Appendix 2: DLS data (Representative).....	251
Appendix 3: FTIR spectra (Representative).....	253
Appendix 4: DSC thermograms (Representative).....	259
Appendix 5: Drug encapsulation efficiency in different techniques	261
Appendix 6: Optimisation of transferring adsorption	262
Appendix 7: Preparation of microbial growth media	262

Appendix 8: Different preparations for Western blot analysis.....	263
Appendix 9: Statistical analysis (Representative)	264
Appendix 10: Freeze-dried nanoparticles (Representative)	265
Appendix 10: Author's Research Engagements and Background.....	266

List of Figures

Figure 1.1: Estimated number of all cancer cases and deaths.....	2
Figure 1.2: Comparative schematic phases between traditional drug discovery and drug repurposing.	3
Figure 1.3: Chemical structure of pimozide.....	8
Figure 1.4: Synthesis of pimozide.	9
Figure 1.5: Antipsychotic mechanism of action of pimozide.....	10
Figure 1.6: Metabolic pathway of pimozide.....	11
Figure 1.7: Graphical representation of genetic mutation of DNA (top) and uncontrolled growth of cells causing cancer (bottom).....	13
Figure 1.8: Illustration of a tumour microenvironment.....	14
Figure 1.9: Cartoon of human brain and an astrocyte (a type of glial cell).....	16
Figure 1.10: Hallmarks of the cancer and possible therapeutic targeting.	17
Figure 1.11: Doxil® vial as marketed by Sequus Pharmaceuticals.....	23
Figure 1.12: Structure of a liposome.	24
Figure 1.13: Molecular structure of PLGA.....	27
Figure 1.14: Biodegradation reaction of PLGA.	28
Figure 1.15: Preparation of PLGA nanoparticles by top-down and bottom-up techniques.	31
Figure 1.16: Preparation of polymeric nanoparticles by single and double emulsion methods. Adapted from Lee, Yun and Park (2016).	31
Figure 1.17: Preparation of polymeric nanoparticles by spray drying method.	32
Figure 1.18: Preparation of polymeric nanoparticles by nanoprecipitation method.	33
Figure 1.19: Preparation of polymeric microparticles by salting-out method.	33
Figure 1.20: Preparation of polymeric nanoparticles by dialysis method.	34
Figure 1.21: Preparation of PGLA nanoparticles by hydrodynamic flow focusing microfluidic method.	35
Figure 1.22: Illustration of a microfluidic device with 69 cycles of staggered herringbone micromixers.....	36
Figure 1.23: Toroidal micromixer introduced in NxGen Microfluidics™.....	37
Figure 1.24: Essential physicochemical properties of nanoparticles required to be tuned for intended therapeutic use.	39
Figure 1.25: Graphical demonstration of targeting strategies of nanoparticles.....	41
Figure 1.26: Potential targets for nanoparticles.	42
Figure 2.1: Simplified schematic diagram of single emulsion-solvent evaporation method in preparation of pimozide-loaded PLGA nanoparticles.	55
Figure 2.2: Phase diagram of water.	56

Figure 2.3: Different stages in freeze-drying.....	56
Figure 2.4: Simplified schematic diagram of microfluidic method in preparation of pimozi- de-loaded PLGA nanoparticles.....	58
Figure 2.5: Workflow of transferrin adsorption on the surface of PLGA nanoparticles.	59
Figure 2.6: Different components used for the determination of particle size by using dynamic light scattering technique.	60
Figure 2.7: Principle of dynamic light scattering (DLS) showing detector receiving scattered light, leading to measurement of average particle size.....	61
Figure 2.8: Movement of small and large particles in a liquid medium.....	62
Figure 2.9: Zeta potential of a negatively charged particle in a liquid medium.	63
Figure 2.10: Different components used for the determination of zeta potential by using laser Doppler anemometry technique.	63
Figure 2.11: Simplified schematic diagram of a scanning electron microscope showing its different components.	65
Figure 2.12: Simplified schematic diagram of a transmission electron microscope showing its different components.	66
Figure 2.13: Simplified schemetic diagram of a Fourier transform infrared (FTIR) spectrophotometer showing its different components.....	67
Figure 2.14: Simplified schematic diagram of a conventional differential scanning calorimeter showing its different components.	69
Figure 2.15: A typical DSC thermogram of a polymer (polyethylene terephthalate).....	69
Figure 2.16: Standard curve of pimozi- de obtained by ultra-high performance liquid chromatography analysis.....	71
Figure 2.17: Standard curve of pimozi- de obtained by UV-visible spectroscopy at 280 nm...75	75
Figure 2.18: Schemetic diagram of an UV-visible spectrophotometer showing its different components.....	76
Figure 2.19: Workflow of in-vitro drug release study of PLGA nanoparticles.....	77
Figure 2.20: Workflow of BCA assay for transferrin analysis in the PLGA nanoparticles.....	78
Figure 2.21: Standard curve of bovine serum albumin (BSA)	79
Figure 2.22: Reaction between cuprous ion (Cu^+) and bicinchoninic acid (BCA).	79
Figure 2.23: General workflow of Western blot.	86
Figure 2.24: Workflow of cell proliferation assay.	87
Figure 3.1: Simplified schematic of an HPLC instrument.	92
Figure 3.2: Simplified structure of a liquid chromatographic column	93
Figure 3.3: Structure of a stationary phase (porous particle).	93
Figure 3.4: Chemical structure of silica with associated functional groups.	94
Figure 3.5: Modification of silica stationary phase by octylsilane (C-8) linkage.	94

Figure 3.6: Separation of toluene and phenol in the column.	96
Figure 3.7: Chromatographic separation process.	96
Figure 3.8: Structure of a chromatographic peak.	97
Figure 3.9: General modes of HPLC.	97
Figure 3.10: Water adsorption to the silica particles in hydrophilic interaction chromatography.	98
Figure 3.11: Representative chromatograms of standard pimoziide in two different solvents of analyte.	102
Figure 3.12: Representative responses of pimoziide after extraction by different solvent systems.	104
Figure 3.13: Effect of syringe filtration on pimoziide's signals.	106
Figure 3.14: Representative chromatograms showing the specificity of the method.	108
Figure 3.15: Regression plot for determining linearity of the method.	109
Figure 3.16: Representative chromatograms of pimoziide stadard concentrations.	110
Figure 3.17: Test of precision by comaparing percent relative standard deviation (%RSD) of pimoziide retention time.	113
Figure 3.18: Test of precision by comaparing percent relative standard deviation (%RSD) of peak area of pimoziide.	114
Figure 3.19: Visual identification of limit of detection (LOD).	115
Figure 4.1: Effect of molecular weight of PLGA on physicochemical properties of PLGA nanoaprticls prepared by microfluic method.	123
Figure 4.2: Overlay of FTIR spectra confirming pimoziide loading within the PLGA.	125
Figure 4.3: Differential scanning calorimetry (DSC) thermograms confirming pimoziide's loading and interaction with PLGA nanoparticles.	126
Figure 4.4: Effect of preparation methods on physicochemical characteristics of PLGA nanoparticles.	129
Figure 4.5: Effect of preparation methods on pimoziide release profile of PLGA nanoparticles.	131
Figure 4.6: Effect of freeze-drying on PLGA nanoparticles particle size.	133
Figure 4.7: Scanning electron microscopy (SEM) images showing larger particle size in freeze-dried nanoparticles.	133
Figure 4.8: Structure of polyvinyl alcohol (PVA).	137
Figure 4.9: Effect of different surfactants on physicochemical properties of PLGA nanoparticles.	140
Figure 4.10: Effect of surfactants on drug release profile of PLGA nanoparticles.	141
Figure 4.11: Chemical structure of polysorbate 80.	141
Figure 4.12: Chemical structure of poloxamer.	143

Figure 4.13: Chemical structure of D- α -Tocopheryl polyethylene glycol 1000 succinate. ...	144
Figure 4.14: Effect of acid and ester terminal groups of PLGA on physicochemical properties of nanoparticles.....	147
Figure 4.15: Fourier transform infrared spectroscopy (FTIR) spectra of acid and ester terminated PLGA and their respective nanoparticles.....	149
Figure 4.16: Effect of acid and ester terminated PLGA nanoparticles on drug release.	150
Figure 4.17: Effect of PLGA terminal group on the stability of PLGA nanoparticles.	152
Figure 4.18: Effect of measuring temperature on both acid and ester terminated PLGA nanoparticles.....	153
Figure 4.19: Representative FTIR spectra confirming PEGylation of the PLGA nanoparticles.	155
Figure 4.20: Effect of two different molecular weights of polyethylene glycol (PEG) on physicochemical properties of formulation F21.....	157
Figure 5.1: Effect of different microfluidic total flow rates (TFR) on the physicochemical properties of PLGA nanoparticles.....	164
Figure 5.2: Effect of different microfluidic flow rate ratio (FRR) on the physicochemical properties of PLGA nanoparticles.....	166
Figure 5.3: Effect of different PLGA concentrations on physicochemical properties of nanoparticles.....	168
Figure 5.4: Effect of different PEG concentrations on physicochemical properties of PLGA nanoparticles.....	171
Figure 5.5: Effect of surfactant concentrations on the physicochemical properties of PLGA nanoparticles.....	173
Figure 5.6: Effect of initial pimozone-load on physicochemical properties of PLGA nanoparticles.....	175
Figure 5.7: Effect of different organic solvent(s) on the physicochemical properties of PLGA nanoparticles.....	178
Figure 5.8: Effect of two different collection techniques on the physicochemical properties of PLGA nanoparticles.	181
Figure 5.9: Confirmation of transferrin adsorption by transmission electron microscopy. ...	185
Figure 5.10: Quantitative analysis of transferrin adsorption by an indirect method using BCA method.	186
Figure 5.11: Stability of optimised PLGA nanoparticles at 4°C temperature.	188
Figure 5.12: Effect of storage temperature on physicochemical properties of PLGA nanoparticles.....	189
Figure 5.13: Bacteria controls on Tryptic Soy Agar (TSA) media.	191
Figure 5.14: Detection of bacterial contamination in PLGA nanoparticles.	191

Figure 5.15:Yeast controls on Malt Agar media.	192
Figure 5.16: Detection of yeast contamination in PLGA nanoparticles.	192
Figure 6.1: Classification of cellular uptake pathways for nanoparticles.	197
Figure 6.2: Schematic diagram showing different mechanisms of endocytosis.	197
Figure 6.3: Schematic diagram of direct cytoplasmic delivery pathways for nanoparticles.	198
Figure 6.4: A typical structure of blood-brain barrier.	200
Figure 6.5: Schematic diagram of transport mechanisms at blood-brain barrier.	201
Figure 6.6: Schematic diagram of transferrin receptor 1-mediated endocytosis of holo-transferrin and ferritin, and recycle of apo-transferrin.	202
Figure 6.7: Schematic diagram of transferrin receptor 2-mediated endocytosis and hypothetical iron transport to the mitochondria.	203
Figure 6.8: Western blot analysis of receptor proteins expressions in glioblastoma cell lines.	206
Figure 6.9: Effect of different pimoziide concentrations on glioblastoma cells proliferation.	209
Figure 6.10: Representative phase contrast images of glioblastoma cells proliferation with and without pure pimoziide treatment.	210
Figure 6.11: Representative phase contrast images of glioblastoma cells after pure pimoziide treatment with fluorescent dye.	211
Figure 6.12: Putative representation of serotonin receptor-7 antagonism and subsequent inhibition mechanism of glioblastoma proliferation.	212
Figure 6.13: Effect of drug free-substances on glioblastoma cells proliferation.	214
Figure 6.14: Representative phase contrast images of E2 cells after treating with empty PLGA nanoparticles.	215
Figure 6.15: Cytotoxic effect pimoziide-loaded PLGA nanoparticles on glioblastoma cells.	216
Figure 6.16: Cytotoxic effect of targeted PLGA nanoparticles on glioblastoma cells.	217
Figure 6.17: Representative phase contrast images of E2 cells after treating with targeted and non-targeted nanoaprticles.	218
Figure 6.18: Representative phase contrast images of E2 cells after treating with fluorescent dye-loaded targeted and non-targeted PLGA nanoaprticles.	219

List of Tables

Table 1.1: Examples of repurposed drugs in the market.	5
Table 1.2: Different classes of antipsychotic drugs with potential anticancer effect.	7
Table 1.3: Recent update on anticancer activity of pimozide.	12
Table 1.4: Targeted therapies with different types of cancer growth blockers.	20
Table 1.5: Examples of personalised therapy for different cancers.....	20
Table 1.6: Current treatment options (chemotherapeutics) for glioblastoma.	22
Table 1.7: List of polymeric nanoparticles in clinical trials for cancer therapy.....	26
Table 1.8: PLGA-based marketed products.....	30
Table 1.9: List of targeting ligands that selectively bind with overexpressed receptors.....	42
Table 1.10: Recent updates of PLGA nanoparticles targeting gliomas.....	44
Table 2.1: Product specifications of pimozide.....	48
Table 2.2: Product specifications of PLGA.....	48
Table 2.3: Product specifications of different surfactants and surface modifying materials. .	49
Table 2.4: Product specifications of reagents and solvents.....	50
Table 2.5: Specifications of instruments and devices.	52
Table 2.6: Gradient profile of the mobile phases.	70
Table 2.7: Analytical method validation parameters and their applicability.	72
Table 2.8: Supplements added to prepare stem cell media	81
Table 2.9: Primary antibodies used in Western blot analysis.	84
Table 2.10: Secondary antibodies used in Western blot analysis	84
Table 3.1: Analysis of pimozide by different techniques.	91
Table 3.2: Detectors used in liquid chromatography	95
Table 3.3: Test of accuracy by recovering the spiked pimozide.	111
Table 3.4: Determination of limit of detection and quantification	115
Table 3.5: Method robustness analysis by changing the flow rate.	116
Table 3.6: Method robustness analysis by changing the column temperature	117
Table 4.1: Formulation compositions with different PLGA molecular weights.	121
Table 4.2: Preliminary formulation compositions with varying parameters.	127
Table 4.3: Characterisation of the preliminary formulations.	128
Table 4.4: Compositions of formulations with different surfactants.	136
Table 4.5: Physicochemical properties of nanoparticles stabilised by different surfactants.	138
Table 4.6: Surface modification of formulation (F21) with two different molecular weight of polyethylene glycol.....	154
Table 5.1: Reproduction of formulation F21 at different microfluidic flow rate.	162
Table 5.2: Reproduction of formulation F21 at different microfluidic flow rate ratio.....	164

Table 5.3: Reproduction of formulation F21 at two different PLGA concentrations.	167
Table 5.4: Reproduction of formulation F21 with different PEG concentrations.	170
Table 5.5: Reproduction of formulation F21 at different TPGS concentrations.....	172
Table 5.6: Reproduction of formulation F21 with different initial drug-loads.	174
Table 5.7: Reproduction of formulation F21 using different organic solvent(s).....	177
Table 5.8: Collection of optimised nanoparticles by two different processes.	180
Table 5.9: Composition and conditions of the final optimised formulation.	183
Table 5.10: Optimised formulation with coumarin-6 and transferrin.	183
Table 5.11: Characterisation of dye-loaded and TF-adsorbed optimised nanoparticles.....	184

Abbreviations and Symbols

AT	Acid terminated
ANOVA	Analysis of variance
BBB	Blood-brain barrier
BCA	Bicinchoninic acid
BSA	Bovine serum albumin
°C	Degree Celsius
CFU	Colony forming unit
CH ₃ CN	Acetonitrile
cm ⁻¹	Per centimetre
CO ₂	Carbon dioxide
D ₂	Dopamine receptor 2
Da	Dalton
DCM	Dichloromethane
dH	Hydrodynamic diameter
DLS	Dynamic light scattering
DMEM	Dulbecco's modified Eagle medium
DMSO	Dimethyl sulfoxide
DSC	Differential scanning calorimetry
DUBs	Deubiquitinates
ECL	Enhanced chemiluminescent
EE	Encapsulation efficiency
EGF	Epidermal growth factor
ELSD	Evaporative light scattering detector
ERK 1/2	Extracellular regulated kinase 1/2
ET	Ester terminated
FDA	Food and Drug Administration
FGF	Fibroblast growth factor
FRR	Flow rate ratio
FTIR	Fourier-transform infrared spectroscopy
GAPDH	Glyceraldehyde 3-phosphate dehydrogenase
H ₂ O	Water
HPLC	High performance liquid chromatography
5-HT ₇	One type of serotonin receptors

ICH	The International Council for Harmonisation of Technical Requirements for Pharmaceuticals for Human Use
IL	Interleukin
kDa	Kilodalton
LDA	Laser Doppler anemometry
LDV	Laser Doppler velocimetry
M	Molar
mAb	Monoclonal antibody
mAU	Milli-absorbance unit
MeOH	Methanol
mM	Millimolar
mRNA	Messenger ribonucleic acid
mV	Millivolt
NaCl	Sodium chloride
Nm	Nanometre
NPs	Nanoparticles
O ₂	Oxygen
o/w	Oil-in-water
p	Value of significance
PAGE	Poly-acrylamide gel electrophoresis
PBS	Phosphate buffered saline
PDI	Poly dispersity index
PEG	Polyethylene glycol
pH	Scale of acidity or basicity
PLGA	Poly (lactic-co-glycolic) acid
PPCI	Protease phosphatase cocktail inhibitor
PTFE	Polytetrafluoroethylene
PVA	Polyvinyl alcohol
R ²	Squared correlation coefficient
RH	Relative humidity
rpm	Revolutions per minute
SD	Standard deviation
SDS	Sodium dodecyl sulfate
SE	Single emulsion-solvent evaporation
SEC	Size-exclusion chromatography
SEM	Scanning electron microscopy

STAT	Signal transducer and activator of transcription
%T	Percent transmittance
TBST	Tris-buffered saline Tween
T _g	Glass transition temperature
TGS	Tris-glycine saline
TEM	Transmission electron microscopy
TF	Transferrin
TFR	Transferrin receptor; Total flow rate
T _m	Melting temperature
TPGS	D- α -Tocopheryl polyethylene glycol 1000 succinate
TSA	Tryptic Soy Agar
UHPLC	Ultra-high-performance liquid chromatography
USP1	Ubiquitin-specific protease 1
μ M	Micromolar
UV-Vis	Ultraviolet visible
V	Volt
w/v	Weight per volume
w/w	Weight per weight

"The most fruitful basis for the discovery of a new drug is to start with an old drug"

- Sir James Black

Chapter 1

Introduction

Chapter 1. Introduction (General)

This chapter describes the context of the overall study, followed by background information on related topics, such as drug repurposing, pimozone, cancer (glioblastoma), and nanomedicines. It further outlines the general aims and objectives of the study, including structure of the thesis.

1.1. Context of the Study

According to World Health Organization (WHO), cancer is one of the leading causes of all deaths globally (WHO, 2021). International Agency for Research on Cancer (IARC), a part of the WHO, has estimated the global cancer cases and deaths for the next two decades (IARC, 2020). It was predicted that 29 million people would be diagnosed with cancer by 2040, while almost half of them would die of it (Figure 1.1), indicating an alarming sign for humanity.

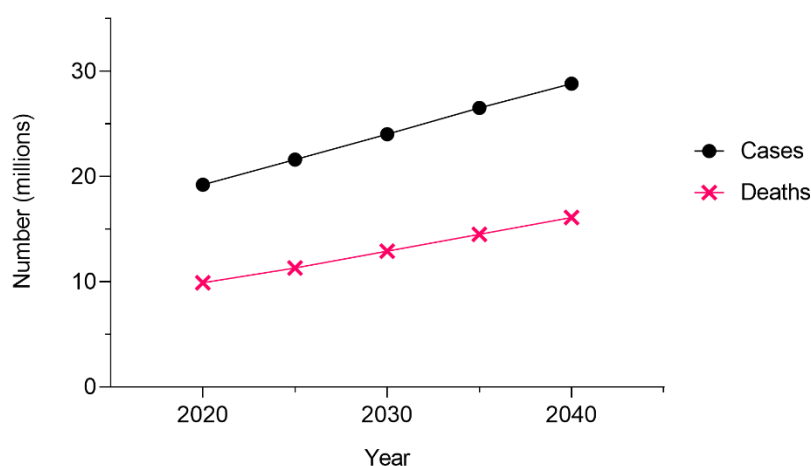


Figure 1.1: Estimated number of all cancer cases and deaths.

Data were adapted and reproduced from 'Cancer Tomorrow' that predicted cancer incidence and mortality burden from the current estimates performed by GLOBOCAN 2020 project, as reported in 'Cancer Today'. Data were based on 36 specific cancer types worldwide (of 185 countries or territories), age group of 0-85+, and all sex group (IARC, 2020).

Of many approaches, drug repurposing is an attractive pharmacological strategy because it is a fast and cost-effective development process for cancer therapeutics (Kirtonia *et al.*, 2020), indeed for any therapeutic. Drug repurposing for cancer utilises existing drugs, which were initially intended for other diseases, thus bypassing several intermediate steps, and consequently accelerating the overall drug discovery and development process (Figure 1.2).

Studies reported that antipsychotics showed antitumor activity in many cancers (Shi *et al.*, 2015; Dong *et al.*, 2017; Yang *et al.*, 2019; Chen *et al.*, 2020; Xue *et al.*, 2020). Pimozide, one of the first-generation antipsychotics with broad spectrum of molecular targets, inhibits cell growth in several cancers, such as glioblastoma (Lee *et al.*, 2016), breast cancer (Dakir *et al.*, 2018), colon cancer (Ren *et al.*, 2018), prostate cancer (Zhou *et al.*, 2016), and more (Elmaci and Altinoz, 2018).

Being a central nervous system (CNS) drug, hydrophobic pimozide can easily cross blood-brain barrier (BBB), which is the major obstacle for many other therapeutic agents to treat CNS disorders (such as, glioblastoma), and shows low and tolerable toxicity. Therefore, pimozide remains as a potential therapeutic candidate for glioblastoma chemotherapy (Kast, 2010; Svenja *et al.*, 2018). However, only a limited number of studies are available in this regard.

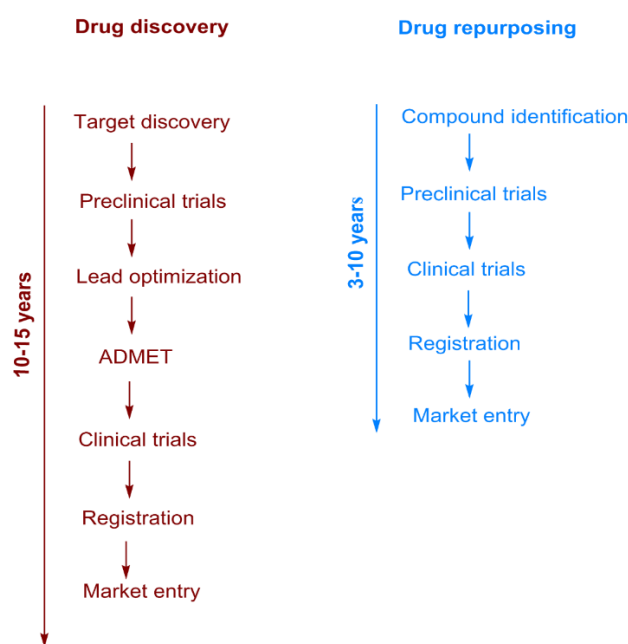


Figure 1.2: Comparative schematic phases between traditional drug discovery and drug repurposing.

With current marketed dosage form of pimozide (tablet), the effective inhibition of glioblastoma cells growth would not be possible as pimozide molecule would enter both normal and cancer cells at the same time, resulting in antipsychotic effect and associated cardiac and extrapyramidal side-effects. To inhibit the growth of cancer cells effectively, a higher dose is required, however, that would further strengthen the severity of the side-effects. To solve this, a targeted delivery of pimozide with an optimal concentration would have potentially (hypothetically) destroyed the glioblastoma cell growth. However, delivery systems carrying pimozide would have to overcome BBB, which restricts entry of any toxic or foreign substance from the bloodstream into the brain.

Nanomedicines, in particular as drug delivery systems, have gained much more attention recently for cancer therapy (Norouzi *et al.*, 2020). Nanoparticles can bypass BBB and deliver therapeutic agents to the targeted sites (such as, glioblastoma in the brain) with no or less systemic toxicity (Bastiancich *et al.*, 2017; Ganipineni, Danhier and Pr eat, 2018; Aparicio-Blanco *et al.*, 2020).

Poly(lactic-co-glycolic acid) (PLGA), a biodegradable synthetic polymer approved by the U.S. Food and Drug Administration (FDA) and European Medicines Agency (EMA) for therapeutic use in human, is being studied extensively as a nanoparticulate drug delivery system. Anticancer agents, such as paclitaxel (Luiz *et al.*, 2019), cisplatin (Dom nguez-R os *et al.*, 2019), doxorubicin (Maksimenko *et al.*, 2019), and many more have been successfully encapsulated in PLGA nanoparticles (Acharya and Sahoo, 2011). However, preparing uniform and reproducible nanoparticles has always been difficult. Some orthodox preparation methods, such as emulsion-solvent evaporation and nanoprecipitation are used to prepare uniform and reproducible nanoparticles in small scale. However, these methods are not reliable for large scale production. Modern microfluidic devices developed by individual research group or commercial platforms are reported to prepare uniform, size controlled, reproducible and scalable nanoparticles. Nevertheless, preparing particles at desired quality requires exploration of many process and formulation parameters.

In short, it appears that repurposing pimozide has not been moved forward since pimozide was reported as a potential anti-glioblastoma agent. In fact, no study has developed pimozide-encapsulated drug delivery systems to evaluate their effect against any cancers, let alone glioblastoma. Therefore, with the advent of pharmaceutical nanotechnology, this study aims to develop pimozide-encapsulated biodegradable polymeric nanoparticles and determine whether pimozide could survive as a repurposing candidate for glioblastoma chemotherapy and move to the next step in the drug discovery and development pipeline.

1.2. Background

1.2.1. Drug Repurposing

Drug repurposing is defined as the re-use of existing drugs for other clinical indications. It reduces time and cost to develop a new drug. Existing drugs are selected for repurposing by serendipitous observations, disease pathways observations, and data mining strategies (Panchapakesan and Pollock, 2018; Paranjpe, Taubes and Sirota, 2019; Luo *et al.*, 2021).

Drug repurposing is being studied for a wide range of diseases: viral infectious diseases (Mercorelli, Palù and Loregian, 2018); bacterial infectious disease (An *et al.*, 2020); kidney diseases (Panchapakesan and Pollock, 2018); neurodegenerative diseases (Paranjpe, Taubes and Sirota, 2019); cardiovascular diseases (Gelosa *et al.*, 2020); and cancer (Sleire *et al.*, 2017). Selected examples of repurposed drugs currently in the market are listed in Table 1.1.

Table 1.1: Examples of repurposed drugs in the market.

Drug	Primary indication	Repurposed indication	Approval date
Zidovudine	Cancer	HIV/AIDS	1987
Minoxidil	Hypertension	Hair loss	1988
Sildenafil	Angina	Erectile dysfunction	1998
Celecoxib	Pain and inflammation	Familial adenomatous polyps	2000
Atomoxetine	Parkinson diseases	ADHD	2002
Duloxetine	Depression	Stress urinary incontinence	2004
Rituximab	Cancers	Rheumatoid arthritis	2006
Thalidomide	Morning sickness	Multiple myeloma	2006
Raloxifene	Osteoporosis	Breast cancer	2007
Fingolimod	Transplant rejection	Multiple sclerosis	2010
Dapoxetine	Analgesia and depression	Premature ejaculation	2012
Topiramate	Epilepsy	Obesity	2012
Ketoconazole	Fungal infection	Cushing syndrome	2014
Aspirin	Analgesia	Colorectal cancer	2015

Adapted from Pushpakom et al. (2019).

Drug repurposing approach can help more than ever in the event of any global emergency, such as COVID-19 pandemic, in which effective drug candidate could be identified and applied to clinical trials very quickly (Luo *et al.*, 2021). However, among the all diseases, cancers are being extensively studied with repurposing strategy that aims to develop cost-effective anti-cancer drugs (Kirtonia *et al.*, 2020).

Drug repurposing for cancer treatment is in high demand because this approach would fast-track the development and approval of novel treatment strategies, while reducing life-threatening risks at the same time (Bertolini *et al.*, 2015). Many drugs of different classes have been repurposed for cancer therapy over the decades (Kirtonia *et al.*, 2020). For example, antidiabetic drug metformin induces cell death of breast cancer (Gonzalez-Angulo and Meric-Bernstam, 2010), gastric cancer (Han *et al.*, 2015), and more (Zhang *et al.*, 2020). Notably, several clinical trials of metformin in cancers have advanced to Phase III and Phase IV, thus indicating the successful outcome of drug repurposing (Zhang *et al.*, 2020). Non-steroidal anti-inflammatory drug aspirin, which inhibits angiogenesis, migration, invasion, and tumorigenesis of human malignancies, such as gastrointestinal and oesophageal cancers, is also on clinical trials (Kirtonia *et al.*, 2020; Zhang *et al.*, 2020).

Antipsychotics are potential target for repurposing because they have been clinically used for decades with history of tolerable safety. Studies report that antipsychotics have potent anticancer activity against many cancers (Huang *et al.*, 2018). Different classes of antipsychotics showing anticancer activity are described in (Table 1.2), indicating they all have the potentials to be repurposed as anticancer therapeutics.

However, according to the aims of this study, further literature review would be based on pimozide and its anticancer activity only.

Table 1.2: Different classes of antipsychotic drugs with potential anticancer effect.

Drugs/class	Primary indications	Primary mechanisms of action	Mechanisms of anticancer activity
Valproic acid	Bipolar disorder Epilepsy Migraine headaches	Blockage of voltage-gated Na ⁺ , K ⁺ , and Ca ²⁺ channels; inhibition of GABA re-uptake	Inhibition of histone deacetylase to reduce cancer cell proliferation but induce apoptosis. Inhibition of angiogenesis.
<i>Phenothiazines</i> Chlorpromazine Levomepromazine Thioridazine	Schizophrenia Psychosis Antiemetic	Antagonism of dopamine receptors; Antagonism of serotonin receptor 7	Boosting of cancer stem cell differentiation through dopamine receptor pathway; inhibition of mitochondrial DNA polymerase and reduction of ATP production.
Olanzapine Pimozide	Schizophrenia Bipolar disorder Tourette syndrome		Disruption of cholesterol homeostasis killing cancer cells.
<i>Selective serotonin reuptake inhibitors (SSRI)</i> Citalopram Fluoxetine Paroxetine Sertraline	Depression Anxiety disorder OCD Eating disorders Stroke recovery	Inhibition of serotonin re-uptake	Reduction of cell proliferation and induction of apoptosis; down-regulation of pAKT to mediate the synergistic anti-proliferative interaction with other chemo-drugs.
<i>Tricyclic antidepressants</i> Imipramine Trimipramine Amitriptyline	Major depression Attention-deficit hyperactivity disorder Insomnia Chronic pain	Blockage of serotonin and norepinephrine transporter	Inhibition of cellular proliferation and induction of cell apoptosis
<i>MAO inhibitors</i> Selegiline Phenelzine Tranylcypromine	Atypical depression Panic disorder Borderline personality disorder	Inhibition of monoamine oxidase, leading to breakdown of MAO neurotransmitters	Inhibition of chromatin modification enzyme (BHC110/LSD1) capable of demethylating histone.

Adapted from Huang et al. (2018).

1.2.2. Pimozide

Pimozide is a first-generation antipsychotic drug indicated for schizophrenia and related psychosis (Mothi and Sampson, 2013; NICE, 2020), including Tourette's syndrome (Regeur *et al.*, 1986; Pringsheim and Marras, 2009; MedlinePlus, 2017). Tourette's syndrome is a neurodevelopment disorder characterised by uncontrolled motor and vocal tics developed in children at early age (Robertson *et al.*, 2017).

Paul Janssen, a renowned physician, discovered pimozide in 1963 (Awouters and Lewi, 2007). Chemical structure shows that pimozide is an organofluorine compound (Figure 1.3), which is a member of benzimidazoles class, and a derivative of diphenylbutylpiperidine (PubChem Database, 2020).

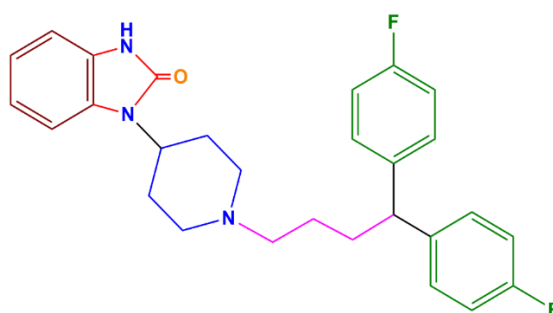


Figure 1.3: Chemical structure of pimozide.
Chemical formula: $C_{28}H_{29}F_2N_3O$; molecular weight: 461.56

Pimozide is synthesised by coupling two intermediates, such as 1-chloro-4, 4-di-(4-fluorophenyl)-butane and 1-(piperidin-4-yl)-1,3-dihydro-2H-benzimidazol-2-one, as shown in the Figure 1.4C, denoted as 1 and 2, respectively. Firstly, as shown in Figure 1.4A, the Grignard reaction between 4-fluorophenylmagnesium bromide (3) and cyclopropane-carboxylic acid ethyl ester (4) yields carbinol (5) that gets chlorinated (by thionyl chloride) to produce alkene (6). Intermediate 1 is produced by hydrogenation of double bond of alkene in presence of palladium on charcoal catalyst. Secondly, as shown in Figure 1.4B, diethyl ester (9) is produced by conjugation reaction between benzylamine (7) and ethyl acrylate (8). Later, oxopiperidine (10) is produced by Diekmann cyclisation of 9. Benzene-1,2-diamine (11) reacts with 10 to produce benzimidazolone (14), by presumably forming 12 and 13. Intermediate 2 is produced by hydrogenation of 14. Intermediate 2 is then alkylated with intermediate 1 in presence of sodium carbonate and potassium iodide to yield final compound pimozide, as shown in (Figure 1.4C).

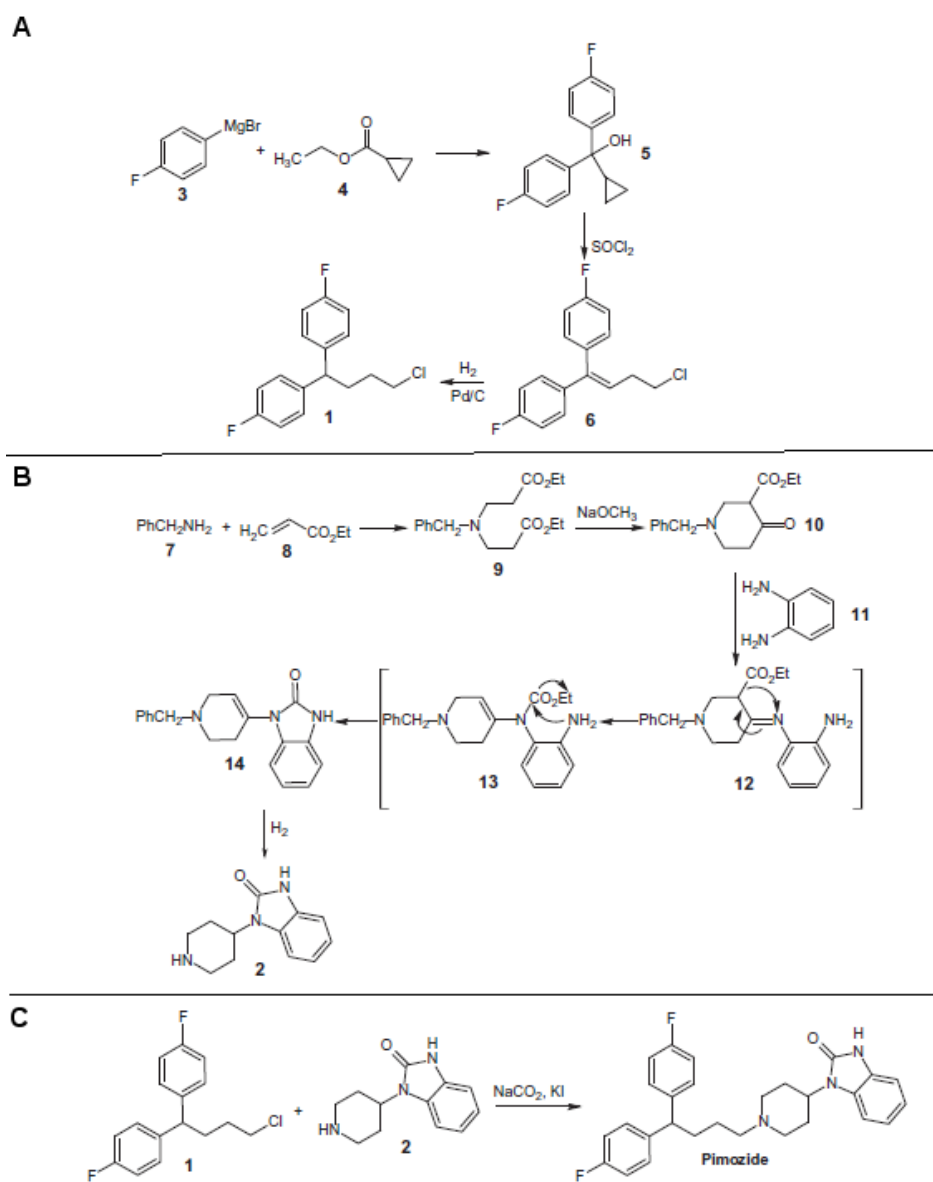


Figure 1.4: Synthesis of pimozide.

Adapted from Smyj, Wang and Han (2012). (A) Reactions to produce intermediate compound 1; (B) reactions to produce intermediate compound 2; (C) Final reaction of intermediate compounds 1 and 2 to produce pimozide.

For antipsychotic activity, the exact mechanism of action is unknown, however, it is believed that pimozide selectively blocks dopamine (D2) receptor in central nervous system, decreasing dopamine neurotransmission (Figure 1.5), which leads to stop the abnormal excitement of the brain (Smyj, Wang and Han, 2012). In addition, pimozide antagonises some other receptors, and blocks some channels: such as, serotonin receptors, alpha-adrenergic receptors, and H1 receptors (PubChem Database, 2020); calcium channels (Gould *et al.*, 1983; Bertolesi *et al.*, 2002), sodium channels, and hERG (human Either-a-go-go-related) potassium channels (Kongsamut *et al.*, 2002).

However, pimozide causes cardiovascular toxicity (such as, long electrocardiogram QT wave interval), and neuroleptic malignant syndrome, including high fever, rigid muscle, and sweating. It also causes extrapyramidal side effects (uncontrolled motor coordination, such as involuntary body movement), such as akathisia and tardive dyskinesia. Therefore, pimozide is kept as a reserved option until other drugs fail to treat the symptoms of Tourette's syndrome (Colvin and Tankanow, 1985; Zemrak and Kenna, 2008; MedlinePlus, 2017).

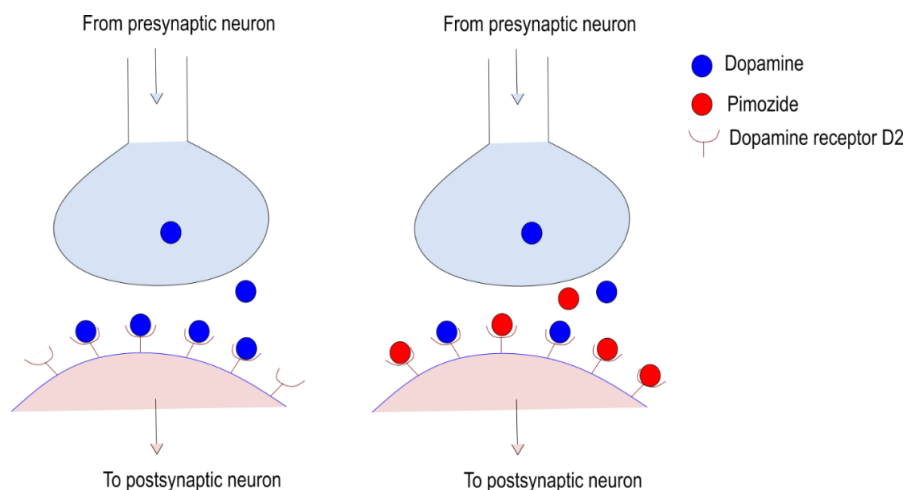


Figure 1.5: Antipsychotic mechanism of action of pimozide.

Pimozide is extensively metabolized in the liver after oral administration, catalysed by CYP3A4 and CYP1A2 enzymes (the metabolic reaction is oxidative N-dealkylation) (Desta *et al.*, 1998). Two major metabolites have been identified (Figure 1.6), which are thought to be pharmacologically inactive (Smyj, Wang and Han, 2012).

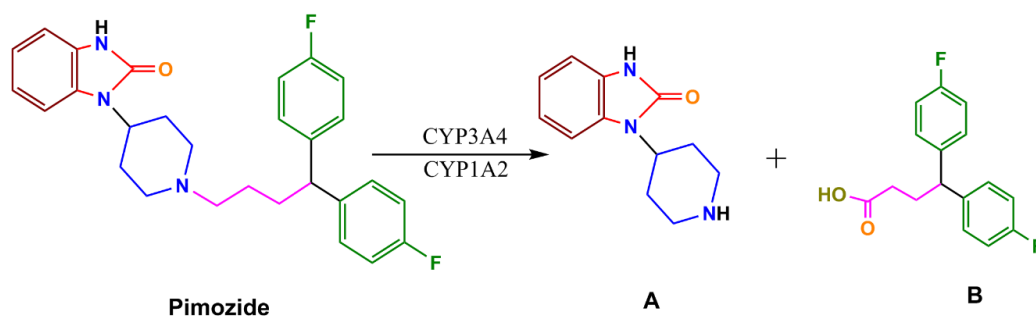


Figure 1.6: Metabolic pathway of pimozide.

(A) 1,3-Dihydro-1-(4-piperidinyl)-2H-benzimidazole-2-one (DHPB); and (B) 4,4-Bis(4-fluorophenyl) butanoic acid (FPBA).

Pimozide and its metabolites are excreted mostly through kidney. In schizophrenic patients, pimozide's mean elimination half-life for both single and multiple doses was 50-60 hours (McCreadie *et al.*, 1979). A common range of blood level concentration was found to be between 1 to 5 ng/mL (as cited in Shaw, Srivastava and Srivastava, 2019). In Tourette's syndrome, pimozide administered in child patients had shorter mean half-life (66 hours) than adult patients (111 hours) (Sallee *et al.*, 1987). It was presumed that prolonged half-life of pimozide caused severe extrapyramidal side effects (Logan *et al.*, 1982).

Besides antipsychotic effect, pimozide was first observed exerting anticancer effect against metastatic malignant melanoma in 1979 (as cited in Elmaci and Altinoz, 2018). However, this study was limited to one patient. Over the years many studies reported anticancer activity of pimozide in different types of cancers that are mentioned in Table 1.3. For example, Dakir *et al.* (2018) found pimozide's anticancer activity both *in vitro* and *in vivo* studies, suggesting it a novel chemotherapeutic option for breast cancer (Dakir *et al.*, 2018). Other studies also found its anticancer activity in breast cancer (Strobl *et al.*, 1990; Wiklund *et al.*, 2010; Ma *et al.*, 2019). However, proposed mechanism of actions varied from one study to another (Table 1.3).

To help understand the mechanism how pimozide exerts its anticancer effect, it is necessary to outline cancer and its progression. Therefore, following sections would describe basic cancer biology, including current treatment strategies.

Table 1.3: Recent update on anticancer activity of pimozide.

Cancer type	Mechanism of action	References
Breast cancer	Calmodulin antagonism; Cell death augmentation during gamma radiation treatment	(Strobl <i>et al.</i> , 1990, 1998; Strobl and Peterson, 1992)
	Dysregulation of cholesterol homeostasis	(Wiklund <i>et al.</i> , 2010)
	Downregulation of RAN GTPase and AKT	(Dakir <i>et al.</i> , 2018)
	Inhibition of USP1	(Ma <i>et al.</i> , 2019)
Colorectal cancer	Inhibition of Wnt/ β -catenin pathway	(Ren <i>et al.</i> , 2018)
Glioblastoma	Inhibition of USP1	(Lee <i>et al.</i> , 2016)
	Autophagy-dependent cell death	(Svenja <i>et al.</i> , 2018)
	Inhibition of EGFRvIII-STAT5	(Roos <i>et al.</i> , 2018)
	Inhibition of ID1 expression	(Sachdeva <i>et al.</i> , 2019)
	Dopamine D2 receptor antagonism	(Weissenrieder <i>et al.</i> , 2020)
Hepatocellular carcinoma	Inducing cell cycle arrest; suppression of STAT3 gene	(Chen <i>et al.</i> , 2017)
	Inhibition of Wnt/ β -catenin signalling	(Fako <i>et al.</i> , 2016)
Chronic myelogenous leukaemia	Inhibition of STAT5 phosphorylation	(Nelson <i>et al.</i> , 2007, 2011, 2012; Rondanin <i>et al.</i> , 2017)
Lung cancer	Dysregulation of cholesterol homeostasis	(Wiklund <i>et al.</i> , 2010)
Lymphoblastoma	Dysregulation of cholesterol homeostasis	(Wiklund <i>et al.</i> , 2010)
Melanoma	Combination of pimozide and L-methyl tryptophan controls cancer proliferation, apoptosis, and migration	(Jia <i>et al.</i> , 2018)
Neuroblastoma	Dysregulation of cholesterol homeostasis	(Wiklund <i>et al.</i> , 2010)
Osteosarcoma	Inhibition of STAT3 and suppression of catalase expression	(Cai <i>et al.</i> , 2017)
Pancreatic cancer	Inhibition of dopamine receptor D2	(Jandaghi <i>et al.</i> , 2016)
Prostate cancer	Suppression of STAT3 activation	(Zhou <i>et al.</i> , 2016)
	Inhibition of STAT5	(Mohanty <i>et al.</i> , 2017)
T-cell lymphoma	Inhibition of STAT5	(Kiel <i>et al.</i> , 2014; Simpson <i>et al.</i> , 2018)

1.2.3. Cancer and its biology

Generally, cancer is defined as a set of diseases that can start any part of the body and spread into nearby tissues or organs. Sometimes, cancer cells travel and attack distant organs. This process is known as metastasis, which is the primary cause of cancer death (WHO, 2021)

Biologically, cancer is defined as a genetic disease caused by genetic error or changes (mutation) in the DNA leading to uncontrolled growth of cells (Figure 1.7). Human body is made up of trillions of cells. Routinely, these cells grow, get old and die, followed by regeneration of new cells. During this life cycle of cells (cell cycle), any mutation in the DNA is repaired naturally. However, sometimes, mutated DNA is skipped from the repairment process. This natural mutation (developed throughout the lifetime), or inherited mutation from parents leads to initiation of cancerous cells. Notably, single mutation is not enough to induce a cancer.

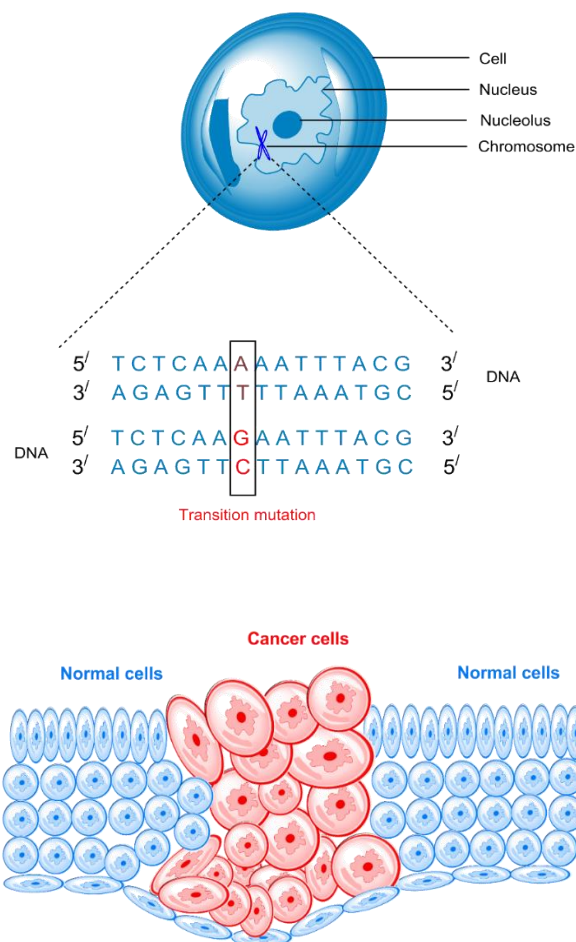


Figure 1.7: Graphical representation of genetic mutation of DNA (top) and uncontrolled growth of cells causing cancer (bottom).

Genetic mutation occurs in proto-oncogenes, tumour suppressor genes, and DNA repair genes. Proto-oncogenes are involved in normal cell growth and division. Tumour suppressor genes control cell growth and division. Finally, DNA repair genes fix DNA damage.

Beside the natural and inherited mutations, mutations can be triggered by some environmental carcinogens: physical carcinogens (ultraviolet and ionizing radiation); chemical carcinogens (asbestos, components of tobacco smoke, aflatoxin, and arsenic); biological carcinogens (infections by viruses, such as human papilloma virus, hepatitis B and hepatitis C virus, and Epstein-Barr virus; infections by bacteria, such as *helicobacter pylori*) (Plummer *et al.*, 2016). Other risk factors include, obesity, unhealthy diet, alcohol consumption, and lack of physical activity. About 30-50% cancer deaths can be prevented by avoiding those risk factors. However, ageing is another (unpreventable) risk factor for cancers.

Once produced, cancerous cells stop receiving signals from surrounding healthy cells and avoid apoptosis (known as programmed cell death). Instead, they induce normal cells to form blood vessels (known as angiogenesis) and get required oxygen and nutrition. Further, cancer cells hide from the immune systems by making genetic changes. Sometimes, they inactivate immune systems by locking immune cells with their cell surface proteins. Cancerous cells build a mass of tissue called tumour or neoplasm (Figure 1.8). Tumour can be malignant (spreading into or invading neighbouring tissues and metastasising) or benign (as opposite to malignant). With exception, blood cancers are malignant, but they do not form solid tumours.

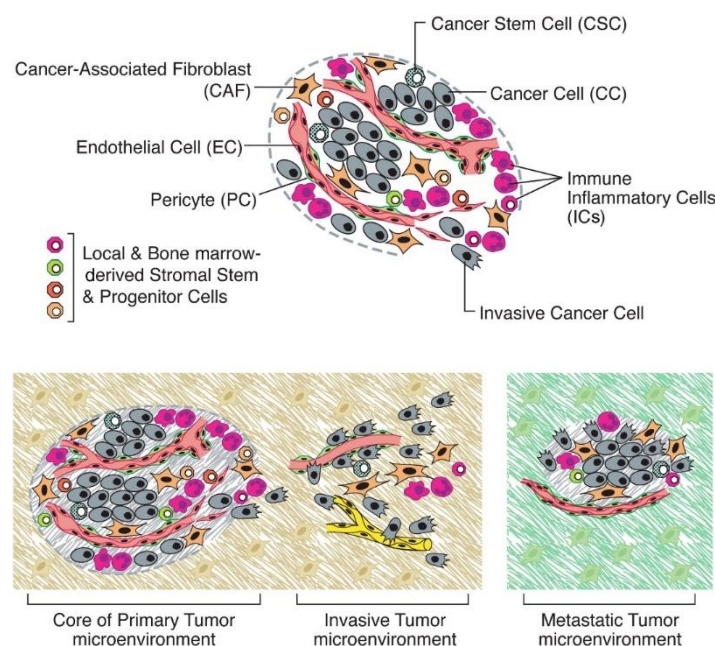


Figure 1.8: Illustration of a tumour microenvironment.
Adapted from Hanahan and Weinberg (2011).

1.2.3.1. Types of cancer

According to World Health Organization (2020), there are more than 200 types of cancer. Normally, they are named after the sources, such as organ, tissue, or cells. Some common categories, based on the tissue type, are known as carcinoma, sarcoma, leukaemia, lymphoma, and central nervous system (CNS) cancers.

Carcinoma, the most common type of cancer, develops in epithelial cells, which cover inside and outside of human organs. Adenocarcinoma develops in fluid-producing cells known as glandular cells. Examples of adenocarcinoma are breast cancer, colon cancer, and prostate cancer. Cancer developing outer layer of the skin is called basal cell carcinoma. Further, cancer could develop in the squamous cells known as squamous cell carcinoma, such as lung cancer, stomach cancer, and kidney cancer.

Sarcoma forms in the connective tissues, such as bone and soft tissues (muscle, fat, blood vessels, lymph vessels, fibrous tissues: tendons and filaments). Sarcoma is less common cancer type compared with carcinoma. There are two types of sarcomas, such as bone sarcoma (osteosarcoma) and soft tissue sarcoma (leiomyosarcoma), which is known as muscle cancer.

Leukaemia begins in blood forming tissue, such as bone marrow, producing too many abnormal white blood cells (WBC). These abnormal WBCs (such as granulocytes, monocytes, and lymphocytes) build up in the blood and cause different types of leukaemia, such as acute myeloid leukaemia, chronic myeloid leukaemia, acute lymphoblastic leukaemia, chronic lymphocytic leukaemia, and many more.

Lymphoma and myeloma (cancers of immune system) develop in the lymphatic system that filters body fluid and fights infections. Specifically, lymphoma starts from immune cells, such as lymphocytes (T cells and B cells). Hodgkin lymphoma (forms in B cells) and non-Hodgkin lymphoma (forms in B and T cells) are the two types of lymphoma. Myeloma (also known as multiple myeloma) starts in plasma cells, which are the types of white blood cells that produce antibodies.

Finally, CNS cancers are the brain and spinal cord cancers. They could be primary (cancer starts in the brain or spinal cord) or secondary (cancer spreads to the brain or spinal cord from other body part). More than 130 brain tumours have been found so far. Among them, most common type of primary brain tumour is called glioblastoma multiforme (Cancer Research UK, 2020).

Glioblastoma is the deadliest, with average survival time is 12-18 months, primary brain tumour, being named after the type of cells (glial cells) they develop from (Cancer Research UK, 2019; Brain Tumour Research, 2020).

Glial cells are the supporting cells of the brain and spinal cord. There are three types of glial cells, namely astrocytes, oligodendrocytes, and ependymal cells. In general, tumours that develop from glial cells are called gliomas. Specifically, tumours develop from astrocytes (Figure 1.9), oligodendrocytes and ependymal cells are called astrocytoma (glioblastoma), oligodendrogliomas and ependymoma, respectively.

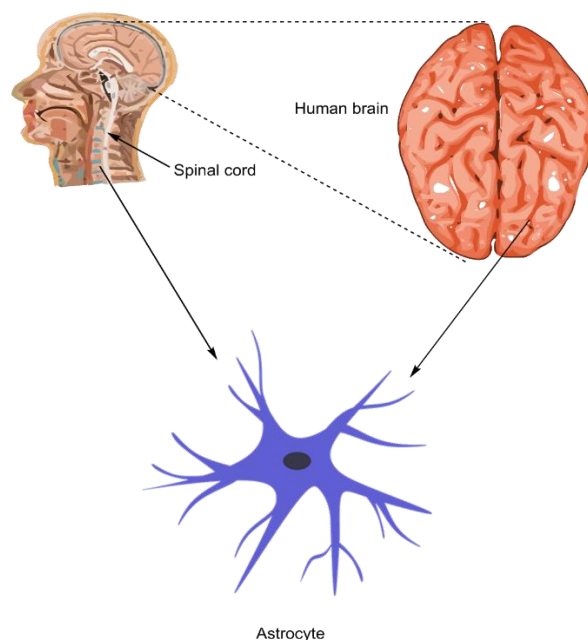


Figure 1.9: Cartoon of human brain and an astrocyte (a type of glial cell).
The star shaped astrocyte cell supports the neurons in the brain and spinal cord.

Gliomas are graded in the scale of 1 to 4; grades 1 and 2 are considered as low grade as they grow slowly; whereas grades 3 and 4 are treated as high grade as they grow quickly. For example, grade 4 astrocytoma are the fastest growing gliomas; they are also known as glioblastoma multiforme (GBM). The diagnosis of glioblastoma is carried out by magnetic resonance imaging (MRI) scan, computed tomography (CT) scan, neurological examination (such as, vision, hearing, alertness, muscle strength, co-ordination, and reflexes), blood test, and biopsy.

1.2.3.2. Current treatment strategies

Treatment depends on the type and severity of the cancer. Generally, current treatment strategies include single approach or combination of approaches, namely surgery, radiotherapy, chemotherapy, immunotherapy, hormone therapy, stem cell transplant, gene therapy, targeted therapy and personalised therapy (Cancer Research UK, 2017a; National Cancer Institute, 2017a). Although there are many possible therapeutic targets (Figure 1.10), only few of them are utilised with current strategies, as described in following sections.

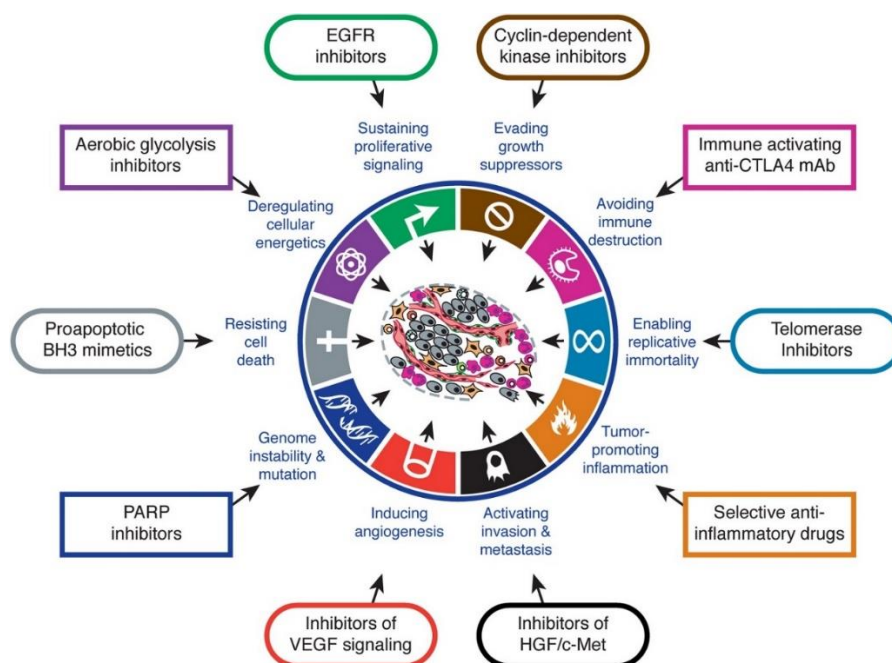


Figure 1.10: Hallmarks of the cancer and possible therapeutic targeting.
Adapted from Hanahan and Weinberg (2011).

Surgery involves removing tumours with scalpels, or other ways: cryosurgery (treatment with extreme cold by liquid nitrogen or argon gas); laser treatment; and hyperthermia (treatment with high heat produced by high energy radio waves). However, if cancer is spread (metastasised) surgery would not be the only treatment option. Furthermore, surgery is impossible for some tumours, such as tumours near to blood vessel or other delicate tissue (National Cancer Institute, 2017b).

Radiotherapy is another conventional treatment option for cancer. It uses high energy x-ray radiation to damage the DNA of cancer cells. Around 50% cancer patients have radiotherapy

at some point during their treatment (Cancer Research UK, 2018). Radiotherapy is given via several ways: external radiotherapy; implants radiotherapy (brachytherapy); radioisotope therapy (injections, capsules, or drinks); and intrabeam radiotherapy during tumour surgery. However, radiotherapy is not straight forward killing of cancer cells, rather it takes days to months. Further, it can also kill normal cells during treatment, inducing side effects, such as hair loss (in the area being treated), tiredness, sore mouth and skin, and diarrhoea.

Chemotherapy is the use of drug molecules to kill cancer cells. It is the conventional and still preferred strategy to treat most cancers. Chemotherapeutic drugs work throughout the body (known as systemic treatment) which can effectively treat metastatic cancers, and cancers that is remained after surgery and radiotherapy (National Cancer Institute, 2017a). Chemotherapeutic drugs attack DNA replication and mitotic processes of fast-growing cancer cells. At present, there are more than 100 chemotherapeutic drugs available and new drugs are being developed (Cancer Research UK, 2017b). Treatment could be with a single chemotherapeutic drug or a combination of drugs, sometimes, with steroids or biological therapies. Common examples of combination therapies are MIC (M, mitomycin; I, ifosfamide; C, cisplatin) and CHOP (C, cyclophosphamide; H, doxorubicin; O, vincristine; P, prednisolone).

Immunotherapy helps immune system fight cancer, by detecting and destroying abnormal cells. Most common immunotherapy includes monoclonal antibodies (MABs), immune checkpoints inhibitors, and T-cell transfer therapy. MABs are the immune system proteins produced in the laboratory, which help mark cancer cells so that immune system better recognize and destroy them. Immune checkpoints proteins (CTLA-4) downregulate body's immune response. Hence, immune checkpoints inhibitors boost the immune system. In T cell transfer therapy, T cells are taken from the tumour. Most active ones are then selected and grown in the laboratory followed by injecting in patients' body.

Hormone therapy (also known as endocrine therapy) can slow down or stop the growth of the cancer, by blocking or lowering the number of hormones in the body. Some types of cancer require hormones to grow, develop or spread, for example breast cancer needs oestrogen and progesterone hormones. Tamoxifen is a common hormone therapy for breast cancer as it blocks oestrogen receptors, stopping the signals from oestrogen. However, hormone therapy does not work for all cancers since many cancer growths are independent of hormones.

Stem cell transplant or sometimes bone marrow transplant can restore blood-forming stem cells of patients' body that was destroyed by previous chemotherapy or radiotherapy. Stem cells are collected from bone marrow, blood, or umbilical cord. Types of stem cell transplant

depend on the donors, such as autologous (from the same patient), allogeneic (from someone else), and syngeneic (from twin). Likewise, bone marrow transplant uses stem cells from patient's or donor's bone marrow.

Gene therapy uses genes to treat cancers. Normally, attenuated viruses are used as a medium (vector) for gene delivery. However, delivery is a difficult aspect in gene therapy, which is still in early stage of research. Gene therapies can function in many ways: boosting the immunity system; making cancer cells sensitive to other treatment; activating pro-drug in the cancer cells; and unblocking processes, such as, apoptosis (programmed cell death). Cancer cells block apoptosis process and they do not die. Further, gene therapy could only be the virus, which has been designed to kill cancer cells alone without any external genes. For example, melanoma skin cancer is treated with a drug talimogene laherparepvec (T-VEC or Imlygic), which uses the strain of herpes simplex virus (Andtbacka *et al.*, 2015).

Targeted therapy targets proteins that are responsible for cancer cells' growth, division, and spreading. Depending on the mechanism of actions, targeted therapies can be grouped into growth blockers, anti-angiogenic drugs, poly-ADP ribose polymerase (PARP) inhibitors, and monoclonal antibodies. Cancer growth blockers targets growth factors, such as epidermal growth factor (EGF) and vascular endothelial growth factor (VEGF), resulting in blocked signals inside the cell. Cancer growth blockers are grouped based on their actions (Table 1.4). Anti-angiogenic drugs prevent cancer cells from growing their own blood vessels. VEGF receptor blockers (TKIs) are also anti-angiogenics as they block signal within the cells; therefore, cells cannot produce new blood vessels. Poly-ADP ribose polymerase (PARP) helps damaged cells to repair themselves. PARP inhibitors, such as Olaparib stops the DNA repairment process, leading cancer cells to die. Finally, MABs as targeted therapies work in many ways, such as blocking growth factors receptors, carrying drugs or radiation to cancer cells, and inducing immune response to kill cancer cells. Example of targeted MABs include trastuzumab, rituximab, and pertuzumab.

Personalised therapy or precision medicine therapy is the genetic understanding of each patient and treating accordingly. In that case, targeted therapy is the foundation of personalised treatment. Genetic changes occur differently in each patient, although they have the same cancer type. Precision medicine therapy focuses the specific proteins that control the cancer growth and spreading of a cancer. For example, trastuzumab is only indicated for the breast cancers that have HER2 proteins on them. Some breast cancers do not overexpress HER2 proteins. Normally, small molecules and monoclonal antibodies are used as precision medicine for personalised therapy. Cancers should be tested first to find

out the changes, such as genes mutation or overexpression of any proteins inside the cells, as some drugs are linked to available tests and indicated accordingly (Table 1.5).

Sometimes, towards precision therapy, another approach known as stratified medicine therapy is applied, which looks for large group of cancer patients to find out the best treatment option.

Table 1.4: Targeted therapies with different types of cancer growth blockers.

Name of the growth blockers	Mechanism of action	Examples
Tyrosine kinase inhibitors (TKIs)	TKIs block tyrosine kinase enzyme → signal cannot pass inside the cell → cell growth stops	Sunitinib, Imatinib, Erlotinib
Proteasome inhibitors (PIs)	PIs block proteasome → unwanted proteins build up in the cell → cells die	Bortezomib
mTOR inhibitors	mTOR inhibitors block mTOR protein (a kinase protein, which produce chemicals, such as cyclins that trigger cell growth) → cell growth and blood vessel development stop	Temsirolimus, Everolimus
Phospho inositide 3 kinase (PI3K) inhibitors	PI3K inhibitors block PI3K protein (acts like switches in the cell for other proteins, such as mTOR) → cell growth, multiplication, and blood vessel development stop	Idelalisib
Histone deacetylase inhibitors (HDAC inhibitors or HDIs)	HDIs block histone deacetylase enzyme so that it cannot remove acetyl groups from histone proteins → cell division stops	Panobinostat, Vorinostat
Hedgehog pathway blockers	They block hedgehog pathway → development of blood vessels and nerves stop	Erivedge
BRAF inhibitors MEK inhibitors	They block cancer cells growth and signal	Vemurafenib Trametinib

Adapted from Cancer Research UK (2021).

Table 1.5: Examples of personalised therapy for different cancers.

Cancers	Available tests look for	Indicated drugs
Chronic myeloid leukaemia	Bcr/Abl gene change	Imatinib
Lung cancer	EGFR-TK mutation Overexpression of ALK enzyme	Erlotinib, afatinib, gefitinib Crizotinib and ceritinib
Breast cancer	Over expression of oestrogen receptors	Tamoxifen
Bowel cancer	K-RAS gene mutation	Cetuximab and panitumumab

Palliative treatment is symptoms-relieve therapy to increase some extra time and improve comfort, although it cannot cure cancer. This treatment includes a variety of drugs, including painkillers, and anticancer drugs.

Complementary therapies are given alongside with conventional anticancer treatment. Arguably, complementary therapies (such as, aromatherapy, acupuncture, herbal medicine, massage, visualization and yoga) help cancer patients feel better, with improving the quality of life (Molassiotis *et al.*, 2005; Wilkinson *et al.*, 2008).

It is known that all these treatment options are not effective against all types of cancer. Treatment options are subject to change due to cancer type, severity, nature, and biology. For glioblastoma, there are only few treatment options are available, namely surgery, followed by concurrent chemotherapy (Table 1.6) with radiotherapy. However, surgery in the brain is very sophisticated process, and it cannot remove all glioma cells as they invade the areas in the brain, where sensory and motor nerves are controlled. Therefore, adjuvant chemotherapy with temozolomide or other chemotherapeutic agents continues to slow down further tumour growth. However, chemotherapy is unselective, killing normal cells in the vicinity of the tumour (National Cancer Institute, 2017a; Senapati *et al.*, 2018), as well as killing fast growing normal cells anywhere in the body, such as hair follicles, skin, and cells lining GI tract. Chemotherapy also induces a set of secondary effects, such as nausea and vomiting, fatigue, peripheral neuropathy and cardiac toxicity, and interference of quality of life (Kayl and Meyers, 2006; Monsuez *et al.*, 2010). These side effects are related to the high mortality rate of cancer patients. Sometimes, glioma cell appears to be resistant to the chemotherapeutic agents. In other words, all glioma cells are not similar in characteristics (heterogenous), which means targeting one type of glioma cells would leave the others to thrive, leading recurrence of glioblastoma unavoidable. This suggests that every glioma cell cannot be destroyed with current treatment strategies, indicating glioblastoma is not fully curable.

Taken together, new therapeutics are warranted for glioblastoma because of the hostile conditions: (a) complete surgical resection is not possible as it can damage the sensitive areas of the brain, (b) CNS is highly protected environment with blood brain barrier for any drug molecule to penetrate, and (c) glioma cells show high drug resistance due to their genetic and epigenetic variation. In this scenario, nanomedicines can work as magic bullets, by delivering the therapeutic molecule safely at the site of action (glioblastoma) with targeted approach.

Table 1.6: Current treatment options (chemotherapeutics) for glioblastoma.

Name (Trade name)	Class; mechanism of action
Temozolomide (Temodal®) Carmustine (BCNU) Lomustine (CCNU) Procarbazine	Alkylating agents; they attach alkyl group to the guanine base of DNA (at the number 7 nitrogen atom of the purine ring), leading to breakage of DNA strands and subsequent cell death.
Carmustine wafer (Gliadel®)	Alkylating agent; it attaches alkyl group to the guanine base of DNA (at the number 7 nitrogen atom of the purine ring), leading to breakage of DNA strands and subsequent cell death
Vincristine	Vinca alkaloid; it binds with tubulin protein inhibiting microtubules formation, leading to apoptosis.
PCV	Combination therapy; it is comprised of procarbazine, lomustine, and vincristine
Methotrexate	Anti-metabolite; it inhibits the folic acid synthesis, leading to cell death.
Bevacizumab (Avastin®)	Monoclonal antibody; it inhibits angiogenesis (formation of new blood vessels) of cancer cells.

Adapted from Cancer Research UK (2019); and Brain Tumour Research (2020)

1.2.4. Nanomedicines

The term 'nanomedicines' and 'nanoparticles' are used interchangeably in this thesis. Theoretically, particles that are below 1000 nm in dimension (diameter or length) are known as nanoparticles. However, in pharmaceutical nanotechnology, particles that are deliberately fabricated between 1 and 100 nm in dimension for clinical uses, such as diagnoses, and therapies are called nanomedicines. US Food and Drug Administration (FDA) has approved more than 50 nanoparticles-based devices or formulations to diagnose or treat diseases by the year of 2016. Among them 20 were in clinical trials between the year 2014 and 2016 (Choi and Han, 2018). Nanomedicines in clinical trials were of various types, such as polymeric nanoparticles, liposomes, inorganic nanoparticles, drug-conjugate, and viral vectors (as cited in Wicki *et al.*, 2015).

First nanomedicine was approved in 1995 by USA Food and Drug Administration (Barenholz, 2012). It was doxorubicin-loaded liposome (Doxil[®]) indicated for several types of cancers, namely Kaposi's sarcoma, breast cancer, and ovarian cancer. It prolonged the biodistribution because of polyethylene glycol on the surface of the liposomal nanoparticles. Doxil[®] being nano sized (~100 nm) targeted tumour cells passively by enhanced permeation and retention (EPR) effect.



Figure 1.11: Doxil[®] vial as marketed by Sequus Pharmaceuticals.
Adapted from Barenholz (2012).

After Doxil[®], FDA approved several nano drug delivery systems: DaunoXome[®] (daunorubicin-loaded liposome to treat HIV associated Kaposi's sarcoma); Abraxane[®] (paclitaxel loaded albumin nanoparticles to treat metastatic breast and pancreatic, advanced

non-small cell lung cancer); and Genexol[®] PM (paclitaxel-loaded polymeric micelles to treat metastatic breast cancer, ovarian cancer, small-cell lung cancer, and gastric cancer (Tran *et al.*, 2017), and more types of nanomedicines in many cancers. To target cancer with nanomedicines, it is necessary to select most potential drug delivery systems. Following sections describe potential types of nanomedicines to be applied in human cancer therapies.

1.2.4.1. Types of nanomedicines

1.2.4.1.1. Liposomes

Liposomes are spherical vesicles made of one or more phospholipid bilayer membrane (Figure 1.12). Different types of therapeutic molecules, such as hydrophilic or hydrophobic small molecule, protein, DNA, and RNA can be encapsulated within the liposome. Again, different types of liposomes can be prepared by altering the lipid composition, vesicle size and dimension, and surface charge.

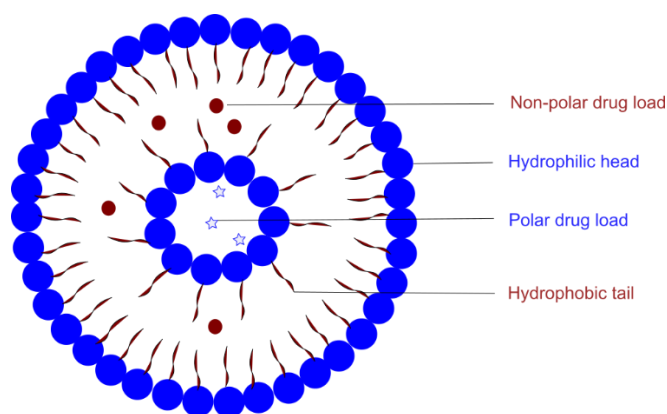


Figure 1.12: Structure of a liposome.

The advantage of liposomes is that they can deliver orally administered therapeutic proteins (such as, insulin) protected from enzymatic and acidic degradation in the stomach (Deb *et al.*, 2019). In addition, liposomes can be fabricated to target specific site, by attaching ligand on their surface. However, phospholipids sometimes undergo oxidation and hydrolysis, resulting in failure of drug delivery (Akbarzadeh *et al.*, 2013).

1.2.4.1.2. Niosomes

Niosomes are also termed as non-ionic surfactant vesicles as their bilayers are formed by non-ionic surfactants. Niosomes are formed by self-clustering of non-ionic surfactants in aqueous phase. Heat or physical agitation is required to form a closed bilayer. The

advantage of niosomes is that they can improve the solubility and sustain release of the drug. Niosomes have better stability (surfactant is more chemically stable than phospholipid) and cost effectiveness than liposomes (Kumar, 2019). Moreover, niosomes can be fabricated in various structures, such as proniosomes, transfersomes, elastic niosomes, bola niosomes, discomes, and aspasome (Khoee and Yaghoobian, 2017; Chen *et al.*, 2019).

1.2.4.1.3. Inorganic nanoparticles

Inorganic nanoparticles (also known as hard nanoparticles) are the potential delivery systems for cancer diagnostics and therapeutics. They are basically named after the inorganic elements (metals and non-metals) that they are made of, for example gold nanoparticles are made of gold metal; and carbon nanotubes are made of graphite (a form of carbon).

1.2.4.1.3.1. *Gold nanoparticles*

Gold nanoparticles have unique physical and chemical properties, which attract many scientists. They can be prepared in various sizes and shapes. However, production of gold nanoparticles that undergoes some physical, chemical, and mechanical synthesis was reported hazardous to human health and environment. Biogenic methods are being used to avoid these hazards. Further, gold nanoparticles can be bioengineered to get desired therapeutic effects, such as anticancer and antimycobacterial activities (Govindaraju *et al.*, 2020).

1.2.4.1.3.2. *Metal oxide nanoparticles*

Iron oxide nanoparticles have been used clinically for 90 years in cancer diagnosis, iron deficiency anaemia, and cancer hypothermia therapy (Soetaert *et al.*, 2020).

1.2.4.1.3.3. *Carbon nanotubes*

Carbon nanotubes are composed of concentric rolled graphene layers. The number of layers results in type of carbon nanotubes, such as single or multi-walled carbon nanotubes. The advantage of carbon nanotubes is that they can provide high surface area with amendable physicochemical properties. Carbon nanotubes can load anticancer drugs and carry them to the target site, by active or passive targeting. Further, they have great potential in diagnostics of cancer, by imaging (Badea *et al.*, 2020).

1.2.4.1.4. Polymeric nanoparticles

Polymeric nanoparticles are of two types, namely natural polymeric nanoparticles, and synthetic polymeric nanoparticles. Both are named after their corresponding polymer type. For safe drug delivery, biodegradable polymers are preferred. Biodegradable polymers get degraded *in vivo*, and produce nontoxic and biocompatible by-products, which are then excreted by normal metabolic pathways.

Abraxane[®] is the only example of natural protein-based polymeric (albumin) nanoparticles that has been approved for clinical use (Wicki *et al.*, 2015). Cyclodextrin-based nanoparticles are also classed as natural polymeric nanoparticles, and couple of them are in clinical trials (Table 1.7). On the other hand, the use of synthetic biodegradable polymers in nanoparticulate drug delivery systems has been dramatically increased in last two decades. For example, docetaxel-loaded polymeric nanoparticles (BIND-014) were in Phase-II clinical trials to treat advanced breast, prostate and lung cancers (Hrkach *et al.*, 2012; Hoff *et al.*, 2016). BIND-014 is made of blend of synthetic polymers (PEG-PLGA/PLA-PEG). However, it is now discontinued (as cited in Operti *et al.* 2021). There are many more synthetic polymeric nanoparticles are in clinical trials, some of them are listed in Table 1.7.

Table 1.7: List of polymeric nanoparticles in clinical trials for cancer therapy.

Product	Company	Polymer type	Therapeutic molecule	Clinical trials
ABI-00	Abraxis/Celgene	Albumin	Docetaxel	Phase-II
ABI-00	Abraxis/Celgene	Albumin	Rapamycin	Phase-I/II
ABI-011	Abraxis/Celgene	Albumin	Thiocolchicine dimer	Phase-I/II
CALAA-01	Calando Pharmaceuticals	Cyclodextrin	siRNA targeting ribonucleotide reductase subunit 2	Phase-I
CRLX-101	Cerulean Pharma	Cyclodextrin	Camptothecin	Phase-I/II
NC-6004	NanoCarrier	PEG-PGA micelles	Cisplatin	Phase-II/III
NK-012	Nippon Kayaku	PEG-PGA micelles	metabolite of irinotecan (SN-38)	Phase-II
NK-105	Nippon Kayaku	PEG-PGA micelles	Paclitaxel	Phase-II/III
NK-911	Nippon Kayaku	PEG-PGA micelles	Doxorubicin	Phase-I

These are some selected clinical trials with polymeric (natural and synthetic) nanoparticles in different types of cancer therapies. Full list can be found in Wicki et al. (2015).

A remarkable achievement for synthetic polymeric nanoparticles is Genexol[®] PM, which is a PEG-PLA polymeric micelle based nanoparticles loaded with paclitaxel to treat breast, lung and ovarian cancers (Kim *et al.*, 2004; Ahn *et al.*, 2014; Tran *et al.*, 2017). It was first approved and marketed in south Korea. Currently, Genexol[®] PM is marketed in India and Indonesia, while it is in Phase-III clinical trials in the United States and Europe (Operti *et al.*, 2021).

Examples of synthetic biodegradable polymers include polylactic acid (PLA), polyglycolic acid (PGA), co-polymer of PLA and PGA (known as PLGA), polycaprolactone (PCL), and polydioxanone (PDO). Among them, PLGA has a wide range of degradation limit that can be manipulated by changing its molecular weight or its monomers' ratio. PLGA nanoparticles can be tuned into desired properties, such as size, shape, and surface charge. A variety of therapeutic molecules, such as small molecules, macromolecules, DNA, RNA, and peptides were already encapsulated in PLGA in different studies (Operti *et al.*, 2021).

The molecular structure of PLGA is illustrated in Figure 1.13. PLGA has an asymmetric alpha (α) carbon in its molecule. In classical stereochemistry, this alpha carbon is denoted as D or L forms (sometimes, as R and S forms respectively) as there could be two possible enantiomers. Therefore, PLGA is an acronym for poly D, L lactic-co-glycolic acid, where both enantiomers are in equal ratio.

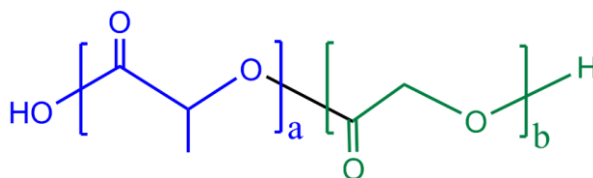


Figure 1.13: Molecular structure of PLGA.
'a' and 'b' are the numbers of lactic acid and glycolic acid units, respectively.

PLGA is synthesised by direct polycondensation of lactic acid and glycolic acid. However, this will yield PLGA with low molecular weight and broad molar mass distribution. Ring-opening polymerisation of cyclic dimers can also produce PLGA of high molecular weight and narrow molar mass distribution (Silva *et al.*, 2015). Molecular weight can be adjusted by changing polymerisation conditions and ratio of monomers. A range of organic solvents such as, dichloromethane, chloroform, acetonitrile, acetone, and tetrahydrofuran dissolve PLGA (Operti *et al.*, 2021). The glass transition temperature of PLGA is reported between 40 and 60^oC, which is above the body temperature.

The biodegradation of PLGA occurs by hydrolysis (cleavage of polymer chains through bulk erosion), releasing its two monomer units (lactic acid and glycolic acid), as shown in Figure 1.14. Lactic and glycolic acids are the natural metabolites of human body. They are excreted by the Krebs's cycle in the form of carbon dioxide and water (Silva *et al.*, 2015). The rate of degradation of PLGA depends on the ratio of monomers and their microstructures. Glycolic acid dominates the degradation rate of PLGA. In other words, higher the glycolic acid units in PLGA, faster the degradation is (Swider *et al.*, 2018).

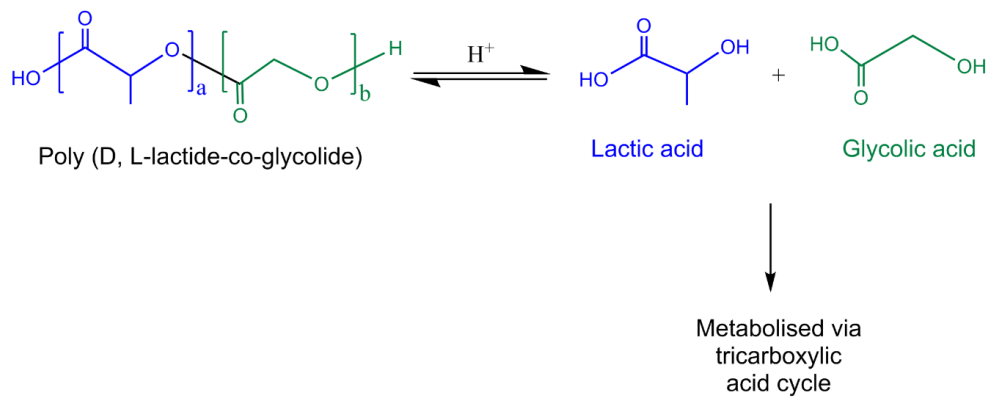


Figure 1.14: Biodegradation reaction of PLGA.

Hydrolysis of PLGA leads to lactic acid and glycolic acid, which are then metabolised via tricarboxylic acid cycle.

It is reported that over 60 PLGA-based products are available in the market with various size and shapes (Operti *et al.*, 2021). However, most of them are macroparticles depot and implant preparations, as listed in

Table 1.8. This indicates that PLGA has long history of its clinical use. Therefore, development of PLGA nanoparticles loaded with various therapeutic molecules is promising approach. In particular, developing cancer therapeutics with PLGA nanoparticles are gaining much more attention in recent years. However, reproducibility and large-scale production of PLGA nanoparticles are still challenging. There are several techniques can be employed to prepare PLGA nanoparticles, as discussed in following section.

Table 1.8: PLGA-based marketed products.

PLGA-based product	Active ingredient	Indication
Decapeptyl®	triptorelin	Prostate cancer
Lupron Depot®	leuprolide acetate	Prostate cancer, breast cancer, endometriosis
Nutropin Depot®	somatropin	Growth hormone failure
Suprecur® MP	buserelin acetate	Prostate cancer and endometriosis
Somatuline® LA	lanreotide acetate	Acromegaly, thyrotropic adenomas, neuroendocrine Tumours
Risperdal® Consta™	risperidone	Schizophrenia, bipolar disorder
Vivitrol®	naltrexone	Alcohol dependency
Zoladex®	goserelin acetate	Prostate cancer
Ozurdex®	dexamethasone	Diabetic macular edema, uveitis
Profact® Depot	buserelin	Prostate cancer
Durysta™	bimatoprost	Intraocular pressure in glaucoma
Sandostatin® LAR Depot	octreotide acetate	Diarrhoea and flushing associated with metastatic carcinoid tumours
Trelstar™ Depot	triptorelin pamoate	Prostate cancer

Adapted and reproduced from Operti et al. (2021).

1.2.4.2. Preparation of PLGA nanoparticles

Bottom-up and top-down techniques can be employed in preparation of PLGA nanoparticles, as shown in Figure 1.15. Bottom-up techniques involve chemical synthesis of PLGA nanoparticles from its two monomers, namely lactic acid, and glycolic acid via polymerisation reaction. Bottom-up techniques can be readily scaled-up, although having limited control over particle size, size distribution and shape. Furthermore, excess impurities are noticed in these techniques. On the other hand, top-down techniques involve physical formation of nanoparticles from already synthesised PLGA, and they have precise control over particle properties (Operti *et al.*, 2021). Therefore, top-down techniques are preferred in preparation of size-controlled nanoparticles. Some frequently used PLGA nanoparticles preparation methods (top-down), including both conventional and modern methods, are described in the following sections.

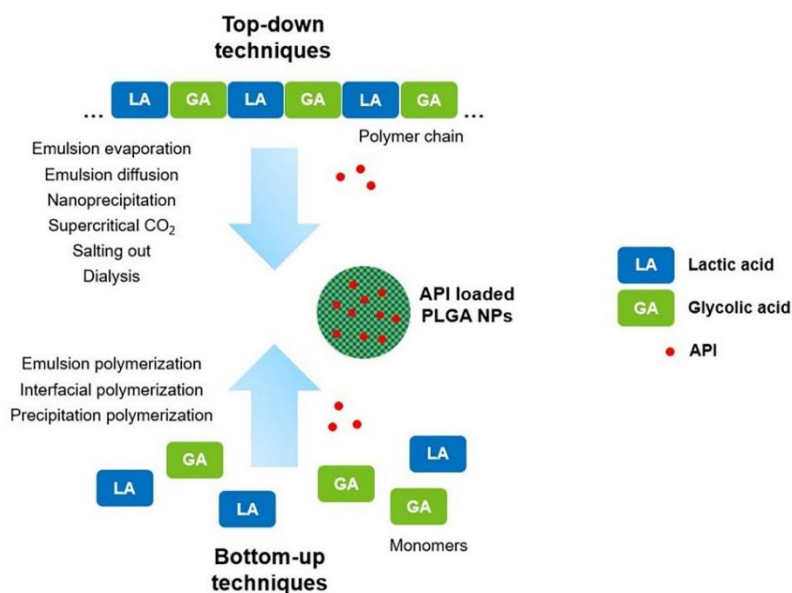


Figure 1.15: Preparation of PLGA nanoparticles by top-down and bottom-up techniques.
 Adapted from Operti et al. (2021).

1.2.4.2.1.1. Emulsion-solvent evaporation

Hydrophobic drugs can be encapsulated into PLGA matrix more conveniently by single emulsion method which requires less time and reagents than that of double emulsion technique. Hydrophilic drugs can be encapsulated into PLGA matrix by double emulsion technique (such as, w/o/w). Several parameters such as drug and polymer ratio, solvent type and volume, surfactant type and concentration, homogenisation/sonication time and rate can be adjusted to optimise the physicochemical properties of nanoparticles produced by this method. However, reproducibility, sometimes in this method, is interfered by manual handling during homogenisation.

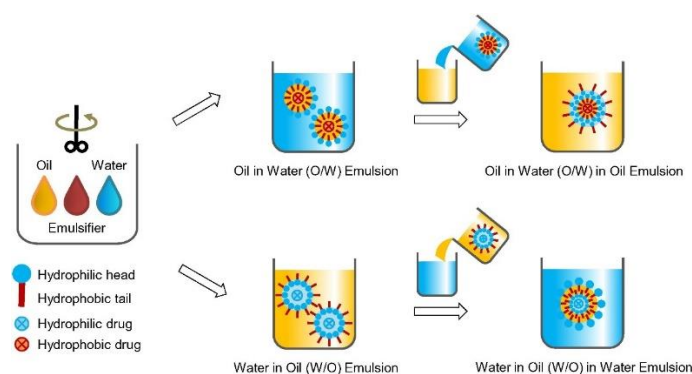


Figure 1.16: Preparation of polymeric nanoparticles by single and double emulsion methods.
 Adapted from Lee, Yun and Park (2016).

1.2.4.2.1.2. Spray-drying

PLGA nanoparticles are produced by spraying solid-in-oil dispersion or water-in oil emulsion in a stream of heated air (Figure 1.17). The organic solvent is instantly evaporated in the chamber. This method is suitable for both hydrophilic and hydrophilic drug molecules. However, it is difficult to control the distribution of the drug molecules in the particles. Also, poor yield due to the aggregation of particles and adhesion of particles to the spray dryer walls is still a major concern. This can be avoided by using anti-adherent (Lee, Yun and Park, 2016; Swider *et al.*, 2018).

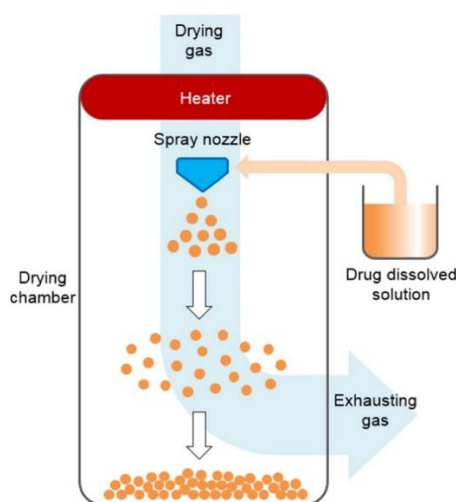


Figure 1.17: Preparation of polymeric nanoparticles by spray drying method.
Adapted from Lee, Yun and Park (2016).

1.2.4.2.1.3. Nanoprecipitation

Nanoprecipitation is also known as solvent displacement method. In this method, PLGA and drug molecule (hydrophobic) are dissolved in a polar solvent, which is later added in a controlled manner to a surfactant solution (Figure 1.18). For hydrophilic drug molecule, aqueous solution containing drug is added to PLGA dissolved in organic solvent. A sub 100 nm particle size and high encapsulation efficiency with hydrophobic molecules are achievable with this method. However, PLGA concentration could change the particle size. Further, low encapsulation efficiency comes with hydrophilic drug molecules since they have poor interaction with PLGA molecules (Lee, Yun and Park, 2016; Swider *et al.*, 2018).

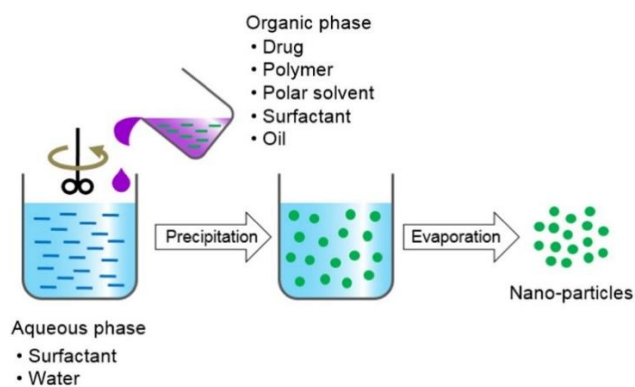


Figure 1.18: Preparation of polymeric nanoparticles by nanoprecipitation method.
Adapted from Lee, Yun and Park (2016).

1.2.4.2.1.4. Salting-out

Like nanoprecipitation, salting-out method is suitable for hydrophobic molecules to encapsulate into PLGA matrix. However, particle size is not significantly manipulated by PLGA concentration. Briefly, this method involves addition of PLGA and drug molecule in a water-miscible solvent to an aqueous solution containing electrolytes (such as, magnesium chloride and calcium chloride) and stabiliser upon high-speed stirring (Figure 1.19). Particles are formed by controlled dilution of electrolytes while organic solvent diffuses into water phase. As heating is not involved in this process, heat-sensitive drug molecules could be safely encapsulated into PLGA particles. However, low yield and low encapsulation efficiency with high polydispersity index are still downsides of this method (Lee, Yun and Park, 2016; Swider *et al.*, 2018).

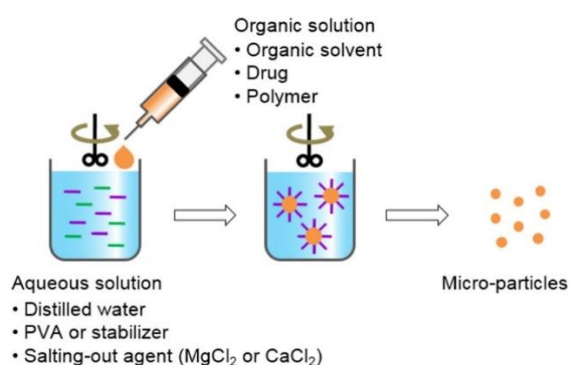


Figure 1.19: Preparation of polymeric microparticles by salting-out method.
Adapter from Lee, Yun and Park (2016).

1.2.4.2.1.5. Dialysis

Dialysis is a simple method to produce PLGA nanoparticles. Briefly, PLGA is dissolved in organic solvent and placed in a dialysis tube. A non-solvent (miscible with organic solvent but it does not dissolve PLGA) is introduced outside the dialysis tube (Figure 1.20). As a result, the organic solvent will be displaced by the non-solvent, leading to decrease PLGA solubility, and subsequently producing PLGA aggregates. Nanosuspension are collected after complete displacement of organic solvent out of the dialysis tube (Lee, Yun and Park, 2016).

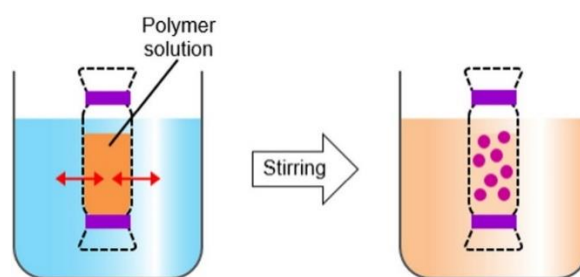


Figure 1.20: Preparation of polymeric nanoparticles by dialysis method.
Adapted from Lee, Yun and Park (2016).

1.2.4.2.1.6. Microfluidics

Microfluidics is an emerging method to produce PLGA nanoparticles. Microfluidics is the control of flow of small volume (from microlitre to litter) of fluids enclosed in microchannels. It has emerged as a multidisciplinary platform with many advantages: cost effectiveness (e.g. reduction in sample and reagents consumption), minimum processing time, enhanced sensitivity, real-time analysis, and automation (Chiu *et al.*, 2017), *in vitro* simulation and cancer diagnosis.

A basic microfluidic device includes network of microchannels (also known as microchip) where fluids of interest can be mixed with controlled manner, producing nanoparticles by nanoprecipitation process. Microchips with different geometric shapes is normally made of glass, silicone, or polymer, such as polydimethylsiloxane (PDMS). Sub-micron particles (10 to 1000 nm) can be produced in this method with high reproducibility. Further, high encapsulation efficiency and high yield is achievable with a wide range of therapeutics.

Based on the mixing arrangement of fluids in a microfluidic device, there are two basic techniques, namely hydrodynamic flow focusing, and chaotic flow that are used to prepare PLGA nanoparticles.

Hydrodynamic flow focusing develops when fluids with different velocities are brought in side by side. Three inlet microfluidics develops hydrodynamic focusing, where main flow containing the sample of interest is sandwiched by side fluids, resulting a homogenous mixing of reagents in a precise manner (Figure 1.21). Studies reported that PLGA nanoparticles were produced with a defined size, low polydispersity, high drug encapsulation efficiency (Karnik *et al.*, 2008; Valencia *et al.*, 2010; Xu *et al.*, 2017). However, hydrodynamic flow focusing is limited to throughput production. Furthermore, PDMS based microfluidic devices are unsuitable for high pressure and some strong organic solvents (Lee, Park and Whitesides, 2003).

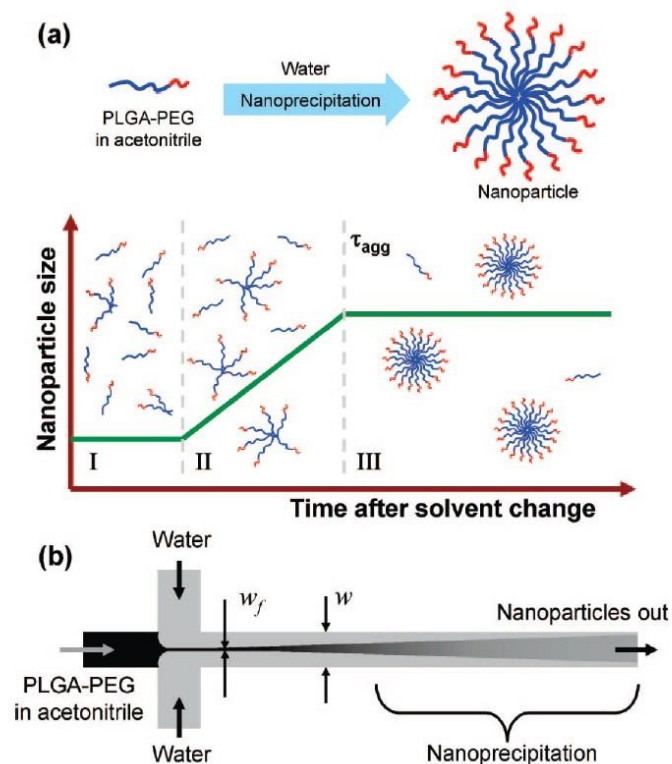


Figure 1.21: Preparation of PLGA nanoparticles by hydrodynamic flow focusing microfluidic method.

(a) Three stages of nanoparticles formation- I. nucleation; II. growth; and III. aggregation. (b) Geometry of a microfluidic device designed for hydrodynamic flow focusing, where PLGA stream is focused into a thin stream between two aqueous streams with high flow, leading to solvent diffusion out of PLGA stream and water diffusion into the PLGA stream, subsequently producing nanoprecipitation of nanoparticles. ' w_f ' denotes width of the focused stream (PLGA stream) and ' w ' stands for width of the channel. Adapted from Karnik *et al.* (2008).

Chaotic flow is the technique that increases mixing efficiency by using geometric patterns. This induces transversal flow components by stretching and folding fluids over the cross section of a microchannel. Chaotic flow can be divided into two sub-groups, namely staggered herringbone mixing (SHM) and toroidal mixing.

Staggered herringbone mixing (SHM) is the use of an array of 'herringbone grooves' on one or more surfaces of a microchannel to induce turbulent mixing within a continuous flow (Stroock *et al.*, 2002). Figure 1.22 is an illustration of a microfluidic device with SHM capacity. In SHM, fluid is redistributed over the entire channel, significantly reducing Taylor dispersion, which is an effect in fluid mechanics in which a shear flow increases the diffusivity of a species, resulting in a nearly even residence time distribution (Stroock *et al.*, 2002; Williams, Longmuir and Yager, 2008). Thus, SHM increases the surface area between two fluids with distance travelled, leading to faster diffusional mixing, compared with hydrodynamic flow focusing technique. Furthermore, mixing performance and particle quality can be increased by adding more herringbone arrays.

Several studies employed SHM to prepare lipid nanoparticles: study found the effect of lipid concentrations and mixing performance on particle size (Maeki *et al.*, 2015, 2017); other studies produced doxorubicin (Zhigaltsev *et al.*, 2012) and siRNA (small interfering RNA) encapsulated lipid nanoparticles (Chen *et al.*, 2012). However, SHM architecture is difficult to make: an expensive process with a limited flow rate capacity. It is also difficult when several herringbone mixers are set in parallel to achieve Good Manufacturing Practice (GMP) scalability.

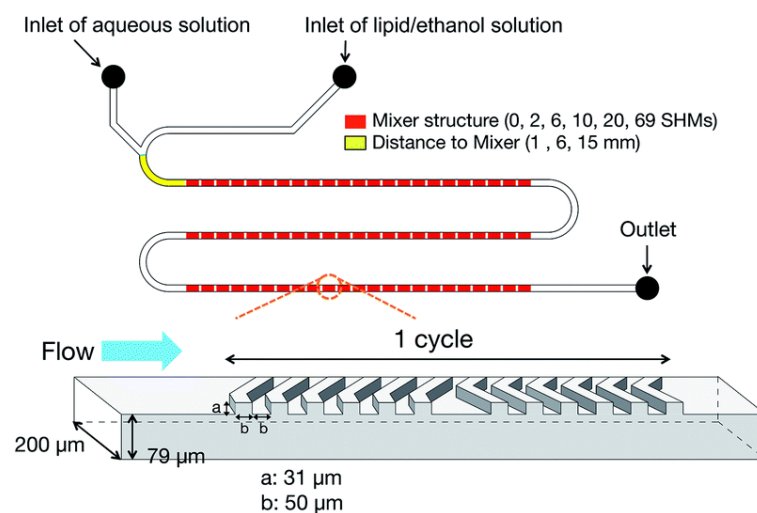


Figure 1.22: Illustration of a microfluidic device with 69 cycles of staggered herringbone micromixers.

Adapted from Maeki *et al.* (2015).

On the other hand, toroidal mixing works under laminar flow at high speed, using circular structures within the flow path. It becomes chaotic flow due to the centrifugal forces created within the architecture, encouraging uniform mixing (Figure 1.23). Toroidal mixing was first reported in a study that compared both SHM and toroidal mixing to produce protein-loaded liposomes (Webb *et al.*, 2020). Authors concluded that this novel toroidal design delivered seamless scale-up production from bench-scale (12 mL/min) to GMP-scale (200 mL/min).

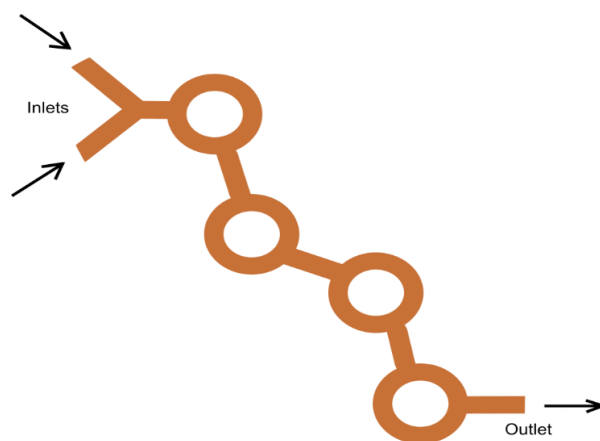


Figure 1.23: Toroidal micromixer introduced in NxGen Microfluidics™.
Adapted and reproduced from (Precision NanoSystems, 2021).

Beside preparation of nanoparticles, microfluidic devices can characterise the particle size and surface charge of nanoparticles (Fraikin *et al.*, 2011). Authors developed a microfluidic analyser that can detect individual nanoparticle, and characterise complex, unlabelled nanoparticle suspension at 500,000 particles per second. The analyser has two components, such as microfluidic channel (that directs the analytes flow driven by pressure to the electrical sensor) and sensor (that is comprised of two voltage-bias electrodes and a readout electrode embedded in the microchannel). Another study reported a real-time detection of sub-100 nm polystyrene particles, viruses and larger proteins based on their polarizability (Mitra *et al.*, 2010). Size tunable elastic pore sensors can simultaneously determine particle size, their concentration and zeta-potential from charge density under electrophoretic force (Kozak *et al.*, 2012). Microfluidic devices can also monitor real-time formation of nanoparticles. One study reported that small angle X-ray scattering (SAXS) embedded microfluidic device monitored the kinetics and mechanisms of nanoparticles' nucleation and growth (Polte *et al.*, 2010). Furthermore, microfluidic-based liquid chromatography (also known as miniaturized HPLC) can analyse drug loading and release, with higher sensitivity and lower sample consumption (Lynch, Chen and Liu, 2018).

Microfluidic-based organ-on-a-chip can produce functionality which is impossible with conventional 2D or 3D culture systems with high-resolution and real-time imaging, and *in vitro* analysis of biochemical, genetic and metabolic activities of living cells (Bhatia and Ingber, 2014). Organ-on-a-chip mimics the multicellular architectures, tissue-tissue interfaces, physicochemical microenvironments, and vascular perfusion of the body. For example, for targeted brain delivery, blood-brain barrier (BBB)-on-a-chip helps study cellular and molecular mechanism of BBB. Further, BBB-on-a-chip can screen drugs to be used in CNS diseases during preclinical studies (Herland *et al.*, 2016; van der Helm *et al.*, 2016).

Microfluidics can be also used for cancer diagnosis. For example, liquid biopsy is one of the cancer detection techniques, capturing cancer derived materials in the body fluids (Nelson, 2018). However, cancer derived materials, such as circulating tumour cells and DNA are present in extremely low quantities, making it difficult for liquid biopsy to detect cancer in question (Gorgannezhad *et al.*, 2018). In this case, microfluidics can handle complex liquid biopsy samples and identify specific targets for cancer diagnosis.

In short, microfluidics is a versatile platform that can be utilised in different steps of cancer nanomedicine development process (such as, preparation, characterisation, and *in-vitro* simulated evaluation), including cancer diagnosis. However, current study only focuses on preparation, and subsequent tuning of PLGA nanoparticles by microfluidics.

1.2.4.3. Tuning PLGA nanoparticles

1.2.4.3.1. Tuning physicochemical properties

The rationale for tuning physicochemical properties of nanoparticles is to influence their cellular uptake and subsequent interactions with cellular components. Figure 1.24 demonstrates some essential physicochemical properties that need to be tuned during the development process of nanoparticles, although there are other factors to be taken into account (Augustine *et al.*, 2020).

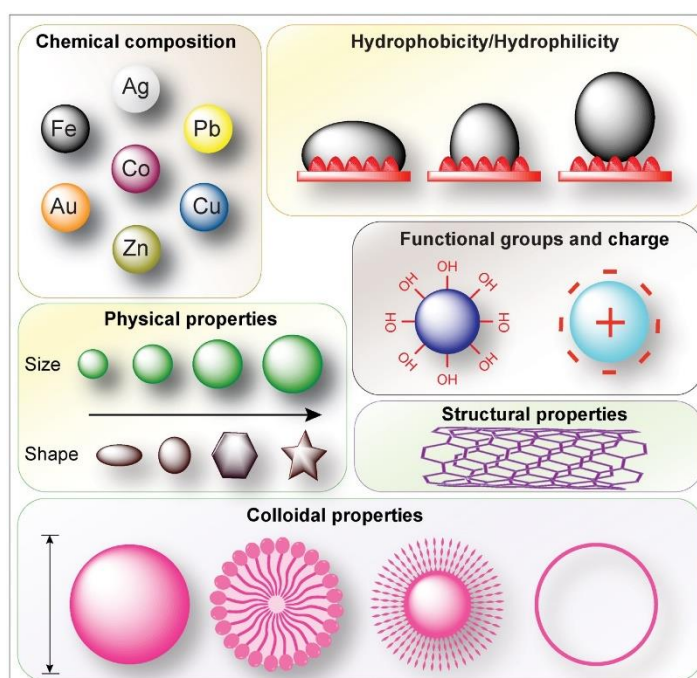


Figure 1.24: Essential physicochemical properties of nanoparticles required to be tuned for intended therapeutic use.

Adapted from Augustine *et al.* (2020).

PLGA nanoparticles can be tuned to desired particle size, surface charge, and drug encapsulation efficiency, by changing process and formulation parameters. Process parameters include types of preparation method, and their respective intermediate steps. For example, emulsion-solvent evaporation method has several intermediate variables that can alter the properties of PLGA nanoparticles. These variables include aqueous-organic phase ratio, homogenisation speed and time, stirring rate, evaporation time, and centrifugation speed and time. Furthermore, during freeze-drying process, there are more variables that could also manipulate the properties of the PLGA nanoparticles, such as freeze-drying time, addition of cryoprotectants (type and concentration of cryoprotectants).

On the other hand, formulation parameters involve the variables in formulation compositions, for example, PLGA type and concentration, drug type and concentration, drug-PLGA ratio, solvent type, and concentration. These parameters can significantly change the properties of PLGA nanoparticles.

Furthermore, PLGA nanoparticles can be functionalised by surface modification. Surface modification is required to prolong the circulation of nanoparticles and prevent them from unwanted interactions with serum proteins. Hydrophobic PLGA nanoparticles can be modified to hydrophilic nanoparticles by attaching a coating material, such as polyethylene glycol (PEG). Particle size of 40-200 nm with hydrophilic surface would circulate long in the blood stream with reduced renal and macrophage clearances, creating more opportunity for delivery systems to reach target tumour site (Torchilin, 2010).

PEGylation, the process of attachment PEG to nanoparticles, is the most common surface modification as this increases the circulation time in the blood. PEG increases the hydrophilicity of the nanoparticles, which lead to avoid interactions with opsonin proteins. Thus, it prevents the nanoparticles from elimination via mononuclear phagocyte system (MPS). Several surfactants have been reported that they also could modify the surface of PLGA nanoparticles. For example, poloxamer 188 decreases the plasma protein adsorption once coated on the PLGA surface (Shubhra *et al.*, 2014). Poloxamers can also enhance proapoptotic signalling and preferentially target cancer cells. However, high dose of poloxamer induces hyperlipidaemia and hypercholesterolemia (as cited in Swider *et al.*, 2018). Polysorbate 80 (Tween[®] 80) is also used as a PLGA coating material that helps in transporting drugs across the blood brain barrier (Escalona-Rayo *et al.*, 2019; Yusuf *et al.*, 2021). However, polysorbate 80 could cause severe non-immunologic anaphylactoid reactions (Coors *et al.*, 2005).

1.2.4.3.2. Tuning nanoparticles for targeted delivery

PLGA nanoparticles can deliver therapeutic molecules in two ways, namely passive targeting, and active targeting, as presented in Figure 1.25.

Passive targeting involves enhanced permeation and retention (EPR) effect. In other words, nanoparticles from the bloodstream would accumulate in a tumour site through fenestrated endothelium of leaky blood vessels, with a gap of 100-780 nm (Figure 1.25A). Doxil[®] and Abraxane[®] are the examples of marketed nanomedicines that work via EPR effect. Several PLGA-based nanoparticulate formulations have been successful for passive targeting, with different therapeutic molecules, such as doxorubicin, paclitaxel, and cisplatin (Dutta, Barick

and Hassan, 2021). However, passive targeting has some drawbacks. For example, some organs (liver and spleen) have fenestrated endothelium, which would potentially accumulate nanoparticles, resulting in unwanted adverse effect (Wicki *et al.*, 2015).

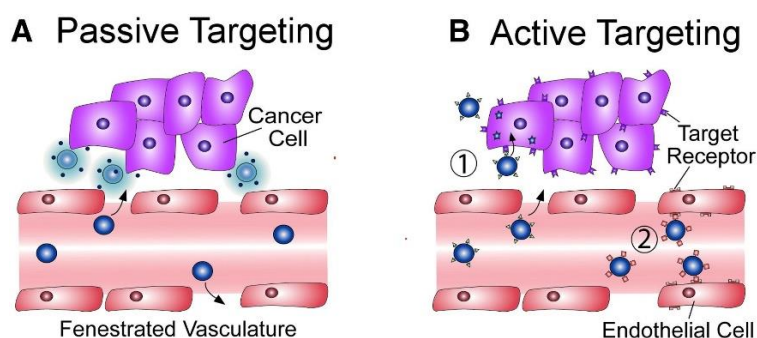


Figure 1.25: Graphical demonstration of targeting strategies of nanoparticles.

(A) Passive targeting of cancer involves EPR effect by which nanoparticles enter and accumulate into the tumour via compromised and leaky vasculatures; and (B) Active targeting involves selective binding between targeted receptor on the cell surface and ligand on the nanoparticles. Adapted from Wicki *et al.* (2015).

In contrast, active targeting involves strong interaction between nanoparticles and targeted receptor on cell surface (Wicki *et al.*, 2015). This is performed by modifying the surface of the nanoparticles with a targeting ligand, which is selective to its corresponding receptor expressed on the cell surface. Subsequently, a ligand-receptor complex is formed, which is later internalised by cells via receptor mediated endocytosis (Raj *et al.*, 2021).

Most tumour cells overexpress certain receptors (Dutta, Barick and Hassan, 2021), such as epidermal growth factor receptors (Nguyen *et al.*, 2021), folate receptors, and transferrin receptors. Breast cancer and adenocarcinoma cells overexpress a growth factor named human epidermal growth factor receptor 2 (HER2 or ErbB2). Active targeting coats or conjugates corresponding ligands on the surface of nanoparticles to selectively bind with these receptor proteins. Figure 1.26 shows some potential targets, to which nanoparticles with targeting ligands can bind.

Targeting ligands can be small molecule (such as, folic acid) or macromolecules, such as protein (such as, transferrin), peptide or aptamers (fragment of DNA or RNA). For example, prostate specific membrane antigen (PSMA) is overexpressed in prostate cancer cells, which can be targeted by an aptamer. Furthermore, short peptides, such as arginine-glycine-aspartic (RGD) sequence has high affinity for $\alpha\beta3$ integrin (a receptor for vitronectin), which are overexpressed in several cancer cells (Cheng and Ji, 2019). Table 1.9 lists some potential targeting ligands that selectively bind with overexpressed receptors on different types of cancer.

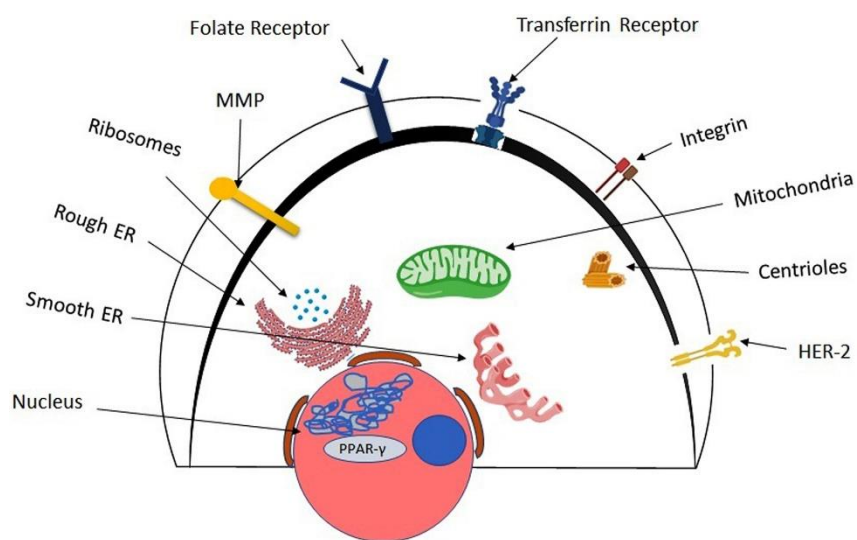


Figure 1.26: Potential targets for nanoparticles.
Adapted from Vyas, Patel and Wairkar (2021).

Table 1.9: List of targeting ligands that selectively bind with overexpressed receptors.

Targeting ligands	Overexpressed receptors	Cancers
Transferrin (TF)	Transferrin receptor (TFR)	Glioma and breast cancer
Folic acid	Folate receptor	Lung, cervical, breast, and liver cancers
anti-EGFR, EGF	EGFR	Breast and oral cancers
anti-HER2	HER2	Breast cancer
anti-CD	CD	Prostate, lymphoma, and breast cancers
Estrone	Estrogen	Breast cancer
RGD peptide	$\alpha\beta 3$ Integrin	Endothelial, glioma, lung, melanoma, and breast cancers
Peptides, mAb	Chemokine (CXCR4)	Lung, lymphoma, breast, and liver cancers
Peptide	LHRH	Breast and ovarian cancers
Biotin	Biotin	Liver and breast cancers
Aptamer, anti-PSMA	PSMA	Prostate cancer
Peptides	IL (4, 13)	Glioma, colon, and lung cancers
Anti-VEGF mAb	VEGF	Pancreatic cancer

Adapted from Dutta, Barick and Hassan (2021).

Particularly, transferrin receptors (TFR) were found to be overexpressed in malignant cells (Byrne, Betancourt and Brannon-Peppas, 2008). This is because cancer cells proliferate uncontrollably, and they require more iron than normal for their growth, leading to overexpression of TFR on the cell surface to attract iron-bound transferrin in the bloodstream (Vyas, Patel and Wairkar, 2021). Several cancer therapeutics targeting TFR are reported to be in clinical trials (Byrne, Betancourt and Brannon-Peppas, 2008).

Transferrin receptors were also reported to be overexpressed on glioma cells (Chirasani *et al.*, 2008). Targeting gliomas, PLGA nanoparticles coated with transferrin was reported to be successful enhancing the anticancer activity of temozolomide (Ramalho *et al.*, 2018). PLGA nanoparticles can be functionalised to perform as transferrin receptor-mediated active targeted drug delivery systems, given the biocompatible, biodegradable and tunable properties of PLGA. A recent study developed transferrin conjugated PLGA nanoparticles for delivery of doxorubicin and methylene blue (Bidkar, Sanpui and Ghosh, 2020).

In short, PLGA nanoparticles coated with transferrin could be the potential active targeted delivery systems for glioblastoma. As PLGA has already proven to encapsulate a variety of therapeutic molecules for targeted glioblastoma chemotherapy (Table 1.10), it is hypothesised that antipsychotic drug pimozide could also be loaded into PLGA nanoparticles and tuned for selective cellular uptake by glioblastoma cells. In other words, pimozide-PLGA nanoparticles could inhibit the glioblastoma cell growth selectively, suggesting a strategy to repurpose pimozide for glioblastoma chemotherapy.

Table 1.10: Recent updates of PLGA nanoparticles targeting gliomas.

Therapeutic molecule	Targeting ligand	Surface coating	References
Mitoxantrone	TRAIL	-	(Hashemi <i>et al.</i> , 2021)
Thiazolidinedione	8D3 mAb	-	(Monge <i>et al.</i> , 2020)
Euphorbia factor L1 (EFL1)	^D WSW and NGR peptides	RBC membrane	(Cui <i>et al.</i> , 2020)
Rapamycin	-	Polysorbate 80	(Escalona-Rayó <i>et al.</i> , 2019)
Temozolomide	Cetuximab	-	(Duwa <i>et al.</i> , 2020)
	OX26 type mAb	PEG	(Ramalho <i>et al.</i> , 2018)
	-	-	(Ananta, Paulmurugan and Massoud, 2016)
3,3'-diindolylmethane	anti-SSTR2 peptide	-	(Bhowmik <i>et al.</i> , 2017)
Paclitaxel and methotrexate	-	PVA and poloxamer 188	(Madani <i>et al.</i> , 2020)
Paclitaxel	-	Polysorbate 80	(Li <i>et al.</i> , 2018)
	-	PEG	(Nance <i>et al.</i> , 2014a)
	AS1411 (aptamer)	PEG	(Guo <i>et al.</i> , 2011)
Paclitaxel and curcumin	T7 peptide and Magnetic NPs	PEG	(Cui <i>et al.</i> , 2016)
Doxorubicin and Methylene Blue	Transferrin	RBC membrane	(Bidkar, Sanpui and Ghosh, 2020)
Doxorubicin and tetrahydrocurcumin	Transferrin	PEG	(Zhang <i>et al.</i> , 2019)
Doxorubicin	-	Poloxamer 188	(Malinovskaya <i>et al.</i> , 2017; Maksimenko <i>et al.</i> , 2019; Pereverzeva <i>et al.</i> , 2019)
	Transferrin	PEG	(Liu <i>et al.</i> , 2013)
Doxorubicin and paclitaxel	Transferrin	Magnetic silica NPs	(Cui <i>et al.</i> , 2013)
	-	Transferrin	BSA

1.3. General Aim and Objectives

1.3.1. General aim

The general aim of this study is to develop functionalised pimozone-loaded PLGA nanoparticles, followed by their evaluation on glioblastoma cell lines.

1.3.2. Specific aims

- a) To prepare and characterise pimozone-loaded PLGA nanoparticles.
- b) To develop and validated an ultra-high-performance liquid chromatography (UHPLC) method for analysis of pimozone in PLGA nanoparticles.
- c) To optimise PLGA nanoparticles by exploring process and formulation parameters.
- d) To functionalise PLGA nanoparticles with polyethylene glycol and transferrin (TF) with the aim of targeting transferrin receptors (TFR) in glioblastoma cells.
- e) To evaluate the developed PLGA nanoparticles on glioblastoma cell lines.

1.3.3. Specific objectives

- i. To select the preparation method by comparing physicochemical properties of PLGA nanoparticles prepared by single emulsion-solvent evaporation and microfluidics.
- ii. To select an appropriate solvent of analyte and sample preparation process prior to validating the UHPLC method according to the ICH guidelines.
- iii. To achieve optimised nanoparticles by exploring the effect of different formulation parameters, such as molecular weight, type, and concentration of individual material in the formulation composition.
- iv. To confirm the PEGylation and investigate its effect on the physicochemical properties of PLGA nanoparticles.
- v. To optimise microfluidic conditions (flow rate and flow ratio of aqueous and organic phases) in preparation of PLGA nanoparticles.
- vi. To determine the appropriate techniques of nanoparticles collection between centrifugation and dialysis.
- vii. To confirm TF adsorption on the surface of PLGA nanoparticles qualitatively and quantitatively.
- viii. To study storage stability of nanoparticles based on their physicochemical properties, and to detect any microbial contamination during the storage.
- ix. To confirm the expression of transferrin receptors (TFR1 and TFR2) on glioblastoma cell lines, followed by investigation of cytotoxicity and cellular uptake of targeted nanoparticles.

1.4. Structure of the Thesis

This thesis consists of further eight chapters. Following paragraphs summarise these chapters (each chapter will have achieved one or more than one aim and objective of this study).

Chapter 2 lists the chemical and biological materials, devices, and instruments. Further, it explains all the experimental methods with their principles.

Chapter 3 describes the development and validation of an ultra-high performance liquid chromatography (UHPLC) method to analyse pimozone in PLGA nanoparticles.

Chapter 4 summarises the findings of the effect of formulation and process parameters on the physicochemical properties of pimozone-loaded PLGA nanoparticles. Briefly, it deals with exploratory investigations of how particle size, charge, and drug encapsulation efficiency are affected by the change of process and formulation parameters, such as preparation method, surfactants, and different types of PLGA. Thus, it achieves a potential formulation with desired physicochemical properties for further study. Furthermore, it introduces surface modification to this potential formulation with polyethylene glycol (PEG) and explores its effect.

Chapter 5 comprises of optimisation, functionalisation, and stability studies. Optimisation are based on further investigation of process and formulation parameters. Functionalisation involves adsorption of transferrin on the surface of PLGA nanoparticles. Finally, this chapter describes the stability of optimised PLGA nanoparticles by storage stability study, including microbial detection study.

Chapter 6 evaluates the optimised and targeted PLGA nanoparticles on glioblastoma cell lines. First, it describes the results of immunoblot analysis whether glioblastoma cells express transferrin receptors. Second, it presents findings of cytotoxicity and cellular uptake studies.

Chapter 7 concludes the study and recommends prospective research directions.

Chapter 8 and 9 list the References and Appendices, respectively.

Chapter 2

Materials and Methods

Chapter 2. Materials and Methods

Current chapter describes all the chemical and biological materials, devices, and instruments used in this study. It further outlines all the experimental methods with related theories.

2.1. Materials

2.1.1. Drug molecule

Pimozide was obtained from Sigma-Aldrich[®], UK (produced in India). A detailed specification is presented in Table 2.1.

Table 2.1: Product specifications of pimozide.

Characteristics	Description
Empirical formula	C ₂₈ H ₂₉ F ₂ N ₃ O
Molecular weight	461.55 g/mol
CAS number	2062-78-4
Product code	P1793
Lot number	SLBQ8725V
Batch number	SLCF5333
Purity	≥ 98 % (TLC)

2.1.2. Carrier molecule

Poly (D, L-lactide-co-glycolide) (PLGA), with 50:50 lactide-glycolide ratio, was used as a drug carrier system in this study. Three different types of PLGA were obtained from Sigma-Aldrich[®], UK (Table 2.2).

Table 2.2: Product specifications of PLGA.

Trade name	Molecular weight (kDa)	Viscosity (dL/g)	Product code	Lot number	Origin of product
Resomer [®] RG 503 H	24-38	0.32-0.44	719870	BCBZ8795	Evonik Rohm GmbH, Germany
Resomer [®] RG 503	24-38	0.32-0.44	739952	BCBT2434	Evonik Rohm GmbH, Germany
LACTEL [®]	30-60	-	P2191	MKBZ5057V	Durect corp., USA

2.1.3. Surfactants and surface modifying agents

D- α -Tocopherol polyethylene glycol 1000 succinate (TPGS), polyvinyl alcohol (PVA, 87-89% hydrolysed), poloxamer 188 (Pluronic[®] F-68) and polysorbate 80 (Tween[®] 80) were used as surfactants. Polyethylene glycol (PEG) was used as surface coating agent of the PLGA nanoparticles. Transferrin ($\geq 97\%$, holo-Transferrin human) was used as targeting ligands. Their detailed specifications are described in Table 2.3.

Table 2.3: Product specifications of different surfactants and surface modifying materials.

Name	Molecular weight (Da)	Product code	Lot number	Supplier
TPGS	574.8	57668	BCBX8795	Sigma-Aldrich, UK
PVA	13-23000	363170	MKBS7627V	Sigma-Aldrich, UK
Poloxamer 188	8400	P5556	RNBF1073	Sigma-Aldrich, UK
Polysorbate 80	1310	59924	BCBJ7603V	Fluka Analytica, UK
PEG 4000	4000	29576	6072870	BDH Chemicals Ltd., Poole, England
PEG 8000	8000	2139	62H0252	Sigma-Aldrich, UK
Transferrin	80000	T0665	SLBZ5500	Sigma-Aldrich, UK

2.1.4. Reagents and solvents

All reagents and solvents used in this study are analytical grade (and HPLC grade). Their specifications are described in Table 2.4.

Table 2.4: Product specifications of reagents and solvents.

Name	Details	Supplier
Acetonitrile	Pierce [®] , LC-MS grade	Thermo Scientific, UK
Accutase [®] cell detachment solution	Corning [™] Accutase [™] , Ref: 25058CI Lot: 25058048	Thermo Scientific UK
Advanced Dulbecco's modified Eagle medium (DMEM)	Cat: 12634010, Lot: 2085134	Thermo Fisher Scientific, USA
Ammonium formate	Analytical reagent grade, Mw: 63.06, CAS: 540692, Lot: 1484211	Fisher Scientific, UK
B-27 [®] supplement	Gibco [™] , Ref: 17504044, Lot: 1933112	Thermo Fisher Scientific, USA
Coumarin-6	98%, Ref: 442631, Lot: MKBR2011V CAS: 38215-36-0	Sigma-Aldrich, UK
Dichloromethane (DCM)	Chromasolv [®] , ≥99.8%, amylene stabilized	Sigma-Aldrich, UK
Dimethyl sulfoxide (DMSO)	≥99.5% (GC), plant cell culture tested, Ref: D4540, Lot: BCBR0695V	Sigma-Aldrich, UK
di-Sodium hydrogen orthophosphate anhydrous	Mw: 141.96, CAS: 7558-79-4	Fisher Scientific, UK
EGF recombinant human protein	Gibco [™] , Invitrogen [®] , Ref: PHG0313, Lot: 1776110A	Thermo Fisher Scientific, USA
Ethanol	Absolute, HPLC grade	Fisher Scientific, UK
FGF-Basic (AA 1-155) Recombinant Human Protein	Gibco [™] , Ref: PHG0263, Lot: 1898331	Thermo Fisher Scientific, USA
Formic acid	CAS: 64186, Lot: 174566	Fisher Scientific, UK
Glutamine	Gibco [™] , L-Glutamine (200 mM) Ref: 25030081	Thermo Fisher Scientific, USA
Heparin sodium salt from intestinal mucosa	Ref: H3393, Lot: SLBP2731V	Sigma-Aldrich, UK
Malt Extract	Malted barley, MC023, Batch: 204407/256	Neogen, UK
Matrigel [™] GFR membrane matrix	Corning [™] , Ref: 11523550	Fisher Scientific, UK
Methanol	99.8%, HPLC grade	Fisher Scientific, UK
Micro BCA [™] Protein Assay Kit	Cat: 23235, Lot: QH221547	Thermo Scientific, UK

N-2 Supplement	Gibco™, Ref:17502048, Lot: 1922476	Thermo Fisher Scientific, USA
Penicillin-Streptomycin	10000 U/mL, Gibco™, Ref: 15140122	Thermo Fisher Scientific, USA
Protein marker	PageRuler™ Prestained Protein Ladder Cat: 26616	Thermo Scientific, UK
Tryptic Soy Agar (TSA)	Cat: 22091, Lot: BCBZ8619	Sigma-Aldrich, UK
Ultra-pure water	Triple Red Laboratory Technology, Barnstead™ Nanopure™	Thermo Scientific, UK

2.1.5. Instruments and devices

List of instruments and devices used in this study is presented in Table 2.5.

Table 2.5: Specifications of instruments and devices.

Instrument/Device	Details	Supplier
Analytical balance	Model: XS204, Capacity: 220 g, 0.1 mg readability Model: MT5	Mettler-Toledo Ltd., UK
Centrifuges	Beckman® J2-21 Centrifuge	Beckman Coulter, USA
	Mikro 200R Centrifuge	Hettich, Germany
Cell culture well plate	Sterile 96 well plate, Cellstar®, cat: 651180	Greiner Bio One International Ltd., UK
Cell culture flask	TC Flasks T75, Ref: 83.3911.002, Lot: 9020811	Sarstedt AG & Co., Germany
Dialysis membrane	Dialysis Tubing- Visking Molecular weight cut-off: 12-14 kDa	Medicell International Ltd., UK
Differential scanning calorimetry (DSC)	DCS Series™ Q1000	TA Instrument, USA
Electron microscopes	Hitachi S-3000N Scanning electron microscope	Hitachi Ltd., Japan
	Hitachi H-7000 Transmission electron microscope	Hitachi Ltd., Japan
FTIR	IRAffinity-1S, Fourier Transform Infrared Spectrophotometer	Shimadzu UK Ltd., UK
Freeze-dryer	Christ® Alpha 2-4 LSC freeze dryer	Martin Christ, Germany
HPLC system	Agilent 1290 Infinity LC system	Agilent, USA
HPLC column	Raptor™ Biphenyl 2.7 µm (100 × 4.6 mm), Serial: 17121693J, Cat: 9309A15, Lot: 170708P	Restek, USA
	Gemini-NX 3 µm C18 110A (150 × 4.6 mm), Serial: 7130118, Cat: 00F4453E0, Batch: 5560048	Chromservis, Czech Republic
	Hypersil™ BDS 5 µm C18 (250 × 4.6 mm), Cat: 28105-254630	Thermo Scientific, UK
	ACE Excel 2 µm super C18 (100 × 2.1 mm), Batch: V14-8386, Part no: EXL-1011-1002U, Serial: A171859	Hichrom Ltd., Reading, UK

Homogenizer	Stuart® laboratory homogeniser, SHM2	Keison Products, UK
Live cell analysis system	IncuCyte® ZOOM	Essen BioScience, UK
Microfluidic mixer	NanoAssemblr® Benchtop	Precision NanoSystems Inc., Canada
Microplate readers	xMark™ Microplate spectrophotometer Multiskan EX microplate spectrophotometer	Bio-Rad Laboratories Inc., USA. Thermo Scientific, UK
Particle analyser	Zetasizer Nano ZSP	Malvern Panalytical, UK
pH meter	HI-8014 pH and ORP Meter	Hanna Instruments, UK
PAGE gel	Mini-Protein® TGX Stain-Free™ Precast Gels, 12%, 15-well comb, 15 µL/well Cat. # 456-8046	Bio-Rad Laboratories Inc., USA
Sonicator	Soniprep 150 Camlab Transsonic T460	MSE Ltd., UK S.H. Scientific, UK
Spreader	L-shaped cell spreader	Fisher Scientific, UK
Syringe filters	KX Syringe Filter, PTFE 25 mm, 0.45 µm PTFE 25 mm, 0.2 µm	Kinesis, UK Fisher Scientific, UK
Trans-Blot apparatus	Trans-Blot® Turbo™ Transfer System (Includes buffer, nitrocellulose membrane, and filter paper)	Bio-Rad Laboratories Inc., USA
UV-Vis Spectrophotometer	M501 Single beam scanning UV-Vis spectrophotometer	Spectronic CamSpec Ltd., UK

2.2. Methods

2.2.1. Preparation of PLGA nanoparticles

This section describes preparation of pimozone-encapsulated nanoparticles by two methods, including preparation of dye-incorporated nanoparticles, and subsequent freeze-drying of all formulations. Further, it outlines the preparation of transferrin-adsorbed nanoparticles.

2.2.1.1. Single emulsion-solvent evaporation method

PLGA nanoparticles were prepared by oil-in-water (o/w) single emulsion-solvent evaporation (SE) method. Figure 2.1 describes the simplified workflow of SE method. Briefly, 100 mg of PLGA (30-60 or 24-38 kDa; acid or ester terminated) was dissolved in 2 mL of dichloromethane (DCM), followed by addition of 2.5 mg of pimozone into the mixture. Then a 5% (w/w) polyethylene glycol (4 or 8 kDa) was added to the mixture. A surfactant solution (PVA or polysorbate 80) of 1.25% (w/v) was emulsified with PLGA-PEG-pimozone mixture by homogenisation using Stuart[®] SHM2 laboratory homogeniser (Keison Products, Essex, UK) for 2 minutes at 1000 rpm. This process was performed on an ice bath to neutralise excess heat produced. The prepared emulsions were magnetically stirred overnight at 80 rpm and room temperature in the fume hood to facilitate DCM evaporation. Nanoparticles were collected by washing the emulsions two times with distilled water, and by subsequent centrifugation using Beckman[®] J2-21 Centrifuge (Beckman Coulter, California, USA) at 10,000 rpm and 4°C for 30 minutes. Pellets were re-dispersed in 5 mL of distilled water in a clear glass vial for further use, such as, initial particle analysis or freezing at -80°C to freeze-dry.

In principle, preparation of polymeric nanoparticles by an oil-in-water (o/w) SE method involves three steps: (a) emulsification of the polymeric dispersed phase (organic phase) in a surfactant-containing aqueous phase under sonication, homogenisation, or milling; (b) solvent removal by evaporation, leading to solidification of emulsion droplets into nanoparticles; and (c) collection of nanoparticles by washing, followed by centrifugation or filtration. Notably, solvent evaporation is usually carried out by continuous stirring at ambient pressure, but its rate can be accelerated under reduced pressure, or under vacuum (McCall and Sirianni, 2013; Lee, Yun and Park, 2016).

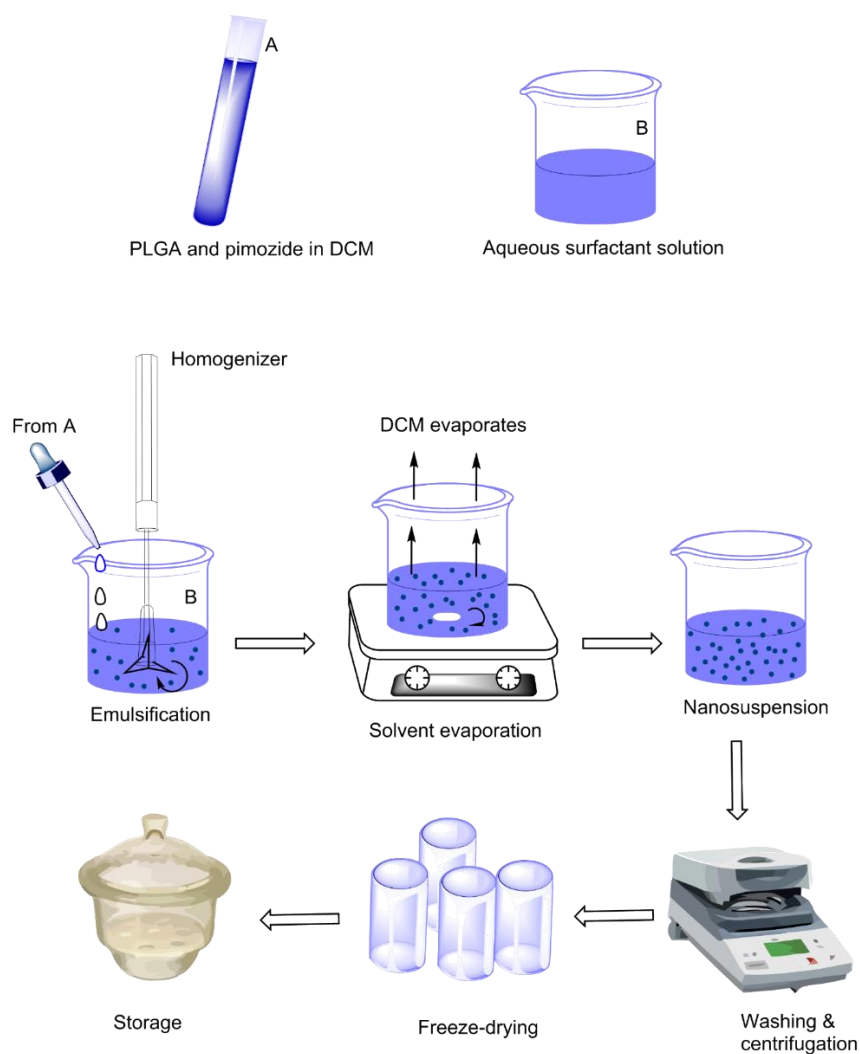


Figure 2.1: Simplified schematic diagram of single emulsion-solvent evaporation method in preparation of pimoziide-loaded PLGA nanoparticles.

To freeze dry, nanoparticles in glass vials were frozen at -80°C for 3 hours and freeze-dried in a Christ[®] Alpha 2-4 LSC freeze dryer instrument (Martin Christ, Osterode, Germany) for 48 hours under vacuum at acquired pressure of 0.035 mbar (with a set pressure of 0.011 mbar) and at shelf temperature of 10°C . Freeze-dried nanoparticles were then stored at appropriate conditions for further characterisations.

Freeze-drying improves the stability of nanoparticles during long-term storage (Trenkenschuh and Friess, 2021). Generally, in freeze-drying technique, aqueous media (such as, water) is removed from frozen nanosuspension by sublimation, which is defined as a process that converts ice into vapour directly, bypassing the liquid state. However, low pressure and heat energy are required to achieve this sublimation state. Phase diagram of

water is an ideal example to understand sublimation (Figure 2.2). In brief, freeze-drying occurs in three stages (Figure 2.3): (a) freezing, which slows down degradation and solidifies the formulation; (b) primary drying, in which sublimation occurs, meaning moisture is removed by vacuum at sub-ambient temperature; and (c) secondary drying, where desorption occurs, meaning the last traces of water is removed by heat (Franks, 1998; Morais *et al.*, 2016).

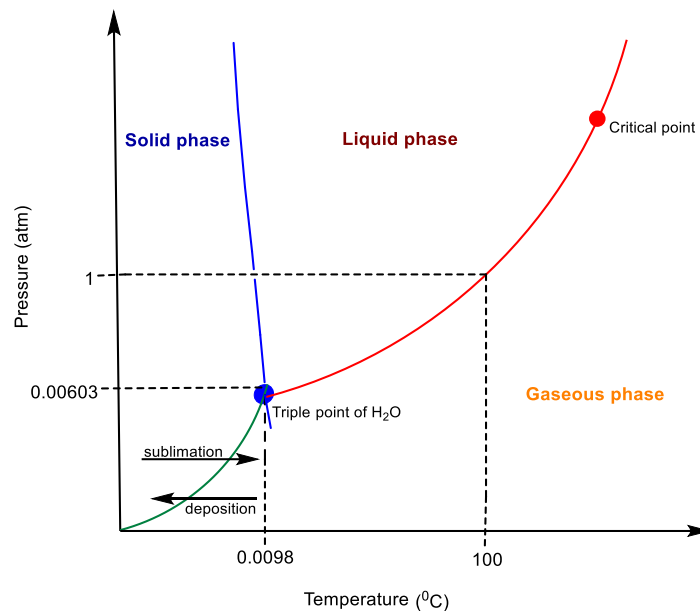


Figure 2.2: Phase diagram of water.

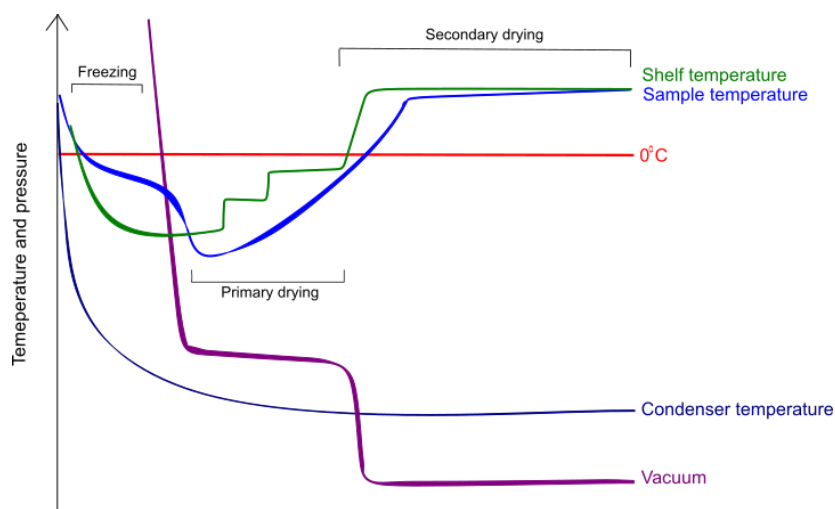


Figure 2.3: Different stages in freeze-drying.

2.2.1.2. Microfluidic method

Nanoparticles were prepared by a microfluidic method that used staggered herringbone mixing technique with a NanoAssemblr[®] Benchtop instrument (Precision NanoSystems, Vancouver, Canada). Briefly, PLGA (100 or 200 mg; acid or ester terminated; 24-38 or 30-60 kDa) and 5 or 10 or 20% (w/w) polyethylene glycol (Mw 4 or 8 kDa) were dissolved in acetonitrile or dimethyl sulfoxide (DMSO), followed by addition of pimozone (2.5 or 5 or 10 mg) that was previously dissolved in methanol or DMSO. PLGA-PEG-pimozone mixture was injected through one inlet of the microfluidic mixing chamber, while aqueous surfactant solution of 1.25% (w/v) [PVA or polysorbate 80 or poloxamer 188 or PVA-TPGS (1:1) or TPGS (0.5 or 1.25 or 2%)] was injected through the other inlet (Figure 2.4). Both organic and aqueous phases were mixed in the microfluidic chamber at a total flow rate of 4 or 8 or 12 or 15 mL/min and at an aqueous-organic phase flow ratio of 1:1 or 1:2 or 2:1. Prepared nanosuspensions were washed and collected by centrifugation (as described in SE method) or by dialysis (Figure 2.4) using Visking dialysis tubing membrane (molecular weight cut-off: 12-14 kDa). Subsequently, nanosuspensions were transferred to a clear glass vial for further use, such as, initial particle analysis and freezing at -80°C to freeze-dry (as described in Section 2.2.1.1). Freeze-dried nanoparticles were then stored at appropriate conditions for further characterisations.

In principle, staggered herringbone mixing (SHM) uses an array of 'herringbone grooves' on one or more surfaces of a microchannel to induce turbulent mixing of fluids, as already described in Chapter 1 (Figure 1.22). With this design, the streams of fluids create counter-rotating vortices, which are repeatedly altered due to the asymmetric geometry, leading to faster and refined mixing, subsequently producing homogenous particles. SHM is an effective mixer for continuous flow since fluids are redistributed over the entire channel, significantly reducing Taylor dispersion, which is an effect in fluid mechanics in which a shear flow increases the diffusivity of a species, resulting in an even residence time distribution (Williams, Longmuir and Yager, 2008; Zhigaltsev *et al.*, 2012).

In case of dye-loading into the nanoparticles, coumarin-6 (a fluorescent dye) was added to PLGA solution at a concentration of 1% (w/w), as the only additional change to the procedure described in this microfluidic method.

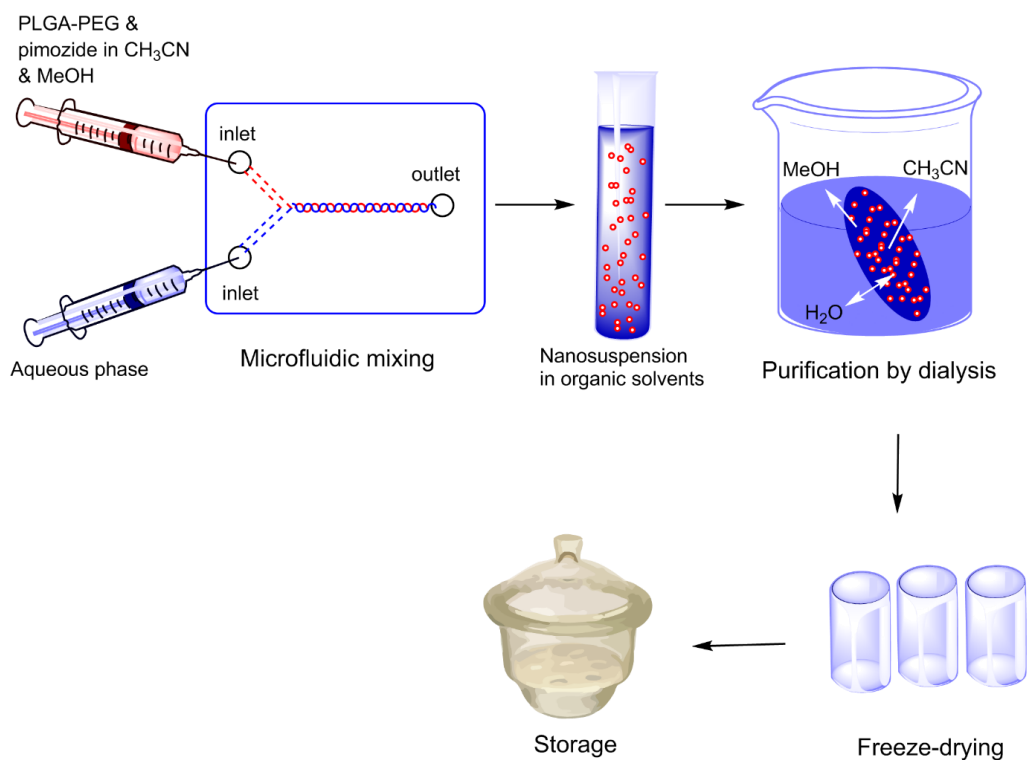


Figure 2.4: Simplified schematic diagram of microfluidic method in preparation of pimoziide-loaded PLGA nanoparticles.

Finally, transferrin receptors targeted PLGA nanoparticles were prepared by physical adsorption of transferrin on the surface of the particles, by following a modified method from Chang *et al.* (2012). Briefly, 20 mg of freeze-dried nanoparticles was incubated with 2 mL of 1 mg/mL transferrin solution (prepared in distilled water) for 2 hours at 4°C (Figure 2.5). Unbound transferrin was removed by centrifugation using Mikro 200R Centrifuge (Hettich, Tuttlingen, Germany) at 10,000 rpm and 4°C for 10 minutes, followed by re-suspending the pellets in 1 mL of distilled water and storing at appropriate condition for future use.

Adsorption of protein molecules on the surfaces of biomaterials is a complex phenomenon that involves multiple non-covalent interactions. Therefore, transferrin adsorption on the surface of PLGA nanoparticles includes a combination of intermolecular interactions, such as hydrogen bonding, van der Waals, hydrophobic, and electrostatic interactions (Vasita and Katti, 2012; Frasco *et al.*, 2015).

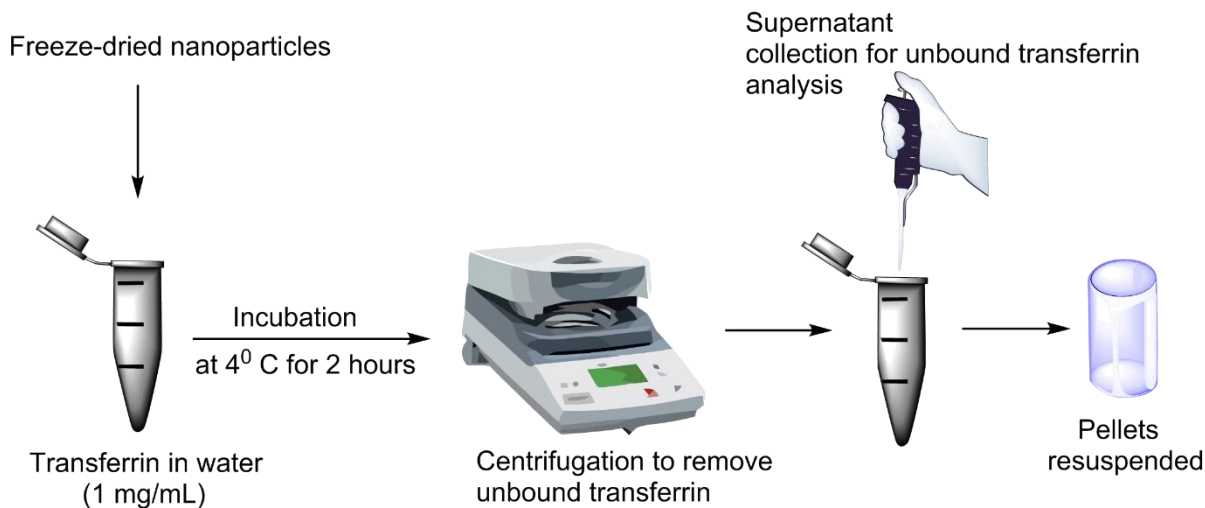


Figure 2.5: Workflow of transferrin adsorption on the surface of PLGA nanoparticles.

2.2.2. Characterisation of nanoparticles

2.2.2.1. Analysis of particle size

Particle size distribution profile that includes size and polydispersity index (PDI) of PLGA nanoparticles was analysed by dynamic light scattering (DLS) technique using a Zetasizer Nano ZSP instrument (Malvern Panalytical, Cambridge, UK), as demonstrated in Figure 2.6. Briefly, freeze-dried nanoparticles were suspended in ultra-pure water at a concentration of 1 mg/mL. Adjustment of sample concentration was made by further dilution to optimise the analysis. Samples before freeze-drying were also prepared at the same concentration. Three measurements were taken for each sample at a measurement angle of 173° , and at a temperature of 25°C .

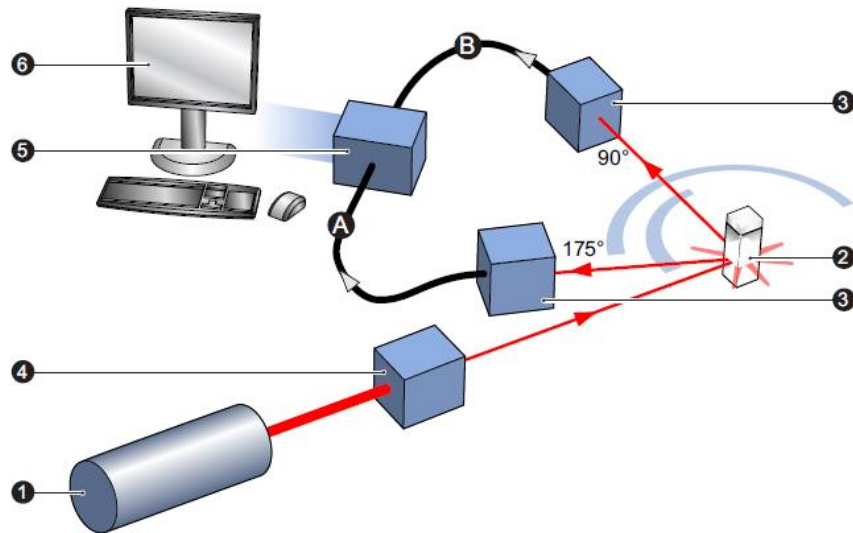


Figure 2.6: Different components used for the determination of particle size by using dynamic light scattering technique.

Adapted from manufacturer brochure of Zetasizer Nano ZSP instrument (Malvern Panalytical, UK). (1) laser, (2) sample cell, (3) detector, (4) attenuator, (5) correlator, and (6) computer.

Dynamic light scattering (DLS), also known as photon correlation spectroscopy (PCS) or quasi-elastic light scattering (QELS), measures the hydrodynamic diameter of particles in a liquid medium. Hydrodynamic diameter is defined as the diameter of an imaginary sphere which is equivalent to an actual particle suspended in a liquid medium. In principle, DLS measures the scattered light intensity at a given angle as a function of time for a population of particles in a liquid medium (Figure 2.7). According to Rayleigh scattering, light scatters in all directions once it hits small particles. The scattering intensity fluctuates over time due to the Brownian motion of the particles, undergoing either constructive or destructive interference. DLS derives this dynamic information from a digital signal processing device named correlator in real time and produces an average size distribution profile of a population of particles based on Stokes-Einstein equation (Pande and Bhaskarwar, 2016).

For more clarity, when nanoparticles are suspended in a liquid medium, they are constantly moving following Brownian motion as they interact with medium's molecules (such as, water molecules in aqueous medium). Brownian motion is the random movement of small particles (in a fluid) caused by the collisions between the particles and fluid molecules. Here, a small particle would move faster than a large particle in a particular fluid (Figure 2.8). However, the movement of particles depends on the fluid medium's viscosity and temperature, including particle size. The relationship between these variables is expressed by Stokes-Einstein equation, and hence the hydrodynamic diameter of the particles can be deduced as follows,

$$d_H = \frac{k_b T}{3\pi\eta D}$$

where d_H is the hydrodynamic diameter, k_b is the Boltzmann constant ($= 1.38 \times 10^{-23} \text{ JK}^{-1}$), T is the temperature, η is the viscosity of the medium, D is the diffusion coefficient, and π is the mathematical constant ($= 3.1416$).

It is to be noted that hydrodynamic diameter is not the actual size of the particle. To understand the difference, further characterisation with other techniques is required. For example, transmission electron microscopy would provide more actual size of the nanoparticles.

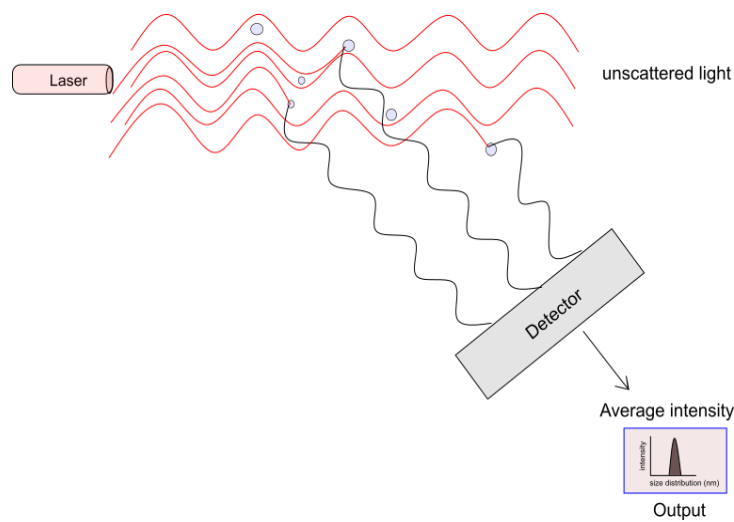


Figure 2.7: Principle of dynamic light scattering (DLS) showing detector receiving scattered light, leading to measurement of average particle size.

The intensity of scattered light at a given angle is calculated as a function of time for a group of particles. Further, the rate of change of this intensity is a function of the movement of the particles, which can be explained by Brownian motion.

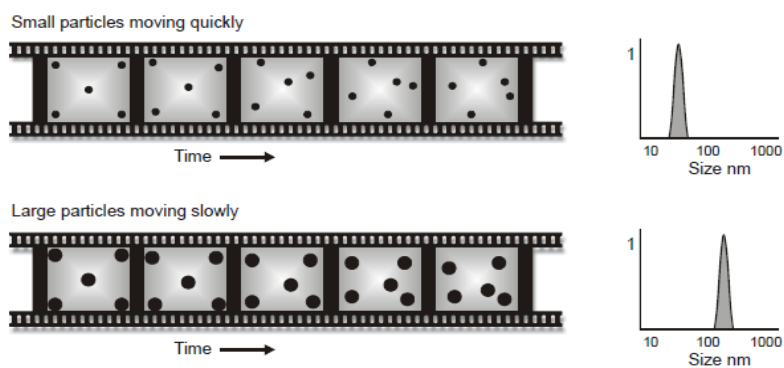


Figure 2.8: Movement of small and large particles in a liquid medium.
Adapted from manufacturer brochure of Zetasizer Nano ZSP instrument, Malvern Panalytical, UK.

2.2.2.2. Determination of zeta potential

Surface charge (zeta potential) is the electric potential developed in a colloidal system. It is used to evaluate the stability of a colloidal system, such as nanoparticles. The zeta potential of negatively charged particle is explained in Figure 2.9. If a negatively charged particle is suspended in a liquid medium, it will attract positively charged ions to be attached around the particle surface. There will be more positively charged ions which are further away from the particles. However, they will be loosely bound forming a layer called diffuse layer. When the particle moves, some of the ions within the diffuse layer moves with it. However, some ions will remain where they are. A boundary called slipping plane can be drawn between these two types of ions. The potential at the slipping plane between particle surface and liquid medium is termed as zeta potential. Its unit is expressed as millivolt (mV).

Zeta potential of PLGA nanoparticles was determined by laser Doppler velocimetry (LDV) using a Zetasizer Nano ZSP instrument (Malvern Panalytical, Cambridge, UK). For the analysis, ultrapure water with 10 mM sodium chloride (NaCl) was used as suspending medium. Briefly, samples were prepared by re-dispersing 5 mg of freeze-dried nanoparticles in 5 mL of 10 mM NaCl, followed by 10 times dilution with same dispersing medium. Samples before freeze-drying were also prepared at the same concentration. Three measurements were taken for each sample at 25° C.

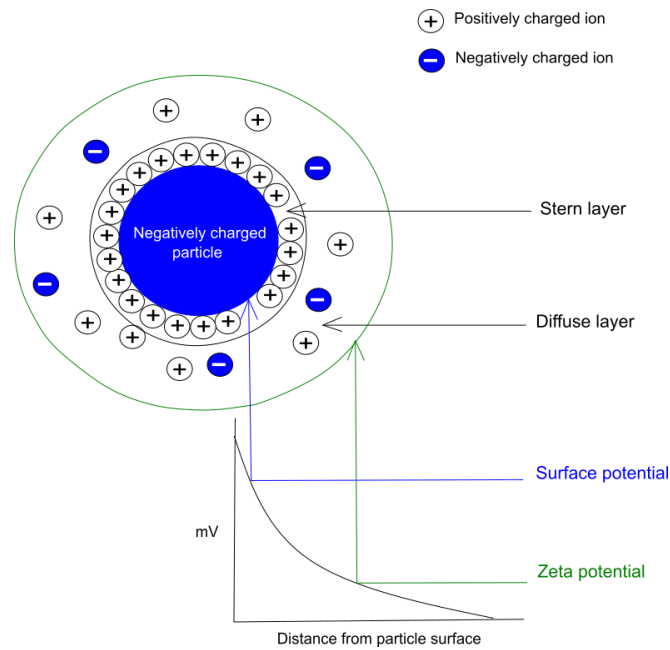


Figure 2.9: Zeta potential of a negatively charged particle in a liquid medium.

LDV is also known as laser Doppler anemometry (LDA). Different components of LDV/LDA for the measurement of zeta potential are illustrated in Figure 2.10. In principle, an electric field is applied across the sample to induce movement of the charged particles. Light scattering is used to determine electrophoretic mobility of the particles.

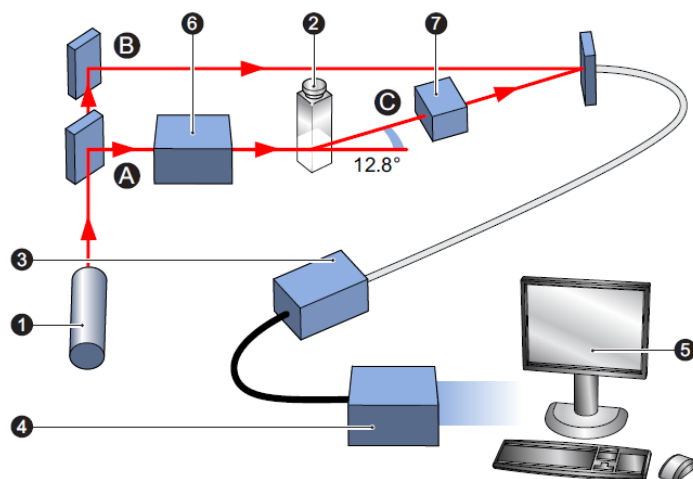


Figure 2.10: Different components used for the determination of zeta potential by using laser Doppler anemometry technique.

Adapted from manufacturer brochure of Zetasizer Nano ZSP instrument (Malvern Panalytical, UK). (1) laser, (2) sample cell, (3) detector, (4) signal processor, (5) computer, (6) attenuator, and (7) compensation optics. (A) incident beam; (B) reference beam; and (C) scattering beam.

Electrophoretic mobility is the ratio of velocity of the particles and external applied electrical field. Subsequently, zeta potential (Z) is deduced from the Henry equation as follows,

$$Z = \frac{3\eta U_E}{2\mathcal{E} f(ka)}$$

where, η is the viscosity of the medium; U_E is the electrophoretic mobility; \mathcal{E} is the dielectric constant; and $f(ka)$ is the Henry function, ka is the ratio of particle radius (a) and Debye length ($1/k$). Debye length is also known as the thickness of the electrical double layer of the particle, which value depends on ionic strength of the medium and temperature of the sample. Debye length ($1/k$) can be calculated as follows,

$$1/k = \sqrt{\frac{\mathcal{E}_o \mathcal{E} k_b T}{2000 e I N_A}}$$

where, \mathcal{E}_o is the permittivity constant of free space ($= 8.854 \times 10^{-12} \text{ Fm}^{-1}$); \mathcal{E} is the dielectric constant; k_b is the Boltzmann constant ($= 1.38 \times 10^{-23} \text{ JK}^{-1}$); T is the temperature; e is the charge of an electron ($= 1.6022 \times 10^{-19} \text{ C}$); I is the ionic strength; and N_A is the Avogadro's number ($= 6.022 \times 10^{23}$). It is to be noted that the value of Henry function becomes maximum ($= 1.5$) in water (polar medium), whereas it becomes minimum ($= 1$) in non-polar medium. These maximum and minimum values are determined by Smoluchowski approximation and Huckel approximation models, respectively.

2.2.2.3. Morphology of nanoparticles

This study used two electron microscopy techniques, namely scanning electron microscopy (SEM) and transmission electron microscopy (TEM) to analyse particle size, shape, surface structure, and porosity.

2.2.2.3.1. Scanning electron microscopy (SEM)

Surface features, such as size, shape, and porosity of PLGA nanoparticles were investigated by using a scanning electron microscope (model no: S-3000N, Hitachi, Tokyo, Japan). Samples were prepared by spreading freeze-dried nanoparticles on aluminium stub in a fine layer with a spatula, tapping excess off and blowing loose particles with compressed air, followed by coating with a mixture of Au/Pd using Quorum SC7620 Sputter Coater before imaging at operating voltage of 5 kV.

A simplified schematic diagram of a scanning electron microscope with its different components is shown in Figure 2.11. Briefly, an electron gun generates an electron beam, which is finely focused onto the sample by condenser lens and objective lens. This causes excitation of electrons presents in the sample, producing different types of electrons, namely backscattered electrons, secondary electrons, and X-rays, which are detected by appropriate detectors. These electrons can convey a variety of information about the sample, such as coarse- and fine-scale topographic features, composition, crystal structure, and local electrical and magnetic fields. SEM can scan the entire surface of the sample. This is due to the presence of scan coils, which can deflect the electron beam, enabling it to scan the sample along X-Y plane. Further, SEM has a motorized sample stage that can be moved in X-Y-Z plane, enabling a complete 360° scan of the sample (Pande and Bhaskarwar, 2016; Goldstein *et al.*, 2017).

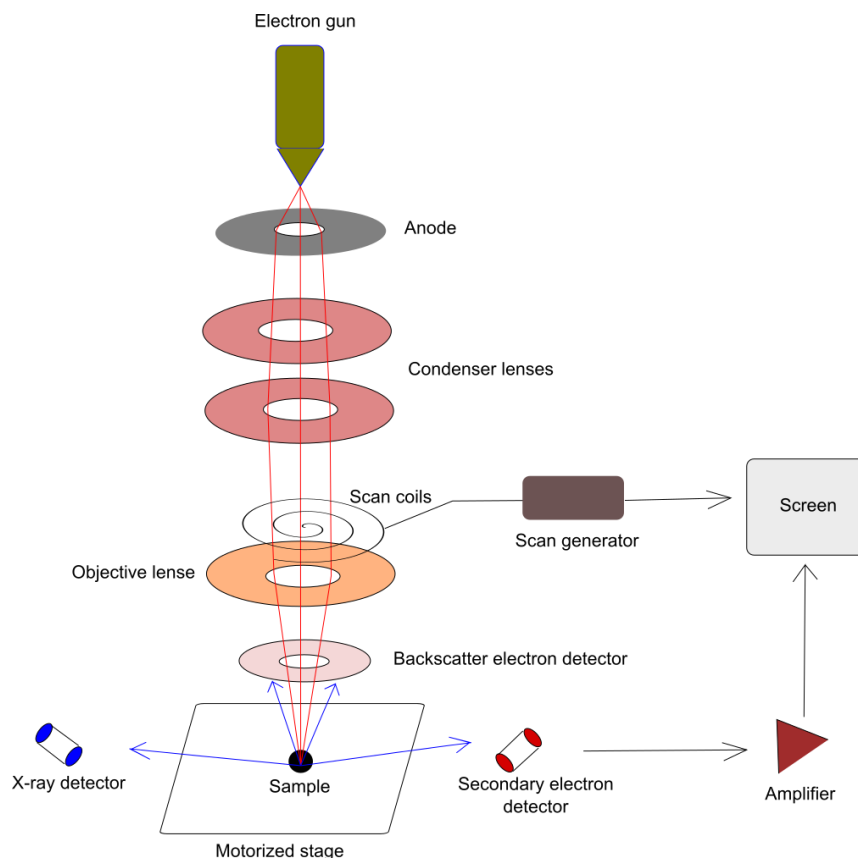


Figure 2.11: Simplified schematic diagram of a scanning electron microscope showing its different components.

2.2.2.3.2. Transmission electron microscopy (TEM)

Particle size and shape were also investigated by a transmission electron microscope (model: H-7000, Hitachi, Tokyo, Japan). Samples were prepared by coating 200 mesh copper grid with re-suspended freeze-dried nanoparticles in deionised water, followed by negative staining with sodium silicotungstate (2% w/v) for 30 seconds and dried in a filter paper at room temperature to remove excess stain prior to imaging at operating voltage of 75 kV.

A simplified schematic diagram of a transmission electron microscope with its different components is shown in Figure 2.12. Briefly, an electron gun generates an electron beam, which is finely focused onto the sample by the condenser lens only, unlike SEM. The electron beam is then transmitted through the sample and passed through the objective lens and other intermediate lens to form a magnified image. The image is recorded either by direct exposure of a photographic emulsion or an image plate inside the vacuum, or by a fluorescent screen coupled to CCD camera (Reimer and Kohl, 2008; Pande and Bhaskarwar, 2016).

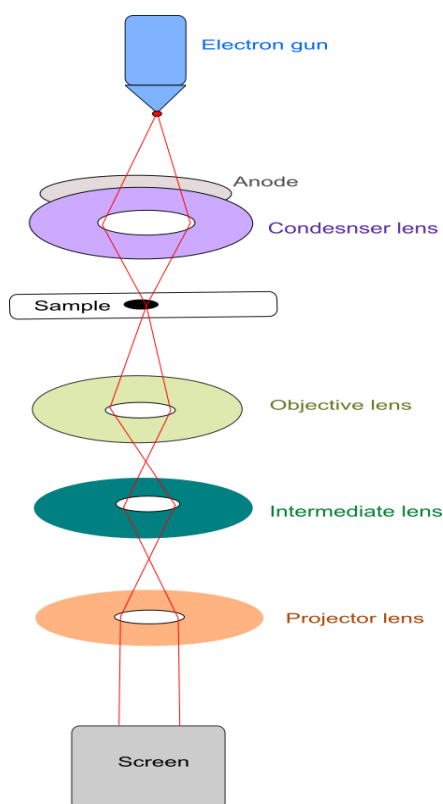


Figure 2.12: Simplified schematic diagram of a transmission electron microscope showing its different components.

2.2.2.4. Investigation of chemical interaction and compatibility

Freeze-dried nanoparticles were evaluated for any chemical incompatibility and thermal instability among drug, PLGA, and other excipients. Two analytical techniques were employed to perform this investigation.

2.2.2.4.1. Fourier-transform infrared spectroscopy (FTIR)

Chemical interactions of individual material and initial confirmation of drug encapsulation within the polymer matrix were analysed by IRAffinity -1S FTIR spectrophotometer (Shimadzu UK Ltd., Buckinghamshire, UK). FTIR spectra of all samples were recorded in both absorbance and transmittance mode in the range of wave number 600-4000 cm^{-1} . Data were manipulated by LabSolutions IR software (Shimadzu UK Ltd., Buckinghamshire, UK). Approximately, 5 mg of freeze-dried nanoparticles, and individual excipient were used directly for analysis, requiring no prior sample preparation.

A schematic diagram of a Fourier-transform infrared spectrophotometer is shown in Figure 2.13. Briefly, the infrared light beam strikes the beam splitter, which is designed to transmit and reflect some of the light incident upon it. The reflected light and transmitted light travel towards the moving mirror and fixed mirror, respectively, where both lights get reflected and travel back to the beamsplitter. Consequently, at the beamsplitter, both reflected light beams combine to a single beam, which interacts with the sample and strikes the detector. Data are interpreted by a mathematical technique called Fourier-transform and expressed into a spectrum (Smith, 2011).

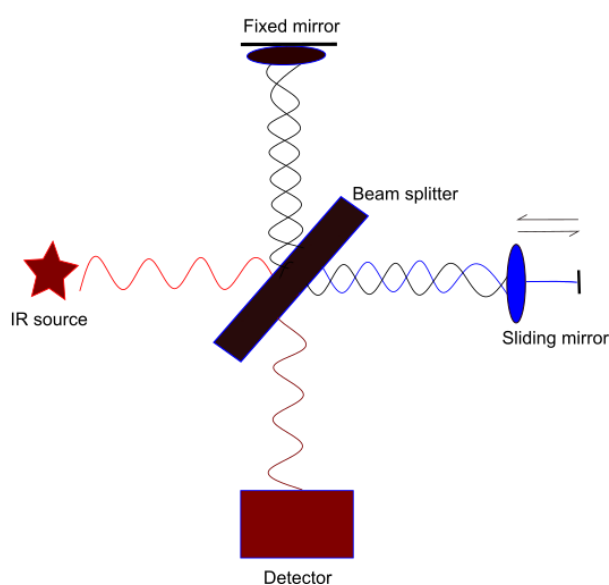


Figure 2.13: Simplified schematic diagram of a Fourier transform infrared (FTIR) spectrophotometer showing its different components.

2.2.2.4.2. Differential scanning calorimetry (DSC)

Thermal analysis of PLGA nanoparticles was performed by differential scanning calorimetry (DSC) using a Q Series™ DSC instrument (Q1000, TA Instruments, Delaware, USA). Prior to running samples, the system was conditioned at 75°C for 120 minutes without a refrigerated cooling system (RCS) with empty cell chamber and then calibrated with pure indium (melting point 156.54°C) with RCS on. Samples were prepared by placing 5 to 10 mg (weighed by MT5 balance, Mettler-Toledo, Leicester, UK) of freeze-dried nanoparticles or individual material in hermetic aluminium pan, followed by running a single heating cycle from 0 to 400°C at a heating rate of 10°C/min in a nitrogen atmosphere (flow rate of 50 mL/min). DSC thermograms were analysed by Thermal Universal Analysis 2000 software (TA Instruments, Delaware, USA).

DSC analyses the thermal properties of materials (such as, polymers). A simple schematic diagram of a conventional DSC instrument is illustrated in Figure 2.14. Briefly, sample and reference are heated and maintained a constant temperature; however, heat requirement would be different for sample and reference due to their varied heat capacities. As a result, DSC plots a thermogram as shown in Figure 2.15, representing heat flux (dH/dt or dQ/dt) on the y-axis and temperature (or time) on the x-axis. The baseline jumps or the peaks (endothermic or exothermic) in the graph denote the transition temperatures of a material, such as glass transition temperature, crystalline temperature, and melting temperature (Elkordy, 2013; Yang, 2018).

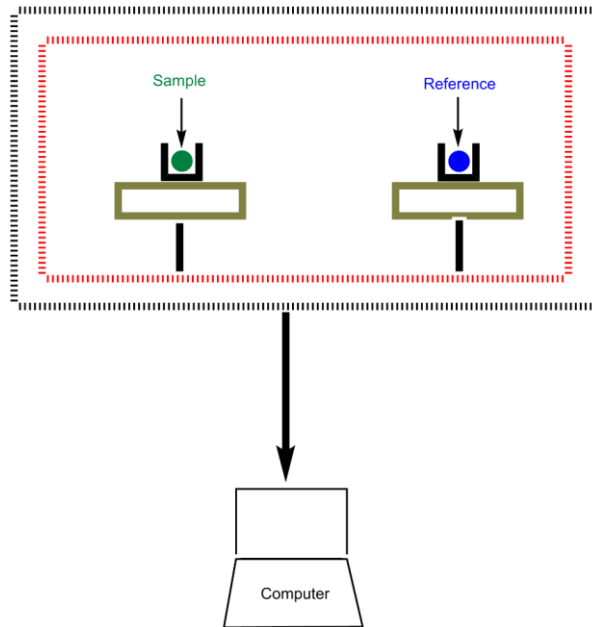


Figure 2.14: Simplified schematic diagram of a conventional differential scanning calorimeter showing its different components.

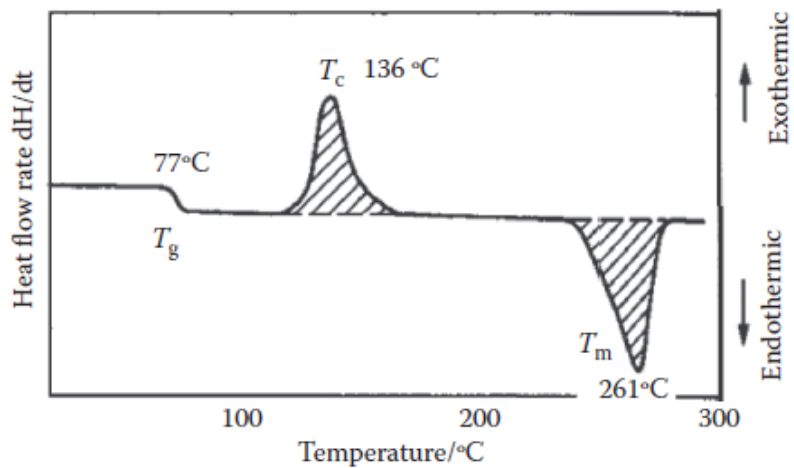


Figure 2.15: A typical DSC thermogram of a polymer (polyethylene terephthalate). T_g , glass transition temperature; T_c , crystallization temperature; and T_m , melting temperature. Shaded area means heat is adsorbed or expelled. Adapted from Yang (2018).

2.2.2.5. Analysis of pimozone in PLGA nanoparticles

2.2.2.5.1. Ultra-High-Performance Liquid Chromatography

All reagents and solvents used in this method were HPLC grade (Table 2.4).

2.2.2.5.1.1. Instrumentation and conditions

This chromatographic technique used an Agilent 1290 Infinity LC system (Agilent, California, USA) for the analysis, with an ACE Excel 2 super C18 column (100 mm × 2.1 mm × 2 μm) as a stationary phase. Aqueous mobile phase was consisted of ammonium formate (0.02 M), formic acid (2 mL/L), and ultra-pure water. pH of the aqueous mobile phase was recorded as of 3.5. Organic mobile phase was consisted of ammonium formate and formic acid (same concentration used in aqueous phase), and methanol. 2 μL sample was drawn from each HPLC vial by the autosampler. Each sample was run for 15 minutes at a flow rate of 0.2 mL/min with a gradient elution of mobile phases (Table 2.6). Column temperature and UV detection wavelength were set to 40°C and 280 nm, respectively.

Table 2.6: Gradient profile of the mobile phases.

Time (minutes)	Aqueous phase (%)	Organic phase (%)
0	85	15
1.7	85	15
8.7	15	85
10.7	15	85
11.2	85	15
15	85	15

2.2.2.5.1.2. Preparation of standard solutions

Pimozone standard stock solution was prepared by dissolving 50 mg of pimozone in 50 mL of methanol in a volumetric flask, achieving a stock concentration of 1000 μg/mL. Subsequently, a range of standard solutions (1, 2, 5, 10, 20, 30, 40, 50, 75, 100 μg/mL) was prepared from the stock solution. Each standard was run in triplicates (n=3). A standard curve of concentrations (along x-axis) vs mean peak area (along y-axis) was drawn (Figure 2.16).

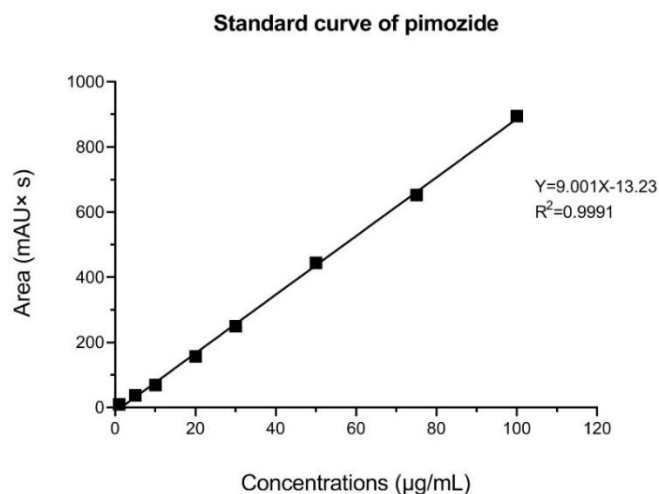


Figure 2.16: Standard curve of pimozide obtained by ultra-high performance liquid chromatography analysis.

Data are mean \pm SD ($n=3$). Error bars are not visible as they are very small numbers.

2.2.2.5.1.3. Method development

Before optimising the current UHPLC method, several preliminary trials were conducted with two different methods, three different columns, and with different solvents of analyte (results not shown). From preliminary findings current method was selected. The method was optimised based on three parameters, such as solvent of analyte, pimozide extraction process, and use of syringe filtration.

2.2.2.5.1.3.1. Optimisation of analyte solvent

Pimozide dissolves in methanol and dichloromethane. Therefore, both solvents were tried as solvent of analyte. Standard solution of pimozide in both solvents were compared in terms of their corresponding signal.

2.2.2.5.1.3.2. Optimisation of pimozide extraction

Effective extraction process helps determine the analyte successfully. Pimozide was extracted out of PLGA nanoparticles by applying five solvent(s) treatment, namely methanol (100%), dichloromethane (DCM) 100%, acetonitrile (100%), DCM: methanol (1:5), and acetonitrile: methanol (1:5). The outcome was evaluated based on the peak height (corresponds to pimozide recovery), and retention time.

2.2.2.5.1.3.3. Recovery of pimozide after membrane filtration

Nanoparticles were subject to syringe filtration prior to auto sampling in the instrument. To see whether pimozide retains in the syringe filter (PTFE 25 mm, 0.2 μ m), the effect of filtration was investigated in pimozide standard solutions in terms of peak area, retention time, and theoretical plate number.

2.2.2.5.1.4. Method validation

Validation is the process demonstration of the suitability of an analytical method for an intended purpose. It is mandatory for any new analytical method. International Council for Harmonisation of Technical Requirements for Pharmaceuticals for Human Use (ICH) has published guidelines for method validation procedure. These guidelines basically define and describe the validation parameters with their accepting value range (Table 2.7).

Table 2.7: Analytical method validation parameters and their applicability.

Validation parameters	Tests for identification	Analysis for impurities		Assays
		Quantitative tests	Limit tests	
Specificity	+	+	+	+
Linearity	-	+	-	+
Accuracy	-	+	-	+
Precision	-	+	-	+
Limit of detection	-	+/-	+	-
Limit of quantitation	-	+/-	-	-
Range	-	+	-	+

Adapted from Pedersen–Bjergaard, Gammelgaard and Halvorsen (2019).

2.2.2.5.1.4.1. Specificity

Specificity is the ability of a method to distinguish the analyte from the other components of a sample. Arguably, specificity is used interchangeably with selectivity. In UHPLC method, specificity is confirmed by complete separation of the analyte's peak from the other peaks of sample (such as, impurities, degradation products, and or matrix).

Specificity was investigated by separately injecting empty nanoparticles (drug-free nanoparticles) and drug (pimozide)-loaded nanoparticles. Also, the effect of empty solvent of analyte (methanol) and phosphate-buffered saline was investigated.

2.2.2.5.1.4.2. Linearity

Linearity is the ability of a method to demonstrate a direct proportional relation between signals and analyte concentrations at a given range.

Briefly, pimozide standard stock solution was diluted with methanol in eight serial concentrations (1, 5, 10, 20, 30, 50, 75, and 100 µg/mL) followed by filtration with 0.2µ PTFE membrane syringe filter.

Linearity was studied by establishing the calibration plot of response vs. concentrations followed by a linear regression analysis, employing least square linear regression method to obtain the slope, intercept, and correlation coefficient.

2.2.2.5.1.4.3. Accuracy

Accuracy is the closeness of agreement between reference value and obtained result value. Accuracy was investigated by determining the recovery (%) of a spiked concentration of analyte into the matrix of the sample.

Briefly, three known pimozide concentrations, such as 10, 20, and 50 µg/mL were spiked in the blank nanoparticles. Each concentration was spiked in triplicates. The accuracy was assessed by comparing the recovered concentration with added concentration.

2.2.2.5.1.4.4. Precision

Precision is the ability of a method to generate reproducible results; it is considered at three levels, such as repeatability, intermediate precision, and reproducibility.

This study evaluated intermediate precision by using different analysts and different laboratory variations, such as different times of injection, and different equipment. Briefly, six standard concentrations of pimozide (10, 20, 30, 50, 75, and 100 µg/mL) were prepared by two analysts, namely A (author) and B (a fellow researcher), and injected in a HPLC instrument, namely 'X'. The responses (retention time and peak area) were analysed and compared. Same samples (prepared by analyst A) were injected in a different HPLC instrument (namely, 'Y') of same make and model. The responses of both instruments were compared. Finally, same samples (prepared by analyst A) were injected after 2 days (at day 3) in instrument 'X' to compare the responses with day 1. Each sample was injected in triplicates in all cases.

2.2.2.5.1.4.5. Limit of detection

Limit of detection (LOD) is the smallest amount of analyte that can be detected, not necessarily quantified, by a given method. Briefly, limit of detection was calculated by the following equation,

$$LOD = 3.3 \times \frac{\sigma}{S}$$

Where, σ is the standard deviation of the response, and S is the slope of the calibration curve.

2.2.2.5.1.4.6. Limit of quantitation

Limit of quantitation (LOQ) is the smallest amount of analyte that can be quantified with accuracy and precision. Generally, LOQ is determined in assays for low levels of impurities and/or degraded products. LOQ is calculated as follow,

$$LOQ = 10 \times \frac{\sigma}{S}$$

Where, σ is the standard deviation of the response, and S is the slope of the calibration curve.

2.2.2.5.1.4.7. Robustness

Robustness is the capacity of a method to remain unaffected by small changes that are made deliberately to the method parameters.

Briefly, robustness was investigated by analysing pimozone standard solutions under different experimental conditions, such as column temperature ($\pm 10^\circ\text{C}$), and flow rate (± 0.1 mL/min). The assessment was performed by calculating the %RSD of the peak area after three consecutive injections of the standard solutions.

2.2.2.5.2. UV-Visible spectroscopy

Pimozone in PLGA nanoparticles was also determined by UV-Visible spectrophotometry using a single beam scanning UV-Vis spectrophotometer (Model: M501, Spectronic CamSpec Ltd., Leeds, UK) at wavelength of 280 nm. Pimozone standard stock solution was prepared by dissolving 50 mg of pimozone in 50 mL of methanol in a volumetric flask, achieving a concentration of 1000 $\mu\text{g/mL}$. Subsequently, a range of standard solutions (1, 2, 5, 10, 20, 30, 40, 50, 75, 100 $\mu\text{g/mL}$) was prepared from the stock solution. A standard curve of concentration (along x-axis) vs corresponding absorbance reading (along y-axis) is drawn (Figure 2.17).

Samples were prepared by a solid-liquid extraction method, as optimised in section 2.2.2.5.1.3.2. Briefly, 10 mg of freeze-dried nanoparticles were treated with 2 mL of acetonitrile, followed by addition of 10 mL methanol. The mixture was sonicated for 10 minutes using Camlab Transonic ultra-sonics (Model: T460, S.H. Scientific, Northumberland, UK), followed by filtration through 0.2 μm PTFE (polytetrafluoroethylene) membrane syringe filter prior to recording absorbance under the spectrophotometer.

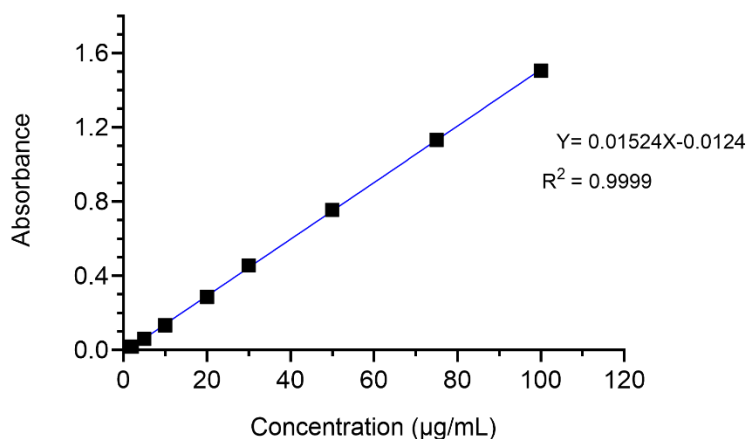


Figure 2.17: Standard curve of pimozide obtained by UV-visible spectroscopy at 280 nm. Data are mean \pm SD ($n=3$). Error bars are not visible as they are very small numbers.

UV-Visible spectroscopy deals with wavelengths of visible light range (380-700 nm) and is based on the Beer-Lambert Law, which states that the light absorbance of a substance in a solution is directly proportional to the concentration of the substance at a constant path length and wavelength of an incident light. The mathematical equation of Beer-Lambert Law can be expressed as follows,

$$A = \log_{10} \frac{I_o}{I} = \epsilon bc$$

where A is the absorbance, I_o is the intensity of incident light, I is the intensity of the transmitted light, ϵ ($=0.03728 \text{ Lmol}^{-1}\text{cm}^{-1}$) is the molar absorptivity coefficient (Lohita *et al.*, 2014), b is the light path length, and c is the concentration of the solution. A schematic diagram of a typical UV-Visible spectrophotometer is illustrated in Figure 2.18. Briefly, an UV light beam is passed through the sample solution. The sample molecule has some functional groups in it, which can absorb maximum light at specific wavelengths. In other words, the electrons in the molecules absorb light and go from ground state to excited state. Subsequently, unabsorbed light (transmitted light) is then detected by a photoelectric detector. The unknown concentration of a sample can be extrapolated from the standard curve of the sample (Gorog, 1995).

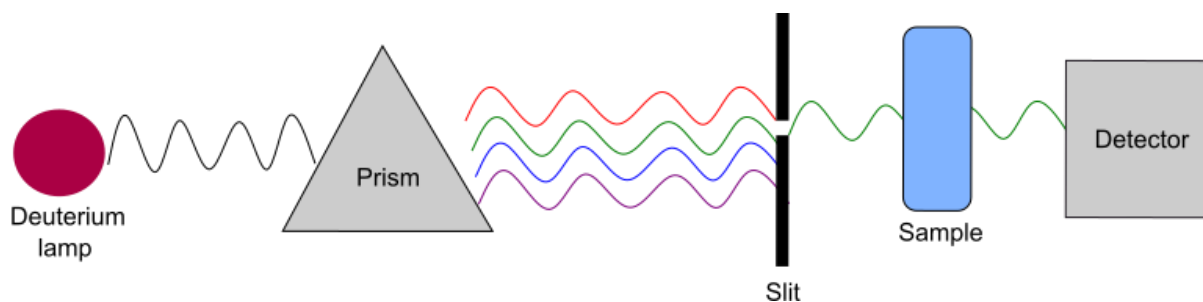


Figure 2.18: Schematic diagram of an UV-visible spectrophotometer showing its different components.

2.2.2.6. Determination of encapsulation efficiency (EE)

Encapsulation efficiency (EE), expressed as percent (%) EE, is the ratio of actual drug found in PLGA nanoparticles and initial drug loaded (also known as theoretical drug loading) during the preparation of formulation. Briefly, actual drug concentration in nanoparticles was determined by extraction of pimozone as described in Section 2.2.2.5.1.3.2, followed by analysis of pimozone using UV-Visible spectroscopy and ultra-high performance liquid chromatography (UHPLC) methods, where unknown pimozone concentration was extrapolated using respective standard curve equations. Each sample was analysed in triplicates. Average pimozone concentration was used in determining EE. Finally, EE was calculated by using the following formula:

$$EE (\%) = \frac{\text{Actual drug extracted from nanoparticles (mg)}}{\text{Initial drug load (mg)}} \times 100$$

Another form of encapsulation known as drug loading capacity (LC) can easily be calculated from the recovered pimozone from the nanoparticles. LC is defined as the amount of drug loaded per unit weight of nanoparticles.

2.2.2.7. In-vitro drug release study

A modified method of Haggag *et al.* (2016) was employed to carry out *in vitro* drug release study. Briefly, as illustrated in Figure 2.19, freeze-dried PLGA nanoparticles (5 mg) were dispersed in 10 mL of phosphate buffered saline solution (PBS) at pH 7.4. The samples were incubated at 37°C with agitation by a reciprocal shaking water bath at 100 RPM. 2 mL of the sample was withdrawn at predetermined time intervals of 1, 4, 24, 72, 96, 120, and

144 hours followed by replenishing equal volume of fresh PBS at each time. Each sample was then centrifugation at 10,000 RPM for 10 minutes using Mikro 200R Centrifuge (Hettich, Tuttlingen, Germany). Supernatant of centrifuged sample was analysed for pimoziide concentration, by using ultra-high-performance liquid chromatography (UHPLC) method.

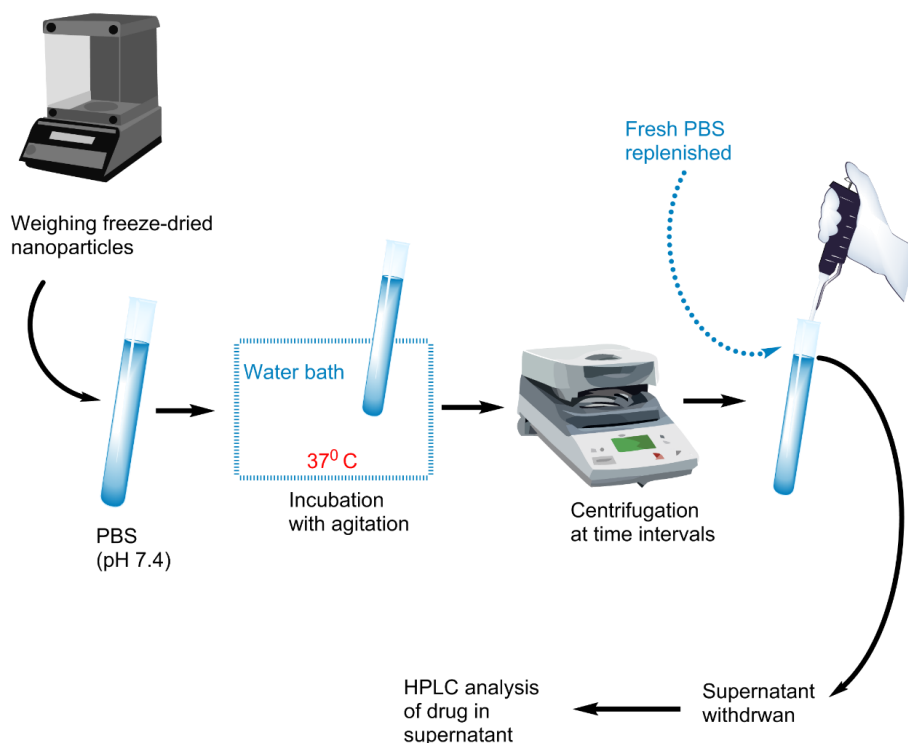


Figure 2.19: Workflow of in-vitro drug release study of PLGA nanoparticles.

2.2.2.8. Determination of transferrin

This study employed an indirect method to analyse transferrin (TF) in the PLGA nanoparticles by bicinchoninic acid (BCA) assay using micro-BCA™ protein assay kit (Thermo Scientific, UK). Briefly, BCA assay method measured the amount of free TF that was not adsorbed to nanoparticles after incubation. Then concentration of total initial incubated TF was deducted from the concentration of free TF to find out adsorbed TF.

$$\text{Adsorbed TF} \left(\mu \frac{g}{mL} \right) = (\text{initial TF concentration} - \text{free TF concentration})$$

Microplate procedure was followed in this experiment. First, a set of standard protein concentrations (0.5, 1, 2.5, 5, 10, 20, 40, and 200 $\mu\text{g/mL}$) was prepared from supplied 2 mg/mL bovine serum albumin (BSA) stock standard. Distilled water was used as diluent. The overall workflow of BCA protein assay is demonstrated in Figure 2.20. BCA working reagent stock was prepared, according to the manufacturer's guidelines, by mixing 25 parts of reagent A (alkaline tartrate-carbonate buffer), 24 parts of reagent B (BCA solution), and 1 part of reagent C (copper sulfate solution). 150 μL of each standard solution, distilled water (as a blank), and sample solution were pipetted into a 96-well plate in triplicates. Subsequently, 150 μL of BCA working reagent was pipetted in each well. The plate was covered with sealing tape to avoid evaporation and mixed thoroughly on a shaker for 30 seconds, followed by incubating it for 2 hours at 37° C. The plate was cooled at room temperature prior to reading absorbance at 562 nm on a plate reader (spectrophotometer). From the reading a standard curve of BSA was drawn (Figure 2.21).

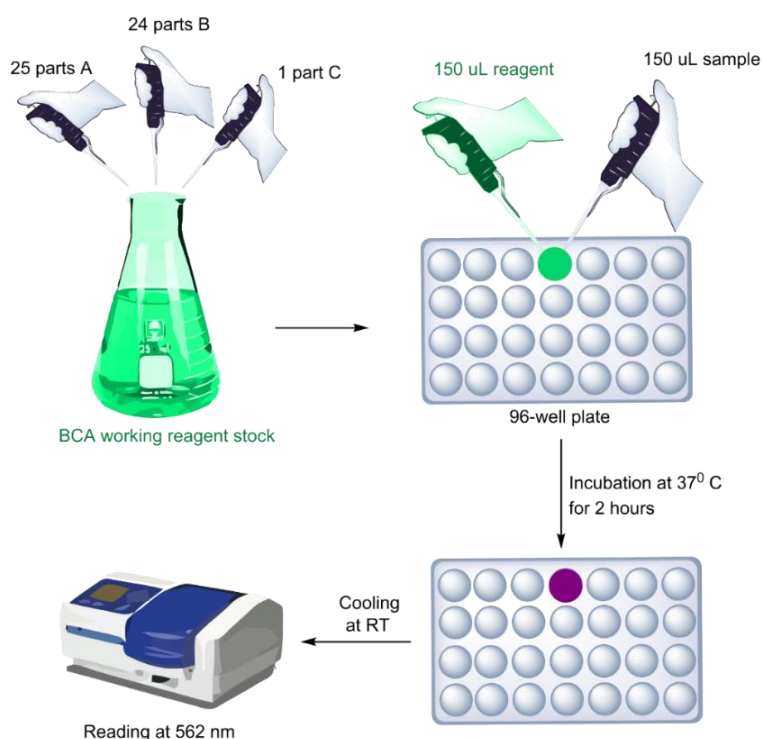


Figure 2.20: Workflow of BCA assay for transferrin analysis in the PLGA nanoparticles. A (alkaline tartrate and carbonate buffer); B (BCA solution); and C (copper sulfate solution).

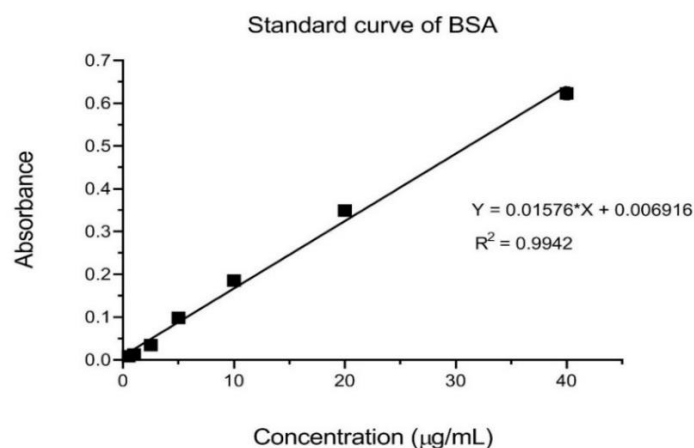


Figure 2.21: Standard curve of bovine serum albumin (BSA)

Bicinchoninic acid (BCA) protein assay, a modified biuret test, is a colorimetric assay to estimate protein in a sample. Briefly, at alkaline medium (pH ~11), BCA stock solutions contains BCA, sodium carbonate, sodium bicarbonate, sodium tartrate, and copper (II) sulfate pentahydrate. Once introduced to protein sample, cupric ion (Cu^{2+}) from copper (II) sulfate is reduced to cuprous ion (Cu^+) by peptide bonds and amino acids cysteine, cystine, tyrosine, and tryptophan present in the protein. Subsequently, two molecules of BCA form a chelate with each Cu^+ ion, changing colour from green to purple (Figure 2.22). The amount chelates that is formed is directly proportional to amount of protein present in a sample. In other words, increased amount of protein will change the colour faster and darker (Bainor *et al.*, 2011; Cortés-Ríos *et al.*, 2020).

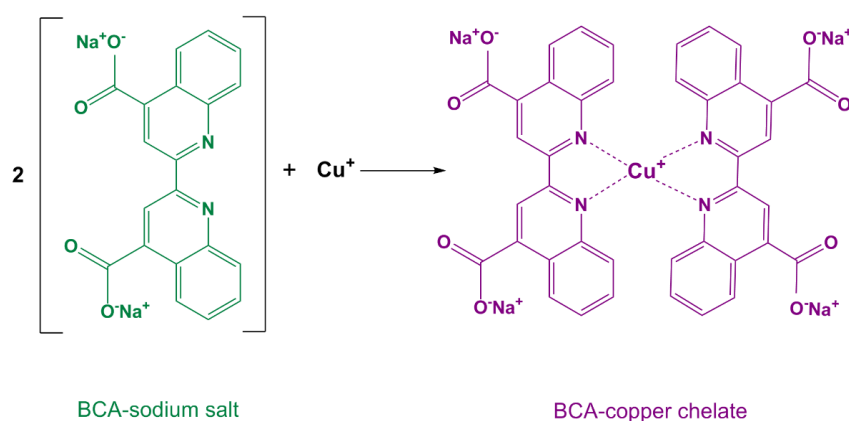


Figure 2.22: Reaction between cuprous ion (Cu^+) and bicinchoninic acid (BCA).

Here, only the final fraction of reactions is shown, where BCA forms chelate with cuprous ion (Cu^+), changing the colour from green to purple. This Cu^+ is formed due to the reduction of copper sulfate and oxidation of protein, once alkaline BCA solution is treated with protein sample.

2.2.2.9. Storage stability study

PLGA nanoparticles in the form of suspension were stored at ambient temperature and 4°C. Samples were drawn at week 0, 1, 2, 8, and 16 to determine particle size, polydispersity index (PDI) and zeta potential by dynamic light scattering (DLS) and laser Doppler velocimetry (LDV) methods.

2.2.3. Detection microbial contamination in nanoparticles

Detection of microbial contamination (bacteria and yeast) in nanoparticles was performed by simple Agar Plate test.

Tryptic Soy Agar (TSA) was obtained from Sigma-Aldrich, UK. Malt extract was obtained from Neogen, UK. *Staphylococcus epidermidis* was used as a standard bacterial cell culture. *Saccharomyces cerevisiae* was used as a standard yeast cell culture. All reagents and devices used were sterile. Detection of bacterial and yeast contamination in nanoparticles was performed by slight modification of the Agar Plate test (Potter *et al.*, 2015). Briefly, nanoparticles were spread on the surface of agar and malt agar media, incubated, and the growth of the colonies was monitored. The assays required 200 µL of the test nanoparticles suspension in distilled water (PLGA concentration 10 mg/mL). All experiments were performed under sterile condition. Results were reported according to the following formula:

$$\text{Colonies} \times \text{Dilution factor} \times \text{Sampling factor} = \text{Colony forming unit} \frac{\text{CFU}}{\text{mL}}$$

2.2.3.1. Detection of bacteria

TSA plates were removed from the refrigerator and allowed to equilibrate to room temperature. All sample plates were prepared in duplicates. Sterile PBS was used as a negative control. *Staphylococcus epidermidis* was used as a positive control. A range of concentrations (10^{-1} to 10^{-7}) of positive control was used. Under sterile condition, 200 µL of samples were spread on the agar surface and evenly distributed by sterile disposable spreader (L-shaped cell spreader, Fisher Scientific, UK). Prior to turning the plates upside down to prevent condensation, samples were allowed enough time to be absorbed on agar medium. All plates were incubated for 48 hours at a nominal temperature of 37°C. After 48 hours, the appearance of colonies was examined, and the numbers were counted.

2.2.3.2. Detection of yeast

Malt agar plates were removed from the refrigerator and allowed to equilibrate to room temperature. All sample plates were prepared in duplicates. Sterile PBS was used as a negative control. *Saccharomyces cerevisiae* (known as baker's yeast) was used as a positive control. A range of concentrations (10^{-1} to 10^{-7}) of positive control was used. Under sterile condition, 200 μ L of samples were spread on the malt agar surface and evenly distributed by sterile disposable spreader (L-shaped cell spreader, Fisher Scientific, UK). Prior to turning the plates upside down to prevent condensation, samples were allowed enough time to be absorbed on malt agar medium. All plates were incubated for 48 hours at a nominal temperature of 25°C. After 48 hours, the appearance of colonies was examined, and the numbers were counted.

2.2.4. Biological evaluation of targeted nanoparticles in glioblastoma cell lines

The effect of optimised nanoparticles was evaluated on glioblastoma cell lines. Following sections are the description of the materials and methods used in this study.

2.2.4.1. Cell lines and culture

Primary glioblastoma cell lines E2, G7, R24 and GLG were generously provided by Dr. Shafiq Ahmed (University of Sunderland). Cell culture experiments were performed using under class II laminar flow biological safety cabinet, using sterile plastic wares and solutions.

2.2.4.1.1. Preparation of stem cell media

Advanced Dulbecco's modified Eagle medium (advanced DMEM; Gibco®, Thermo Fisher Scientific, USA) was used as a basic medium. To prepare stem cell media, required concentrations of supplements (Table 2.8) were added to the basic medium.

Table 2.8: Supplements added to prepare stem cell media

Name of the supplements	% v/v added to the basic medium
Heparin	0.1
L-Glutamine	1.0
Penicillin	0.5
N-2 supplement	0.33
B-27 supplement	0.66

2.2.4.1.2. Preparation of complete media

Complete media was prepared only before use, by adding 0.02% (v/v) EGF (Invitrogen™, Thermo Fisher Scientific, USA) and 0.01% (v/v) FGF (Invitrogen™) to the stem cell media.

2.2.4.1.3. Preparation of extracellular matrix-coated flask

Stem cells were cultured as 2D monolayer in Matrigel™ coated flask. Briefly, 2 mL of Matrigel™ (2% v/v in stem cell media, after defrosting on ice) was spread evenly on the base of T75 flask and incubated for 45 minutes at 37°C with 5% CO₂, followed by removal of media. Flasks were stored at 4°C until required.

2.2.4.1.4. Thawing cells

Stocked cells (frozen at -80°C in cryogenic vial) were defrosted at 37°C for 2 minutes followed by transferring cells to a Matrigel-coated T75 flask containing 13.5 mL of complete media. Flask was then incubated at 37°C with 5% CO₂. After 24 hours, the media was replenished to remove residual DMSO.

2.2.4.1.5. Routine 2D cell culture

Cells were checked under microscope for confluence and split (passaged) every 4/5 days. This was carried out by aspirating media, followed by washing cells with 5 mL of PBS and detaching cells from the Matrigel™ base with 1.5 mL of Accutase® (Corning™, Thermo Scientific, UK) for 5 minutes at 37°C. Cell suspension was centrifuged for 5 minutes at 100g RCF after adding 5 mL of basic media. Cell pellets were re-suspended in complete media. A cell count was performed using a haemocytometer, prior to plating out in a new Matrigel-coated flask.

2.2.4.2. *Determination of targeted receptor protein expression*

Western blot was used to analyse targeted receptor proteins (transferrin receptors) on glioblastoma cells.

2.2.4.2.1. Sample preparation

Cells were centrifuged for 3 minutes at 4°C and 2000 RPM, followed by re-suspending pellets in 1 mL of basic media. Cell suspension was transferred to an Eppendorf and centrifuged again with same conditions. Further, pellets were washed with PBS and centrifuged for 2 minutes at 4°C and 2000 RPM, prior to storing pellets at -80°C.

2.2.4.2.2. Cell lysis

Protease phosphatase cocktail inhibitor (PPCI) was used to prevent protease and phosphatase from protein denaturation and dephosphorylation, respectively. Inhibitor mixer (PPCI and SDS lysis buffer, Appendix 8) was added to pellets in 1:50 v/w ratio, followed by vortexing for 5 seconds, sonicating for 20 seconds in 5 cycles (Soniprep 150, MSE Ltd., UK), and heating for 5 minutes at 95°C. Cell lysates were further vortexed for 2 minutes, followed by diluting 5 times with distilled water (total volume 10 µL).

2.2.4.2.3. Protein estimation

2 mg/mL bovine serum albumin (BSA) was used as protein standard stock solution. Standard concentrations (0.2, 0.4, 0.8, 1, 1.5 mg/mL) were prepared with distilled water. 10 µL sample (standard and lysate) was loaded in each well of a 96 well plate in triplicates, followed by addition of 190 µL mixed reagents (previously prepared according to the manufacturer protocol) of BCA Protein Assay Kit (Fisher Scientific, UK). After 30 minutes incubation, the absorbance was read at 594 nm by Multiskan Ex microplate spectrophotometer (Thermo Scientific, USA). Total protein concentration present in the lysate was calculated from the calibration curve of the BSA standards.

2.2.4.2.4. Running SDS-PAGE

According to the protein estimation, required volume of cell lysate (containing 50 µg of protein) was transferred to a 500 µL Eppendorf, followed by addition of 5 µL of loading buffer (Appendix 8) to break the di-sulphide bonds in the proteins. Samples were heated for 5 minutes at 95°C. Each sample (<15 µL) and 4 µL protein marker (PageRuler™ Prestained protein ladder, Thermo Scientific, UK) were loaded into a Mini-PROTEAN® TGX Stain-Free™ precast gel (Bio-Rad Laboratories Inc., USA) after it was immersed in TGS (1X) buffer (Appendix 8) in the electrophoresis tank (Bio-Rad Laboratories Inc., USA). Glyceraldehyde-3-phosphate dehydrogenase (GAPDH, molecular weight of 35 kDa, dilution of 1:1000) was used as loading control. The gel was run for 60 minutes (or until the marker reached at the bottom of the cassette) at 130V.

2.2.4.2.5. Transferring gel (protein)

The gel was then transferred into a nitrocellulose membrane by using a Trans-Blot® Turbo™ Transfer System (Bio-Rad Laboratories Inc., USA) after 15 minutes at 25V. The membrane was interacted with 5% w/v milk-TBST, used as a blocking agent (Appendix 8), and left on shaker for 60 minutes. After washing three times with TBST, the membrane was transferred to 3 mL blocking agent. Required volumes (based on antibody dilution) of primary antibodies (Table 2.9) were added to the blocking agent with the membrane, followed by leaving on a shaker overnight at 4°C. The membrane was washed three times with TBST, followed by

transferring the membrane to 3 mL blocking agent again and adding secondary antibodies (Table 2.10) to it. After leaving the membrane with blocking agent on a rotary shaker for 2 hours at room temperature, it was then washed with TBST, followed by shaking for 10 minutes (washing and shaking were repeated two more times).

2.2.4.2.6. Membrane imaging (detection of protein band)

For membrane imaging (protein visualisation), an enhanced chemiluminescent (ECL) reagent (Bio-Rad Laboratories Inc., USA) was added to the membrane. Images were captured (within exposure time of 1-100 seconds) with ChemiDoc™ system (Bio-Rad Laboratories Inc., USA).

Table 2.9: Primary antibodies used in Western blot analysis.

Antibody	Type	Molecular weight (kDa)	Dilution	Product catalogue	Supplier
5-HT ₇ ^a	Rabbit polyclonal	54	1:500	GTX108157	GeneTex, USA
USP1 ^b	Rabbit polyclonal	88	1:500	GTX130252	GeneTex, USA
CD71/ TFR1 ^c	Mouse monoclonal	85-95	1:250	SC-65882-S	Santa Cruz Biotechnology, USA
TFR2 ^d	Rabbit polyclonal	89	1:500	GTX110441	GeneTex, USA
TFR2	Mouse monoclonal	97-105	1:250	SC-32271-S	Santa Cruz Biotechnology, USA

^aSerotonin receptor; ^bUbiquitin-specific protease 1; ^cTransferrin receptor 1; ^dTransferrin receptor 2

Table 2.10: Secondary antibodies used in Western blot analysis

Antibody	Dilution	Product catalogue	Supplier
Anti-rabbit IgG	1:2000	7074S	Cell Signalling Technology, USA
Anti-mouse IgG	1:2000	7076S	Cell signalling Technology, USA

Western blotting is a widely used bioanalytical technique to detect and quantify specific proteins in a sample. This technique employs SDS-PAGE (sodium dodecyl sulfate - polyacrylamide gel electrophoresis) that separates proteins based on their molecular weight, followed by probing them antibodies and subsequently detecting the protein bands by chemiluminescence or colorimetric method.

Figure 2.23 describes the general principle and workflow of Western blot. At first, protein sample is treated with sodium dodecyl sulfate (SDS), a detergent that unfolds the protein into linear chain and coats with negative charge. Proteins are then separated according to their sizes (large protein molecule travels slowly down to the gel, and vice versa) by an electrophoresis method using polyacrylamide gel.

Separated proteins are then transferred onto a hydrophobic blotting membrane (such as, a nitrocellulose membrane). The membrane is treated with blocking agent (such as, skimmed milk) to prevent antibodies from binding any nonspecific target on the membrane. The membrane is treated and incubated with a primary antibody, which will only bind with targeted protein. Following washing unbound primary antibody, the membrane is then treated with secondary antibody, which binds specifically to the primary antibody. The secondary antibody is labelled with an enzyme (such as, horseradish peroxidase or alkaline phosphatase) that catalyses a reaction emitting light or colour to be detected as band for targeted protein.

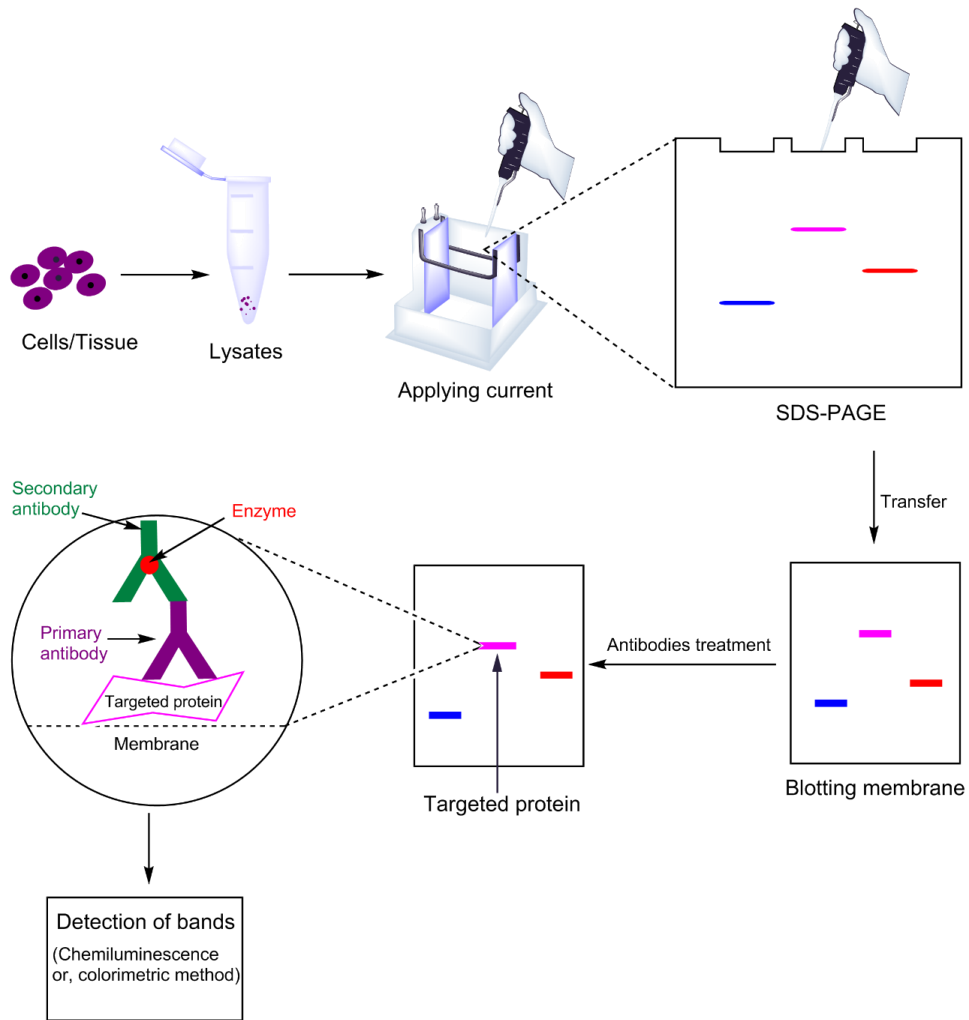


Figure 2.23: General workflow of Western blot.

2.2.4.3. Cell proliferation assay

The cell proliferation assay was performed by IncuCyte ZOOM[®] live-cell analysis system (Essen BioScience, Michigan, USA). Figure 2.24 demonstrates the workflow of cell proliferation assay. Briefly, glioblastoma cells (100 μ L) were seeded in a 96-well plate at a density of 3000 cells/well (10-20% confluent). After incubation for 24 hours at 37^oC, 5% CO₂ (when cells attach to the extracellular matrix), cells were treated with pimoziide, nanoparticles, and controls (all diluted in growth media). Pimoziide encapsulation efficiency data, acquired from ultra-high-performance liquid chromatography analysis, was used to determine the required concentration of nanoparticles carrying equivalent pimoziide. Cell growth was monitored up to 140 hours by IncuCyte[®] system (at 37^oC, 5% CO₂), capturing phase contrast images (4X) in each well every 4 hours, and analysing data with the integrated confluence algorithm.

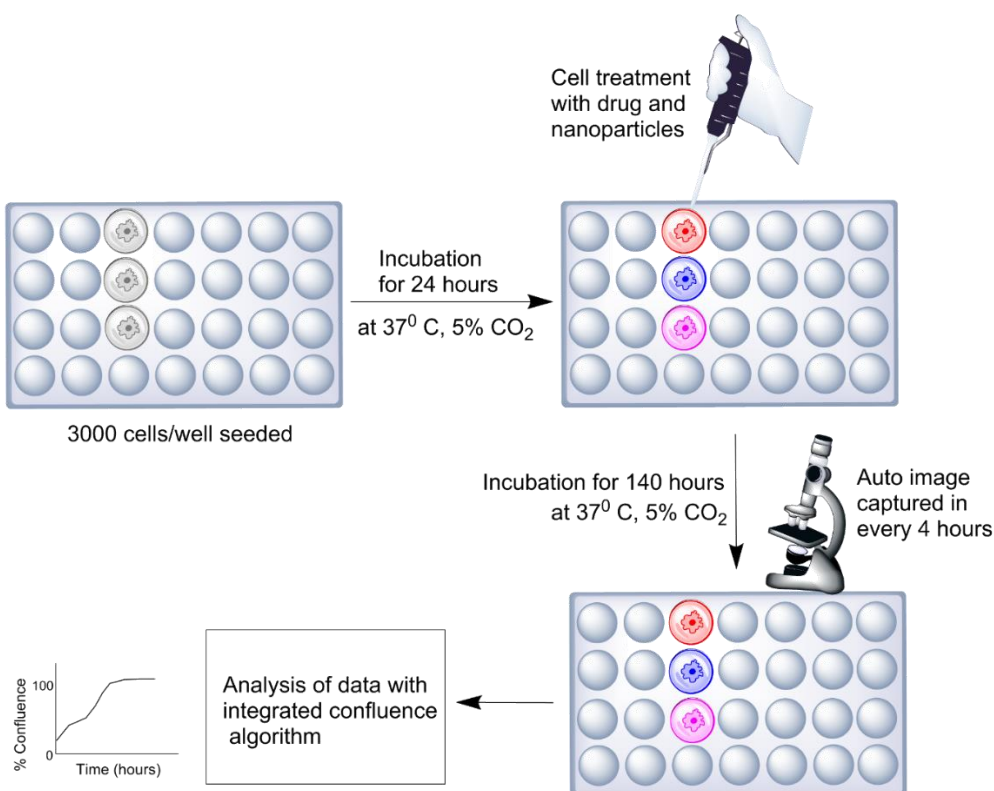


Figure 2.24: Workflow of cell proliferation assay.

2.2.5. Statistical analysis

Results are expressed as mean \pm standard deviation (SD) of at least three measurements unless otherwise stated. Statistical analysis was performed by GraphPad Prism Software version 9.0.2 (161), GraphPad Software Inc., California, USA. Statistical significance of two group data was analysed either by paired *t*-test, Wilcoxon test, or unpaired *t*-test. Three or more than three group data was analysed by one-way ANOVA, followed by Tukey's multiple comparison test. A p-value of <0.05 was considered as statistically significant (* $p=0.033$; ** $p=0.002$; and *** $p<0.001$).

Chapter 3

Development and validation of an ultra-high-performance liquid chromatography method for pimozide analysis in PLGA nanoparticles

Chapter 3. Development and validation of an ultra-high-performance liquid chromatography method for pimozone analysis in PLGA nanoparticles

This chapter describes how an ultra-high-performance liquid chromatography (UHPLC) method was developed and validated according to guidelines of the International Council for Harmonisation of Technical Requirements for Pharmaceuticals for Human Use (ICH) for pimozone analysis in PLGA nanoparticles.

3.1. Introduction

Pharmacopoeias, such as the United States Pharmacopeia (USP), the European Pharmacopeia (Ph. Eur.), and British Pharmacopeia (BP) prescribe several methods to analyse pimozone. For instance, ultraviolet absorption, infrared absorption, thin layer chromatography (TLC), and high-performance liquid chromatography (HPLC) are the most common methods for identification and quantification.

High performance liquid chromatography (HPLC) is widely used as an analytical technique to separate, identify, and quantify the analyte of interest. In drug discovery and development process, HPLC has been used extensively since late 1960s (Pedersen–Bjergaard *et al.*, 2019).

HPLC has been a versatile method to analyse nanoparticles and their loaded individual materials. Active pharmaceutical ingredients, which are loaded in PLGA nanoparticle, can be analysed by HPLC quite efficiently (Ebrahimzadeh *et al.*, 2013; Furman *et al.*, 2017; Bhandari *et al.*, 2019). Further, PLGA itself can be analysed (into their monomers: lactic acid and glycolic acid) by HPLC. This way the monomer ratio can be calculated and hence drug release profile can be understood (Pourasghar *et al.*, 2019).

Studies report several techniques to analyse pimozone in pure or dosage form, such as tablet (Table 3.1). However, some of them are not specific to pimozone. There has been no study for pimozone analysis in complex matrix, such as polymeric nanoparticles (PLGA nanoparticles).

Table 3.1: Analysis of pimozide by different techniques.

Analytical technique	Description	Reference
Spectro fluorometry	Pimozide was determined in oral preparations	(Baeyens, 1977)
Thin layer chromatography	Pimozide was detected and differentiated in the presence of other compounds	(Pluym, 1979)
	A combined use of normal and reverse phase to detect and determination of pimozide	(Ojanperä <i>et al.</i> , 1991)
Spectrophotometry and conductometry	Interaction of pimozide with DDQ as π acceptor to form coloured product	(Kelani <i>et al.</i> , 1997)
	Used conductometric titration and spectrophotometry	(Kurzawa <i>et al.</i> , 2004)
	UV determination of pimozide in bulk and tablet dosage form	(Lohita <i>et al.</i> , 2014; Alamein <i>et al.</i> , 2015)
Potential pulse voltammetry	Use of oxidative peak current	(Özkan <i>et al.</i> , 2002; Punde <i>et al.</i> , 2018)
High performance liquid chromatography	Radio detection	(Michiels <i>et al.</i> , 1982)
	Fluorescence detection	(Kerbusch <i>et al.</i> , 1997)
	Electrochemical detection	(Özkan <i>et al.</i> , 2002)
	Mass spectroscopy detection	(Yan <i>et al.</i> , 2010)
	Ultraviolet detection	(Kabra <i>et al.</i> , 2014)

3.1.1. Basic instrumentation

An HPLC instrument is a set of individual modules. The fundamental modules are mobile phase reservoir, high pressure pump, sample injector, column, and detector (Figure 3.1). Briefly, mobile phase(s) are forced to pass through the column, by high pressure produced by the pump. Sample solution is injected manually, or automatically by autosampler. Sample is detected by the detector, producing an electronic response.

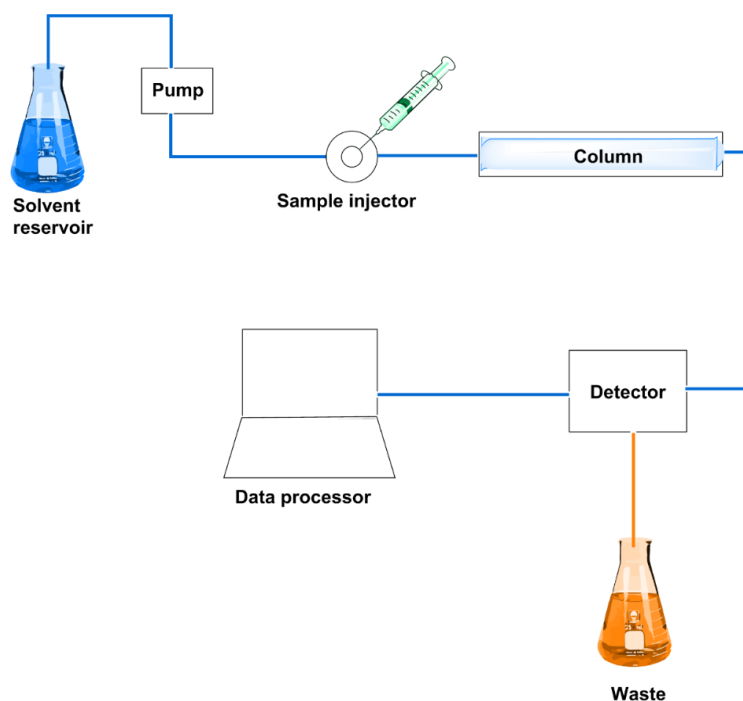


Figure 3.1: Simplified schematic of an HPLC instrument.

Mobile phases are contained in the reservoir, from where they are pumped through polyethylene tubing to the column. Mobile phase solvents should have some criteria, such as they should be of analytical grade indicating solvents are sufficiently pure with low viscosity and low toxicity; and they should not be detected by the detector. Depending on the modes of liquid chromatography (refer section 3.1.3), mobile phase solvent can be aqueous or organic.

A pump in HPLC generates high pressure that forces mobile phase to flow through the column. The small particles in the column produce a back pressure up to 350 or 500 bar, sometimes up to 1500 bar in ultra-high-performance liquid chromatography (Section 3.1.4). The pump maintains the flow accuracy and precision at any flow rate (from 0.1 mL/min to 5 or 10 mL/min)

The column is the foundation of the separation process. An HPLC column is made of stainless-steel tubing, known as grade 316 (chromium-nickel-molybdenum). Column could also be made of glass or plastic that are resistant to usual HPLC pressure and inert to chemical corrosion. The column is packed with small particles, known as stationary phase or column bed, through which mobile phase transports sample component with it. Stationary phase particles could be porous, non-porous, porous layered beads, perfusive, and monolithic. A liquid chromatography column tubing packed with porous particles is shown in Figure 3.2. Porosity of these particles can be further understood in Figure 3.3.

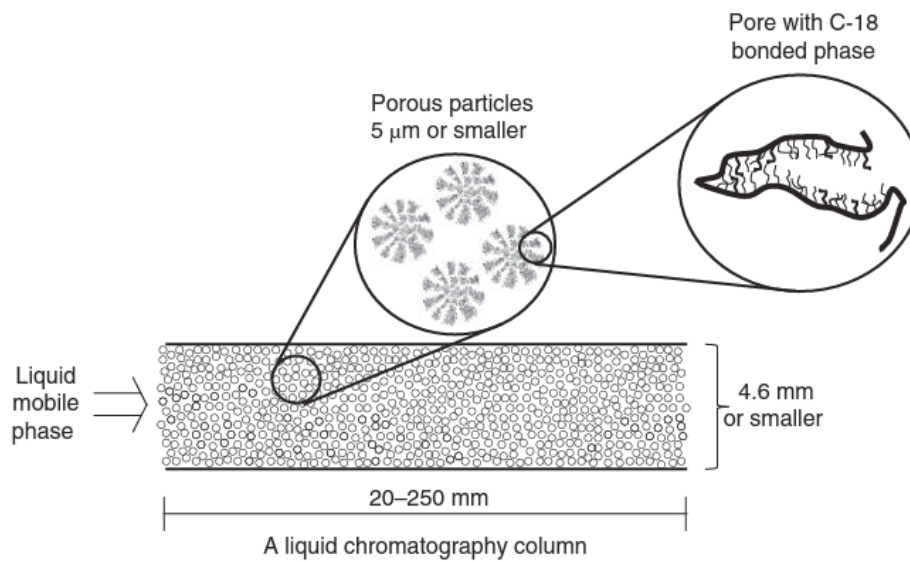


Figure 3.2: Simplified structure of a liquid chromatographic column
Adapted from Vitha (2017).

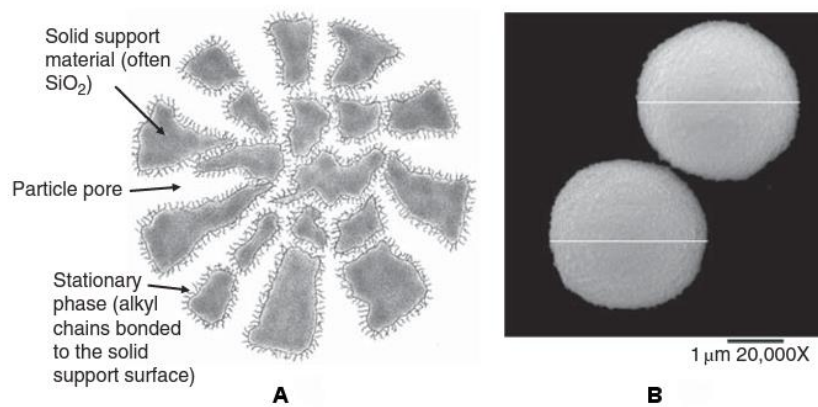


Figure 3.3: Structure of a stationary phase (porous particle).
(A) Cross-section illustration; and (B) Scanning electron microscopy image of an actual porous 3 μm particle
Adapted from Vitha (2017).

Silica is commonly used as stationary phase as it has outstanding adsorbent properties with active adsorptive functional groups at the surface (Figure 3.4). Further, silanol groups on the surface of silica can be chemically modified to achieve specific properties (Figure 3.5). Some other stationary phases include alumina, magnesium silicate, methacrylate gels, agarose, titania, and zirconia.

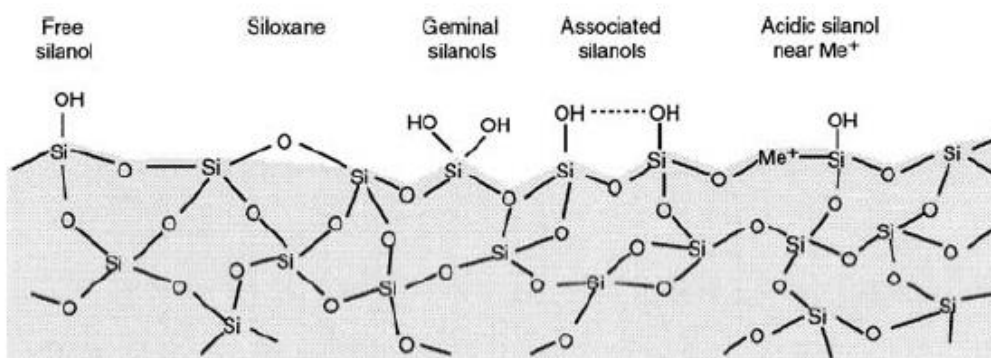


Figure 3.4: Chemical structure of silica with associated functional groups.
Adapted from Meyer (2010).

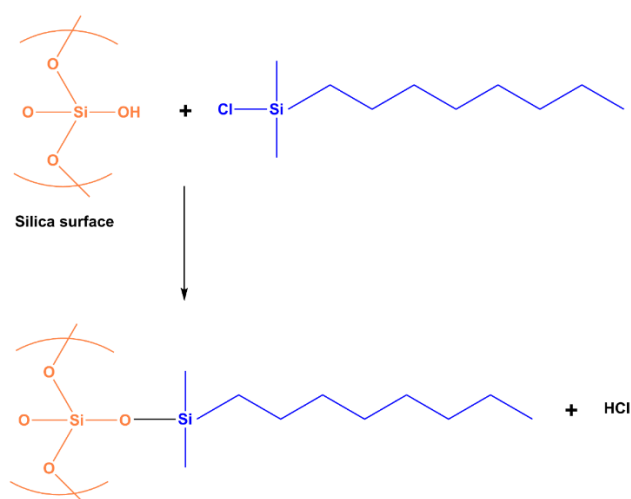


Figure 3.5: Modification of silica stationary phase by octylsilane (C-8) linkage.
Adapted and reproduced from (Vitha, 2017).

The function of the detector is to generate electrical signal once it has detected the analyte; the signal is proportional to either concentration or mass of the analyte. Quantitative analysis of the analyte is carried out from that signal (from calculated peak area or peak height). In pharmaceutical analysis, UV detector is extensively used due to its sensitivity. However, it only detects analyte that absorbs UV or visible light. Other detectors include refractive index detectors (when analyte does not absorb UV light), fluorescence detectors (lower detection for specific analyte), electrochemical detectors, light scattering detectors, and spectroscopy-coupled detectors, such as HPLC-UV (diode array detector), HPLC-FTIR, HPLC-MS, and HPLC-NMR. A list of common detectors with their performance is shown in Table 3.2.

Table 3.2: Detectors used in liquid chromatography .

Detector	Lower limit of detection (ng)	Gradient elution
Ultraviolet (UV)	0.1-1.0	√
Refractive index	100-1000	×
Fluorescence	0.001-0.01	√
Electrochemical	0.01-1.0	×
Light scattering	0.1-1.0	√
Mass spectroscopy	0.001-0.01	√
Charged aerosol	0.1-1.0	√

Adapted from Pedersen–Bjergaard et al. (2019)

3.1.2. Separation principle

Separation process in liquid chromatography is explained by distribution of a sample component or a mixture of sample components between two phases in the column bed. The components reside in the stationary phase and mobile phase according to their chemical interactions. The component that prefers mobile phase will migrate faster and vice versa. A simple separation process of toluene and phenol is shown in Figure 3.6. To further understand the separation process, a mixture of two sample components and their separation is shown in Figure 3.7.

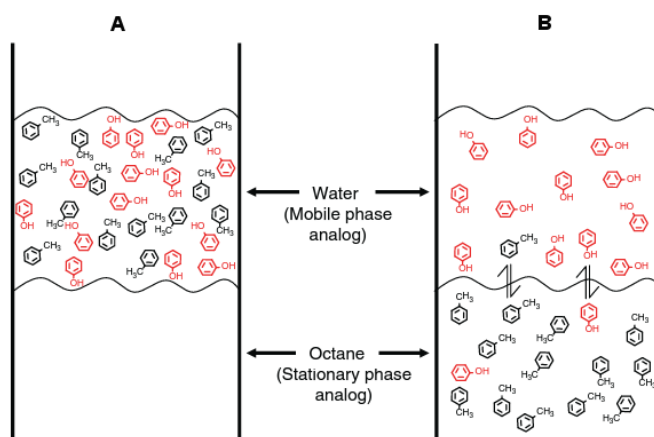


Figure 3.6: Separation of toluene and phenol in the column.

(A) Introduction of toluene and phenol in water (polar mobile phase) and octane (non-polar stationary phase); and (B) Toluene resides in stationary phase, and phenol stays with mobile phase due to hydrogen bonding and dipole-dipole interactions. Adapted from Vitha (2017).

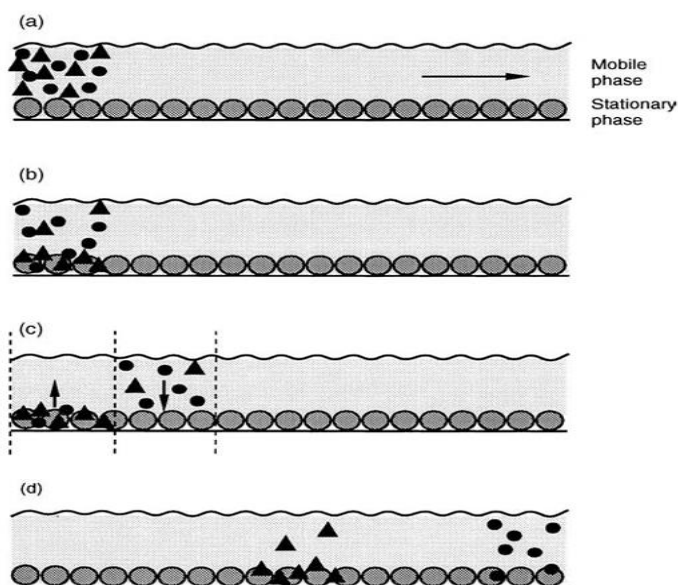


Figure 3.7: Chromatographic separation process.

(a) Application of a mixture of two components in the column bed; (b) Residence of components in two phases according to their preference; (c) New equilibrium after introduction of fresh mobile phase previously adsorbed components in the stationary phase appear in the mobile phase; and (d) Separation of two components after repeating the previous step many times. Adapted from Meyer (2010).

Subsequently, the eluted sample component is detected and recorded as a peak, which is a Gaussian (bell-shaped) curve. A peak provides information about a sample component qualitatively (with retention time) and quantitatively (with the area and height). The structure of a sample peak is shown in Figure 3.8.

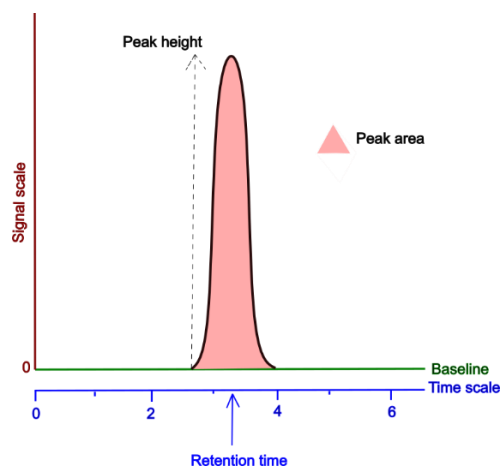


Figure 3.8: Structure of a chromatographic peak.

3.1.3. Modes of liquid chromatography

Liquid chromatography varies based on nature of the stationary phase and mobile phase, type of the interactions for separation, concentration of solvent in the mobile phase, and so on. Common modes of HPLC are shown in Figure 3.9.

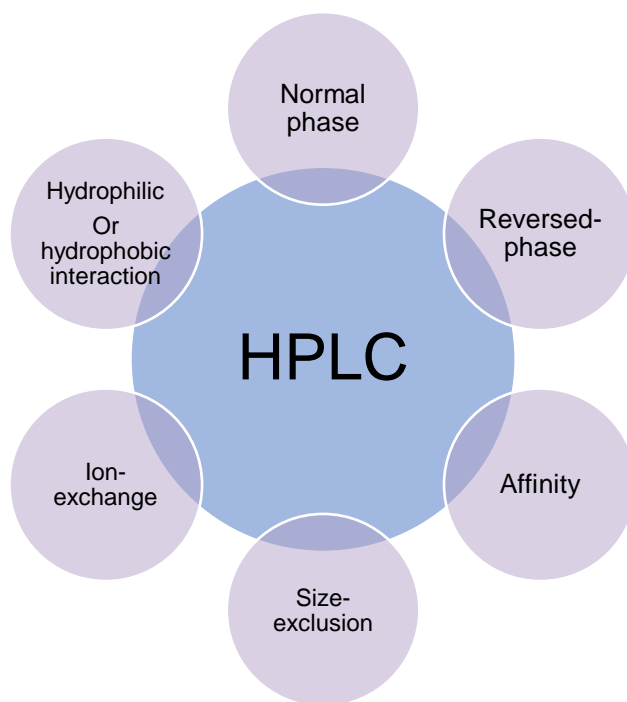


Figure 3.9: General modes of HPLC.

Normal phase chromatography is comprised of a relatively polar stationary phase (such as, silica, alumina, and magnesium oxide), and a relatively nonpolar mobile phase (such as, heptane).

Reversed-phase chromatography is comprised of a relatively less or non-polar stationary phase (such as, chemically bonded octadecylsilane, an n-alkane with 18 carbon atoms; C8 and shorter carbon chains; and cyclohexyl and phenyl group), and relatively polar mobile phase (such as, water, methanol, acetonitrile, and ethanol). Reversed-phase liquid chromatography (RP-HPLC) can separate a wide range of compounds which are hydrophobic in nature.

In ion-exchange chromatography, the stationary phase has ions (such as, SO_3^{2-} , COO^- , NH_3^+ and NR_3^+) on its surface, and it can exchange ions. Sample ion and mobile phase ions compete each other for the ions on the stationary phase.

Hydrophilic interaction chromatography (HILIC) separates very polar sample component in a normal-phase mode. The separation is explained as the water is adsorbed to the silica particle surface with hydrogen bonding (Figure 3.10). Polar molecules are attracted toward this water molecule or directly silanol group.

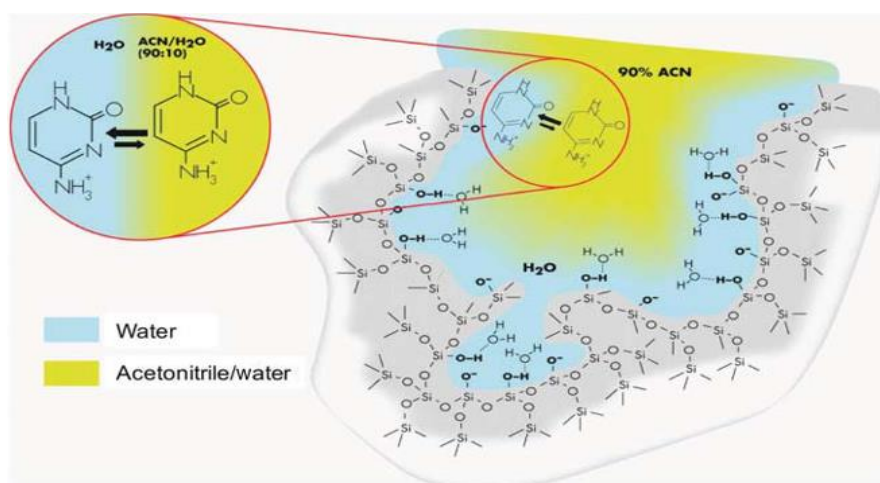


Figure 3.10: Water adsorption to the silica particles in hydrophilic interaction chromatography.

Adapted from Vitha (2017).

Size exclusion chromatography (SEC) is also known as gel permeation chromatography; its separation is based on the molecular size of the analyte in the solution. The column is packed with a semi-rigid gel, which has an inert porous surface. Smaller molecules diffuse completely into the pores and elute at last. Contrarily, larger molecules fail to enter the pores and elute at first.

Affinity chromatography deals with biochemical interaction in nature, such as antigen-antibody, enzyme-inhibitor, and hormone-carrier. It is a specific chromatographic method, where a ligand is bonded to a support and other (sample) is absorbed from solution. In this way, a specific sample is retained by the specific stationary phase, where other components are removed by the mobile phase.

3.1.4. Ultra-high-performance liquid chromatography

Liquid chromatography that can run at very high pressure is known as ultra-high-performance liquid chromatography (UHPLC or UPLC). The practice of liquid chromatography has come to a new era with the introduction of UHPLC commercially in 2004, although it was developed in academic laboratories in late 1990s (Xu, 2013). UHPLC is getting more attention recent years in pharmaceutical industries because of its high speed, high resolution, high sensitivity, and cost effectiveness using minimum amount of solvents.

UHPLC can be achieved either by coupling sub-2 μm particle column packing, which can withstand extremely high pressure (up to 1500 bar), or by core shell (fused core) particle column packing, which can endure column back pressure up to 400 bars.

As it is known that there are many established HPLC methods for commercial and new investigational drug products, these can be converted to UHPLC systematically, by selecting appropriate column, experimenting to verify conditions, and validating the method.

Therefore, as mentioned earlier that there has been no study that developed a chromatographic method to analyse pimozide in complex matrix, such as PLGA nanoparticles, this study aims to develop an UHPLC method for that. To do so, it also aims to optimise and validate the method.

3.2. Aims and Objectives

Aims

- a) To develop an UHPLC method for the analysis of pimozide in PLGA nanoparticles.
- b) To validate the method according to the ICH guidelines.

Specific objectives

- i. To optimise an appropriate solvent of analyte.
- ii. To evaluate whether there is any loss of pimozide recovery due to the interaction between membrane molecule of the syringe filter and pimozide.
- iii. To optimise the solvent/solvent extraction of pimozide out of PLGA nanoparticles.
- iv. To validate the method by evaluating specificity, linearity, accuracy, precision (intermediate precision), limit of detection and limit of quantification, and robustness according to the ICH guidelines.

3.3. Results and Discussions

3.3.1. Development of the UHPLC method

Details of the method (instrumentation and conditions) can be found in Chapter 2 (Section 2.2.2.5.1).

3.3.1.1. Selection of solvent of analyte

Selecting an appropriate solvent of analyte (or diluent) is vital for any chromatographic separation as failing to do so could lead to an inaccurate quantification of the analyte (Stoll and Mack, 2019). Pimozide was dissolved in dichloromethane (DCM) and methanol separately, and respective standard concentrations were prepared. Pimozide was then analysed by an UHPLC method, as described in chapter 2 (section 2.2.2.5.1). Both solvents of analyte were compared in terms of retention time and peak shape.

The retention time of pimozide was detected at 11.2 minutes (Figure 3.11). It remained almost same when analysed in both solvents of analyte. However, peak height (~75 mAU) was higher in methanol than DCM (~55 mAU). This indicates that pimozide was recovered more when it was analysed in methanol than analysed in DCM.

It is known that the analyte of interest must be dissolved in the solvent that is miscible with the mobile phase (Pedersen–Bjergaard, Gammelgaard and Halvorsen, 2019). Further, the solvent of analyte should not have stronger elution strength than the mobile phase. Therefore, mobile phase is the first choice as a solvent of analyte. It is possible that DCM, being a stronger solvent in strength than methanol, produced unwanted peaks (Figure 3.11a). Distorted peak shape is also due to the effect of stronger solvent of analyte (Stoll and Mack, 2019).

However, in reversed-phase chromatography, the use of neat methanol or acetonitrile should be avoided as solvent of analyte and mobile phase simultaneously, as this would increase strength of analyte solution, preventing the retention of analyte in the stationary phase, resulting in faster elution and broader peaks. In this case, either a small injection volume of analyte in same solvent as mobile phase, or large injection volume of analyte with solvent of weaker strength than mobile phase could prevent the peak broadening (Pedersen–Bjergaard, Gammelgaard and Halvorsen, 2019). However, too much weak solvent could lead to phase separation or precipitation of the analyte (Stoll and Mack, 2019). Therefore, care should be taken during determining the level of solvent of analyte to be used, as this varies according to the nature of the compound.

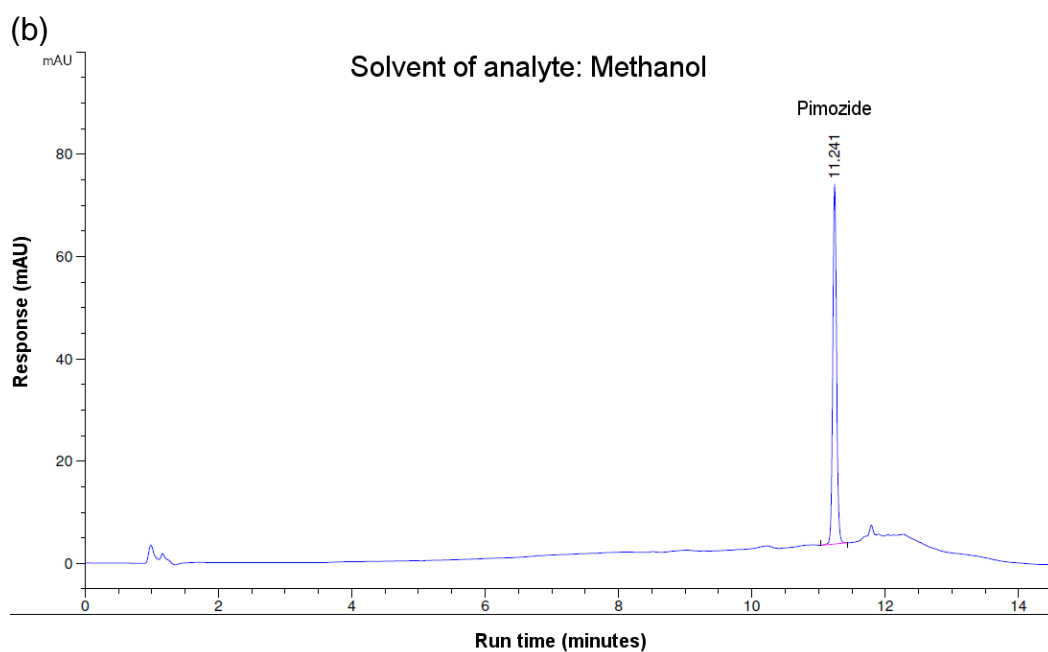
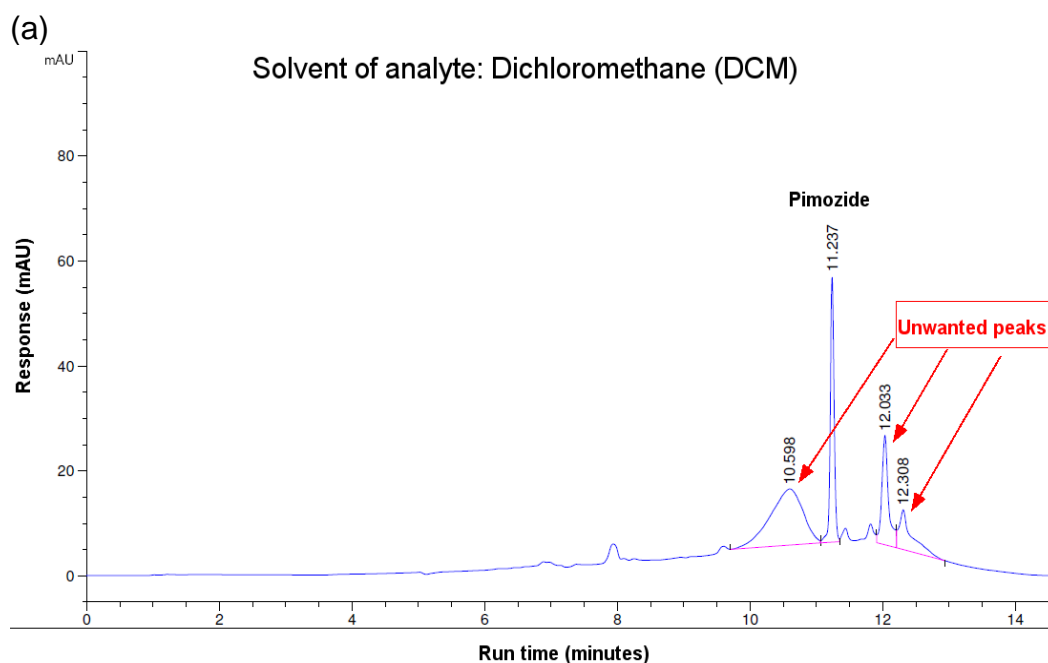


Figure 3.11: Representative chromatograms of standard pimozone in two different solvents of analyte.

50 $\mu\text{g}/\text{mL}$ pimozone standard solution was prepared in (a) dichloromethane; and (b) methanol. Each sample (2 μL) was injected three times. Detection was by UV absorption at 280 nm. Pimozone's peak was integrated on the same scale by Agilent ChemStation software.

3.3.1.2. Optimisation of pimozone extraction

Analyte extraction from a complex matrix, such as PLGA nanoparticles is vital for accurate detection and quantitation. It could be performed in one step by a single solvent or multiple steps by different solvents.

At first, initial softening or dissolution of PLGA was confirmed with an organic solvent followed by subsequent dilution with another solvent for pimozone extraction. Sonication and filtration aided this procedure prior to sample injection. Therefore, a solid-liquid multi-step extractions protocol was followed using five different solvent system(s), such as methanol, dichloromethane (DCM), acetonitrile, dichloromethane-methanol, and acetonitrile-methanol. The latter two dual-solvent systems were in 1:5 v/v ratio, respectively.

As shown in

Figure 3.12, pimozone's responses (in peak heights) were found to be 125, 128, 155, 182, and 190 mAU when extracted with methanol, DCM, acetonitrile, DCM-methanol, and acetonitrile-methanol, respectively. This indicates that pimozone was recovered most once extracted with acetonitrile-methanol solvent systems, while the pimozone recovery was least with methanol only. It is possible (in case of methanol treatment only) that nanoparticles were not completely broken down or softened due to the sonication. There were still some pimozone molecules trapped inside the PLGA matrix, resulting lowest response (

Figure 3.12a). On the contrary, in case of acetonitrile-methanol treatment, acetonitrile dissolved PLGA by forcing pimozone out of the PLGA matrix and then let methanol dissolve pimozone, leading to the maximum recovery (

Figure 3.12e).

In case of DCM treatment, although DCM dissolved both pimozone and PLGA, low response could be due to the strength of this solvent, as DCM is stronger solvent than the mobile phase (methanol).

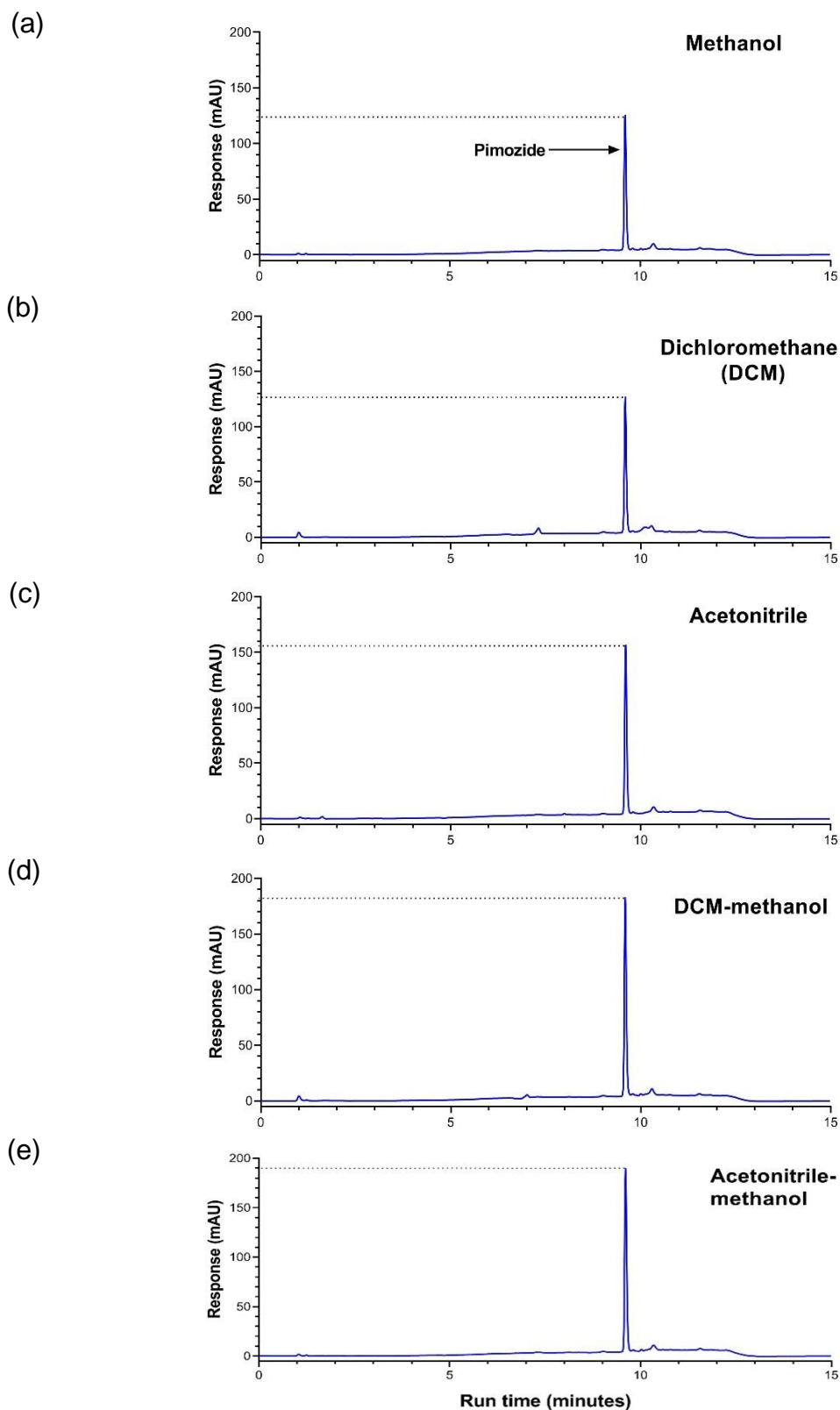


Figure 3.12: Representative responses of pimozone after extraction by different solvent systems.

PLGA nanoparticles were treated with (a) methanol; (b) dichloromethane (DCM); (c) acetonitrile; (d) DCM-methanol (1:5); and (e) acetonitrile-methanol (1:5) followed by sonication and filtration. Pimozone's peak was integrated by Agilent ChemStation software and reproduced by GraphPad Prism software.

3.3.1.3. *Effect of membrane filtration*

Filtration is considered as a simple and cost-effective measure in HPLC analysis. Successful filtration of a sample achieves accurate results since it avoids blockage of the column that increases the backpressure resulting incorrect signals. Furthermore, filtration increases the lifetime of the column and the instrument. However, adsorption of analyte to the filter membrane (leading to loss of analyte) and interference of filter extractables to the analyte solution (leading to unwanted peaks or deformed peaks) are two major downsides. Membrane filters are made of polymeric films, such as cellulose esters, nylon, polyvinylidene difluoride (PVDF), and polytetrafluoroethylene (PTFE) that are arranged as open and colloidal structures (Carlson and Thompson, 2000).

This experiment aimed to investigate whether pimozone was lost (retained in the membrane) during filtration by analyte-membrane binding. Eight standard pimozone concentrations (5 to 100 µg/mL) were injected before and after filtration with a 0.2 µm PTFE syringe filter. UHPLC responses, such as retention time, peak area, and theoretical plate number were then compared to identify any loss of pimozone.

As demonstrated in Figure 3.13a, the retention time for both filtered and non-filtered remains same (11.1 minutes). The difference in retention time was found to be statistically not significant ($p=0.724$, paired t -test). Figure 3.13b compares the peak area before and after filtration. It was found that maximum 0.000129% pimozone was lost during filtration. This indicates there was insignificant pimozone-PTFE membrane binding (adsorption) or there was insignificant solvent (methanol) incompatibility between pimozone and membrane. In this regard, Carlson and Thompson (2000) found significant analyte loss after filtration with three types of polymer-based membrane filter. Authors concluded that basic and neutral analytes dissolved in methanol could pass three types of filters, such as cellulose acetate, nylon, and polyvinylidene difluoride (PVDF) without any significant loss. However, acidic analyte was significantly adsorbed (up to 53.6%) by the membrane. Their study presumed similar results would have been found when PTFE filter would be used, opposing current study findings.

It is known that column efficiency is determined by the number of theoretical plates – the higher the plate numbers, the better is the column efficiency (Stauffer, Dolan and Newman, 2008). An efficient column will produce narrower peaks, whereas an inefficient column will produce broader peaks. Figure 3.13c depicts the comparison between filtered and non-filtered pimozone standard solution in terms of theoretical plate numbers. Here, the plate numbers range from 185,000 to 200,000. This study found no significant difference in plate numbers after filtration. This indicates that the filtration did not have any effect on column efficiency.

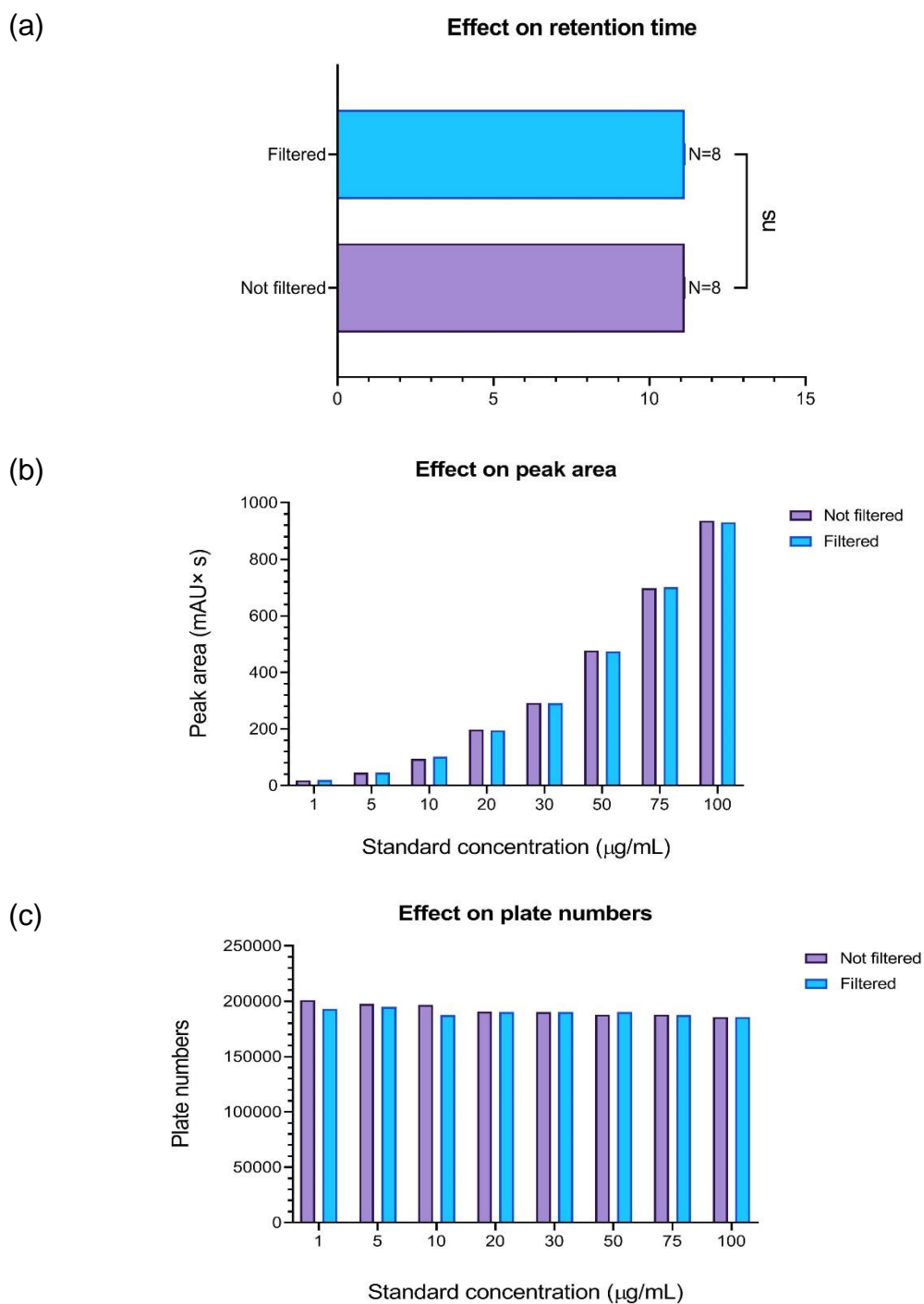


Figure 3.13: Effect of syringe filtration on pimozide's signals. Effect of PTFE syringe filter on (a) retention time; (b) peak area; and (c) plate numbers. Data are presented as mean \pm SD ($n=3$, unless otherwise stated). A syringe filter of 0.2 μm was used to filter the standard solutions. Mean difference of retention time in Figure A is not statistically significant (ns), paired t -test.

Therefore, it was concluded that during filtration of samples, pimozide did not interact with the 0.2 PTFE membrane molecule, and hence no significant loss of pimozide was observed.

3.3.2. Method validation

Current method was validated for specificity, linearity, accuracy, precision, limit of detection, limit of quantification, and robustness in line with the guidelines provided by the International Council for Harmonisation of Technical Requirements for Pharmaceuticals for Human Use (ICH, 2005).

3.3.2.1. *Specificity*

To confirm the specificity of the method, empty nanoparticles and drug-loaded nanoparticles were injected separately along with the solvent only (methanol).

Figure 3.14 demonstrates and compares the chromatograms of solvent, pimozone-loaded nanoparticles, and empty nanoparticles. Pimozone peak was found at 9.6 minutes (Figure 3.14b). At this retention time, the peak was absent for both methanol (Figure 3.14a) and empty nanoparticles (Figure 3.14c). This indicates that the method is specific for pimozone since any possible interference by the solvent or excipients was absent at 9.6 minutes.

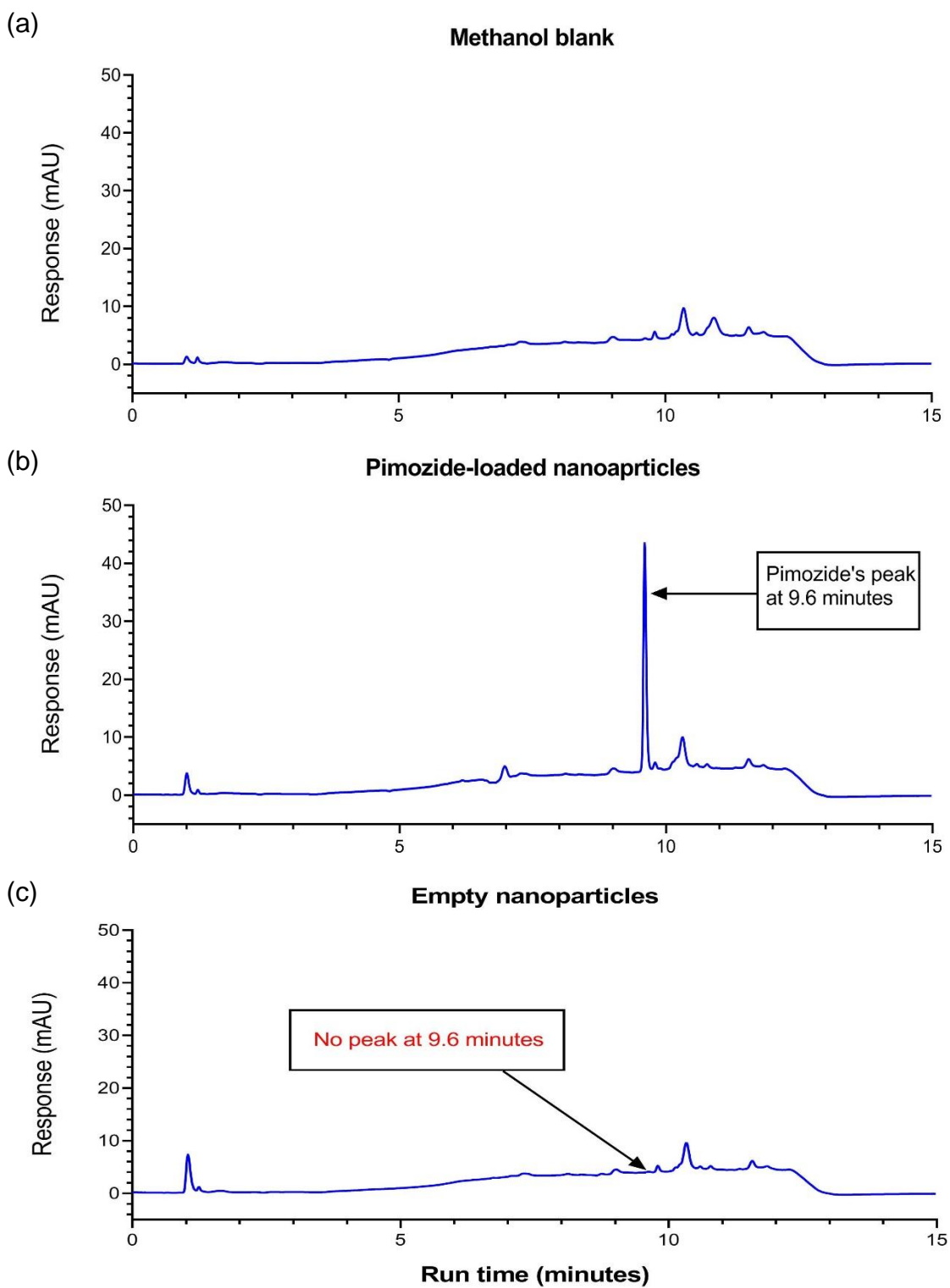


Figure 3.14: Representative chromatograms showing the specificity of the method. (a) Blank solvent; (b) Pimozide-loaded nanoparticles; and (c) Empty nanoparticles. Nanoparticles was comprised of PLGA, PEG 4000, and TPGS.

3.3.2.2. Linearity

Linearity was determined by preparing standard curve plotted with peak area (mAU × s) against concentrations (µg/mL). A linear regression equation was obtained that provided slope, y-intercept, and correlation coefficient (denoted as R²).

As shown in Figure 3.15, pimoziide standard curve is drawn with concentration range of 1-100 µg/mL. The regression equation was calculated as of $y = 9.001x - 13.23$, where 'y' is the peak area, and 'x' is the pimoziide concentration (µg/mL). This equation reveals slope as of 9.001 and y-intercept as of -12.23. The regression analysis also finds correlation coefficient (R²) as of 0.9991, indicating that the method is linear over the studied concentration range of 1 to 100 µg/mL. Figure 3.16 demonstrates representative chromatograms of pimoziide standard concentrations.

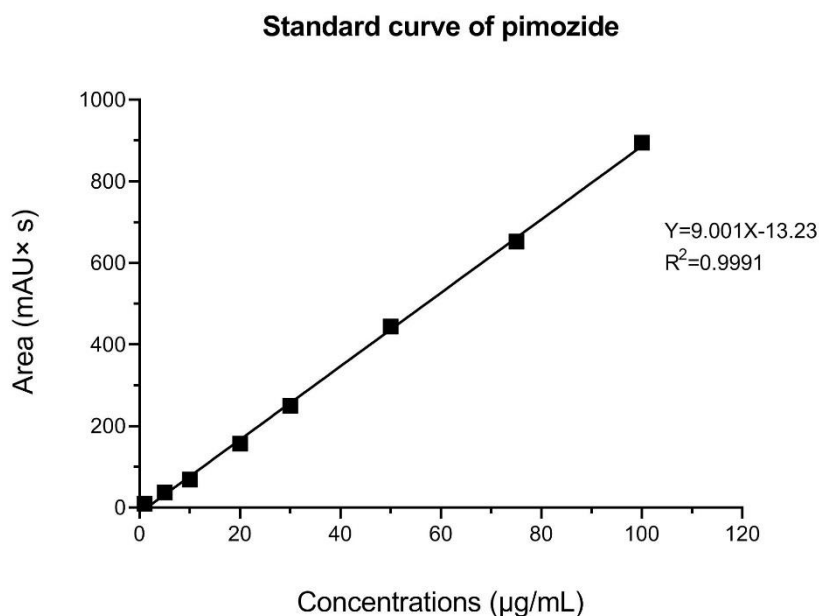


Figure 3.15: Regression plot for determining linearity of the method.

Standard curve was determined by external calibration method, with eight pimoziide standard solutions in methanol (each standard was measured in triplicates).

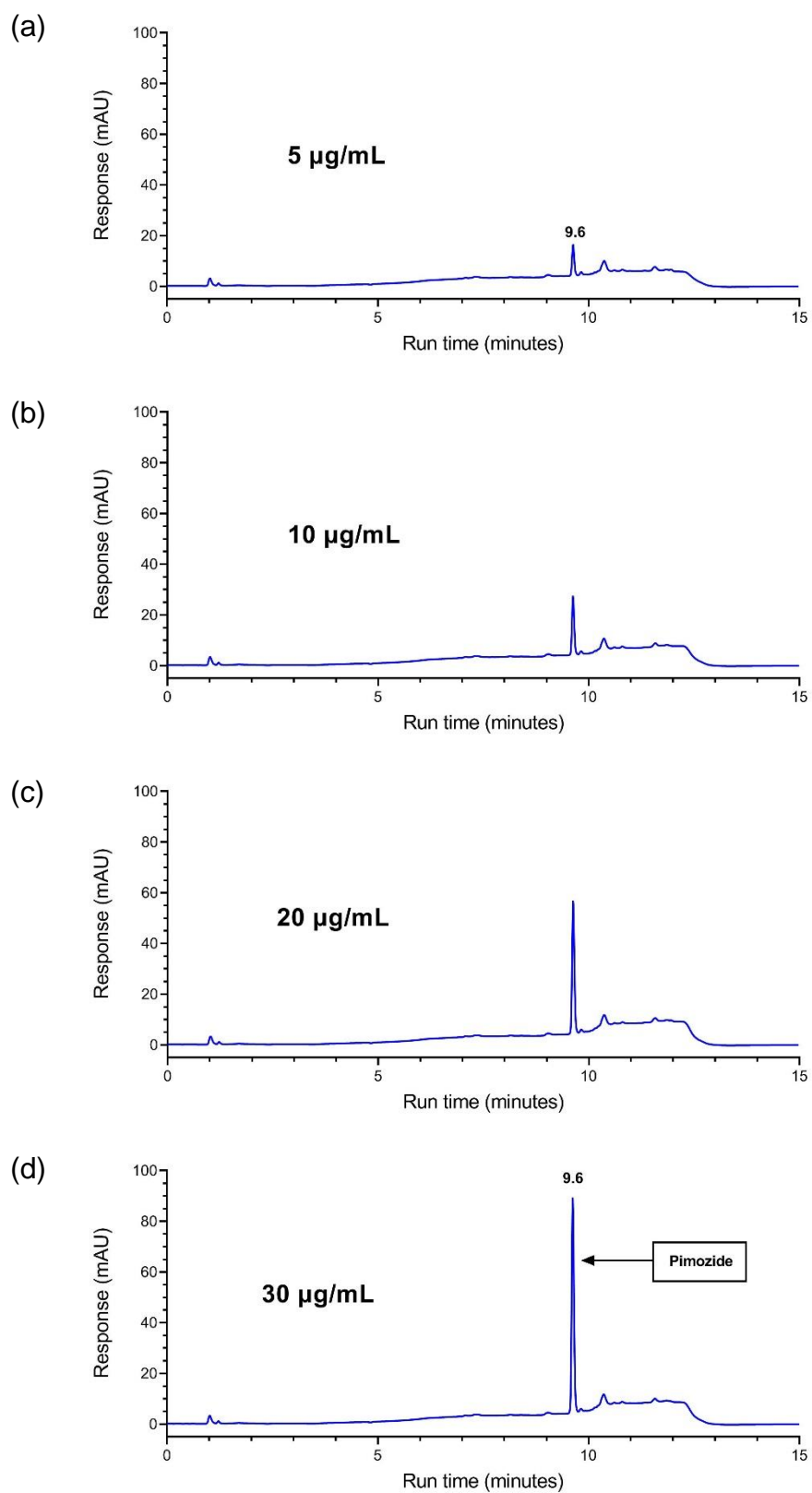


Figure 3.16: Representative chromatograms of pimoziide standard concentrations. Chromatogram of pimoziide at its standard concentration of (a) 5 µg/mL; (b) 10 µg/mL; (c) 20 µg/mL; and (d) 30 µg/mL.

3.3.2.3. Accuracy

Three standard pimozide concentrations (10, 20, and 50 µg/mL) were spiked in empty nanoparticles. Each concentration was spiked in triplicates. Each sample was then injected in triplicates.

As shown in Table 3.3, the recovered pimozide concentration is between 99.8% and 101.9%. This indicates that the current method complies with the acceptance criteria for accuracy ($\leq 2\%$ RSD).

Table 3.3: Test of accuracy by recovering the spiked pimozide.

Spiked concentration (µg/mL)	Mean recovered concentration (µg/mL)	%RSD	%Recovery
10	10.1	1.3	101.9
20	20.5	1.3	101.9
50	49.8	0.2	99.8

RSD, relative standard deviation

3.3.2.4. Precision

This study confirmed intermediate precision of the method by comparing retention time and peak area of pimozide achieved by two different analysts, two different times of injection, and two instruments. Six standard concentrations of pimozide (10, 20, 30, 50, 75, and 100 µg/mL) were prepared for this experiment. Each sample concentration was injected in triplicates.

Results are expressed in percent relative standard deviation (%RSD) of retention time and peak area for different analysts, times, and instruments (Figure 3.17 and Figure 3.18).

Two analysts were named as analyst A (author) and analyst B (a fellow researcher). Analyst B prepared all pimozide standard solutions following same protocol as followed by analyst A. Results show that %RSDs of the retention time were 0.013% and 0.014% for analyst A and B, respectively (Figure 3.17a). The mean difference %RSD between those two analysts was found to be statistically not significant ($p=0.945$, paired *t*-test). %RSDs of peak area were

obtained as of 0.54% and 0.66%, respectively (Figure 3.18a). Likewise, the mean difference was statistically not significant ($p=0.794$, paired t -test).

Also, responses were obtained from different times (day 1 and day 3) of injection of same samples prepared by analyst A. %RSDs of retention time were calculated as of 0.014% and 0.018% for day 1 and day 3, respectively (Figure 3.17b). The mean difference was statistically not significant ($p=0.364$, paired t -test). In case of peak area, %RSD were obtained as of 0.66% and 0.47% for day 1 and 3, respectively (Figure 3.18b). The mean difference was statistically not significant ($p=0.519$, paired t -test).

Finally, samples (prepared by analyst A) were also injected in a different instrument of same make and model, named as instrument 'Y'. It should be noted previous analyses (different analysts and times of injection) were performed in instrument 'X'. Here, responses of instrument X and instrument Y were compared. %RSDs of retention time were obtained as of 0.007% and 0.084% for X and Y, respectively (Figure 3.17c). The mean difference was statistically not significant ($p=0.262$, paired t -test). In case of peak area, %RSDs were found of as 0.69% and 0.45% for instrument 'X' and 'Y', respectively (Figure 3.18c). The mean difference was found to be statistically not significant ($p=0.433$, paired t -test).

In summary, all comparisons of responses were found to be statistically insignificant, indicating that the method is reproducible. %RSDs in all cases were below 2%. Therefore, it is confirmed that current method demonstrates acceptable precision.

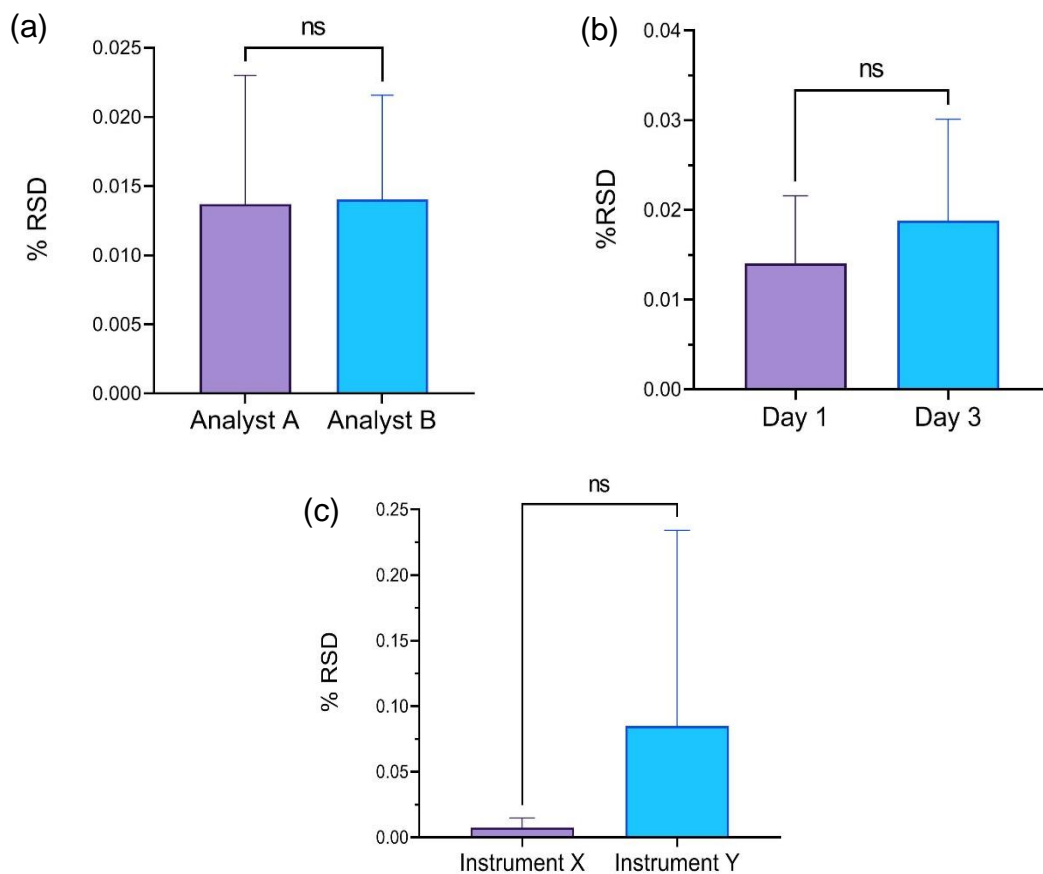


Figure 3.17: Test of precision by comparing percent relative standard deviation (%RSD) of pimozide retention time.

(a) Comparison between two analysts; (b) Comparison between two different days; and (c) Comparison between two HPLC instruments. Data presented are mean of the %RSD \pm SD ($n=3$). Mean differences are not statistically significant (ns), paired t-test.

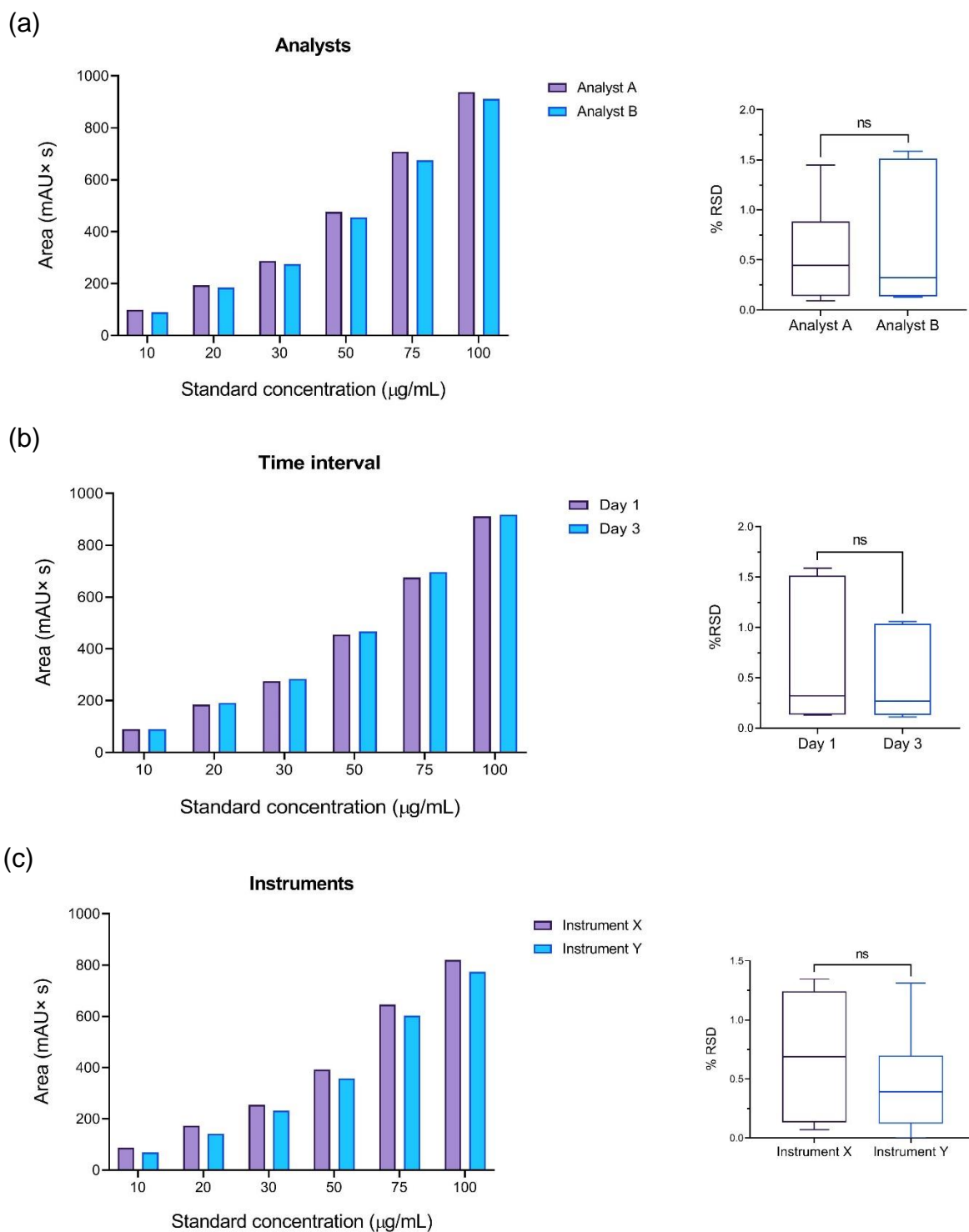


Figure 3.18: Test of precision by comparing percent relative standard deviation (%RSD) of peak area of pimozide.

(a) Comparison between two analysts; (b) Comparison between two different times of injection; and (c) Comparison between two different instruments. Data presented in bars are mean peak area ($n=3$). Box plots are the mean %RSD \pm SD ($n=6$). Mean differences of %RSD are not statistically significant (ns), paired t -test.

3.3.2.5. Limit of detection and quantification

Limit of detection (LOD) and limit of quantification (LOQ) were calculated by using standard deviation of response (peak area) and slope of the calibration curve. LOD and LOQ were found to be 0.6 µg/mL and 2.1 µg/mL, respectively (Table 3.4). A comparative inspection of chromatograms confirms that pimozone's peak (at 9.6 minutes) is visible at concentration of 0.5 µg/mL (Figure 3.19).

Table 3.4: Determination of limit of detection and quantification

Limit of detection (µg/mL)	Limit of quantification (µg/mL)
0.6	2.1

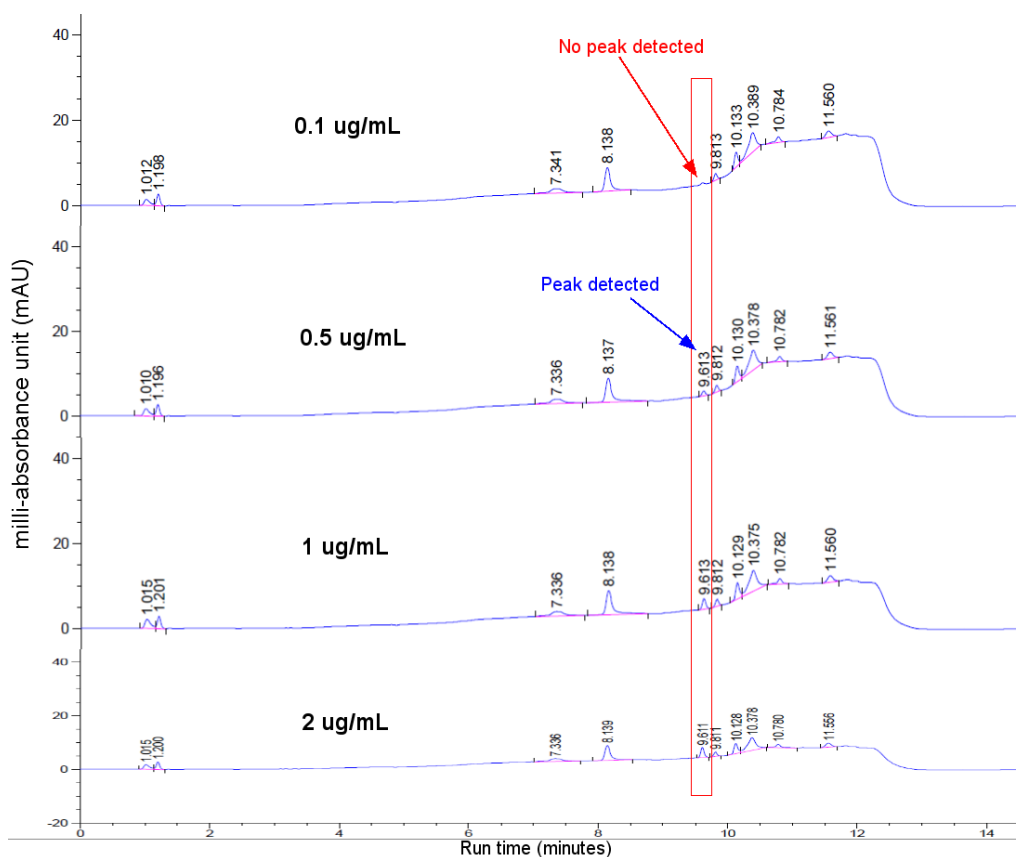


Figure 3.19: Visual identification of limit of detection (LOD).
Pimozone is retained at 9.6 minutes.

3.3.2.6. Robustness

Robustness of the method was evaluated by changing flow rate (± 0.1 mL/min) and column temperature ($\pm 10^\circ$ C). Results are expressed as percent relative standard deviation (%RSD) of peak area produced from three concentrations of pimozone (10, 20, and 30 μ g/mL).

As shown in Table 3.5, at flow rate of 0.2 mL/min, %RSD of peak area of all three concentrations is between 0.1% and 0.7%, which is well below 2%. However, with a slight change (± 0.1 mL/min), the method is not robust because %RSD increases to 6% for both 10 and 20 μ g/mL sample concentration, exceeding the acceptance criteria. Contrarily, at concentration 30 μ g/mL, %RSD remains 0.5% for both flow rates.

Table 3.5: Method robustness analysis by changing the flow rate.

Sample concentration (μ g/mL)	% RSD of peak area		
	0.1 mL/min	0.2 mL/min	0.3 mL/min
10	4	0.5	6
20	4	0.7	0.7
30	0.5	0.1	0.5

With almost similar trend, at column temperature 40° C, %RSD of peak area is between 0.1% and 0.8%, which is less than 2% (Table 3.6). However, with a change in column temperature ($\pm 10^\circ$ C), at sample concentration 10 μ g/mL, %RSD are found to be 3% and 7%, both exceeding the acceptance criteria ($\leq 2\%$). Contrarily, at sample concentration 10 and 20 μ g/mL, %RSD remains between 0.1% and 0.8% for both flow rates.

In short, current method is proven to be robust when the sample concentration is more than ≥ 20 μ g/mL with flow rate ≥ 0.1 mL/min.

Table 3.6: Method robustness analysis by changing the column temperature

Sample concentration ($\mu\text{g/mL}$)	% RSD of peak area		
	30° C	40° C	50° C
10	3	0.5	7
20	0.8	0.8	0.2
30	0.5	0.1	0.5

3.4. Conclusion

This chapter aimed to develop and validate an ultra-high-performance liquid chromatography (UHPLC) method to determine pimozone in PLGA nanoparticles. Whilst optimising the method, it was found that methanol was an appropriate solvent of analyte. Acetonitrile-methanol (1:5) mixture was observed as an efficient solvent system to extract pimozone out of PLGA nanoparticles with maximum recovery. It was also confirmed that syringe filtration used in this study did not affect the overall recovery of pimozone. Finally, optimised method was validated by evaluating specificity, linearity, accuracy, precision, limit of detection, limit of quantification, and robustness. All results complied with the acceptance criteria provided by the ICH guidelines. Therefore, in the following chapters (4 and 5), this validated UHPLC method would be used to determine drug encapsulation efficiency of the PLGA nanoparticles.

Chapter 4

Development of Pimozide-Loaded PLGA Nanoparticles: Exploration of Process and Formulation Parameters

Chapter 4. Development of Pimozide-Loaded PLGA Nanoparticles: Exploration of Process and Formulation Parameters

This chapter describes the design and development of pimozide-encapsulated PLGA nanoformulations, by investigating the effect of several independent process and formulation variables (such as, different preparation methods, and different formulation compositions) on the physicochemical characteristics of nanoparticles to achieve a potential formulation.

4.1. Introduction

PLGA nanoparticles are potential drug delivery systems that can carry variety of therapeutic candidates to the site of action. As discussed in chapter 1, PLGA has already been approved by leading international medicines regulatory agencies to be used as an excipient in production of long acting injectables and other medical devices, yet there is no PLGA-based nanomedicine on the market (Operti *et al.*, 2021).

However, numerous research work is published every year regarding PLGA based nanomedicines, to overcome many formulations related obstacles, specifically scalability and reproducibility with desired particle properties. One of the attractive features of PLGA nanoparticles is that their physicochemical properties can be finely tuned by altering many process and formulation parameters. Therefore, it was hypothesised that, in line with the general aims and objectives of the study, hydrophobic drug candidate (pimozide) could be encapsulated within PLGA nanoparticles, producing a novel drug delivery system to repurpose pimozide for glioblastoma chemotherapy.

Several hydrophobic drug molecules were reported to be successfully encapsulated within PLGA nanoparticles, and optimised to desired properties making them potential drug delivery systems for particular cancer types (Mu and Feng, 2003; Acharya and Sahoo, 2011; Zhu *et al.*, 2014; Sufi *et al.*, 2020; Bacanlı *et al.*, 2021).

In vitro and *in vivo* performances of PLGA nanoparticles are dependent on their key physicochemical properties, such as particle size, size distribution, charge, morphology, surface functionality, drug encapsulation efficiency, and stability (Operti *et al.*, 2021). These key properties are manipulated by many process and formulation parameters, consequently affecting the efficacy of nanoparticles. For example, type of surfactant, as one of the formulation parameters, can change the size and stability of the nanoparticles (Shkodra-Pula

et al., 2019). In case of process parameters, preparation methods and their intermediate steps, even with a subtle change, can alter the final product, leading to affect their therapeutic outcomes (Operti *et al.*, 2021). Therefore, this chapter aims to explore several process and formulation parameters during the development of pimozone-encapsulated PLGA nanoparticles, leading to a potential formulation that is to be further developed for targeted glioblastoma therapy.

4.2. Aim and Objectives

Aim

- a) To achieve a potential formulation by exploring several process and formulation parameters based on the physicochemical properties of PLGA nanoparticles.

Specific objectives

- i. To study the effect of using two different molecular weights of PLGA (24-38 kDa and 30-60 kDa).
- ii. To confirm chemical interaction and compatibility between pimozone and PLGA.
- iii. To investigate the effect of two preparation methods, namely single emulsion-solvent evaporation (SE) and microfluidics.
- iv. To address the effect of freeze-drying on particle size.
- v. To study the effect of five different surfactant systems, namely polyvinyl alcohol (PVA), polysorbate 80, poloxamer 188, TPGS, and PVA-TPGS.
- vi. To examine the effect of two chemical terminal groups of PLGA (namely, acid and ester).
- vii. To modify the surface of PLGA nanoparticles by coating them with polyethylene glycol (PEG); and to investigate the effect of two molecular weights of PEG (4 and 8 kDa).

4.3. Results and Discussions

4.3.1. Preliminary findings

4.3.1.1. Effect of PLGA molecular weight

PLGA can be of different types, such as different molecular weights, ratio of monomers (lactic acid and glycolic acid), and free chemical terminal groups (such as, carboxyl, ester, and hydroxy terminated group). Changing any of these types can affect physicochemical properties of PLGA nanoparticles, such as particle size, surface charge, drug stability, drug encapsulation efficiency, release kinetics, and *in vivo* behaviour (Li *et al.*, 2021).

This study initially designed two formulations with two different molecular weights of PLGA (24-38 kDa and 30-60 kDa PLGA), while keeping other parameters constant (Table 4.1). Both PLGAs were ester terminated. Nanoparticles were prepared by single emulsion-solvent evaporation (SE) method, as described in Chapter 2 (Section 2.2.1.1). Results are demonstrated in Figure 4.1.

Table 4.1: Formulation compositions with different PLGA molecular weights.

Formulation code	MW of PLGA (kDa)	Pimozide load (2.5% w/w)	Surfactant	Preparation method
S1	24-38	+	PVA ¹	SE ²
S2	30-60	+	PVA	SE

¹Polyvinyl alcohol; ²Single emulsion-solvent evaporation

Particle size, the basic aspect of nanoparticulate drug delivery systems, is the principle determinant of bio-distribution and retention in targeted sites (Cho *et al.*, 2013). Orally administered carriers or drug particles should range around 300 nm or less to be absorbed readily by epithelial cells (M cells) of the gut-associated lymphoid tissues. For injectable nanoparticles, particle size plays a crucial role in delivering the drug at the site of action. First, it determines whether particles can flow in blood avoiding aggregation or blockage. Second, in targeted delivery, it determines particle's capacity to adsorb targeting ligand (such as, transferrin) on the surface. Smaller particles having larger surface area would adsorb more targeting ligands. Third, cellular uptake (endocytosis) of particles is also size dependent. Finally, extravasation (escape of particles from the bloodstream into the target site) happens more readily with smaller particles.

The mean particle sizes were found to be 265 ± 7 nm and 345 ± 26 nm for 24-38 kDa and 30-60 kDa PLGA nanoparticles, respectively (Figure 4.1a). This indicates that particle size was increased with the increase of PLGA molecular weight. The mean difference was significantly different ($p=0.028$, paired *t*-test). However, in both cases, mean polydispersity index was recorded as of ≤ 0.3 , with no significant difference (Figure 4.1b). Large particle size can be explained by the increased viscosity of PLGA solution. High molecular weight PLGA makes more viscous solution at a constant solvent volume. At the same homogenisation speed, more viscous solution might have produced larger emulsion droplets compared to less viscous solution. Similarly, Mittal *et al.* (2007) found that particle size was increased proportionally from 90 to 143 nm with the increase of PLGA molecular weight from 14.5 kDa to 213 kDa. Authors also explained that the large particle size was due to the increased viscosity. A recent study with PLGA microspheres also observed large particle size with increased molecular weight of PLGA (Kohno *et al.*, 2020).

In case of zeta potential, no significant difference was observed in both types of formulations (Figure 4.1c). It is known that zeta potential of PLGA nanoparticles is influenced by type of surfactant used.

Another important characteristic of PLGA nanoparticles is their drug encapsulation efficiency (EE). Figure 4.1d shows that drug EEs are $67 \pm 15\%$ and $71 \pm 10\%$ in 24-38 kDa and 30-60 kDa PLGA nanoparticles, respectively. This finding indicates that high molecular weight of PLGA encapsulated more drug molecules than that of low molecular weight PLGA. This can be explained by the hydrophobic nature of PLGA. Higher molecular weight of PLGA facilitated more hydrophobic interactions with pimozone, resulting in increased entrapment. However, the mean difference of EE between two formulations were not statistically significant (paired *t*-test). Kohno *et al.*, (2020) observed no significant difference in drug (risperidone) loading after using four different molecular weights of PLGA.

In contrast, Graves *et al.* (2004) found that drug EE was lower in high molecular weight PLGA nanoparticles than in low molecular weight PLGA nanoparticles. Interestingly, authors observed a blend of high and low molecular weights of PLGA (1:7) encapsulated maximum drug molecule in their study.

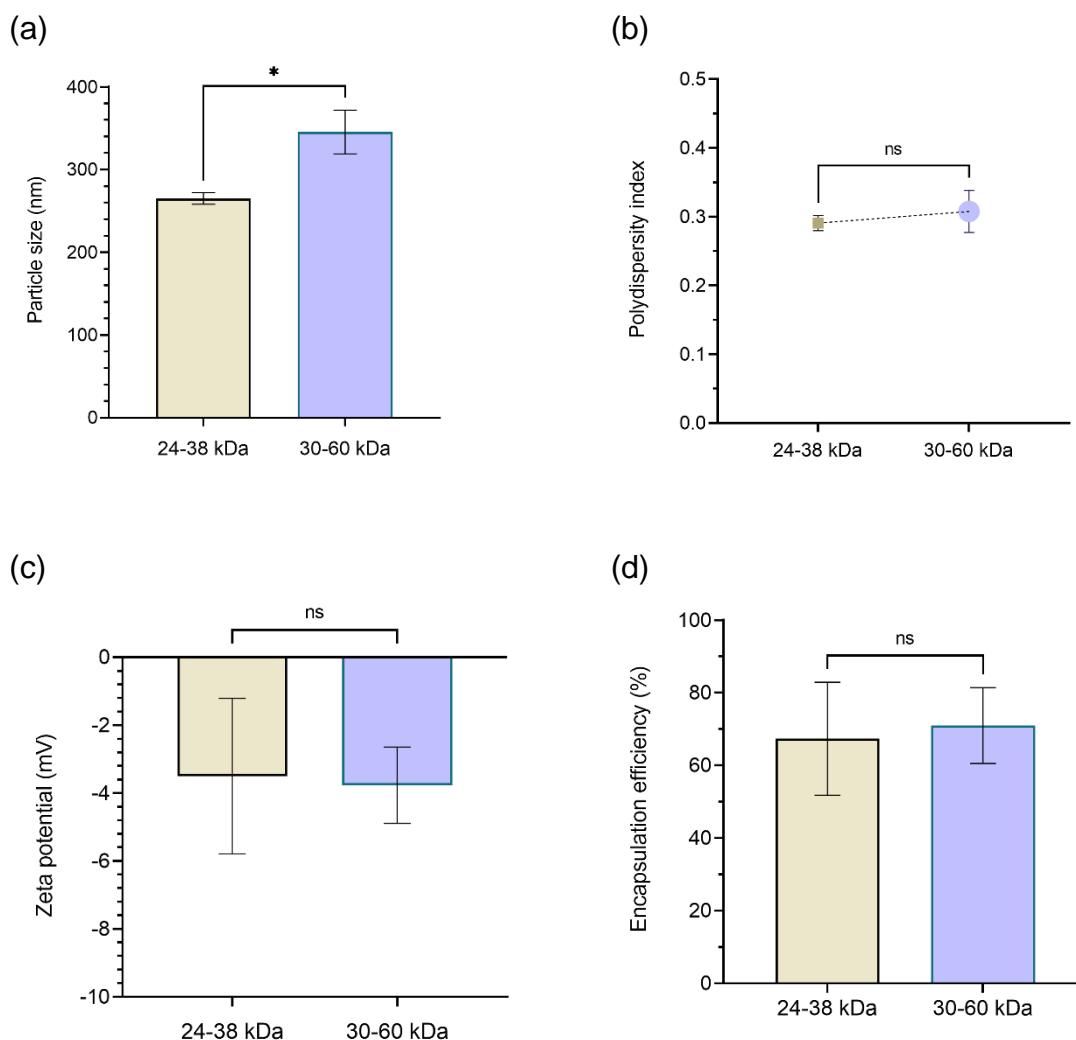


Figure 4.1: Effect of molecular weight of PLGA on physicochemical properties of PLGA nanoparticles prepared by microfluidic method.

Difference between 24-38 kDa PLGA nanoparticles and 30-60 kDa PLGA nanoparticles in terms of (a) Particle size (nm); (b) Polydispersity index; (c) Zeta potential (mV); and (d) Drug encapsulation efficiency (%). Data are mean \pm SD (n=3). Particle size, polydispersity index, and zeta potential were analysed by dynamic light scattering; and drug encapsulation efficiency was calculated from the recovered pimozone in nanoparticles by HPLC analysis. Asterisk (*) indicates that the mean difference is statistically significant ($p < 0.05$), while 'ns' denoting statistically not significant (paired t-test).

Molecular weight is a key factor that also affects drug release profile of PLGA nanoparticles. High molecular weight of PLGA has long polymer chains, resulting increased hydrophobicity of the polymer. In other words, PLGA would be more hydrophobic with high molecular weight. Consequently, its degradation (hydrolysis) would be slower than low molecular weight PLGA (Mittal *et al.*, 2007). During drug release, larger core pores are reported to be formed with molecular weight more than 20 kDa, while smaller peripheral pores formed

below that molecular weight. The formation of large core pores could delay the drug release by enabling drug sequestration (Mylonaki *et al.*, 2018).

Therefore, it was concluded that 30-60 kDa molecular weight of PLGA would be excluded in the following studies due to producing large particle size (~350 nm). Although 24-38 kDa PLGA nanoparticles were found to be <300 nm in size with more than 65% of drug EE, it was necessary to confirm that all materials in the nanoparticles were compatible to each other, especially pimozone with PLGA, prior to preparing further formulations.

4.3.1.2. Confirmation of chemical interactions and compatibility

Formulation S1 (24-38 kDa PLGA nanoparticles) was further characterised to evaluate chemical interactions, and determine the compatibility between materials comprising nanoparticles, such as drug molecule (pimozone) and excipients (such as, PLGA and surfactant).

Initial confirmation of drug loading and chemical interaction were achieved by Fourier-transform infrared (FTIR) spectroscopy. FTIR spectra of nanoparticles and individual pure material were obtained and compared (Figure 4.2). The peak at 1693 cm^{-1} confirms the presence of imidazolidine-2-one (C=O) stretch of pimozone (Figure 4.2). In the literature, this peak was reported at the wavenumber of 1698 cm^{-1} (Smyj, Wang and Han, 2012), 1696 cm^{-1} (PubChem, 2021), and 1685 cm^{-1} (Vengala, Dintakurthi and Subrahmanyam, 2013). On the other hand, the peak at 1751 cm^{-1} confirms the presence carbonyl group (C=O) found in the two monomers of PLGA (Figure 4.2). This was again verified by a literature values of 1758 cm^{-1} (Frasco *et al.*, 2015), 1746 (Abrego *et al.*, 2014), and 1739 cm^{-1} (Girotra, Singh and Kumar, 2016).

It can be noticed that pimozone's peaks (C=O, and other functional groups) are absent in nanoparticles (Formulation S1), as shown in Figure 4.2. This indicates that pimozone was loaded within the PLGA matrix. Also, any other major shifting or loss of functional groups of PLGA was absent in nanoparticles. In other words, the spectrum of pure PLGA resembled with the spectrum of nanoparticles, confirming that all materials were compatible to each other within the nanoparticles. However, the peak intensity at 1751 cm^{-1} was noticed to be reduced slightly in nanoparticles. This could be due to the stretching vibration of C=O group of pimozone within PLGA matrix.

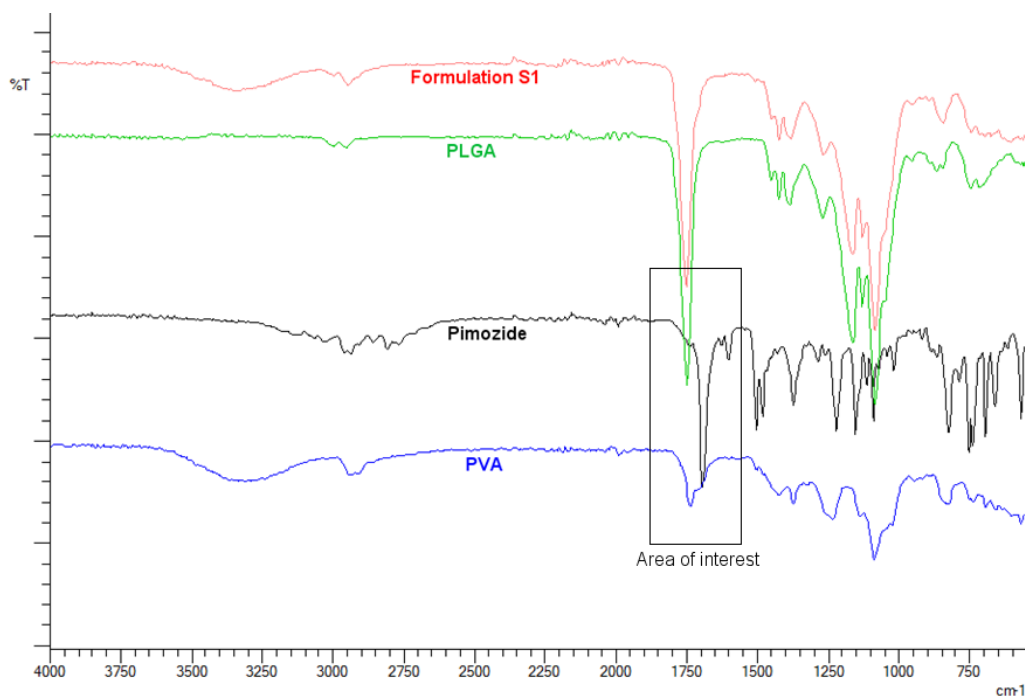


Figure 4.2: Overlay of FTIR spectra confirming pimozide loading within the PLGA. Formulation S1 was comprised of 24-38 kDa PLGA, pimozide, and PVA (Table 4.1).

Drug loading, chemical interactions, and compatibility were further confirmed by differential scanning calorimetry (DSC) analysis. DSC thermograms define the physical state of the drug and polymer within the nanoparticles and, are useful in detecting their interactions. Drug molecule can either crystallise or remain dispersed within PLGA matrix after encapsulation. If the drug crystallizes, its melting peak will appear in the DSC thermogram of the nanoparticles. If the drug molecule was dispersed with PLGA matrix, the melting peak of the drug would be absent (Graves *et al.*, 2004).

Figure 4.3 demonstrates the confirmation of pimozide loading within PLGA and any possible interactions within the excipients. An endothermic peak of pimozide was found at 220.66°C, indicating its melting temperature (Figure 4.3a). Pimozide-loaded PLGA nanoparticles showed glass transition temperature (T_g) peak at 53.45°C (Figure 4.3b). It can be observed that pimozide's melting temperature peak is absent in PLGA nanoparticles, confirming the absence of its crystalline form in the PLGA nanoparticles (Figure 4.3b). The other minor peaks were due to the presence of surfactant (polyvinyl alcohol) in small amount in the formulation. Therefore, it can be confirmed that the pimozide was present in the amorphous phase and it was homogeneously dispersed in the PLGA matrix. Further, any incompatibility between pimozide and excipients was absent.

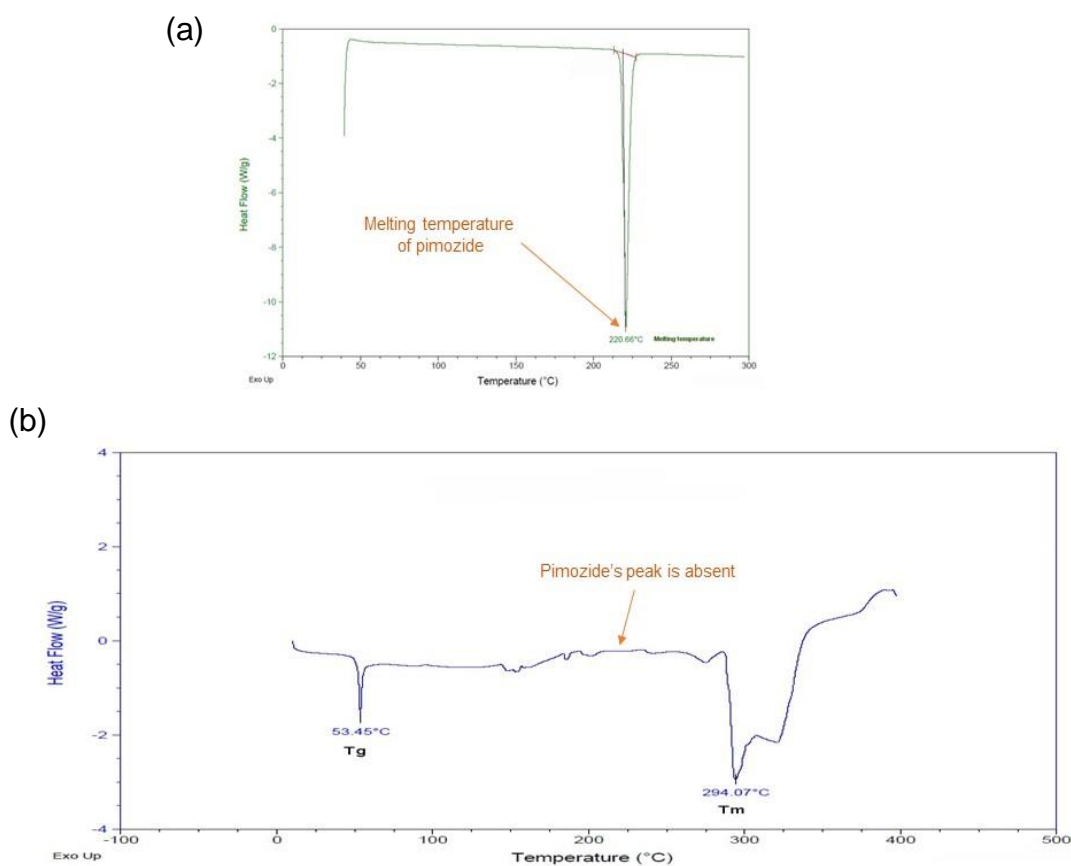


Figure 4.3: Differential scanning calorimetry (DSC) thermograms confirming pimozone's loading and interaction with PLGA nanoparticles.

(a) Thermogram of pimozone showing its melting temperature peak at 220°C. (b) Thermogram of pimozone-loaded PLGA nanoparticles (Formulation S1). Downward peak represents endothermic reactions. T_g, glass transition temperature; and T_m, melting temperature of PLGA.

Taken together, PLGA nanoparticles prepared by SE method has shown successful pimozone loading within PLGA matrix. Furthermore, there was no chemical incompatibility found between pimozone, PLGA, and PVA. Based on this finding, further formulations would be prepared by varying preparation method, surfactant, and chemical type of PLGA.

4.3.2. Effect of preparation method

PLGA nanoparticles can be prepared by several methods as described in chapter 1 (Section 1.2.4.2). This study selected single emulsion-solvent evaporation (SE) and microfluidic (MF) methods. SE is the most common method that is used to prepare hydrophobic small molecule loaded PLGA nanoparticles. This was already proven in previous section. On the other hand, microfluidic is the advanced version of nanoprecipitation method that is used for controlled production of either hydrophobic, or hydrophilic, or both drug-loaded PLGA nanoparticles (Xu *et al.*, 2017).

Initially, eight formulations were designed, with varying compositions. These formulations were prepared by both SE and MF methods, according to the procedures described in chapter 2 (Section 2.2.1), leading to a total of sixteen preliminary formulations (Table 4.2). Beside the preparation method, further independent variables were two different surfactants (PVA and polysorbate 80), and two different terminal groups of PLGA (acid and ester terminated PLGAs).

Table 4.2: Preliminary formulation compositions with varying parameters.

Formulation code	Preparation method	Pimozide load (2.5% w/w)	Type of PLGA	Surfactant
F1	SE ¹	+	AT ³	PVA ⁵
F2	SE	+	AT	Tween
F3	SE	+	ET ⁴	PVA
F4	SE	+	ET	Tween
F5	SE	-	AT	PVA
F6	SE	-	AT	Tween
F7	SE	-	ET	PVA
F8	SE	-	ET	Tween
F9	MF ²	+	AT	PVA
F10	MF	+	AT	Tween
F11	MF	+	ET	PVA
F12	MF	+	ET	Tween
F13	MF	-	AT	PVA
F14	MF	-	AT	Tween
F15	MF	-	ET	PVA
F16	MF	-	ET	Tween

¹Single emulsion; ²Microfluidics; ³Acid terminated; ⁴Ester terminated; ⁵Polyvinyl alcohol

Prepared formulations were characterised in terms of particle size, polydispersity index (PDI), zeta potential, and encapsulation efficiency (EE), as summarised in Table 4.3. Two methods were then compared based on these properties and their comparisons were presented in Figure 4.4.

Table 4.3: Characterisation of the preliminary formulations.

Formulation code	Preparation method	Particle size (nm)	PDI ³	Zeta potential (mV)	EE ⁴ (%)
F1	SE ¹	246 ± 3.4	0.218 ± 0.02	-2.6 ± 0.8	72 ± 7.8
F2	SE	289 ± 96	0.359 ± 0.08	-17 ± 4.1	34 ± 12
F3	SE	276 ± 19	0.291 ± 0.05	-1.1 ± 0.2	47 ± 0.1
F4	SE	357 ± 22	0.510 ± 0.06	-8.2 ± 0.3	35 ± 8.5
F5	SE	242 ± 7.9	0.201 ± 0.03	-3 ± 1.2	-
F6	SE	272 ± 4.3	0.328 ± 0.01	-22 ± 3.2	-
F7	SE	247 ± 11	0.221 ± 0.02	-2 ± 0.9	-
F8	SE	301 ± 37	0.324 ± 0.03	-21 ± 2.4	-
F9	MF ²	235 ± 9.5	0.285 ± 0.05	-2.2 ± 0.1	80 ± 6.7
F10	MF	145 ± 20	0.363 ± 0.02	-21 ± 1.1	74 ± 4.5
F11	MF	198 ± 10	0.270 ± 0.03	-3.5 ± 0.4	71 ± 4.3
F12	MF	128 ± 6.3	0.137 ± 0.04	-14 ± 1.8	51 ± 3.8
F13	MF	165 ± 3.1	0.097 ± 0.02	-3.5 ± 1.7	-
F14	MF	187 ± 2.4	0.192 ± 0.02	-31 ± 1.8	-
F15	MF	228 ± 12	0.166 ± 0.02	-1.7 ± 0.4	-
F16	MF	202 ± 9.2	0.210 ± 0.02	-30 ± 0.6	-

¹Single emulsion; ²Microfluidics; ³Polydispersity index; ⁴Encapsulation efficiency. Data are mean ± SD (n=3). EE was calculated by both UV-Visible spectroscopy and ultra-high-performance liquid chromatography. However, the mean differences of EEs found in these two techniques were not statistically significant (Appendix 5).

As demonstrated in Figure 4.4a, mean particle sizes were found to be 278 ± 38 nm and 186 ± 37 nm prepared in SE and MF methods, respectively. Statistical analysis indicated that significantly smaller particles were produced by MF method compared to SE method (**p=0.007, paired *t*-test). Predictably, lower polydispersity index (PDI) value (~0.2), although not statistically significant, was observed in MF-based nanoparticles than that of SE-based nanoparticles (Figure 4.4b). This indicates that more monodispersed nanoparticles were produced in MF method.

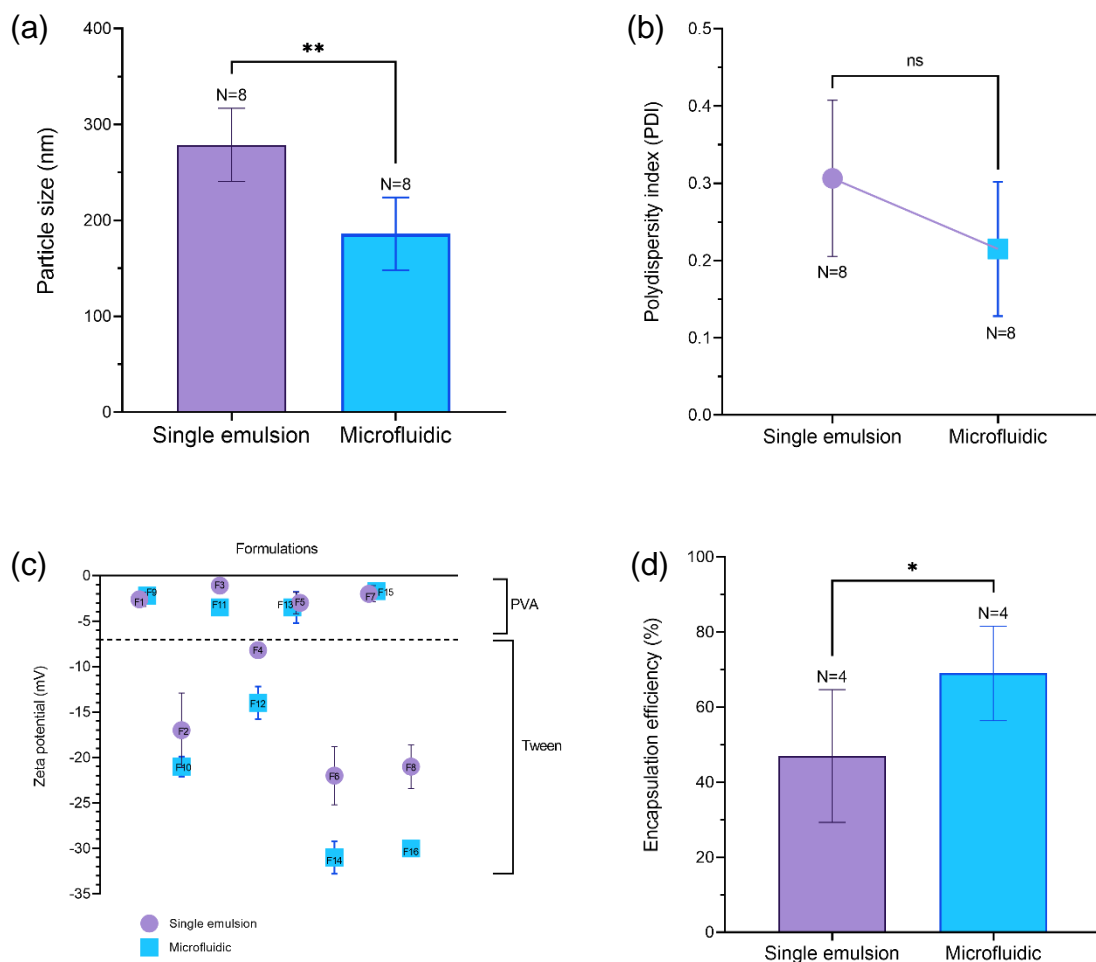


Figure 4.4: Effect of preparation methods on physicochemical characteristics of PLGA nanoparticles.

(a) Effect on particle size (nm); (b) Effect on polydispersity index; (c) Effect on zeta potential (mV); and (d) Effect on drug encapsulation efficiency (%). Data presented are mean \pm SD (of N), where 'N' is the total number of independent formulations, as described in Table 4.2. Asterisks (* $p=0.033$ and ** $p=0.002$) denote that the mean difference is statistically significant ($p<0.05$), while 'ns' stands for statistically not significant (paired t-test).

Similar trend in particle sizes due to using different preparation methods was observed in a study that observed that rutin-loaded PGLA nanoparticles prepared by MF method were significantly smaller and more homogenous than that of nanoparticles prepared by SE method (Vu *et al.*, 2019). It could be because MF method provided homogenous reaction environment, ultrafast and controlled mixing, and mixing at a fixed temperature. On the other hand, these properties were absent in SE method. Xie and Smith (2010) found that particle size and size distribution differed from one method to another even they used same PLGA concentration and solvent.

Apparently, zeta potential values of PLGA nanoparticles vary with types of surfactants used. Almost neutral zeta potential value (-1 to -3.5 mV) was observed in all PVA stabilised formulations, while more negative values (-8 to -31 mV) were observed in tween stabilised formulations (Table 4.3). As shown in Figure 4.4c, preparation method did not have any significant effect on zeta potential value of PVA stabilised nanoparticles. However, tween stabilised nanoparticles produced by MF method showed higher negative value than that of nanoparticles produced by SE method ($p < 0.05$, paired *t*-test). Differently, Vu *et al.* (2019) found high negative zeta potential value in PVA stabilised PLGA nanoparticles, this could be due to the use of a different drug molecule (rutin) than pimozone. Notably, their MF method produced higher negative zeta potential value (-32 mV) than that of SE method (-16 mV). This difference could be due to the use of more concentrated PVA (3.4%) in SE method than in MF method (1%). In this case, the use of same concentration in both methods would have provided conclusive results of comparison.

Drug encapsulation efficiency (EE) of PLGA nanoparticles is compared in Figure 4.4d. It can be observed that mean EE of MF-based nanoparticles is higher ($69 \pm 12\%$) than that of SE-based nanoparticles ($47 \pm 17\%$). The mean difference was found statistically significant ($p = 0.049$, paired *t*-test). Low EE in SE-based nanoparticles can be explained by the intermediate steps of the method. During solvent evaporation process, which was facilitated by magnetic stirring, there could be a chance of pimozone diffusion out of the PLGA nanoparticles, resulting in loss of entrapped drug. Vu *et al.* (2019) also found higher EE ($34 \pm 2\%$) in MF-based PLGA nanoparticles than in SE-based nanoparticles ($27 \pm 1\%$). Similarly, another study found EEs of 48.79% and 1.29% of a drug candidate (cucurbitacin I) in MF and SE-based based nanoparticles, respectively (Alshamsan, 2014). This could be due to the relative polarity of the drug that might have interfered with its loading into PLGA matrix in emulsion method.

To further compare the preparation method, drug release profile of two representative formulations, namely F1 and F9 (Table 4.2), from each method were investigated following the procedure, as described in Chapter 2, Section 2.2.2.7. Cumulative drug release was calculated from the recovered drug in the released sample and drug EE of the corresponding formulation.

As shown in Figure 4.5, MF-based PLGA nanoparticles burst released $10 \pm 4\%$ of pimozone in the first hour. After 4 hours, the cumulative release reached to $18 \pm 6\%$. In contrast, burst release of pimozone was absent in SE-based nanoparticles in the first hour, however, it was observed after 4 hours with only $6 \pm 3.9\%$ pimozone released. After 144 hours, cumulative pimozone releases for MF and SE-based nanoparticles were $68 \pm 4\%$ and $37 \pm 6\%$,

respectively. The mean difference of drug releases at each time interval was found to be statistically significant ($p < 0.05$, paired t-test). These results indicate that SE-based nanoparticles delayed the release of pimozone than that of MF-based nanoparticles. This could be due to the solvent evaporation process during nanoparticles preparation in SE method. Emulsions were solidified by removal of solvent. It was possible that nanoparticles were hardened too much in this process, causing slow degradation of PLGA that led to slow pimozone release. Vu *et al.* (2019) found similar trend when release profile of rutin-loaded PLGA nanoparticles was studied in PBS at pH 7.4. Authors found released rutin of 78% and 64% in MF and SE-based nanoparticles after 24 hours. Slower release of drug in SE-based nanoparticles can be further explained by the larger particle size. Larger particles have lesser surface area, resulting in slower degradation of PLGA that leads to slower release of entrapped pimozone. On the contrary, MF-based smaller particles have larger surface area, leading to faster degradation of PLGA and subsequently faster pimozone release.

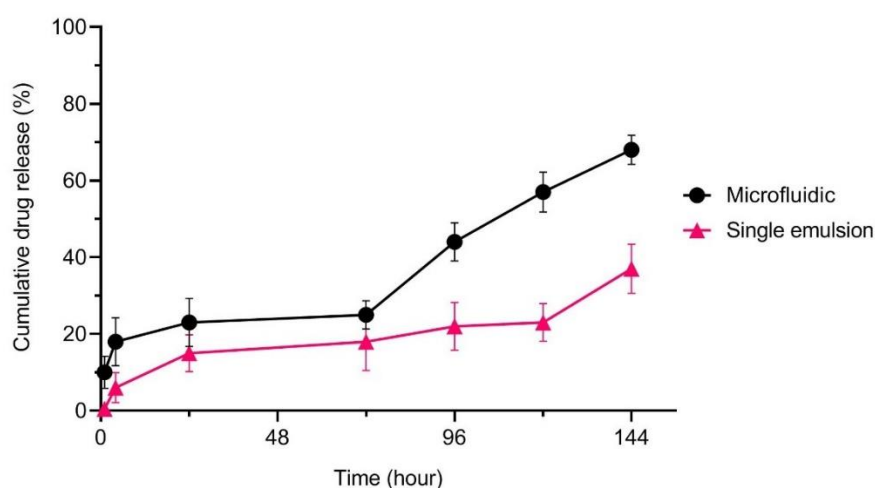


Figure 4.5: Effect of preparation methods on pimozone release profile of PLGA nanoparticles
 Data presented are mean \pm SD ($n=3$). Microfluidic and single emulsion methods correspond to the formulation F1 and F9, respectively in Table 4.2. Freeze-dried nanoparticles were incubated in phosphate-buffered saline (PBS) with agitation at 37°C, pH 7.4 for 144 hours. Sample collection at each time interval was followed by replenishing fresh PBS. The mean difference of drug releases at each time interval was statistically significant ($p < 0.05$, paired t-test).

Pimozone was efficiently encapsulated into PLGA nanoparticles by both SE and MF methods. However, both methods exhibited differences in terms of particle, size, shape, and drug encapsulation efficiencies. It is known that microfluidic method produces PLGA nanoparticles in controlled manner, resulting uniform particles. Further, tuning the flow and rate of aqueous and organic phases enables microfluidic method to produce desired smaller

particles with highly loaded drug molecules than emulsion method. Moreover, microfluidic becomes ultimately a cost-effective nanomedicine production method as it saves significant amount solvent waste compared to emulsion-solvent evaporation method. Therefore, given all advantages of microfluidic method, this study would exclude single emulsion method in further experiments.

4.3.3. Effect of freeze-drying

Nanosuspension undergoes physical and chemical instabilities with time. Removal of water (by freeze-drying) from nanosuspension can avoid hydrolytic degradation of PLGA matrix. However, freeze-drying could alter the properties of PLGA nanoparticles, such as particle size.

This study investigated the effect of freeze-drying on particle size by comparing six formulations before and after freeze-drying. As demonstrated in Figure 4.6, it was observed that particles before freeze-drying are sub 400 nm in all formulations. In contrast, after freeze-drying, a significant rise of particle size in each formulation was observed. The mean difference was statistically significant ($p=0.013$, paired t -test). These results confirm freeze-drying process increased the particles size. This could be due to the absence of cryoprotectants in nanoparticles prior to freeze-drying. Yet, particles have uniform smooth spherical appearance, with absence of pores on surface (Figure 4.7).

Often freeze drying is used to preserve unstable materials, by increasing their shelf lives. For example, heat-sensitive materials such as, proteins, pharmaceuticals, microbes, tissues, and plasma can be preserved for longer time. Freeze drying can reduce the weight of the products, which are easy to transport. Freeze drying enhances the solubility of an insoluble material. However, freeze-drying leads to several physical instability of the nanoparticles, such as aggregation, fusion and drug leakage (Trenkenschuh and Friess, 2021).

Freeze-drying process aggregates PLGA nanoparticles and results poor dispersibility once they are rehydrated in the aqueous medium (Murakami *et al.*, 1997). Further, it increases porosity of the particles, leading to undesirable initial burst release of drug. However, on the bright side, freeze-drying increases colloidal stability, by maintaining smooth spherical shape. Further, it slows the drug release once PGLA nanoparticles are treated with cryoprotectants (Fonte *et al.*, 2015).

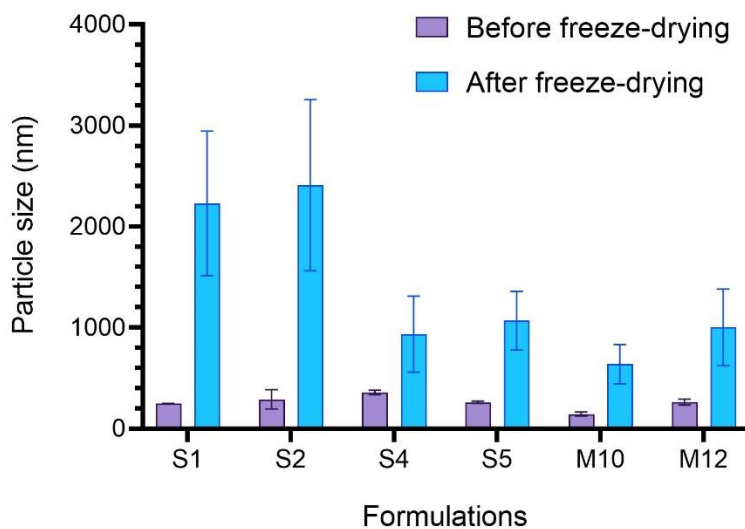


Figure 4.6: Effect of freeze-drying on PLGA nanoparticles particle size.

Data are mean \pm SD ($n=3$). Particle size was measured immediately after the collection of prepared nanoparticles. Again, particle size of freeze-dried nanoparticles was measured by resuspending particles in distilled water. Compositions of formulations (S1, S2, S4, S5, M10, and M12) can be found in Table 4.2.

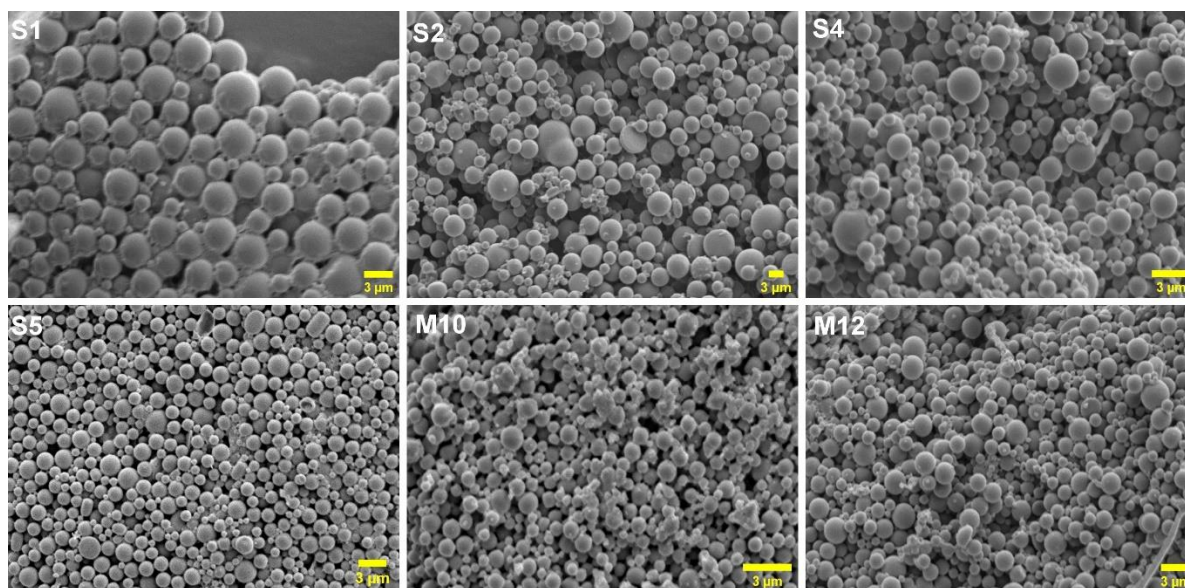


Figure 4.7: Scanning electron microscopy (SEM) images showing larger particle size in freeze-dried nanoparticles.

Montage of SEM images was produced from formulations S1, S2, S4, S5, M10, and M12 (refer Table 4.2 for formulation compositions). Scale bar indicates 3 μ m.

Cryoprotectants, such as glucose, lactose, sucrose, trehalose, and mannitol prevent PLGA nanoparticles from aggregation. They affect glass transition temperature (T_g) of PLGA nanoparticles, resulting high redispersion speed and more stability upon storage (Yesenia Hernández-Giottonini *et al.*, 2020).

In particular, sucrose and trehalose as cryoprotectants increase the T_g of PLGA nanoparticles, by forming an amorphous mass, subsequently maintaining the integrity of the nanoparticles during the storage or after reconstitution (Holzer *et al.*, 2009).

Increased stability by cryoprotectant can be also explained in terms of zeta potential. Addition of trehalose, sucrose, fructose, glucose, and sorbitol individually increases the anionic nature of PLGA nanoparticles. In other words, these sugars, once added with PLGA nanoparticles, show higher negative zeta potential than PLGA nanoparticles alone. This leads to occur more particle-particle repulsion, thus preventing particles aggregation, consequently increasing stability of the particles (Fonte *et al.*, 2015). Notably, freeze-drying PLGA nanoparticles with cryoprotectant preserves the drug molecule (insulin) better than nanoparticles without cryoprotectants (Fonte *et al.*, 2016).

Hydroxypropyl- β -cyclodextrin (HP β CD) is also used as a cryoprotectant, which does not allow PLGA nanoparticles to aggregate (Parra *et al.*, 2015). This attributes to the cyclic structure of these oligoglucoside compounds that ensured better adsorption on the surface of PLGA nanoparticles during freeze-drying.

Interestingly, Abrego *et al.* (2014) found that particle size remained similar when compared before freeze-drying PLGA nanoparticles with after freeze-drying nanoparticles. Authors explained that PVA acted as both surfactant and cryoprotectant, which was attributed to its high molecular weight that prevented agglomeration of particles during freeze-drying. However, PVA and tween stabilised PLGA nanoparticles were found to be aggregated after freeze-drying in current study. Therefore, further surfactants would be investigated to avoid this problem, and to improve particle properties.

4.3.4. Effect of surfactants on particle size, charge, drug encapsulation and drug release profile

Surfactants are also known as surface-active agents that decrease the surface tension of the emulsion droplets. Surfactants allows emulsions to be broken into smaller droplets during mixing. They have both hydrophilic and hydrophobic tails in their molecules. These tails react with respective water and oil phase at the interface, resulting formation of barriers around the dispersed droplets, preventing them from aggregation, consequently maintaining the stability of the emulsions. The barriers are formed by electrostatic repulsion, steric hindrance, and creation of bound water layer. In fact, the formation of barriers depends on the types of surfactants used (Miller, 2016). Further, different types and concentrations can alter the properties of colloidal droplets, such as particle size, distribution, charge, and stability (Shkodra-Pula *et al.*, 2019; Esim *et al.*, 2020).

It was aimed to investigate the effect of four surfactants (and one dual surfactants system) on the physicochemical properties of PLGA nanoparticles. Selected surfactants at a fixed concentration of 1.25% w/v were polyvinyl alcohol (PVA), polysorbate 80, poloxamer 188, D- α -tocopheryl polyethylene glycol succinate (TPGS), and PVA-TPGS (1:1). Surfactant-free formulation was used as a control. Among them PVA and tween stabilised nanoparticles were already prepared in previous experiments (Table 4.2 and Table 4.3). Therefore, further nanoparticles were prepared with rest of the surfactants (Table 4.4). Recorded physicochemical properties are demonstrated in Table 4.5. All surfactants were compared based on the physicochemical properties of drug-loaded nanoparticles (Figure 4.9).

Table 4.4: Compositions of formulations with different surfactants.

Formulation code	Pimozide load (2.5% w/w)	Type of PLGA	Surfactant (1.25% w/v)
F17	+	AT	Poloxamer
F18	+	ET	Poloxamer
F19	-	AT	Poloxamer
F20	-	ET	Poloxamer
F21	+	AT	TPGS
F22	+	ET	TPGS
F23	-	AT	TPGS
F24	-	ET	TPGS
F25	+	AT	PVA-TPGS
F26	+	ET	PVA-TPGS
F27	-	AT	PVA-TPGS
F28	-	ET	PVA-TPGS
F29	+	AT	Distilled water
F30	+	ET	Distilled water
F31	-	AT	Distilled water
F32	-	ET	Distilled water

AT, acid terminated; ET, ester terminated; PVA-TPGS (1:1)

4.3.4.1. Polyvinyl alcohol (PVA)

Polyvinyl alcohol (PVA) is extensively used as a surfactant during the preparation of nanoparticles. PVA is a water-soluble synthetic polymer (Figure 4.8), which can be classified into two groups, such as partially hydrolysed and fully hydrolysed. Highly hydrolysed PVA (such as, 91-99%) has more adhesion to hydrophilic surfaces and is more stable in presence of organic solvents than that of less hydrolysed PVA (such as, 87-89%). In other words, partially hydrolysed PVA is more water soluble and has more adhesion to hydrophobic surfaces (Rivera-Hernández *et al.*, 2021). Partially hydrolysed PVA provides desired stability to the PLGA nanoparticles (Shkodra-Pula *et al.*, 2019).

PVA is prepared from polyvinyl acetate by replacing acetate groups with hydroxyl groups (PubChem Database, 2021). These hydroxyl groups create inter and intra molecular hydrogen bonding, which is responsible for its rheological and mechanical properties. Basically, the density and spatial arrangement of hydroxyl groups determine its properties. These hydrogen bonds also produce phase separation and gelation, meaning solutions are

time-dependant. Furthermore, PVA solutions are rheologically heterogenous, indicating they exhibit Newtonian and non-Newtonian flow behaviour (Rivera-Hernández *et al.*, 2021).

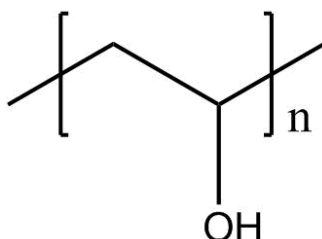


Figure 4.8: Structure of polyvinyl alcohol (PVA).

Addition of surfactants increases the particle size of PLGA nanoparticles (Shkodra-Pula *et al.*, 2019). It was observed that PVA stabilised PLGA nanoparticles were significantly larger in size (216 ± 26 nm) compared to control, which are surfactant-free nanoparticles (

Figure 4.9a). However, in both cases polydispersity index value was found to be less than 0.3 (Figure 4.9b). PVA are adsorbed on the surface of PLGA nanoparticles by hydrophobic interactions. Abundant hydroxyl groups of PVA could be hydrated at the surface to stabilise PLGA nanoparticles. Strong hydrogen bonds are formed between inter or intra molecules of PVA. Solvent from oily phase hinders the hydration of PVA at the interface, leading to create PVA-PVA network. Once the degree of hydrolysis gets higher, the hydration is again obstructed because of increased hydrogen bonds between inter and intra molecules of PVA. Consequently, this produces aggregated PLGA nanoparticles, leading to larger particle size (Murakami *et al.*, 1997).

Other studies also reported large particle size (>300 nm) in PVA stabilised PLGA nanoparticles (Abrego *et al.*, 2014; Sharma, Madan and Lin, 2016). In contrast, another study reported that PVA stabilised nanoparticles became significantly smaller (<300 nm) compared to surfactant free nanoparticles (Haggag *et al.*, 2018).

Table 4.5: Physicochemical properties of nanoparticles stabilised by different surfactants.

Formulation code	Particle size (nm)	PDI ^a	Zeta potential (mV)	EE ^b (%)
F17	390 ± 49	0.470 ± 0.05	-20 ± 2.5	54 ± 9.9
F18	324 ± 20	0.372 ± 0.10	-19 ± 8.2	43 ± 9.6
F19	173 ± 2	0.392 ± 0.03	-33 ± 3.5	-
F20	162 ± 0.6	0.349 ± 0.01	-23 ± 2.9	-
F21	52 ± 2	0.241 ± 0.05	-21 ± 1.4	72 ± 5
F22	91 ± 5	0.190 ± 0.02	-19 ± 1.1	60 ± 9
F23	225 ± 1	0.187 ± 0.02	-39 ± 1.3	-
F24	231 ± 6	0.186 ± 0.02	-40 ± 0.9	-
F25	191 ± 0.7	0.071 ± 0.02	-3.7 ± 0.2	74 ± 3.8
F26	219 ± 11	0.116 ± 0.03	-5.6 ± 0.6	69 ± 4.7
F27	192 ± 1	0.108 ± 0.01	-7.1 ± 1.9	-
F28	213 ± 2	0.093 ± 0.03	-5.9 ± 0.6	-
F29	79 ± 4	0.195 ± 0.01	-23 ± 3.8	54 ± 3.6
F30	86 ± 5.8	0.205 ± 0.02	-21 ± 4.1	51 ± 4.8
F31	197 ± 9	0.104 ± 0.01	-38 ± 1.3	-
F32	205 ± 8	0.164 ± 0.02	-38 ± 2.0	-

^aPolydispersity index; ^bDrug encapsulation efficiency

Particle size is also PVA concentration dependent. Abdelkader *et al.*, (2018) observed particle size of ~250 nm at 1.25% w/v PVA concentration. However, nanoparticles were prepared by double emulsion-solvent evaporation method in their study. Authors concluded that particle size was directly proportional to the PVA concentration. Similar trend was observed by Roces, Christensen and Perrie (2020), reporting largest particle size (~300 nm) with highest PVA concentration (2% w/v) used in their microfluidic-based study. In contrast, a SE method-based study found smaller particles when PVA concentration was increased from 3 to 4%, however, authors observed larger particles when PVA concentration was further increased from 4 to 6% (Vu *et al.*, 2019). Interestingly, another study found comparatively smaller particle size (150-200 nm) in 5% PVA stabilised PLGA nanoparticles (Mathew *et al.*, 2012).

As demonstrated in

Figure 4.9c, a significant difference was observed in zeta potential between PVA-stabilised nanoparticles (-2 ± 0.9 mV) and control (-20 ± 1.4 mV). Other studies also found almost neutral zeta potential value in PVA-stabilised PLGA nanoparticles (Abrego *et al.*, 2014; Sahin *et al.*, 2017; Abdelkader *et al.*, 2018; Robin *et al.*, 2021). The neutral zeta potential can be explained by the presence of residual PVA chains that shield the anionic surface charge of PLGA (Robin *et al.*, 2021). In contrast, Mathew *et al.* (2012) found negative zeta potential (-20 to -30 mV) in 5% w/v PVA stabilised curcumin-loaded PGLA nanoparticles prepared by single emulsion-solvent evaporation method.

Figure 4.10 demonstrates the drug release profile from PLGA nanoparticles stabilised by different surfactants. A slow drug release profile in PVA stabilised nanoparticle was observed. After 10% initial burst release, a total of $68 \pm 3\%$ pimoziide is released in 6 days. Low burst release of drug indicates that there is less amount of drug molecule attached on the PLGA surface, while rest of the drug molecules are trapped within the PLGA matrix that get released slowly over the time based on degradation profile of PLGA (El-Hammadi *et al.*, 2017).

Haggag *et al.* (2018) found more (19 to 47%) initial burst release of 5-fluorouracil from PLGA nanoparticles prepared by double emulsion method. Notably, authors observed that initial burst release and total release of drug decreased due to the addition of PVA.

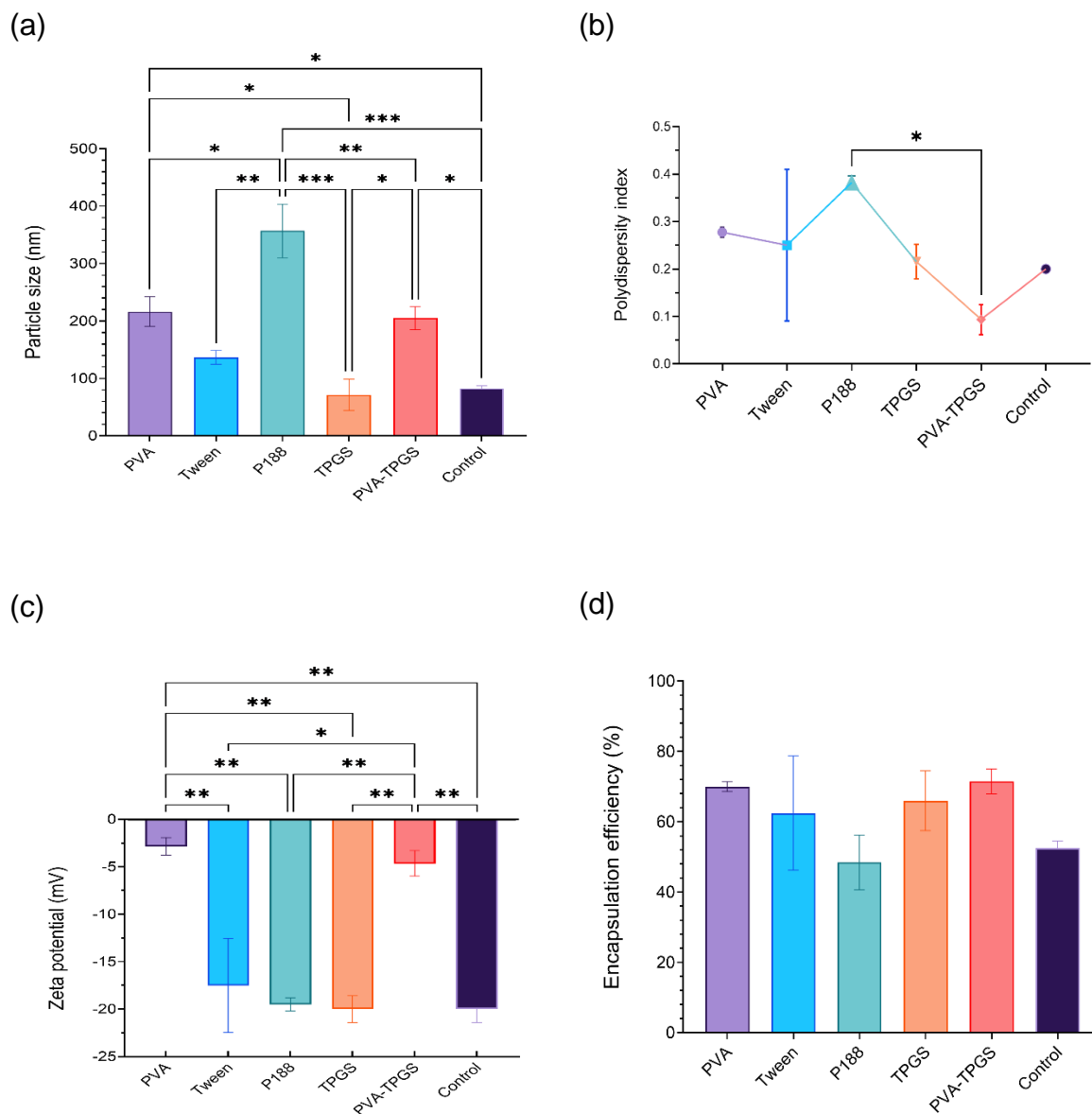


Figure 4.9: Effect of different surfactants on physicochemical properties of PLGA nanoparticles.

Effect of surfactant on (a) Particle size; (b) polydispersity index; (c) zeta potential (d) drug encapsulation efficiency. Data presented are mean \pm SD (n=6). Mean differences were compared by one-way ANOVA (* $p=0.033$, ** $p=0.002$ and *** $p<0.001$ denote statistically significant). Surfactant-free (distilled water only) formulations were used as control. Concentration of all surfactants was 1.25 w/v.

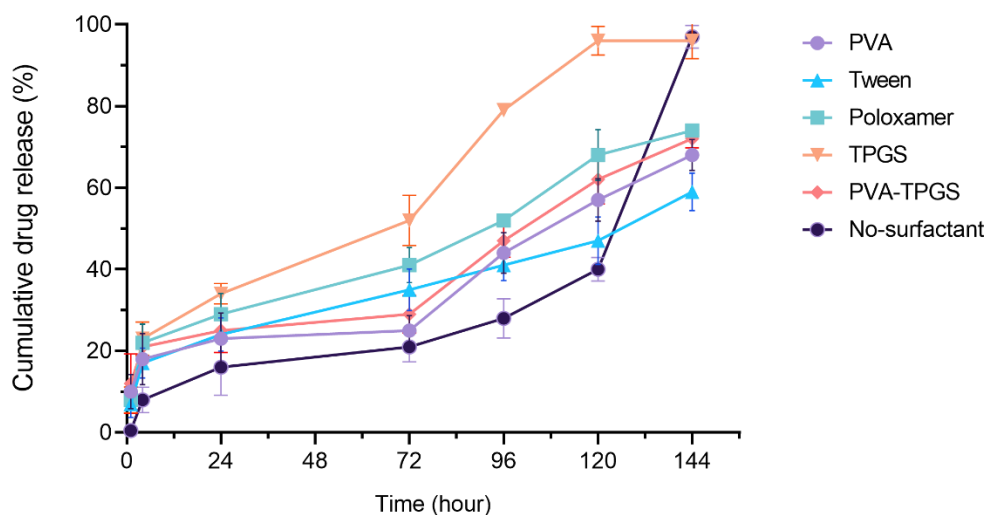


Figure 4.10: Effect of surfactants on drug release profile of PLGA nanoparticles.

Data are mean \pm SD ($n=3$). Surfactant stabilised nanoparticles (freeze-dried) were suspended in phosphate-buffered saline (pH 7.4). Released drug (pimozide) was analysed by HPLC in different time interval up to 144 hours.

4.3.4.2. Polysorbate 80

Polysorbates are synthetic nonionic surfactants used in pharmaceutical preparation. They are derived from ethoxylated sorbitan and fatty acids (such as, lauric, palmitic, stearic, and oleic acids) by esterification. Polysorbates are classified into different types, such as polysorbate 20, 40, 60, and 80 depending on the fatty acids. Figure 4.11 demonstrates the chemical structure of polysorbate 80, which contains oleic acid and total 20 polyoxyethylene.

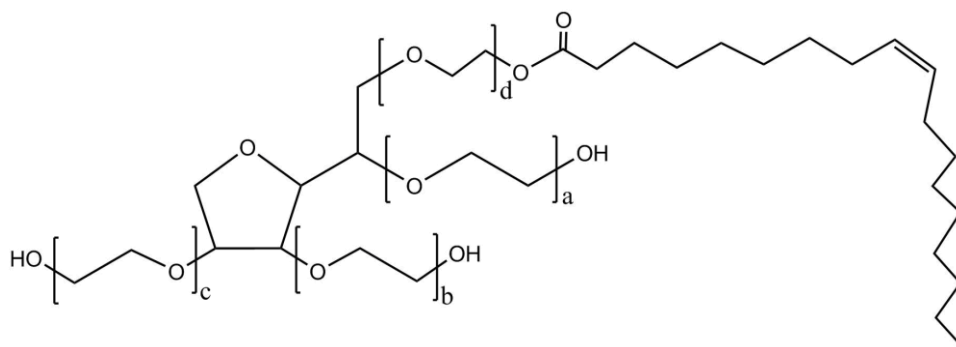


Figure 4.11: Chemical structure of polysorbate 80.

Here, total number of polyoxyethylene is 20 ($a+b+c+d=20$), where '80' denotes monooleate, which is a naturally occurred fatty acid.

Tween 80 is a trade name of polysorbate 80. It was observed that tween stabilised PLGA nanoparticles had mean particle size of $136 \pm 12\text{nm}$ (PDI <0.3), which was larger than the control but smaller than PVA stabilised particles (

Figure 4.9a and

Figure 4.9b). However, the mean differences were not statistically significant.

Studies reported particle size of 50-150 nm in polysorbate 80 stabilised PLGA nanoparticles at a concentration of 1% v/v (Hoda *et al.*, 2016; Sufi *et al.*, 2020). Notably, both studies encapsulated different drug molecules by different preparation methods, however, both studies observed that the empty nanoparticles were smaller than the drug-encapsulated nanoparticles. Shkodra-Pula *et al.* (2019) observed $159 \pm 2\text{ nm}$ particle size with 3% w/v Tween 80, prepared by nanoprecipitation method.

It was observed Tween 80 stabilised nanoparticles had high negative zeta potential value of $-17 \pm 4\text{ mV}$ (

Figure 4.9c). This finding was consistent with Monge *et al.* (2020) who reported zeta potential value of -17 to -22 mV in all formulations.

Tween stabilised PGLA nanoparticles release $59 \pm 4\%$ pimozone in 6 days, which was lower than PVA, however, not statistically significant (Figure 4.10). Sufi *et al.*, (2020) reported $93 \pm 5\%$ drug release after 96 hours.

4.3.4.3. Poloxamer 188

Poloxamers are nonionic triblock copolymers arranged in the form of ABA (Figure 4.12). The central block is made of polypropylene oxide, which is hydrophobic in nature. Two side blocks are made of hydrophilic polyoxyethylene. Thus, poloxamers can provide amphiphilic properties. Properties of poloxamers can be customised by changing the length of constituting blocks. For example, poloxamer 188 is one specific type that has 80% hydrophilic polyoxyethylene on both sides and 1800 g/mol hydrophobic polypropylene oxide on the centre.

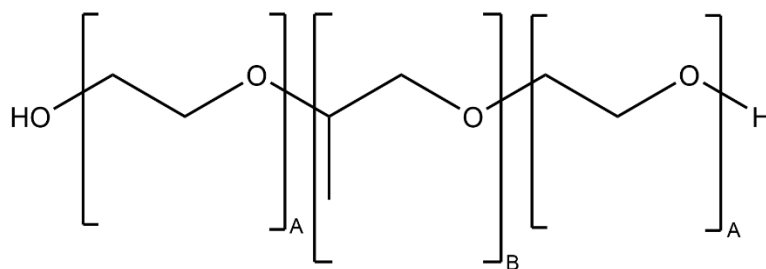


Figure 4.12: Chemical structure of poloxamer.

'A' denotes the hydrophilic chain polyethylene oxide and 'B' denotes hydrophobic chain polypropylene oxide.

Significantly larger particle size (357 ± 46 nm, PDI 0.382) was observed in poloxamer stabilised nanoparticles compared to surfactant-free nanoparticles, as demonstrated in

Figure 4.9a and

Figure 4.9b. PLGA interacts with poloxamer by hydrophobic interactions, meaning polypropylene oxide chain of poloxamer interacts with PLGA, while extending its two hydrophilic side chains towards aqueous phase, thus stabilising PLGA nanoparticles. Increased particle size and size distribution can be explained by lesser number of hydrophobic units than hydrophilic units present in the poloxamer. Therefore, washing off freshly prepared PLGA nanoparticles could potentially break the hydrophobic interactions between PLGA surface and polypropylene oxide chain of poloxamer. As a result, unstable polydisperse particles are formed after purification, leading to increased particle size and PDI (Shkodra-Pula *et al.*, 2019).

Contrary to these findings, Lababidi *et al.* (2019) observed that 1% w/v poloxamer helped reduce particle size from 90 nm to 70 nm. Other studies also found smaller particles size (<200 nm), however with different drug molecules and preparation methods (Frasco *et al.*, 2015; Shkodra-Pula *et al.*, 2019).

Current study found high negative zeta potential (-19.5 ± 0.7 mV) in poloxamer stabilised nanoparticles, which is slightly less negative compared to control (

Figure 4.9c). More negative value (-27 mV) has been observed by Frasco *et al.* (2015) while preparing proteasome inhibitor-loaded PLGA nanoparticles by SE method.

Poloxamer stabilised PLGA nanoparticles show $74 \pm 1.1\%$ cumulative pimozone release in 6 six days (Figure 4.10).

release almost 100% drug within 5 days, which was significantly different from other surfactant stabilised nanoparticles (Figure 4.10).

4.3.4.1. PVA-TPGS

Particle size of PVA stabilised nanoparticles was reduced to ~205 nm when TPGS is added as co-surfactant (

Figure 4.9a). PVA-TPGS (1:1) dual surfactants stabilised nanoparticles have the most monodispersed particles with lowest PDI value of 0.094 ± 0.03 among all surfactants used. The monomers of TPGS might align on the organic/aqueous interface along with PVA to cover the organic phase droplets more efficiently. Thus, the interfacial tension between organic and aqueous phase reduces significantly, leading to smaller particle size (Sharma, Madan and Lin, 2016). In terms of surface charge, mean zeta potential value was found to be -4 ± 1.3 mV, which was slightly higher than PVA but significantly lower than TPGS (** $p=0.004$), as demonstrated in Figure 4.9c.

Findings of current study were in line with a study by Sahin et al. (2017), who compared PVA and PVA-TPGS stabilised ibuprofen loaded nanoparticles in terms of particle size, PDI, and zeta potential. Notably, authors found that drug encapsulation efficiency became almost double in PVA (0.5%)-TPGS (0.1%) stabilised nanoparticles than that of PVA (0.5%) stabilised nanoparticles. In case of drug release profile, burst release of ibuprofen within 1 hour was found to be less in PVA-TPGS stabilised nanoparticles than that of PVA stabilised nanoparticles. Same study also evaluated cytotoxic effect of PLGA nanoparticles stabilised by PVA and PVA/TPGS on human breast adenocarcinoma cells (MCF-7) and human epithelial colorectal adenocarcinoma cells (Caco-2). On both occasions PVA/TPGS stabilised nanoparticles showed higher cytotoxicity than that of PVA stabilised nanoparticles alone. However, the effect of TPGS stabilised PLGA nanoparticles alone was not explored.

PLGA nanoparticles can be prepared without any surfactants. For example, Venugopal *et al.* (2018) reported ~ 300 nm particle size with $PDI \leq 0.3$ with no surfactant. A recent study also prepared surfactant free-PLGA nanoparticles by a microfluidic method (Roces, Christensen and Perrie, 2020). In fact, authors observed that surfactant-free particles are smaller than surfactant stabilised nanoparticles and remained stable up to 4 weeks. However, Shkodra-Pula *et al.* (2019) found that surfactant-free nanoparticles aggregated after washing or shortly after storage (Shkodra-Pula *et al.*, 2019).

In summary, based on the small particle size, narrow size distribution, high negative zeta potential, high drug encapsulation efficiency, including almost 100% drug release within 5 days, this study selected TPGS stabilised formulations, F21 and F22 (Table 4.4 and Table 4.5), for further studies.

4.3.5. Effect of PLGA terminal groups

Ester group terminated PLGA (PLGA-COOR) nanoparticles and carboxylic acid group terminated PLGA (PLGA-COOH) nanoparticles were compared in terms of their physicochemical properties. Molecular weight of both types of PLGA was 24-38 kDa.

A trend was noticed in formulations F10 to F32, indicating that mean particle sizes were always smaller in acid terminated (AT) PLGA nanoparticles compared to ester terminated (ET) PLGA nanoparticles (Table 4.2; Table 4.3; Table 4.4; and Table 4.5). In addition, negative zeta potential values and drug encapsulation efficiencies were always higher in AT-PLGA nanoparticles than that of ET-PLGA nanoparticles. In particular, comparison between formulation F21 (AT-PLGA nanoparticles) and formulation F22 (ET-PLGA nanoparticles) is demonstrated in Figure 4.14.

It was found that AT-PLGA nanoparticles were significantly smaller than ET-PLGA nanoparticles (Figure 4.14a). However, an opposite trend, although statistically not significant, was observed in case of polydispersity index (PDI), where both types of particles had PDI value less than 0.3 (Figure 4.14b). This indicates that particles were monodispersed in both formulations. These results were supported by transmission electron microscopy images, in which it was observed that nanoparticles were well separated from each other (monodispersed) and are within sub 100 nm in size (Figure 4.14c and Figure 4.14d). A recent study found that free chemical end groups (-COOH, -COOR, and -OH) of PLGA did not affect the particle size distribution (Li *et al.*, 2021).

In terms of surface charge, slightly higher negative zeta potential was observed in AT-PLGA nanoparticles compared to ET-PLGA nanoparticles (Figure 4.14e). However, the mean difference was not significantly different. Yesenia Hernández-Giottonini *et al.* (2020) found significant difference in zeta potential between AT and ET-PGLA nanoparticles. Authors observed high negative zeta potential (-20 to -30 mV) in AT-PLGA nanoparticles, while having almost neutral zeta potential (-5 mV) in ET-PLGA nanoparticles. It is known that PLGA is intrinsically anionic. Positive ester terminal group creates more hydrophobic nature to the PLGA, leading to the neutral surface charge. On the other hand, negative acid terminal end creates more hydrophilic nature to PLGA, resulting high negative surface

charge. Frasco *et al.* (2015) also found high negative zeta potential (-27 mV) in acid terminated PLGA nanoparticles.

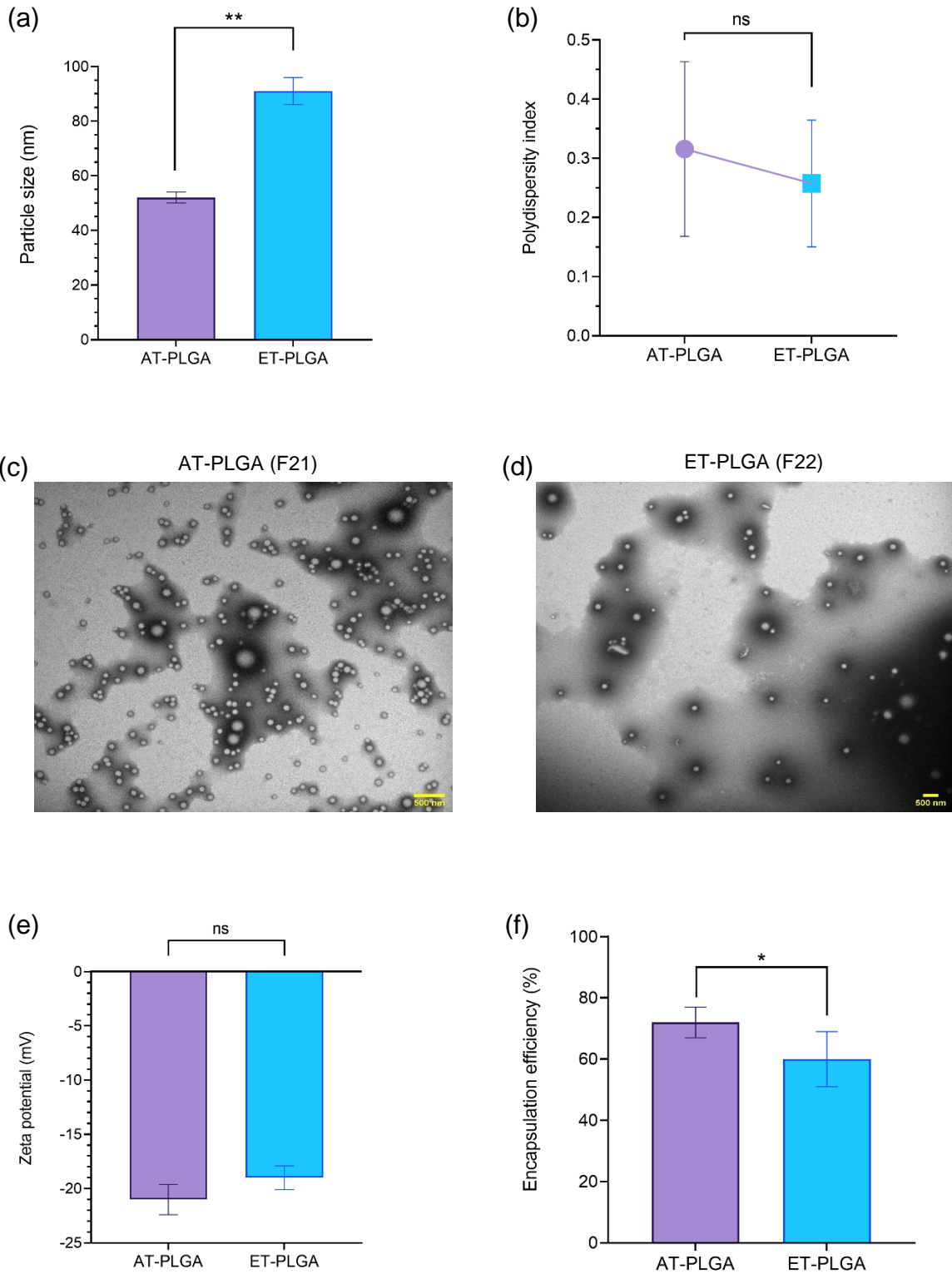


Figure 4.14: Effect of acid and ester terminal groups of PLGA on physicochemical properties of nanoparticles.

(a) Effect on particle size; (b) Effect on polydispersity index; (c) TEM image of AT-PLGA nanoparticles; (d) TEM image of ET-PLGA nanoparticles; (e) Effect on zeta potential; and (f) Effect on encapsulation efficiency (%). Data are mean \pm SD ($n=3$). Statistical significance was denoted by $*p=0.033$ and $**p=0.002$ (paired t -test). ns, statistically not significant; AT, acid terminated; ET, ester terminated; and TEM, transmission electron microscopy. Scale bar indicates 500 nm in both (c) and (d).

Drug encapsulation efficiency (EE) was found to be significantly higher in AT-PLGA nanoparticles compared to ET-PLGA nanoparticles (Figure 4.14f). Similar trend was also observed by Li *et al.* (2021), who reported that encapsulation of ropivacaine was higher in AT-PLGA nanoparticles than that of ET-PLGA nanoparticles.

Overlay of FTIR spectra confirmed that there was no major chemical shift between AT and ET-PLGA and their respective nanoparticles (Figure 4.15). Thermal analysis shows that both AT and ET-PLGA have almost same glass transition temperature and melting temperature (Appendix 4c and Appendix 4d).

Different chemical end group of PLGA affects its degradation, hence affecting release profile of encapsulated drug within its matrix. Pimozide release profiles from AT-PLGA and ET-PLGA nanoparticles were compared (Figure 4.16). It was found that $52 \pm 4\%$ pimozide was released from AT-PLGA nanoparticles in 72 hours, while $71 \pm 3\%$ pimozide was released from ET-PLGA nanoparticles at the same time (Figure 4.16a). The mean difference was found to be statistically significant. This outcome can be backed up by scanning electron microscopy images, in which it was observed that after 72 hours of drug release, many AT-PLGA nanoparticles remained intact, while all ET-PLGA nanoparticles were already degraded (Figure 4.16b). Furthermore, at the end of the six days, AT-PLGA nanoparticles released total $91 \pm 4\%$, while ET-PLGA nanoparticles released almost 100% of total encapsulated pimozide (Figure 4.16a).

Results of the current study were in consistent with a study by Li *et al.* (2021), however, with a different drug molecule. Authors found that AT-PLGA nanoparticles released 67.3% ropivacaine in 8 days, while ET-PLGA nanoparticles did 89.5% in 4 days. PLGA undergoes degradation leading to release of the drug incorporated within its matrix. Degradation involves hydrolysis of ester bonds within PGLA. Drug release is also influenced by physicochemical properties of encapsulated drug and its interactions with PLGA matrix. For example, hydrolysis of PLGA creates an acidic environment that could damage the loaded drug.

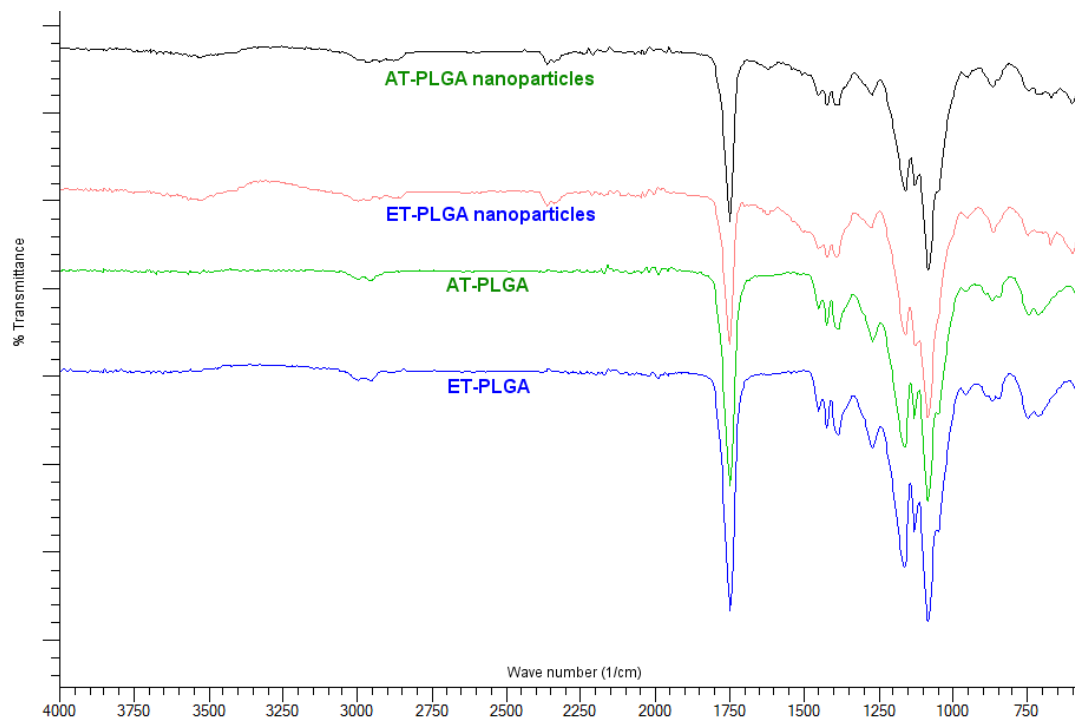
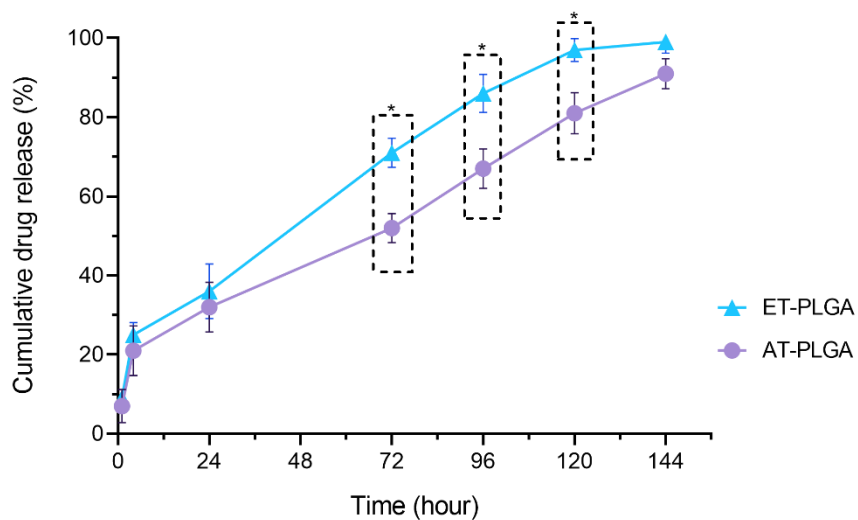


Figure 4.15: Fourier transform infrared spectroscopy (FTIR) spectra of acid and ester terminated PLGA and their respective nanoparticles.

(a)



(b) Nanoparticles after 72 hours of drug release

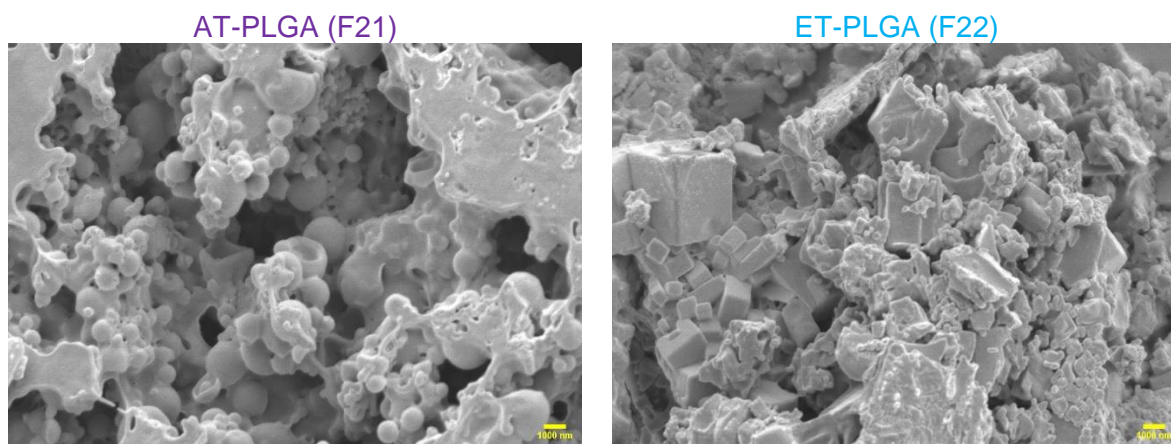


Figure 4.16: Effect of acid and ester terminated PLGA nanoparticles on drug release. (a) Cumulative drug release profile, where data are mean \pm SD ($n=3$); (b) Scanning electron microscopy image of nanoparticles after 72-hour drug release in phosphate-buffered saline (pH 7.4). Scale bar indicates 1000 nm.

The storage stability of both chemical groups terminated PLGA nanoparticles was investigated for 16 weeks in terms of particle size, polydispersity index, and zeta potential. Results show that particle size of AT-PLGA nanoparticles was increased from 52 ± 3 nm to 68 ± 10 nm after 16 weeks (Figure 4.17a), while ET-PLGA nanoparticles having their particle size from 91 ± 6 nm to 95 ± 5 nm in the same time range. Likewise, any significant change was absent in their polydispersity index (Figure 4.17b) and zeta potential (Figure 4.17c). These results indicate that both types of formulations were stable up to 16 weeks.

Furthermore, the effect of two different measuring temperatures (25°C and 37°C) on particle size and zeta potential was investigated. When measuring temperature was increased from 25°C to 37°C , a slight increase in particle size (12 nm for AT-PLGA and 2 nm for ET-PLGA nanoparticles, respectively) was observed (Figure 4.18a). However, polydispersity index in each type of formulation remains almost unchanged (Figure 4.18b). In case of zeta potential, only a slight decrease (1 mV for both types of nanoparticles) was observed at 37°C (Figure 4.18c).

In summary, based on smaller particle size, higher negative zeta potential, higher drug encapsulation efficiency, and better storage stability, Formulation F21 (AT-PLGA nanoparticles) was selected for further developments, such as surface modification with polyethylene glycol.

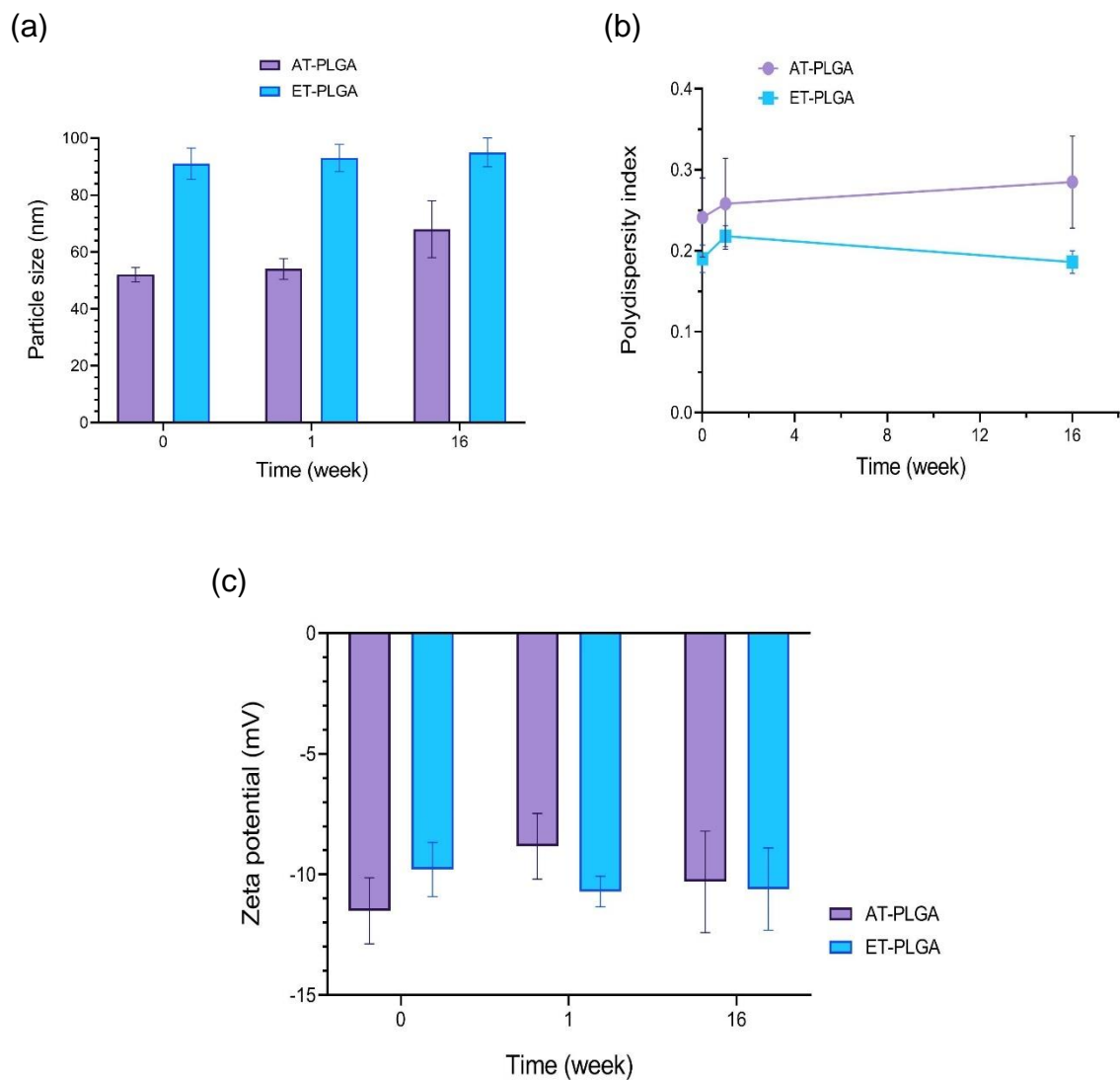


Figure 4.17: Effect of PLGA terminal group on the stability of PLGA nanoparticles. Effect of acid and ester terminated PLGA on (a) Particle size; (b) Polydispersity index; and (c) Zeta potential. Data are mean \pm SD ($n=3$). Formulations were stored at 4° C after preparation. Measurements were taken at 25° C.

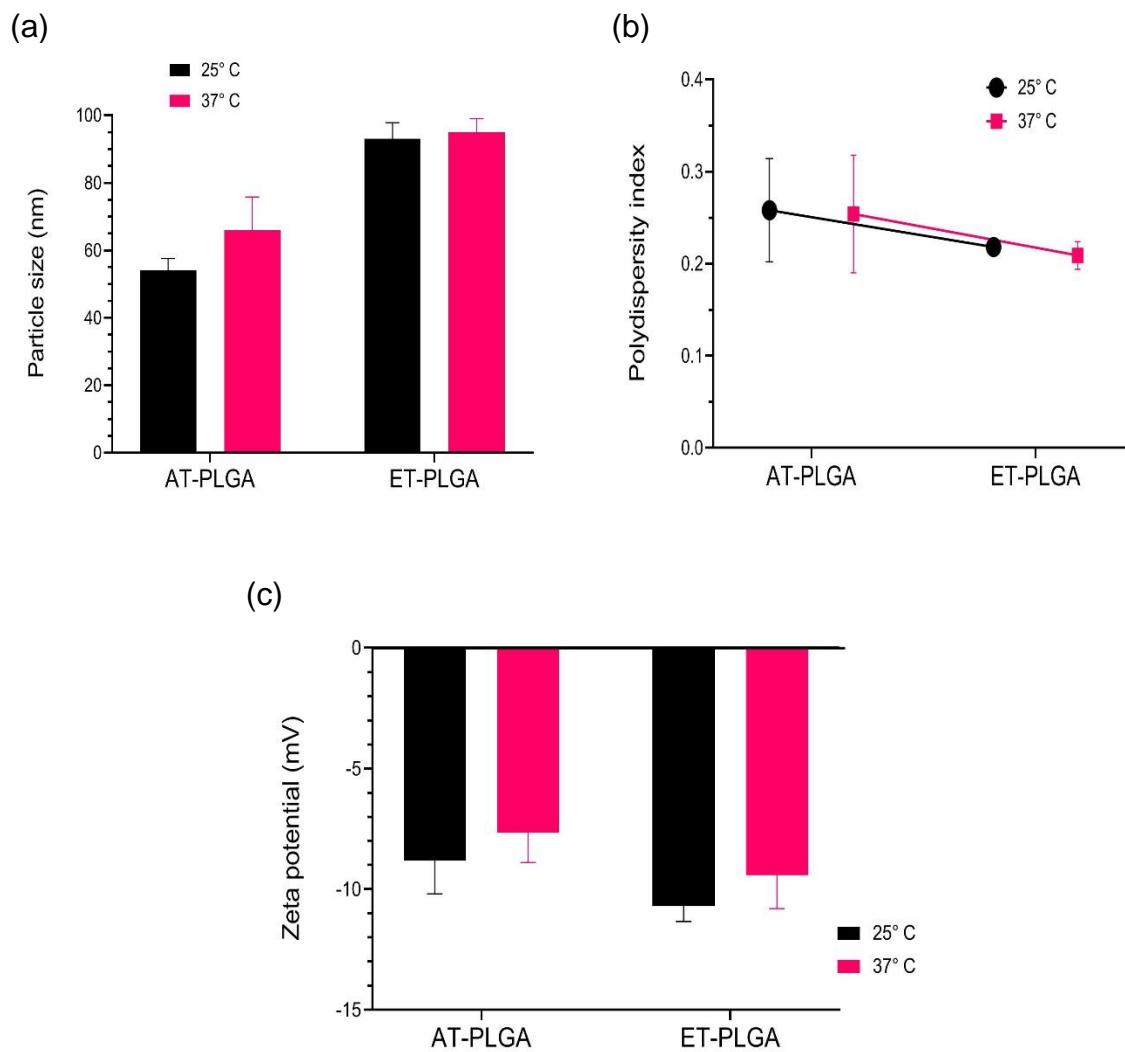


Figure 4.18: Effect of measuring temperature on both acid and ester terminated PLGA nanoparticles
 Effect on (a) particle size; (b) polydispersity index; and (c) zeta potential. Data are mean \pm SD ($n=3$).

4.3.6. Effect of PEGylation

Polyethylene glycol (PEG) is an amphiphilic polymer, and it is used as a surface coating or modifying material for PLGA based nanoparticles. PEG can be added to PLGA nanoparticles either by surface adsorption or covalent bonding or direct addition during nanoparticles preparation. The process of adding PEG to the surface of PLGA nanoparticles is termed as PEGylation.

Once administered intravenously, PEG helps PLGA nanoparticles to escape blood proteins, which are prone to adsorb on hydrophobic PLGA and subsequently remove them from the circulatory system. PEGylation would delay the degradation of nanoparticles and increase stability by staying longer in the blood circulation (Suk *et al.*, 2016). Also, PEGylated nanoparticles can diffuse brain tumour cells 100 fold faster than PEG-free nanoparticles (Nance *et al.*, 2014b).

Effect of two different molecular weights of PEG (4 and 8 kDa) with a fixed concentration of 5% w/w was investigated. The composition of these formulations is described in Table 4.6. PEG was directly added to PLGA during the preparation of nanoparticles.

Table 4.6: Surface modification of formulation (F21) with two different molecular weight of polyethylene glycol.

PEG molecular weight (kDa)	PEG (% w/w)	PLGA type	TPGS (1.25% w/v)	Drug (% w/w)
4	5	AT	1:1	2.5
8	5	AT	1:1	2.5

AT, acid terminated

At first, PEG coating was confirmed by FTIR analysis. It was found that the spectrum of PEGylated nanoparticles resembled with the spectrum of pure PEG (Figure 4.19). This indicated that PEG was coated on the surface of PLGA nanoparticles. Also, increased change in particle size (Figure 4.20a) and decreased change in negative zeta potential (Figure 4.20c) confirmed the PEG coating.

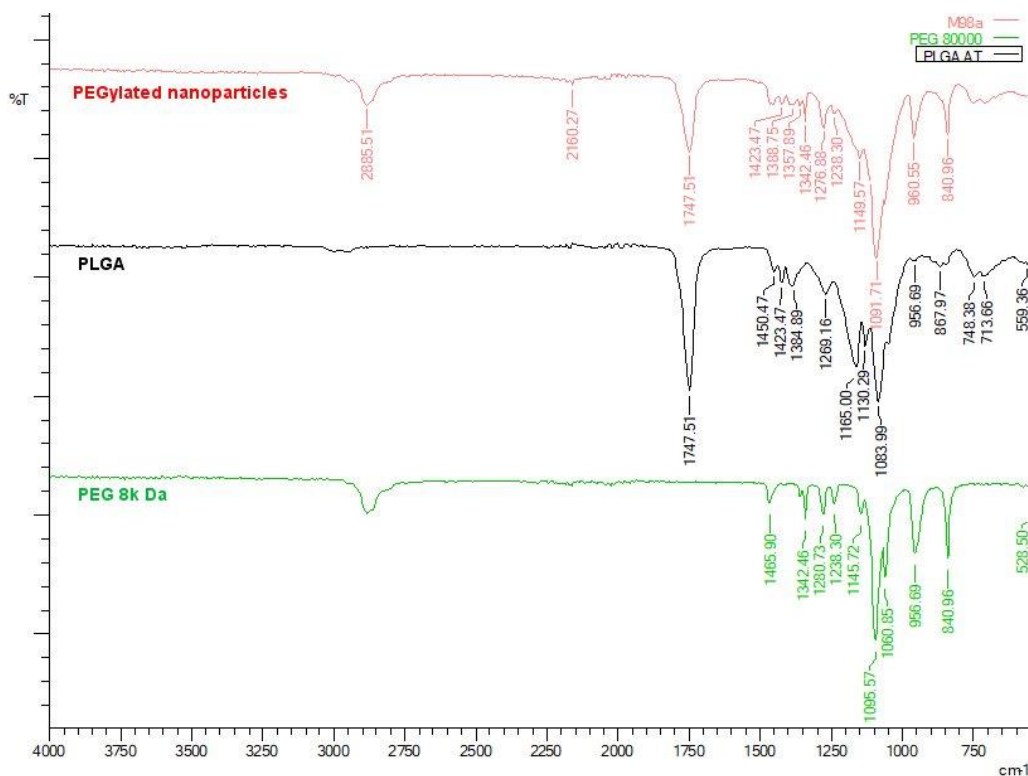


Figure 4.19: Representative FTIR spectra confirming PEGylation of the PLGA nanoparticles.

Effect of PEGylation, with two different molecular weights, is demonstrated in Figure 4.20 in terms of physicochemical properties of nanoparticles. Molecular weight of PEG was found to have significant effect on particle size. Particle size was increased by 9 nm and 32 nm once coated with PEG 4 kDa and PEG 8 kDa, respectively compared to PEG-free PLGA nanoparticles (Figure 4.20a). This indicates that particle size was directly increased with the increase of the molecular weight of PEG. However, in case of polydispersity index (PDI), no significant difference was observed (Figure 4.20b). Notably, PDI value was less than 0.3 in both formulations.

Abdelkader *et al.*, (2018) reported that PEG with low molecular weight (200 Da) significantly increased the particle size, however, PEG with high molecular weight (2 kDa and 5 kDa) produced smaller particles. Notably, 2 kDa of PEG-coated PLGA nanoparticles were the smallest in size. The coating of PEG alters the association of polymers during the formation of nanoparticles, leading to larger particle size. It was explained that PEG with higher molecular weight (more than 1000 Da) had better solubility in organic solvent with the PLGA, leading to decreased particle size. Contrarily, low molecular weight (200-800 Da) PEG

remained poorly soluble in organic solvent, resulting larger particle size. Similarly, studies with PLGA-PEG diblock copolymers (PEG with molecular weight of 5 kDa) found significantly reduced particle sizes compared to PLGA nanoparticles alone (Haggag *et al.*, 2016, 2017).

In terms of surface charge, it was observed that anionic nature of PEGylated nanoparticles decreased significantly with the increase of molecular weight of PEG. A decrease of negative 3 and 2 mV were observed in 4 kDa and 8kDa PEG-coated PLGA nanoparticles, respectively compared to PEG-free PLGA nanoparticles (Figure 4.20c). Notably, change in zeta potential also confirmed the surface coating with PEG. Similarly, Haggag *et al.*, (2016, 2017, 2019) found significant reduction of negative zeta potential value (high negative value reduced to neutral) with diblock copolymers PLGA-PEG nanoparticles compared to PLGA only nanoparticles. This was explained by the shielding property of PEG. As PEG is an amphiphilic polymer, its chains shield the surface of PLGA that is prominent for its high negative zeta potential value, resulting less negative or neutral value (Haggag *et al.*, 2019).

In contrast, Abdelkader *et al.*, (2018) did not observe any significant effect of three different molecular weights of PEG (200, 2000, and 5000 Da) on zeta potential value of PLGA-PEG nanoparticles. Notably, authors coated PLGA nanoparticles by physical addition, which could be responsible for unchanged zeta potential value.

Pimozide encapsulation efficiency (EE) was almost similar in PEG-free and PEG 4kDa-coated nanoparticles (Figure 4.20d). Only a slight increase of EE was noticed in PEG 8kDa-coated nanoparticles. However, mean difference with PEG-free nanoparticles was not significantly different.

In summary, based on the smaller particle size, and higher negative zeta potential, PEG 4 kDa-coated PLGA nanoparticles were selected for further optimisation.

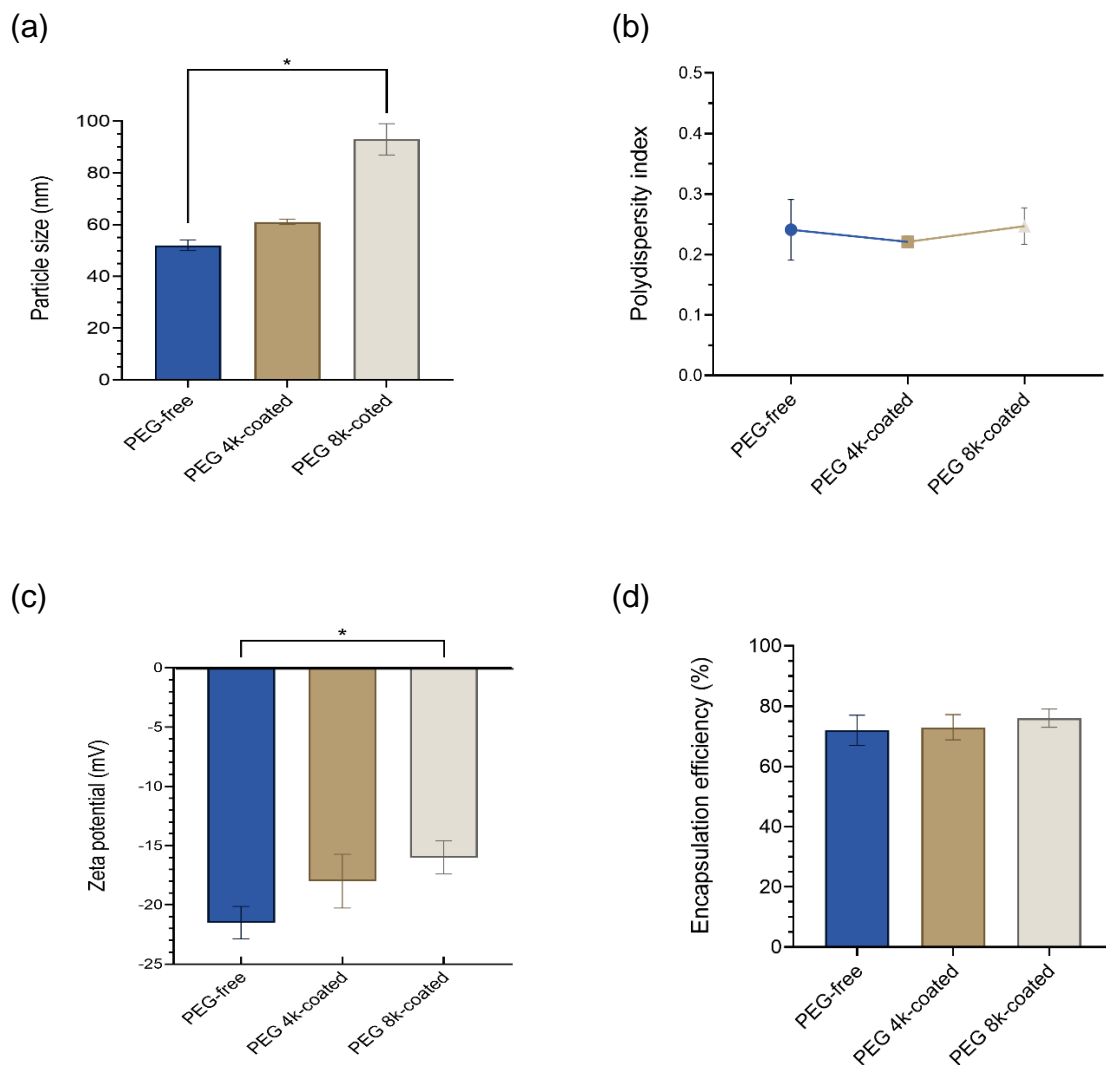


Figure 4.20: Effect of two different molecular weights of polyethylene glycol (PEG) on physicochemical properties of formulation F21. Effect on (a) particle size; (b) polydispersity index; (c) zeta potential, and (d) drug encapsulation efficiency. Data presented are mean \pm SD $n=3$. Asterisk (*) denotes statistically significant ($p=0.033$).

4.4. Conclusion

In this chapter, several process and formulation parameters on the experimental responses, such as particle size, charge, morphology, drug encapsulation efficiency, and *in vitro* drug release and stability of PLGA nanoparticles were explored.

Both single emulsion-solvent evaporation (SE) and microfluidic (MF) methods present opportunities for alteration of formulation and process variables that lead to changed physicochemical properties of nanoparticles. It was found that microfluidic method produced significantly smaller particles than SE method. Also, significantly higher drug encapsulation efficiency was observed in MF-based nanoparticles. In terms of drug release, SE-based nanoparticles were observed to release pimozone in a more delayed fashion than MF-based nanoparticles. Taking all into account, MF method was selected for further optimisation studies.

Type of PLGA affects physicochemical properties of nanoparticles. It was found that high molecular weight of PLGA led to increase the particle size. While investigating the effect of PLGA terminal groups, it was found that acid terminated (AT) PLGA nanoparticles had significantly smaller particle size than its counterpart ester terminated (ET) PLGA nanoparticles. Drug encapsulation efficiency seemed to be significantly higher in ATPLGA nanoparticles. In terms of drug release, significantly faster release was noticed in ET-PLGA nanoparticles.

Freeze-drying is essential for stability of PLGA nanoparticles for long time storage. However, it was observed that particle size became significantly large after freeze-drying. Clearly, it was noticed that surfactants played a critical role in changing the physicochemical properties of PLGA nanoparticles. Of all surfactants used in this study, TPGS was found to be to produce significantly smaller particles with narrow size distribution. Physicochemical properties remained almost unaltered after freeze-drying. Furthermore, TPGS stabilised nanoparticles released pimozone quick manner (almost 100% by 120 hours) than other surfactants stabilised nanoparticles.

PEGylation seemed to increase particle size. It was found that particles became significantly larger with high molecular weight of PEG. In addition, anionic nature of the PLGA nanoparticles was reduced significantly due to the PEGylation.

Based on physicochemical characteristics, TPGS stabilised, and acid terminated AT-PLGA-PEG (4 kDa) nanoparticles was found to be a potential formulation (F21) for further optimisation and targeting.

Chapter 5

Development of Transferrin Receptors Targeted PLGA Nanoparticles: An Optimisation Study

Chapter 5. Development of Transferrin Receptors Targeted PLGA Nanoparticles: An Optimisation Study

In the previous chapter, a potential formulation was achieved based on the physicochemical properties of nanoparticles. This chapter describes how that formulation was optimised, by investigating further process and formulation parameters. Furthermore, it outlines the development of transferrin receptors targeted PLGA nanoparticles, including their storage stability study, and potential microbial contamination detection study.

5.1. Introduction

PLGA nanoparticles can be finely tuned (optimised) by exploring many process and formulation parameters. Microfluidic is a versatile method to produce PLGA nanoparticles with desired properties. It is proven, according to many studies, that it could produce small, uniform nanoparticles loaded with a variety of therapeutics. Most common parameters that are used to tune the nanoparticles are total flow rate (TFR) and flow rate ratio (FRR) of aqueous and organic phases. Different flow rates and ratio were found to manipulate the characteristics of the nanoparticles. Similarly, concentration of individual material in a formulation also plays a vital role. Therefore, to achieve the desired properties one should explore every aspect of these parameters, as a subtle change could significantly affect the final product.

Transferrin receptors are overexpressed in almost all types of cancer. Therefore, targeting transferrin receptors (TFR) with transferrin (TF) tagged PLGA nanoparticles would be one approach of many. To implement this approach certain properties of PLGA nanoparticles should be optimised, such as a minimum particle size (<100 nm) that are monodispersed, an appropriate surface charge to prevent nanoparticles from agglomeration, and enough drug encapsulation efficiency to exert its therapeutic effect at the target site.

In general, it is challenging to achieve PLGA nanoparticles with all these required properties at the same time. Furthermore, like any other pharmaceutical formulations, developed nanoparticles must be stable, and sterile or containing a minimum microbial population during production and handling. Otherwise, *in vitro*, and *in vivo* experiments would be hampered. In keeping with general aims and objectives of the study, this chapter aims to develop transferrin receptors targeted nanoparticles, while taking above mentioned issues into account.

5.2. Aims and Objectives

Aims

- a) To optimise TPGS-stabilised PLGA-PEG nanoparticles (Formulation F21) by investigating the effect of further process parameters (such as, different microfluidic conditions and particle purification processes) and formulation parameters (such as, concentrations of PLGA, PEG, and TPGS, and type of solvents).
- b) To develop glioblastoma targeted formulations by tagging transferrin on the surface of the optimised PLGA nanoparticles
- c) To study storage stability of targeted nanoparticles, by characterising particles at different times (16 weeks) and different temperatures (4°C and 25°C).
- d) To confirm whether nanoparticles are free from bacteria and yeast prior to *in vitro* investigation on glioblastoma cell lines.

Specific objectives

- i. To study the effect of different microfluidic conditions, such as total flow rates (4, 8, 12, and 15 min/mL) and flow rate ratio of aqueous and organic phase (1:1, 1:2, and 2:1)
- ii. To evaluate the effect of different concentrations of PLGA (20 and 40 mg/mL), PEG (5,10, and 20% w/w), TPGS (0.5, 1.25, and 2% w/v), and pimozone (2.5, 5, and 10% w/w).
- iii. To assess the effect of three different solvent systems during the preparation of nanoparticles.
- iv. To address the difference between two collection processes of nanoparticles, such as centrifugation and dialysis.
- v. To confirm the surface adsorption of transferrin both qualitatively and quantitatively.
- vi. To optimise transferrin adsorption by different times of incubation.
- vii. To understand the effect of using a fluorescent dye (coumarin-6) on nanoparticles.

5.3. Results and Discussions

5.3.1. Optimisation study

Formulation F21, a potential formulation obtained in chapter 4, was optimised in terms of particle size, polydispersity index (PDI), zeta potential, and drug encapsulation efficiency (EE), by investigating different microfluidic conditions, concentrations of individual excipients, solvents, and nanoparticles collection processes.

5.3.1.1. Microfluidic conditions

At first, formulation F21 was reproduced varying the total flow rate (TFR), as shown in Table 5.1. During preparation of nanoparticles at different TFRs, other parameters were kept constant. Total four TFRs (4, 8, 12 and 15 mL/min) were investigated. Figure 5.1 demonstrates the summary effect of different microfluidic TFRs of aqueous and organic phases on the physicochemical properties of PLGA nanoparticles.

Table 5.1: Reproduction of formulation F21 at different microfluidic flow rate.

Total flow rate (TFR) (mL/min)	Flow rate ratio (FRR) (aqueous/organic)	PLGA (mg/mL)	PEG (% w/w)	TPGS (% w/v)	Drug (% w/w)
4	1:1	20	5	1.25	2.5
8	1:1	20	5	1.25	2.5
12	1:1	20	5	1.25	2.5
15	1:1	20	5	1.25	2.5

Results show that faster flow rate produced significantly smaller particles (Figure 5.1a). Notably, the smallest particle size of 50 ± 1 nm with PDI value of 0.032 ± 0.01 was observed at total flow rate of 15 mL/min. Similar to this finding, Roces, Christensen and Perrie (2020) found that TFR of 15 mL/min (the fastest in their study) produced the smallest particles, with PDI value of ≤ 0.2 . Also, Xie and Smith (2010) found smaller particles with higher TFR.

Zeta potential values of PLGA nanoparticles prepared at 4, 8, 12, and 15 mL/min of TFR were found to be -17 ± 1 , -19 ± 3 , -18 ± 2 , and -16 ± 1 , respectively (Figure 5.1b). This indicates, in all cases, zeta potential value remains negative, although not highly negative as native PLGA. High negative zeta potential value (-30 to -40 mV) is an intrinsic nature of PLGA nanoparticles due to the presence of carboxyl group in PLGA matrix. However, all formulations compared here were PEGylated, which led PLGA nanoparticles to be slightly less anionic compared to native PLGA, as already observed in previous chapter. Furthermore, an internal phase of methanol that dissolved the drug within the organic continuous phase (acetonitrile) could also possibly responsible for the reduced anionic properties. Roces, Christensen and Perrie (2020) reported nanoparticles with mean zeta potential of ~ -40 mV, and there was no significant difference among different TFRs (5, 10, and 15 mL/min). High negative value was produced because authors did not require any internal phase to dissolve their hydrophilic drug molecules. Alternatively, it could be because PLGA nanoparticles were not surface modified.

Figure 5.1c demonstrates that drug encapsulation efficiency (EE) was found to be $70 \pm 3.9\%$, $71 \pm 2.2\%$, 73 ± 4.2 , and 49 ± 4 in pimozide-encapsulated PLGA nanoparticles produced at TFRs of 4, 8, 12, and 15 mL/min, respectively. This indicates that EE increases slightly with the increase of TFR up to 12 mL/min. However, further increase in TFR (15 mL/min) resulted in significantly low EE (49%). On the contrary to this finding, Roces, Christensen and Perrie (2020) reported higher EE at faster TFR (15 mL/min) in PLGA (50:50) nanoparticles.

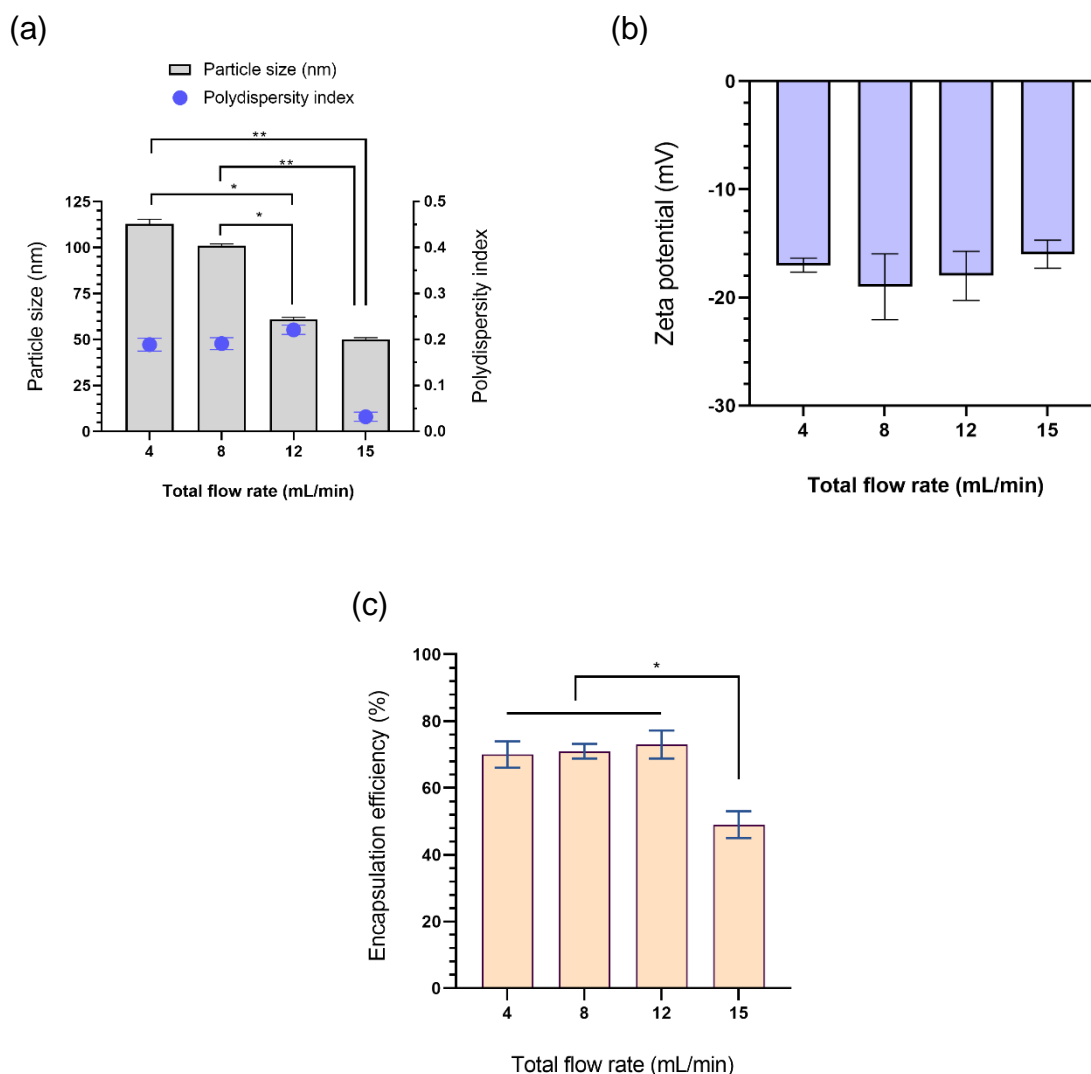


Figure 5.1: Effect of different microfluidic total flow rates (TFR) on the physicochemical properties of PLGA nanoparticles.

Effect of total flow rate (TFR) on (a) particle size & polydispersity index (PDI); (b) zeta potential; and (c) encapsulation efficiency (EE). Data are mean \pm SD ($n=3$). At different TFRs, the FRR was set to constant (1:1). * $p=0.033$ and * $p=0.002$ indicate statistical significance.

Secondly, formulation F21 was reproduced at three flow rate ratios (1:1, 1:2, and 2:1) of aqueous and organic phases (Table 5.2). In both cases, TFR was kept constant (12 mL/min). Results are summarised in Figure 5.2.

Table 5.2: Reproduction of formulation F21 at different microfluidic flow rate ratio.

Flow rate ratio (FRR) (aqueous/organic)	Total flow rate (TFR) (mL/min)	PLGA (mg/mL)	PEG (% w/w)	TPGS (% w/v)	Drug (% w/w)
1:1	12	20	5	1.25	2.5
1:2	12	20	5	1.25	2.5
2:1	12	20	5	1.25	2.5

Figure 5.1a shows that mean particle sizes were found to be 61 ± 1 , 123 ± 1.4 , and 114 ± 1.05 nm at FRR of 1:1, 1:2, and 2:1, respectively. In all cases, PDI value was ≤ 0.25 . This finding indicates that significantly larger particles are produced at higher organic phase (ratio 1:2) or high aqueous phase (ratio 2:1) compared to their equal phase ratio (1:1). High organic phase ratio leading to large particle size can be explained by the viscosity of the colloidal system during the formation of particles. Increased organic phase volume means there are more drug and PLGA molecules dissolved. As a result, more growth and agglomeration occur immediately after the nucleation process. However, this hypothesis does not apply to the increased aqueous phase ratio. Instead, larger particles were also observed in nanoparticles produced in higher aqueous phase ratio.

Lababidi *et al.* (2019) found substantial particle size reduction from 150 nm to 70 nm when FRR changed from 1:1 to 20:1, respectively. In other words, increased aqueous phase during the mixing process reduced the particle size. Similar trends were observed by other studies (Karnik *et al.*, 2008; Xu *et al.*, 2017).

Figure 5.1b depicts that anionic PLGA nanoparticles were produced at all FRRs. Zeta potential values were found to be -18 ± 2.3 , -14 ± 1.2 , and -27 ± 1.2 mV at FRR of 1:1, 1:2, and 2:1, respectively. These finding indicates that nanoparticles produced at aqueous phase dominated solvents are significantly highly anionic than that of organic phase dominated or equal phased solvents. However, Roces, Christensen and Perrie (2020) observed no difference in zeta potential among various FRR after preparation of PLGA (50:50) nanoparticles. It should be noted that authors only evaluated equal ratio (1:1) and aqueous phase dominated ratios only (3:1 and 5:1).

In terms of EE, a significant reduction ($p < 0.05$, paired *t*-test) was observed at FRR of 2:1 compared to FRR of 1:1 and 1:2 (Figure 5.2c). On the contrary, only a slight increase of EE was noticed at FRR of 1:2 compared to FRR of 1:1. This indicates that at higher organic phase ratio, more pimozone was encapsulated. This can be explained by the solubility of the PLGA and pimozone in the organic phase (acetonitrile-methanol). In other words, higher volume of organic solvents helped encapsulate pimozone more and vice versa.

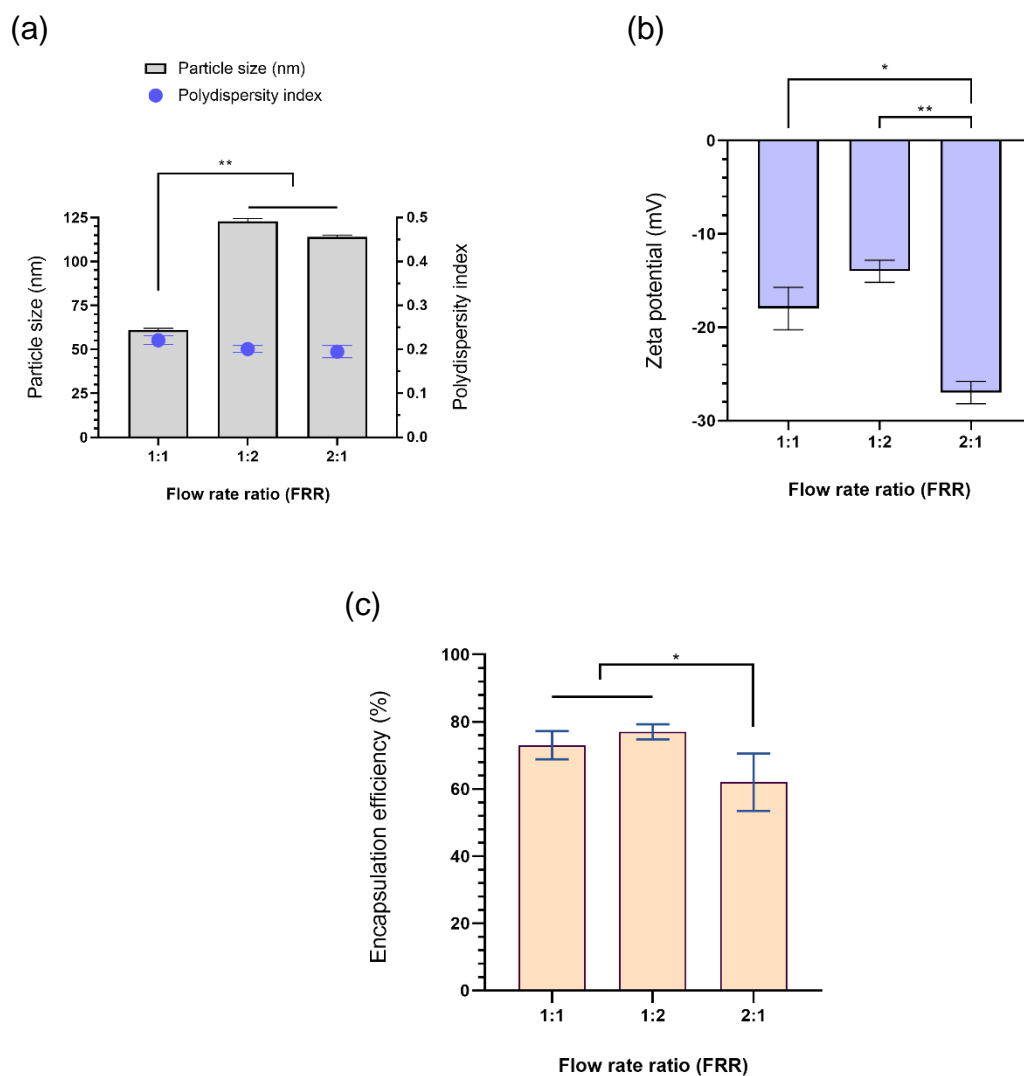


Figure 5.2: Effect of different microfluidic flow rate ratio (FRR) on the physicochemical properties of PLGA nanoparticles.

Effect of flow rate ratio (FRR) on (a) particle size & polydispersity index (PDI); (b) zeta potential; and (c) encapsulation efficiency (EE). Data are mean \pm SD (n=3). At different FRRs, the TFR was set to constant (12 mL/min). *p=0.033 and *p=0.002 indicate statistical significance.

Based on the significantly smaller particle size with high negative zeta potential and high drug encapsulation efficiency, TFR of 12 mL/min and FRR of 1:1 were selected as optimal microfluidic conditions for further optimisation of the nanoparticles.

5.3.1.2. PLGA concentration

Nanoparticles were prepared with two concentrations of PLGA, such as 20 mg/mL and 40 mg/mL in organic solvent(s). These two concentrations become 10 mg/mL and 20 mg/mL, respectively in the final formulation (after microfluidic mixing). The effect of these two PLGA concentrations were investigated on pimozone-encapsulated PLGA nanoparticles in terms of their physicochemical properties, while other parameters were kept constant (Table 5.3).

Table 5.3: Reproduction of formulation F21 at two different PLGA concentrations.

PLGA concentration (mg/mL)	Microfluidic conditions		PEG (% w/w)	TPGS (% w/v)	Initial drug loading (% w/w)
	TFR (mL/min)	FRR (aqueous/organic)			
20	12	1:1	5	1.25	2.5
40	12	1:1	5	1.25	2.5

TFR, total flow rate; FRR, flow rate ratio

Figure 5.3 illustrates the summary effect on physicochemical characteristics of nanoparticles. It was observed that particle size increased from 61 ± 1 to 146 ± 7 when PLGA concentration was increased from 20 to 40 mg/mL, respectively, although PDI value was less than 0.25 in both cases (Figure 5.3a). Significantly larger particle size at increased PLGA concentration is presumably due to the increasing viscosity of organic phase. Therefore, many nuclei are formed followed by increased particle growth, leading to formation of large nanoparticles.

Xu *et al.* (2017) observed an overall particle size increase while increasing PLGA concentrations from 5 mg/mL to 15 mg/mL. Similarly, Xie and Smith (2010) found larger particle in more concentrated PLGA, while comparing among 10, 20, and 40 mg/mL PLGA nanoparticles. Another study found that 100 nm size PLGA nanoparticles increased to 170 nm when PGLA concentration increased from 5 to 20 mg/mL (Vu *et al.*, 2019). Their findings are consistent with another study that found particle size increased from 65 to 150 nm when PGLA concentration also increased from 1 to 10 mg/mL, respectively (Lababidi *et al.*, 2019). Interestingly, authors also reported that PLGA concentration more than 10 mg/mL clogged their microfluidic mixing channel, while less than 1 mg/mL failed to produce monodispersed nanoparticles.

Cheng *et al.*, (2007) found a trend of increasing particle size with the increase of polymer (carboxyl group terminated PLGA-b-PEG) concentration after preparing nanoparticles with

nanoprecipitation method. Sharma, Madan, and Lin (2016) using single emulsion method observed similar trend with 10, 15, and 20% PLGA concentrations.

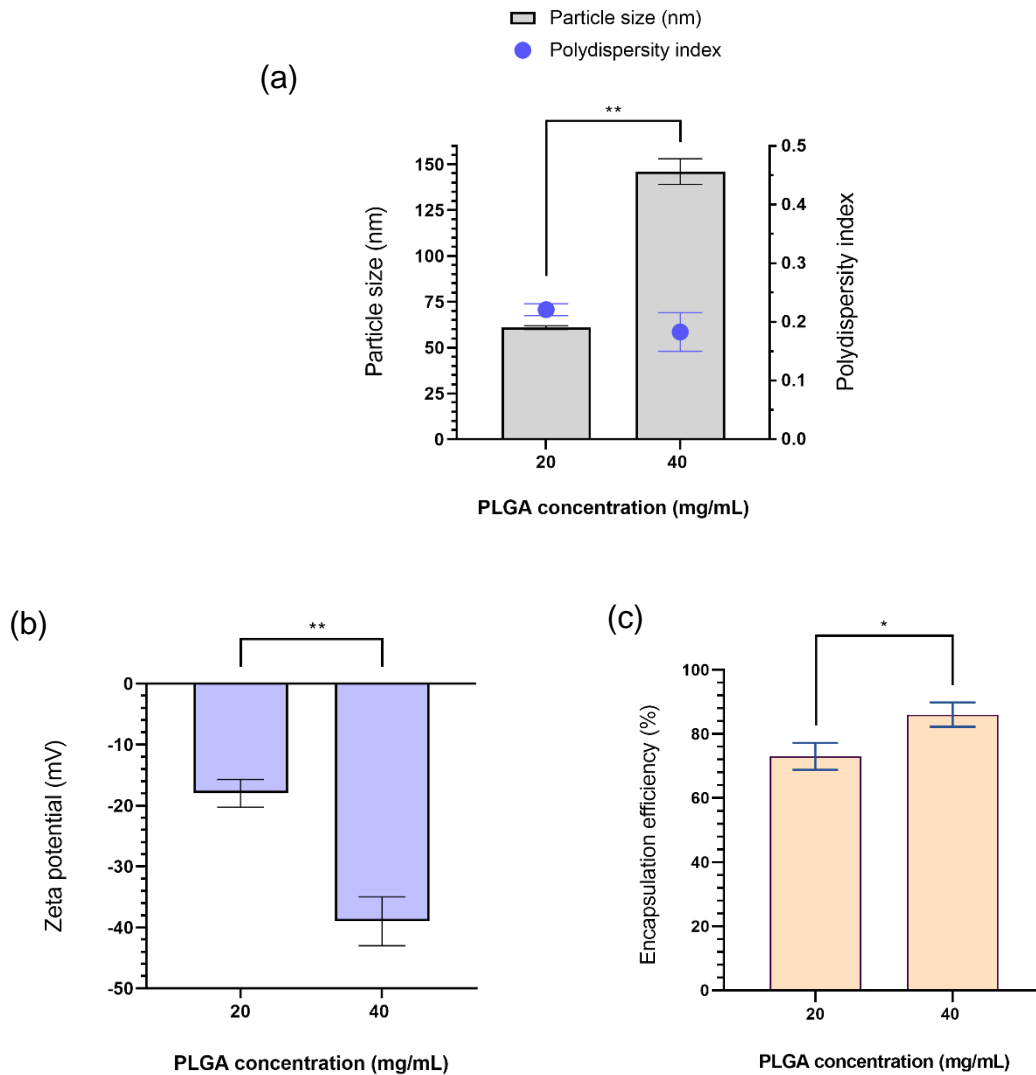


Figure 5.3: Effect of different PLGA concentrations on physicochemical properties of nanoparticles.

Effect of PLGA concentrations on (a) particle size and polydispersity index; (b) zeta potential; and (c) encapsulation efficiency. Data are mean \pm SD ($n=3$). Microfluidic conditions were 12 mL/min and 1:1. * $p=0.033$ and ** $p=0.002$ indicate statistical significance.

Abdelkader *et al.*, (2018) studied the effect of three concentrations (2.5, 5, and 7 mg/mL) with similar PLGA type (acid terminated and molecular weight) as used in this study. Authors observed that particle size increased with the increase of PLGA concentration. This was explained by the increased resistance of organic phase to flow. In other words, increased PLGA concentration increases the consistency of the droplets leading to larger particle size.

However, their preparation method was double emulsion-solvent evaporation, while this study evaluated this effect by microfluidic method only.

In contrast, Yesenia Hernández-Giottonini *et al.*, (2020) found no significant difference in particle size while investigating the effect of three different concentrations of PLGA (5, 10, and 15 mg/mL) on PLGA nanoparticles prepared by single emulsion method. However, in nanoprecipitation-based nanoparticles, they found significantly increased particle size with the increased PLGA concentrations.

The effect of PLGA concentration on zeta potential is demonstrated in Figure 5.3b. Higher negative zeta potential from -18 ± 2.2 to -39 ± 4 mV was observed when concentration was increased from 20 to 40 mg/mL. The mean difference was found to be statistically significant ($p < 0.05$, paired *t*-test). Abdelkader *et al.*, (2018) found similar trend with 7.5 mg/mL PLGA, however, 2.5 and 5 mg/mL had no such effect. It is known that high negative zeta potential is due to the presence of terminal carboxylic group found in the surface of PLGA nanoparticles. Therefore, concentrated PLGA means more carboxylic acid groups on the surface, resulting in high negative value. However, Yesenia Hernández-Giottonini *et al.*, (2020) found no effect of PLGA concentrations on zeta potential value.

Figure 5.3c shows the effect of PLGA concentration on encapsulation efficiency. Pimozide encapsulation efficiency was found to be significantly increased from $73 \pm 4.2\%$ to 86 ± 3.8 ($p < 0.05$, paired *t*-test) when PLGA concentration was increased from 20 to 40 mg/mL. High PLGA concentration increases the hydrophobicity of PLGA solution. Addition of a hydrophobic drug (pimozide in this case) into the PLGA solution would increase hydrophobic interactions between drug and PLGA, resulting in high drug encapsulation efficiency (Karnik *et al.*, 2008).

Although both drug encapsulation efficiency and negative zeta potential values were high in more concentrated (40 mg/mL) PLGA nanoparticles, it was concluded that a lower concentrated (20 mg/mL) PLGA nanoparticles would move forward for further optimisation, since it produced significantly smaller particles (< 100 nm) with reasonable surface charge for stability, and drug encapsulation efficiency.

5.3.1.3. PEG concentration

It was observed in previous chapter that higher molecular weight of PEG (8 kDa) produced larger nanoparticles than its lower molecular weight (4 kDa). Here, three formulations were designed to further optimise the nanoparticles with three different PEG (4 kDa) concentrations (5, 10, and 20% w/w), while other parameters were kept constant (Table 5.4).

Table 5.4: Reproduction of formulation F21 with different PEG concentrations.

PEG concentration (% w/w)	Microfluidic conditions		PLGA (mg/mL)	TPGS (% w/v)	Initial drug loading (% w/w)
	TFR (mL/min)	FRR (aqueous/organic)			
5	12	1:1	20	1.25	2.5
10	12	1:1	20	1.25	2.5
20	12	1:1	20	1.25	2.5

TFR, total flow rate; FRR, flow rate ratio. Molecular weight of PEG was 4 kDa.

Figure 5.4 shows the effect of three different PEG concentrations on the physicochemical properties of drug encapsulated-PLGA-PEG nanoparticles. It was found that 5, 10, and 20% (w/w) PEGylated nanoparticles had mean particle size of 61 ± 1 , 83 ± 3 , and 101 ± 3 nm, respectively with PDI value less than 0.35 in all cases (Figure 5.4a). This indicates that particle size increases with the increase of PEG concentration. This finding is not consistent with other studies, in which it was observed that particle size was reduced significantly with the increase of PEG concentration from 5 to 10% (Haggag *et al.*, 2016, 2017, 2018, 2019). This could be because the authors used PLGA-PEG block co-polymer in preparing nanoparticles, while this study added PEG into PLGA by physical mixing.

In terms of zeta potential, the value ranged between -20 ± 1.7 and -18 ± 2.3 mV, while the most concentrated PEGylated nanoparticles had the least negative value of -13 ± 1 mV (Figure 5.4b). This indicates that with the increase of PEG concentration, the negative value zeta potential was reduced. This could be explained by the shielding effect of PEG. Amphiphilic PEG attaches with PLGA by hydrophobic interactions with its hydrophobic part, while leaving hydrophilic part toward the solvent molecules, resulting in an overall hydrophilic nature of the nanoparticles. Subsequently, negative zeta potential of native PLGA is hindered, leading to less negative value.

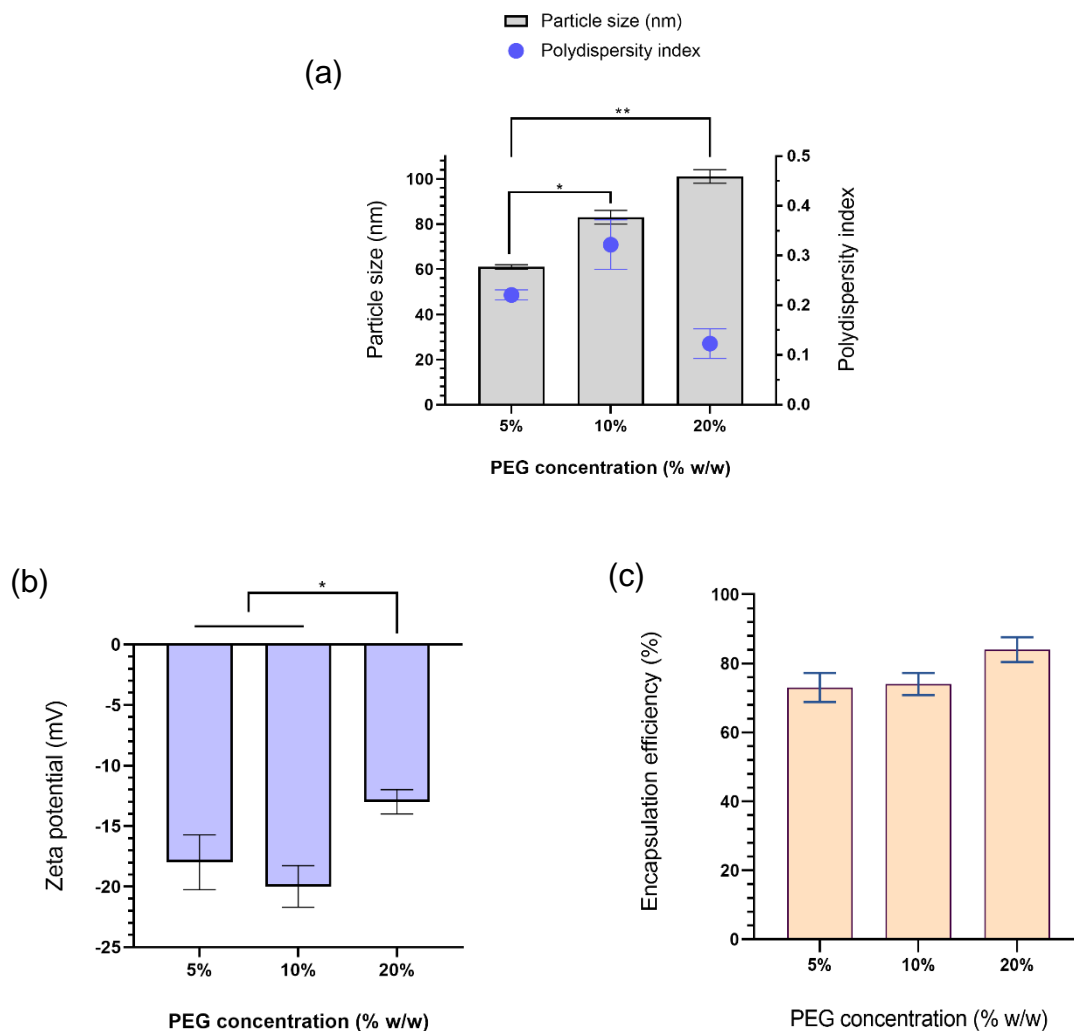


Figure 5.4: Effect of different PEG concentrations on physicochemical properties of PLGA nanoparticles.

Effect of PEG concentrations on (a) particle size with polydispersity index; (b) zeta potential; and (c) encapsulation efficiency. Data are mean \pm SD ($n=3$). PEG (4000 Da) was added to PLGA before microfluidic mixing with a flow rate of 12 mL/min and flow rate ratio of 1:1. * $p=0.033$ and ** $p=0.002$ indicate statistical significance.

Similarly, Nance *et al.* (2014) observed almost neutral zeta potential (-2.2 mV) in densely PEGylated PLGA nanoparticles, whereas authors found high negative zeta potential (-48 mV) in PEG-free nanoparticles. Haggag *et al.* (2018) also found that increasing PEG content significantly decreased overall surface charge (from ~ -20 to ~ -8 mV) of the 5-fluorouracil encapsulated PGLA nanoparticles.

Differently, few other studies did not find any effect of different PEG content (5 and 10%) on zeta potential of protein or peptide loaded PLGA nanoparticles (Haggag *et al.*, 2016, 2017, 2019; Abdelkader *et al.*, 2018).

In case of drug encapsulation efficiency (EE), a slight increase (1%) was observed when PEG concentration was increased from 5 to 10% (Figure 5.4c). A high EE (84%) was found when PEG concentration was increased to 20% (w/w). These findings indicate that EE increased with the increase of PEG concentration. This outcome was in consistency with other studies, however with different drug molecules (Haggag *et al.*, 2018, 2019).

In conclusion, both of 5 and 10% (w/w) PEG could be optimal concentrations for PEGylation of PLGA nanoparticles, based on the small particle size (<100 nm) and negative zeta potential (<-15 mV) and high EE (>70%). As this study aimed to add targeting ligand to the surface of the nanoparticles, it was expected that particle size would further increase. Therefore, formulation with significantly smaller particles after 5% PEGylation (in this case 61 nm) was selected for further optimisation.

5.3.1.4. TPGS concentration

Vitamin E-TPGS is a non-ionic surfactant. It stabilises the PLGA nanoparticles and avoids their aggregation during and after the formation of nanoparticles. The physicochemical properties of nanoparticles are manipulated by the concentration of TPGS. Therefore, investigation aimed to evaluate the effect of three different TPGS concentrations (0.5, 1.25, and 2% w/v), while keeping other parameters constant, as described in Table 5.5.

Table 5.5: Reproduction of formulation F21 at different TPGS concentrations.

TPGS concentration (% w/v)	Microfluidic conditions		PLGA (mg/mL)	PEG (% w/w)	Initial drug loading (% w/w)
	TFR (mL/min)	FRR (aqueous/organic)			
0.5	12	1:1	20	5	2.5
1.25	12	1:1	20	5	2.5
2	12	1:1	20	5	2.5

TFR, total flow rate; *FRR*, flow rate ratio

Figure 5.5 illustrates the effect of different TPGS concentrations on particle size, polydispersity index (PDI), zeta potential, and encapsulation efficiency (EE). It was found that particle size remained almost same (~95 nm, PDI <0.25) in both 0.5 and 2% (w/v) TPGS concentrations (Figure 5.5a). Interestingly, at concentration 1.25% (w/v), particle size was reduced by ~40 nm. Esim *et al.* (2020) observed that increasing TPGS concentrations (from

0.3% to 2%) generated larger particles. An early study found that only 0.015% w/v TPGS was enough to stabilise paclitaxel-loaded PLGA nanoparticles (Mu and Feng, 2003). Zeta potential value was in the range of -18 and -16 mV in all cases, with only a slight change (less negative by 2 mV) in 2% TPGS stabilised nanoparticles (Figure 5.5b). In case of encapsulation efficiency (EE), it was observed that 1.25% TPGS stabilised nanoparticles had the maximum EE ($73 \pm 4\%$) among all formulations (Figure 5.5c).

Based on the significantly smaller particle size and slightly higher EE, 1.25% TPGS stabilised nanoparticles were selected for further optimisation.

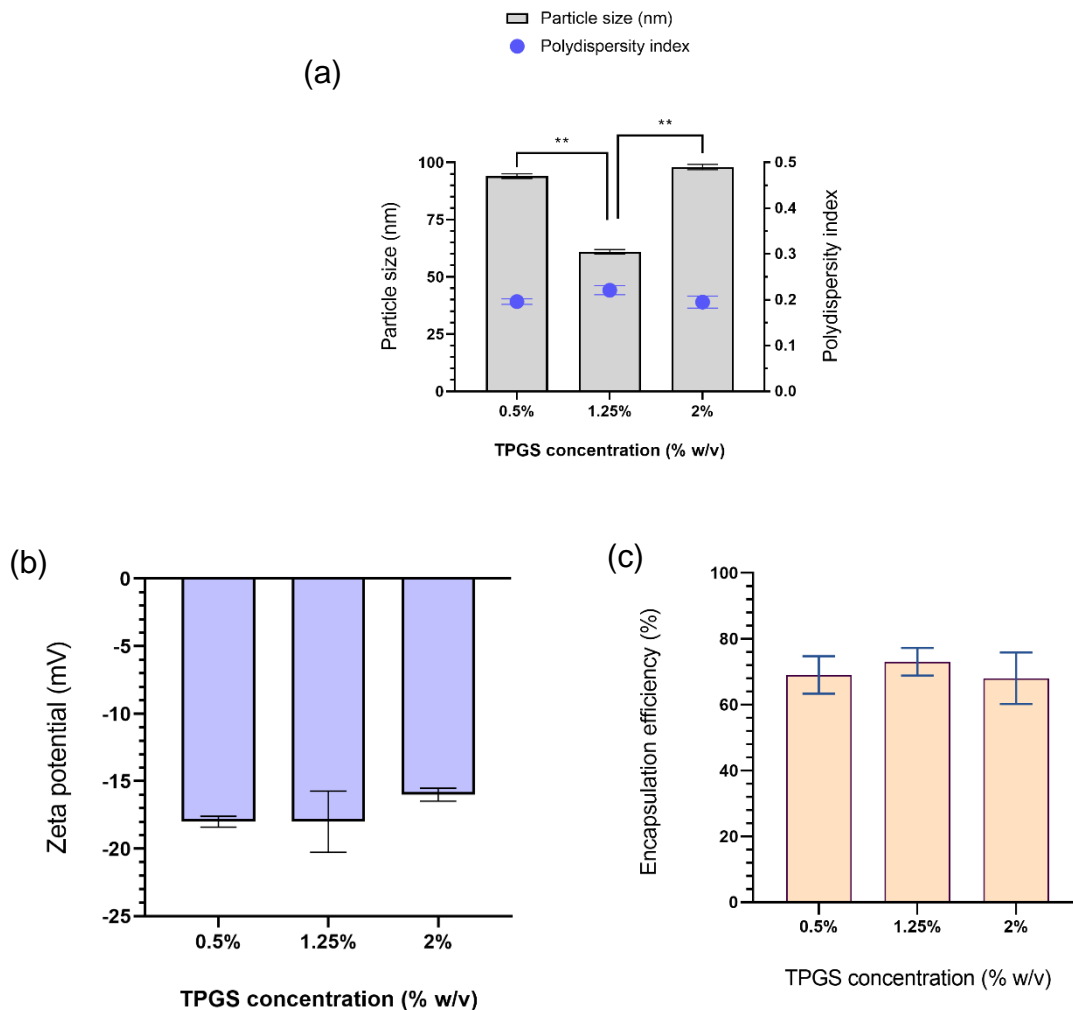


Figure 5.5: Effect of surfactant concentrations on the physicochemical properties of PLGA nanoparticles.

Effect of different TPGS concentrations (% w/v) on (a) particle size & polydispersity index; and (b) zeta potential; and (c) encapsulation efficiency. Data are mean \pm SD ($n=3$). * $p=0.002$ indicates statistical significance.

5.3.1.5. Initial drug-load

The effect of three different concentrations of pimozone (2.5, 5, and 10% w/w), which were loaded during the preparation of nanoparticles, was investigated on the physicochemical properties of nanoparticles, while keeping the other parameters constant (Table 5.6).

Table 5.6: Reproduction of formulation F21 with different initial drug-loads.

Initial drug-loading (% w/w)	Microfluidic conditions		PLGA (mg/mL)	PEG (% w/w)	TPGS (% w/v)
	TFR (mL/min)	FRR (aqueous/organic)			
2.5	12	1:1	20	5	1.25
5	12	1:1	20	5	1.25
10	12	1:1	20	5	1.25

TFR, total flow rate; FRR, flow rate ratio

Figure 5.6 demonstrates the effect of different initial pimozone loading concentrations on particle size, polydispersity index (PDI), zeta potential, and encapsulation efficiency (EE).

Studies suggest, with different drug molecule, that particle size increases with increase of initial drug loading (Cheng *et al.*, 2007; Sharma, Madan and Lin, 2016; Sufi *et al.*, 2020). This study found mean particle sizes as of 61 ± 1 , 82 ± 25 , 76 ± 22 nm in 2.5, 5, and 5% w/w initial drug loaded PLGA nanoparticles, respectively (Figure 5.6a). PDI values were recorded as of 0.22, 0.21, and 0.35, respectively (Figure 5.6a). These findings indicate that increasing the initial drug loading led to slightly larger particle size and higher PDI value. However, this trend discontinued at loading concentration of 10%, where particle size slightly reduced, however PDI value was increased, compared to 5% loading concentration.

A study observed that when initial feed of curcumin was increased more than 10% w/w, uncoated curcumin crystals were found among PLGA nanoparticles investigated by scanning electron microscopy (Mathew *et al.*, 2012). Therefore, it could be possible that poorly water soluble free pimozone had aggregated and resulted in increased particle size and PDI.

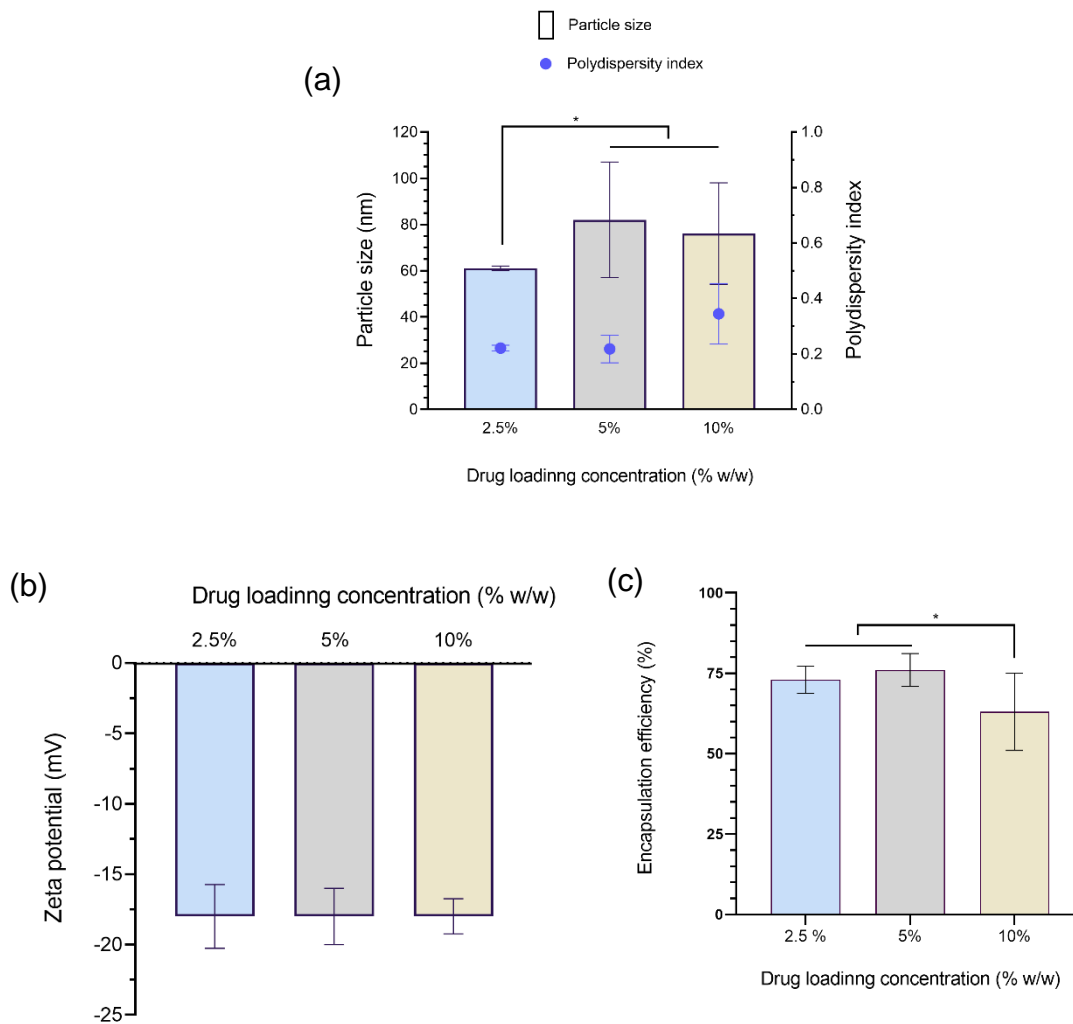


Figure 5.6: Effect of initial pimoziide-load on physicochemical properties of PLGA nanoparticles.

Effect on (a) particle size and polydispersity index; (b) zeta potential; and (c) encapsulation efficiency. Pimoziide was loaded to acid terminated PLGA with PEG 4 kDa (5% w/w). Nanoparticles were stabilised by TPGS (1.25% w/v). Microfluidic total flow rate was 12 mL/min, and flow rate ratio was 1:1 (aqueous: organic). Data are presented as mean \pm SD (n=3). *p=0.033 indicates statistical significance.

Furthermore, increased particle size can also be explained by the viscosity of the dispersed phase. In other words, more drug molecules make the organic phase more viscous, resulting larger particle size (Sharma, Madan and Lin, 2016).

Roces, Christensen and Perrie (2020) found that particle size remained almost similar, while investigating the effect of three different initial protein loading concentrations (0.2, 0.5, and 1 mg/mL).

This study found that nanoparticle in all formulations had negative value of ~ -18 mV (Figure 5.6b). This indicates that different pimoziide loadings had no significant effect on surface charge of the nanoparticles. Similarly, Roces, Christensen and Perrie (2020) found no effect of different drug loadings on zeta potential.

In case of drug encapsulation efficiency (EE), a slight increase (from 73% to 76%) was observed when initial pimoziide loading concentration was increased from 2.5 to 5% (w/w) as shown in Figure 5.6c. However, at concentration 10% (w/w), EE became lower (63%). It was possible that higher drug concentration of pimoziide was not dissolved completely at constant volume of methanol (same volume was used for 2.5 and 5%), resulting in lower drug encapsulation. In contrast, it was possible that 2.5 and 5% w/w pimoziide were completely dissolved in methanol, leading high EE. This indicates that higher is the drug feed (up to a certain concentration), the higher would be the EE. This trend was supported by the comparison of FTIR spectra of both types of formulations (Appendix 3g). It was noticed that C=O group's peak at 1751 cm^{-1} of 5% pimoziide-loaded nanoparticles were shorter than that of 2.5% pimoziide-loaded nanoparticles. This indicated that more pimoziide molecules were present within 5% drug loaded nanoparticles. This can be explained by stretching vibration of carbonyl group (C=O). In other words, C=O group of PLGA is interfered by C=O group of pimoziide, leading to reduced intensity of this peak in nanoparticles. More pimoziide molecules produced more interference, leading to shorter peak. Furthermore, thermal analysis showed no change in DSC thermograms of both types of formulations (Appendix 4e). This indicates that increase in initial pimoziide-load did not change its physical state within the PLGA nanoparticles.

Sharma, Madan and Lin (2016) observed a downward trend of drug encapsulation efficiency from 94% to 77% when initial drug (paclitaxel)-load increased from 1 mg to 5 mg, respectively. This could be because drug concentration in the PLGA nanoparticles depends on drug-PLGA interaction and miscibility of drug within PLGA, as different drug molecules have different interactions within PLGA.

In brief, both 2.5, 5 and 10% (w/w) initial drug concentration have the potential to be used as optimised loading concentration. However, this study would exclude 5% and 10% loading concentration for further study, as 2.5% drug loaded nanoparticles were significantly smaller in size.

5.3.1.6. Organic solvent(s)

Physicochemical properties of nanoparticles could be manipulated by using different types of solvent or a mixture of solvents during the preparation of PLGA nanoparticles. All formulations in previous experiments were prepared by using a mixture of organic solvents namely acetonitrile and methanol at a ratio of 4:1.

Solvent(s) optimisation was performed by using more safe solvents, namely dimethyl sulfoxide (DMSO), and acetonitrile-DMSO (4:1). Accordingly, formulation F21 was reproduced using these solvent(s), while keeping the other parameters constant (Table 5.7).

Table 5.7: Reproduction of formulation F21 using different organic solvent(s).

Optimisation parameters						
Solvent/s	Microfluidic conditions		Concentrations			
	TFR (mL/min)	FRR	PLGA (mg/mL)	PEG (% w/w)	TPGS (% w/v)	Drug-load (% w/w)
acetonitrile-methanol (4:1)	12	1:1	20	5	1.25	2.5
acetonitrile-DMSO (4:1)	12	1:1	20	5	1.25	2.5
DMSO	12	1:1	20	5	1.25	2.5

Figure 5.7 shows the effect of using different organic solvent/s on particle size, PDI, zeta potential, and encapsulation efficiency.

As demonstrated in Figure 5.7a, acetonitrile-methanol (4:1) solvent mixture produced smallest particles (61 ± 1 nm, PDI 0.22 ± 0.01), while DMSO alone producing the largest (192 ± 21 nm, PDI 0.38 ± 0.03). However, when DMSO was added as a fraction (25%) into acetonitrile, particle size was reduced to 107 ± 1 nm with PDI value of 0.15 ± 0.02 . The reduction of particle size can be explained by the miscibility of solvents with water. Methanol, acetonitrile, and DMSO are all water miscible solvents. However, their relative polarity is different from each other (methanol > acetonitrile > DMSO). Being least polar solvent, DMSO produced largest particles. Acetonitrile-DMSO (4:1) particularly is more polar than DMSO alone, resulting in smaller particle comparatively. Further particle size reduction was noticed once more polar solvent mixture (acetonitrile-methanol) was introduced.

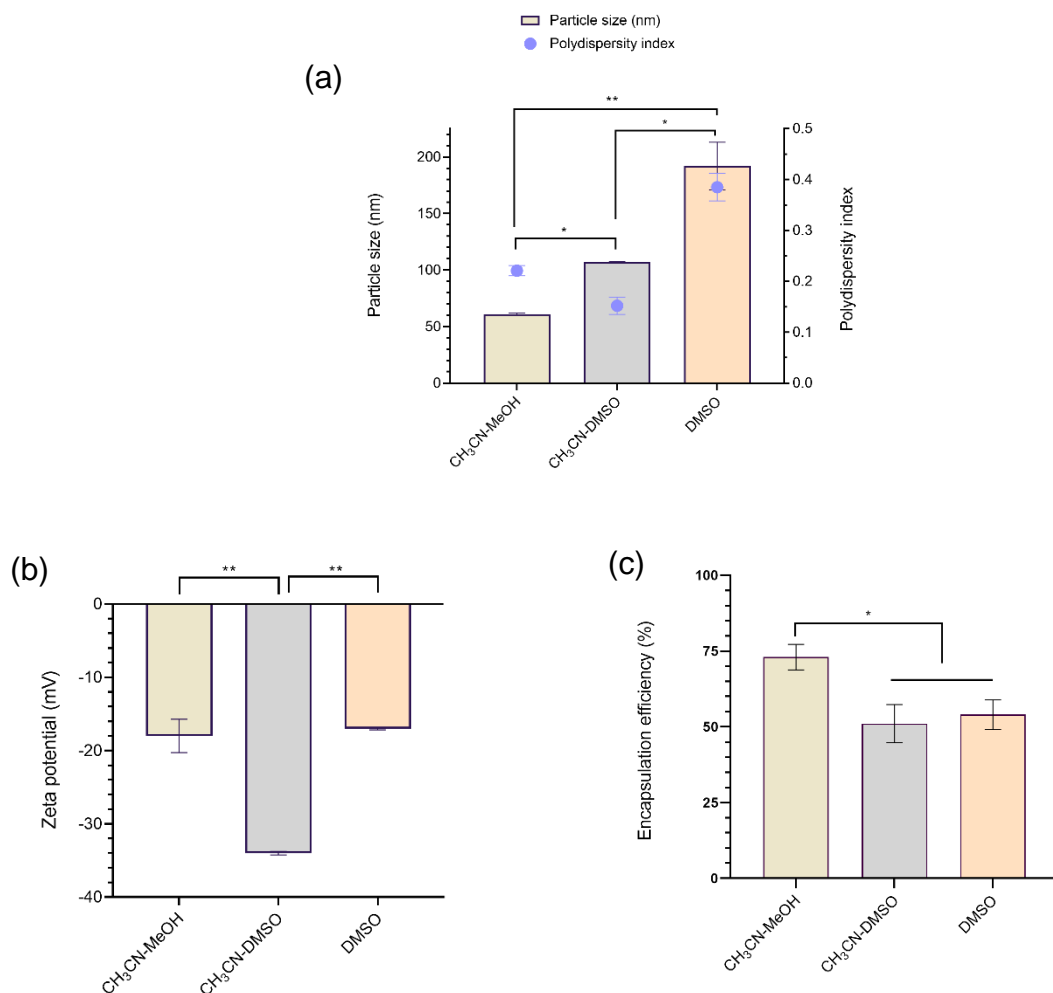


Figure 5.7: Effect of different organic solvent(s) on the physicochemical properties of PLGA nanoparticles.

Effect of solvent(s) on (a) particle size and poly dispersity index; (b) zeta potential; and (c) encapsulation efficiency. Data presented are mean \pm SD ($n=3$). CH₃CN, acetonitrile; MeOH, methanol; and DMSO, dimethyl sulfoxide. Microfluidic total flow rate was 12 mL/min, and flow rate ratio was 1:1 (aqueous: organic), where the ratio of organic phases, such as acetonitrile-methanol, and acetonitrile-DMSO was 4:1. * $p=0.033$ and ** $p=0.002$ indicate statistical significance.

These findings are consistent with other studies. Cheng *et al.*, (2007) found a correlation between particle size and water-miscibility of four solvents. Authors observed the smallest PLGA-PEG nanoparticles with most water-miscible solvent used in their study. Similarly, Xie and Smith (2010) introduced different fraction of methanol (20, 50, and 80% v/v) to acetonitrile and observed that higher methanol fractions produced smaller particles.

In a coaxial microfluidic device (using microfluidic flow-focusing method), Xu *et al.* (2017) managed to produce ~ 60 nm particles using DMSO as a solvent. Authors observed that using a partially water miscible solvent systems, dichloromethane-DMSO as 1/10 and 1/20, increased the overall particle size of PLGA nanoparticles.

Lababidi *et al.* (2019) found a correlation between Hildebrand solubility parameter (HSP) and formation of smaller particle size. Authors observed that particle size reduced from 100 nm to 40 nm once organic solvent was changed from acetonitrile to DMSO. HSP estimates interaction between materials and indicates their solubility, indicating similar HSP value of two materials is the indication that they are likely to be miscible. HSP values of DMSO and acetonitrile are 26.65 and 24.28, respectively.

Figure 5.7b depicts that acetonitrile-DMSO mixture produced nanoparticles with high negative zeta potential value (-34 ± 0.3 mV). In contrast, DMSO alone and acetonitrile-methanol mixture produced nanoparticles with similar less negative zeta potential (~ -18 mV).

In case of encapsulation efficiency (EE), acetonitrile-methanol mixture-based nanoparticles had the maximum drug EE ($73 \pm 4.2\%$) compared to the other two solvent(s)-based nanoparticles (Figure 5.7c).

In summary, at a constant aqueous phase (TPGS 1.25% w/v), acetonitrile-methanol (4:1 v/v) mixture as an organic phase produced significantly smaller particles with high drug encapsulation and moderately negative zeta potential. Therefore, further optimisation would be continued with only acetonitrile-methanol mixture as an organic phase.

5.3.1.7. Collection of nanoparticles

Prepared nanoparticles need be free from organic solvent(s) and free drug molecules or surfactants. Therefore, nanoparticles are washed off and collected with different techniques. This study investigated two techniques of collecting optimised PLGA nanoparticles, while keeping other parameters constant (Table 5.8).

Table 5.8: Collection of optimised nanoparticles by two different processes.

Collection techniques	Optimised parameters					
	Microfluidic conditions		Concentrations			
	TFR (mL/min)	FRR	PLGA (mg/mL)	PEG (% w/w)	TPGS (% w/v)	Drug-load (% w/w)
Centrifugation	12	1:1	20	5	1.25	2.5
Dialysis	12	1:1	20	5	1.25	2.5

Organic phase was a mixture of acetonitrile and methanol at a ratio of 4:1 (v/v).

The effect of centrifugation and dialysis are compared in Figure 5.8 in terms of particle size, polydispersity index, zeta potential, and drug encapsulation efficiency (EE).

Particle size was found to be 76 ± 22 nm (PDI 0.345 ± 0.1) and 50 ± 1 nm (0.032 ± 0.01) in centrifuged and dialysed nanoparticles, respectively (Figure 5.8a). These findings indicate that dialysis-based nanoparticles were smaller than centrifuged-based nanoparticles. Increased particle size and PDI value can be explained by the intermediate steps of centrifugation process. Collection of nanoparticles by centrifugation requires 2/3 times washing of the nanoparticles with distilled water. Each washing up is followed by centrifugation of nanoparticles with high speed until sedimentation. Sediments in the form of pellets are resuspended again to repeat the process. It is possible that some particles remained agglomerated during redispersion step, leading to increased particle size and PDI. Yesenia Hernández-Giottonini *et al.* (2020) showed that an increase in particle size was consistent across the centrifugation cycles used in the purification.

On the other hand, dialysis process removes the loose particles and solvent by diffusion through a semipermeable membrane. As a result, the size of PLGA nanoparticles remain unaltered.

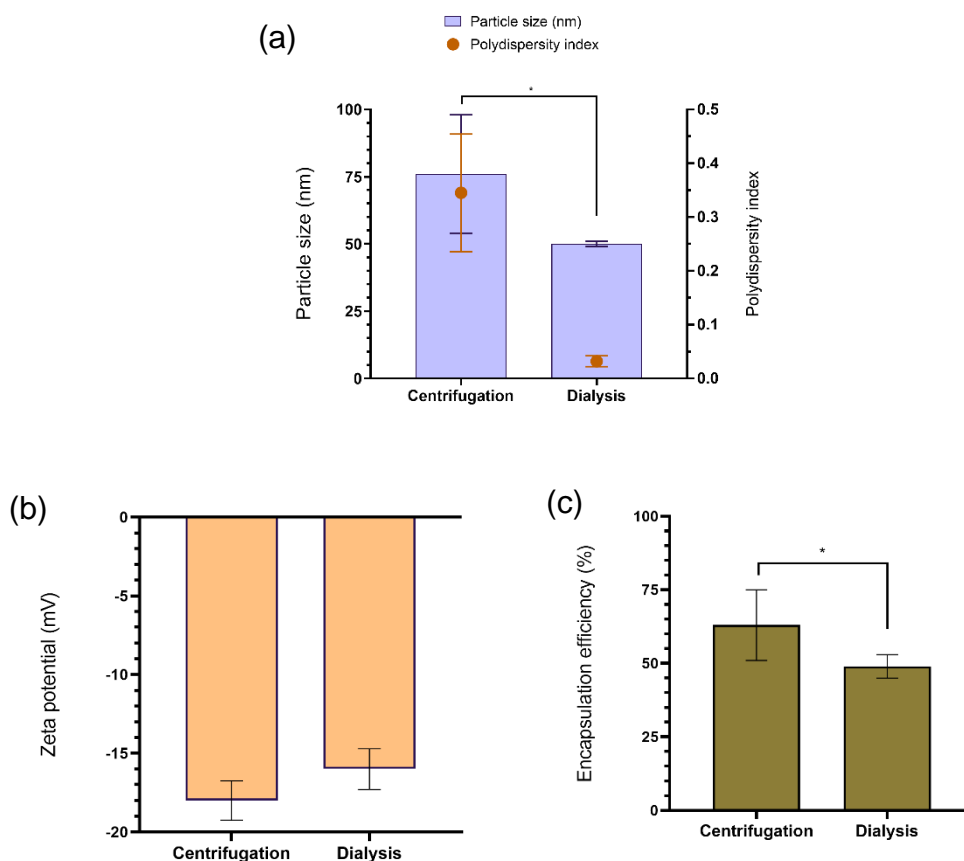


Figure 5.8: Effect of two different collection techniques on the physicochemical properties of PLGA nanoparticles.

Effect on (a) particle size and polydispersity index; (b) zeta potential; and (c) encapsulation efficiency. Data are mean \pm SD (n=3). *p=0.033 indicates statistical significance.

As displayed in Figure 5.8b, a slightly less negative zeta potential value (-16 ± 1 mV) was observed in dialysed nanoparticles compared to centrifuged nanoparticles (-18 ± 1 mV). This can be explained by the removal of TPGS layer from the surface of the PLGA nanoparticles due to high-speed centrifugation. As a result, carboxyl group of PLGA becomes exposed and increases the anionic nature of PLGA nanoparticles. In other words, zeta potential becomes more negative once PLGA nanoparticles are purified with high-speed centrifugation, while it remains unaltered after dialysis.

Figure 5.8c illustrates that centrifuged nanoparticles have higher drug EE ($63 \pm 12\%$) than that of dialysed nanoparticles ($49\% \pm 4$). This can also be explained by the steps of both techniques. In centrifugation, the washing up steps was rapid. Therefore, loss of superficially loaded pimozone was minimum. On the contrary, dialysis techniques required long time (approximately, 6 hours) washing up (by diffusion). As a result, loss of pimozone was

maximum. In other words, in dialysis technique, there was a chance of initial burst release of drug, resulting in lower EE compared to centrifuged nanoparticles.

In general, both techniques lose loaded drug during the washing up processes. Furthermore, both are time consuming and not suitable for scale up. Tangential flow filtration (TFF) can be an efficient alternative purification process for scale up production of PLGA nanoparticles (Roces, Christensen and Perrie, 2020).

However, this study selected dialysis as an optimised technique of nanoparticles collection based on the significantly smaller particle size. Therefore, targeting nanoparticles (including dye-loaded nanoparticles) would be developed from dialysis-based nanoparticles only.

5.3.2. Active targeting with transferrin

So far, this study has reached to an optimised formulation. Its compositions and conditions are described in Table 5.9. This optimised formulation was used to target transferrin receptors (TFR) in glioblastoma cells. To do that, transferrin (TF) was adsorbed on the surface of the nanoparticles. Furthermore, to monitor the targeted nanoparticles during cellular uptake and cytotoxicity studies, fluorescent dye coumarin-6 (C6) was loaded within PLGA nanoparticles. Investigated formulations are described in Table 5.10.

Physicochemical properties of optimised nanoparticles are altered due to the addition of targeting ligand and fluorescent dye. Table 5.11 demonstrates the effect of adding transferrin and coumarin-6 on the particle size, polydispersity index (PDI), zeta potential, and drug encapsulation efficiency (EE).

Table 5.9: Composition and conditions of the final optimised formulation.

Parameters	Optimised compositions and conditions
Total flow rate	12 mL/ min
Flow rate ratio (aqueous/organic)	1:1
PLGA concentration	20 mg/mL
PEG concentration	5% (w/w)
TPGS concentration	1.25% (w/v)
Initial drug loading concentration	2.5% (w/w)
Organic phase	acetonitrile-methanol (4:1)
Collection technique	dialysis

Table 5.10: Optimised formulation with coumarin-6 and transferrin.

Formulation code	Pimozide	Coumarin-6 (1% w/w)	Transferrin (1 mg/mL)
NPs (empty)	-	-	-
NPs-C6	-	+	-
NPs-drug	+	-	-
NPs-drug-C6	+	+	-
NPs-C6-TF	-	+	+
NPs-drug-C6-TF	+	+	+

+ present; - absent; NPs, nanoparticles; C6, coumarin-6 (fluorescent dye); TF, transferrin

The adsorption of transferrin (TF) was confirmed qualitatively, by the measuring particle size. From dynamic light scattering (DLS) analysis, it was found that particle size increased by 44 nm after incubating drug-free nanoparticles (blank nanoparticles) into the TF solution (Table 5.11). For drug-dye-loaded nanoparticles, an increase of 24 nm was also observed (Table 5.11). Similarly, an increase of ~45 nm was observed in TF-incubated nanoparticles, analysed by transmission electron microscopy (Figure 5.9a). Increased particle size could be due to the adsorbed TF molecular layer on the surface of the nanoparticles. Thus, it confirmed the addition of transferrin in PLGA nanoparticles.

Other studies also reported increased particle size after adding targeting ligand into the PLGA nanoparticles (Frasco *et al.*, 2015; Venugopal *et al.*, 2018). In particular, Frasco *et al.* (2015) observed a slight increase in particle size after adding the transferrin. Using a different targeting ligand (anti-EGFR), Venugopal *et al.* (2018) found that particle size increased from 317 nm to 335 nm.

Zeta potential value for both blank and drug-loaded nanoparticles became less negative (from -36 to -19 mV and from -16 to -10 mV, respectively) after transferrin adsorption (Table 5.11). Less negative zeta potential (from -12.7 mV to -3.5 mV) was noticed due to the addition of antibody protein on the surface of the PLGA nanoparticles (Venugopal *et al.*, 2018).

Table 5.11: Characterisation of dye-loaded and TF-adsorbed optimised nanoparticles.

Formulation code	Particle size (nm)	PDI	Zeta potential (mV)	EE (%)
NPs (empty)	146 ± 7	0.183 ± 0.03	-39 ± 4	-
NPs-C6	177 ± 6	0.149 ± 0.02	-36 ± 1	-
NPs-drug	61 ± 1	0.221 ± 0.01	-18 ± 2	73 ± 4
NPs-drug-C6	50 ± 1	0.032 ± 0.01	-16 ± 1	49 ± 4
NPs-C6-TF	221 ± 13	0.230 ± 0.04	-19 ± 5	-
NPs-drug-C6-TF	74 ± 6	0.331 ± 0.06	-10 ± 2	47 ± 3

NPs, nanoparticles; TF, transferrin; PDI, polydispersity index; EE, encapsulation efficiency; C6, coumarin-6; drug, pimozone. Data are mean ± SD (n=3).

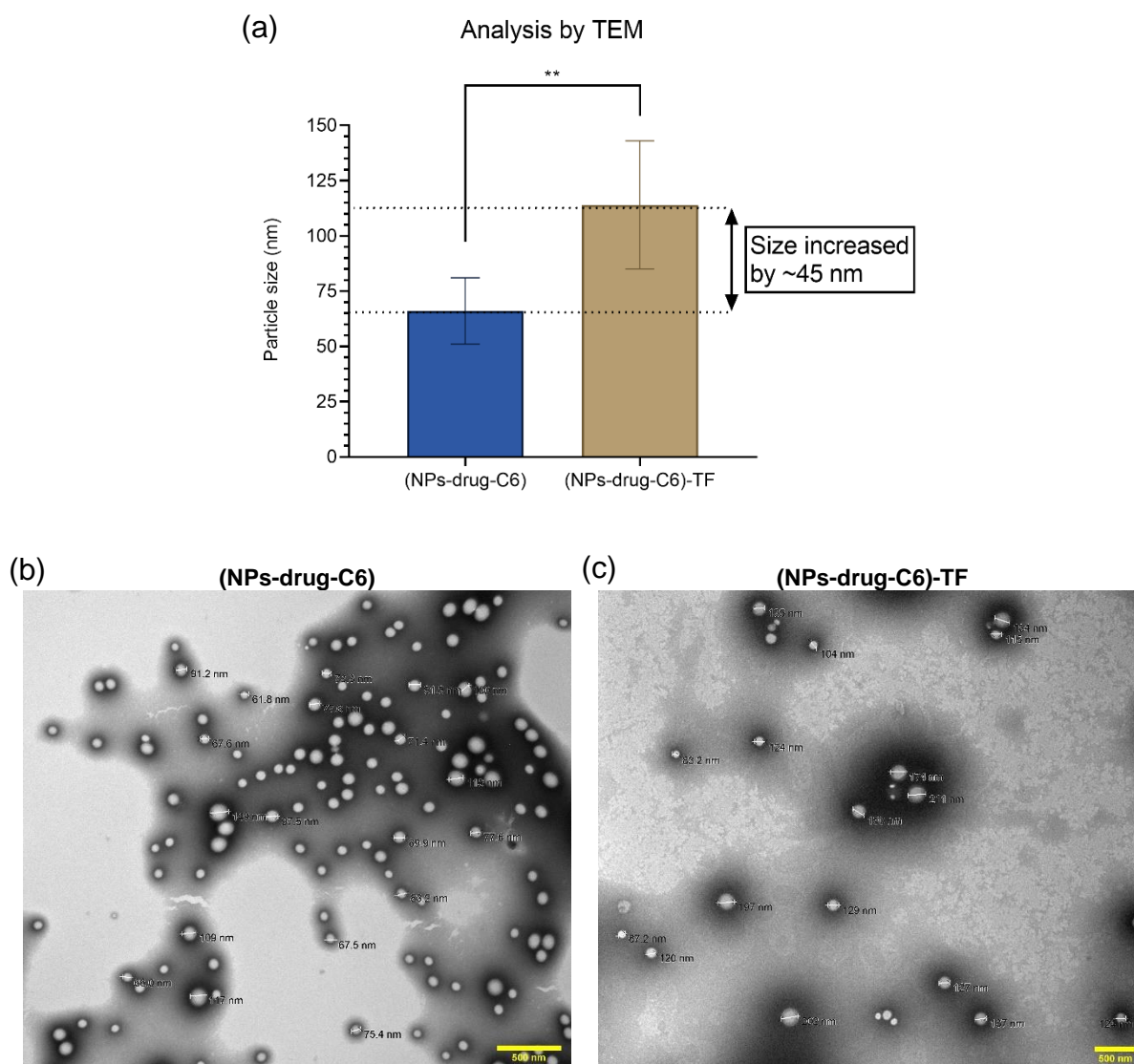


Figure 5.9: Confirmation of transferrin adsorption by transmission electron microscopy. (a) Particle size difference between nanoparticles and TF-adsorbed nanoparticles; (b) Transmission microscopy (TEM) image of nanoparticles; and (c) TEM image of TF adsorbed nanoparticles. Scale bars indicate 500 nm. Data in (a) are mean \pm SD ($n=50$, where n is the number of randomly selected individual particle). $**p=0.002$ indicates statistical significance.

Active targeting is influenced by transferrin content on the PGLA surface. To analyse the adsorbed transferrin quantitatively, a bicinchoninic acid (BCA) protein assay was used. Previously, adsorption of transferrin was optimised by incubating drug loaded PLGA nanoparticles in 1 mg/mL transferrin solution for 2 hours and 24 hours. It was found that that $\sim 150 \mu\text{g}$ transferrin was recovered from 2 hours incubated PLGA nanoparticles, and $\sim 120 \mu\text{g}$ recovered from 24 hours (Appendix 6).

Figure 5.10 shows that ~120 µg of transferrin was recovered from 1 mL of drug-loaded nanoparticles. However, the amount was higher (~180 µg) in empty nanoparticles. This finding also confirmed the successful transferrin adsorption on PLGA nanoparticles quantitatively. Frasco *et al.* (2015) recovered 49 ± 7 µg/mg adsorbed transferrin using similar adsorption technique.

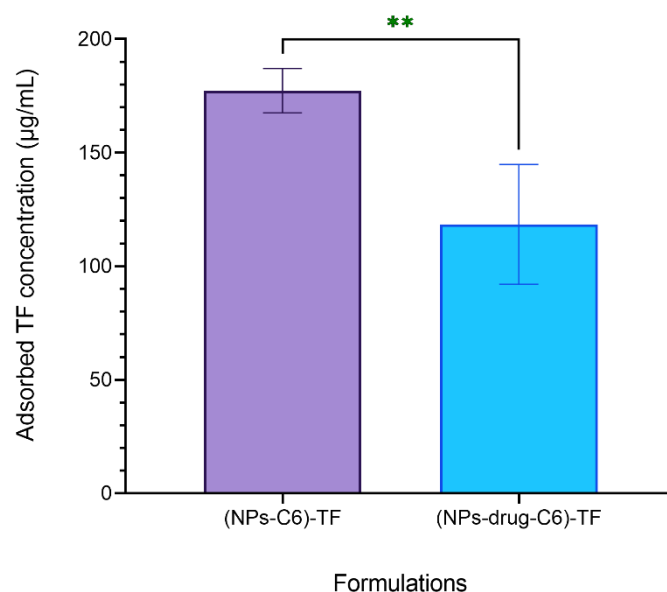


Figure 5.10: Quantitative analysis of transferrin adsorption by an indirect method using BCA method.

Comparison of transferrin adsorption between empty nanoparticles (NPs-C6-TF) and drug-loaded nanoparticles (NPs-drug-C6-TF). Data are mean \pm SD (n=6). Transferrin was adsorbed by incubating PLGA nanoparticles in 1 mg/mL transferrin solution for 2 hours.

It was observed that fluorescent dye-loaded nanoparticles were smaller by 11 nm than dye-free nanoparticles (Table 5.11). However, blank nanoparticles did not show this trend. Instead, particle size increased from 146 nm to 177 nm with the addition of dye (Table 5.11). In terms of zeta potential, a slight decrease in anionic nature (by 2 mV) was observed in dye-loaded nanoparticles. Notably, a lower drug EE was found in dye-loaded nanoparticles (Table 5.11).

In brief, both qualitative and quantitative analysis confirmed that TF was successfully adsorbed on the surface of the nanoparticles. That leads to formation of a transferrin receptor targeted PLGA nanoparticles. As coumarin-6 did not significantly affect particle size and surface charge, it could now be used as a fluorescent dye to monitor the targeted nanoparticles within the cells.

5.3.3. Storage Stability Study

Storage conditions, such as temperature and duration of storage, can affect the stability of the nanoparticles. Unstable nanoparticles tend to agglomerate over time, increasing the particle size and polydispersity index. Also, degraded nanoparticles will have changed zeta potential over time.

Previously, in chapter 4, it was shown that both acid and ester terminated PLGA nanoparticles remained stable up to 16 weeks at 4°C temperature.

Here, transferrin adsorbed optimised nanoparticles (in suspension) were stored at room temperature, and 4°C temperature. Particle size, polydispersity index (PDI) and zeta potential were evaluated up to 16 weeks.

Figure 5.11 demonstrates the change in physicochemical properties of transferrin adsorbed PLGA nanoparticles over the 16 weeks period stored at 4°C temperature. No significant change was noticed in particle size (Figure 5.11a), polydispersity index (Figure 5.11b) and zeta potential (Figure 5.11c) after 16 weeks. These results indicate that transferrin adsorbed PLGA nanoparticles remain stable up to 16 weeks at 4°C temperature.

However, at room temperature, particle size became 5 times larger in 16 weeks, indicating particles have agglomerated (Figure 5.12a). It was also observed that polydispersity index increased from 0.2 to 0.6 (Figure 5.12b). Further, a less negative zeta potential was noticed after 16 weeks (Figure 5.12c). These results indicate that transferrin adsorbed PLGA nanoparticles are not stable at 16 weeks of storage in 25° C.

Roces, Christensen and Perrie (2020) investigated the stability of PVA stabilized PLGA nanoparticles at 4°C for 4 weeks. Authors found no significant difference in particle size, PDI, and zeta potential after this time.

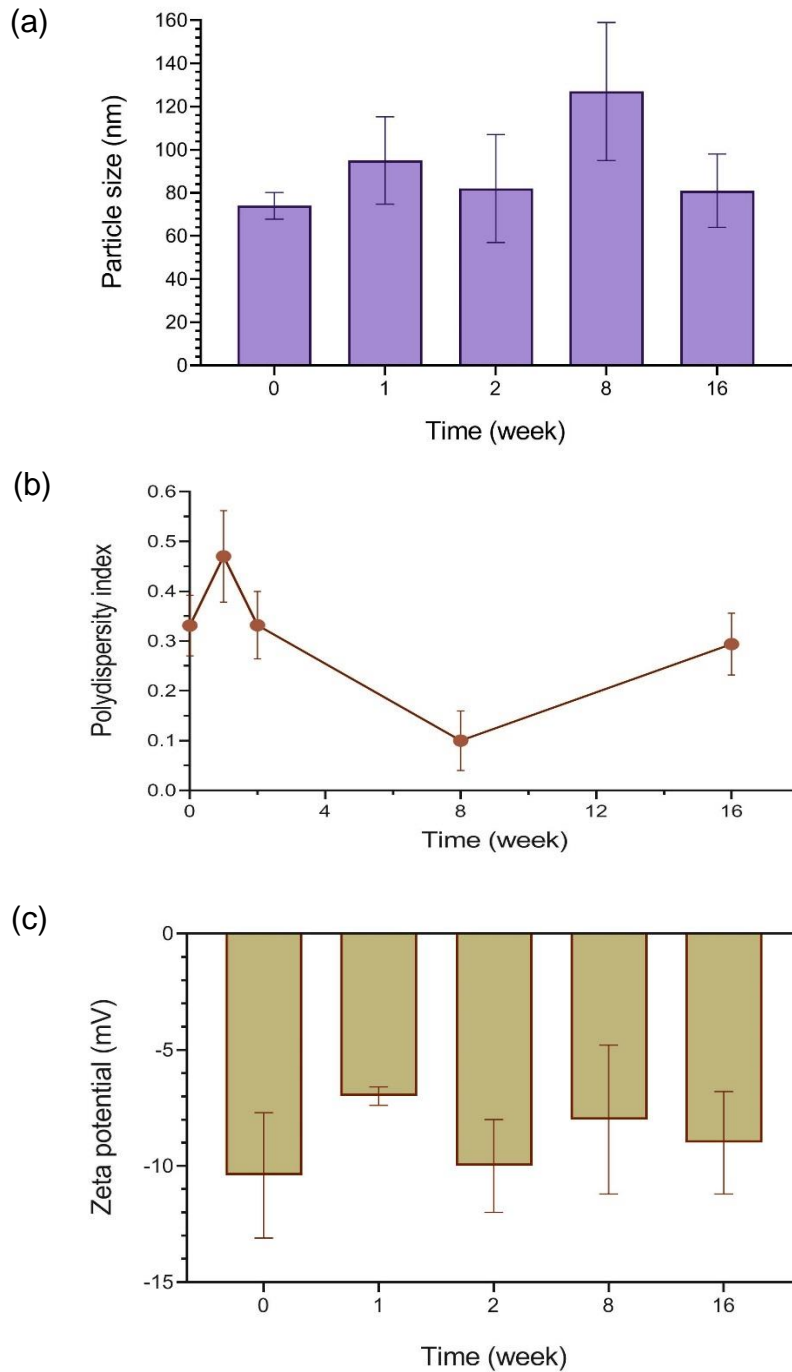


Figure 5.11: Stability of optimised PLGA nanoparticles at 4°C temperature.

(A) Particle size; (B) Polydispersity index; and (C) Zeta potential. Data are mean \pm SD ($n=3$). Nanosuspension were stored at cold temperature (4°C) up to 16 weeks. Measurement of parameters were taken at week 0, 1, 2, 8, and 16.

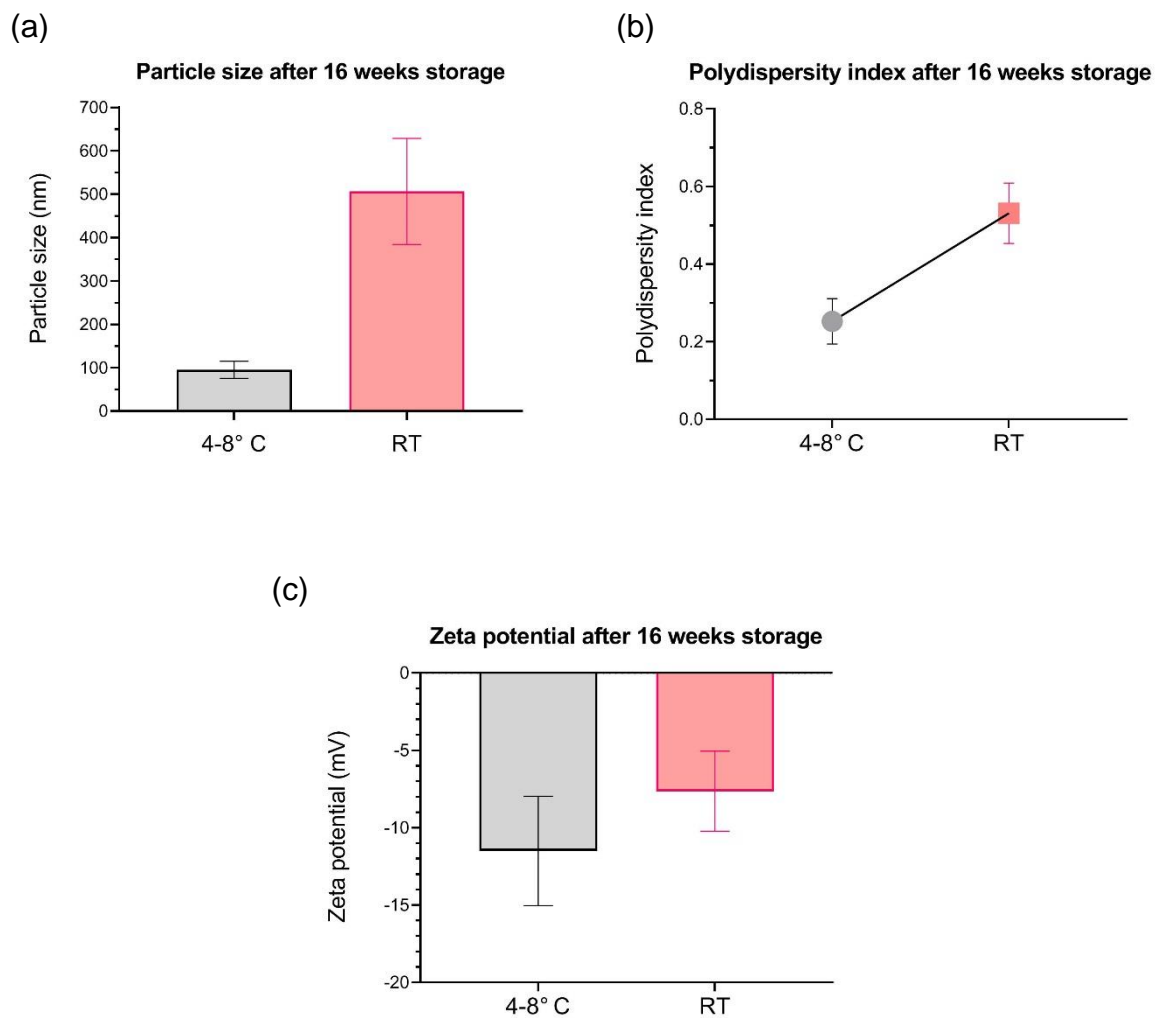


Figure 5.12: Effect of storage temperature on physicochemical properties of PLGA nanoparticles.

Effect on (A) Particle size; (B) Polydispersity index; and (C) Zeta potential after 16 weeks of storage at room temperature (RT). Data are mean \pm SD ($n=3$). Recorded room temperature was $25^{\circ}\text{C} \pm 2$ (RH 60%).

5.3.4. Detection of Microbial Contamination in Nanoparticles

Pharmaceutical formulations, such as nanoparticles are considered susceptible for microbial attack in suitable environmental conditions. The excipients in the formulations, once spoiled, provide enough nutrition for microbial growth, unless steps are taken to reduce it.

Study found that microorganisms could metabolise a variety of active ingredients, leading to the loss of their activity, for example, β -lactamase producing bacteria inactivate the penicillin injections; esterase producing bacteria inactivate aspirin in suspension; and fungi metabolise damp tablets and steroid cream.

This experiment demonstrates a qualitative detection of microbial contamination in PLGA nanoparticles. The rationale for this investigation is to avoid contamination in cell cultures, and transmission to animals in preclinical studies for toxicity, efficacy, and biodistribution. In particular, the aim of this investigation was to detect bacteria and yeast contamination in prepared PLGA nanoparticles to avoid microbial interference in glioblastoma cell cultures during cell treatment assays.

For bacteria, sterile phosphate-buffered saline (PBS) was used as a negative control, and *Staphylococcus epidermidis* as positive control. Figure 5.13(0) represents negative control and it shows absence of bacterial growth, while the growth of bacteria (as colony) was observed in positive controls, as shown in Figure 5.13(1-7). Four formulations (NPs-C6; NPs-drug-C6; NPs-C6-TF; and NPs-drug-C6-TF), which were stored in refrigerator at 4°C for 16 weeks, were investigated. Compositions of the formulations can be found in Table 5.10. Results show that all formulations were overwhelmed by the growth of bacteria (Figure 5.14). This indicates that the storing of nanoparticles as suspension is subject to bacterial contamination.

For yeast, *Saccharomyces cerevisiae* was used a positive control. Figure 5.15(0) demonstrates the negative control, indicating absence of yeast once phosphate buffered saline was spread on Malt Agar media. A serial dilution of positive controls showed the growth of yeast, as presented in Figure 5.15(1-7). Same formulations (used in bacteria detection) were used for the detection of yeast. Results showed that all formulations were contaminated with yeast, except for Formulation NPs-C6-TF for unknown reason (Figure 5.16), indicating that PLGA nanoparticles are also subject to yeast contamination upon long time storage.

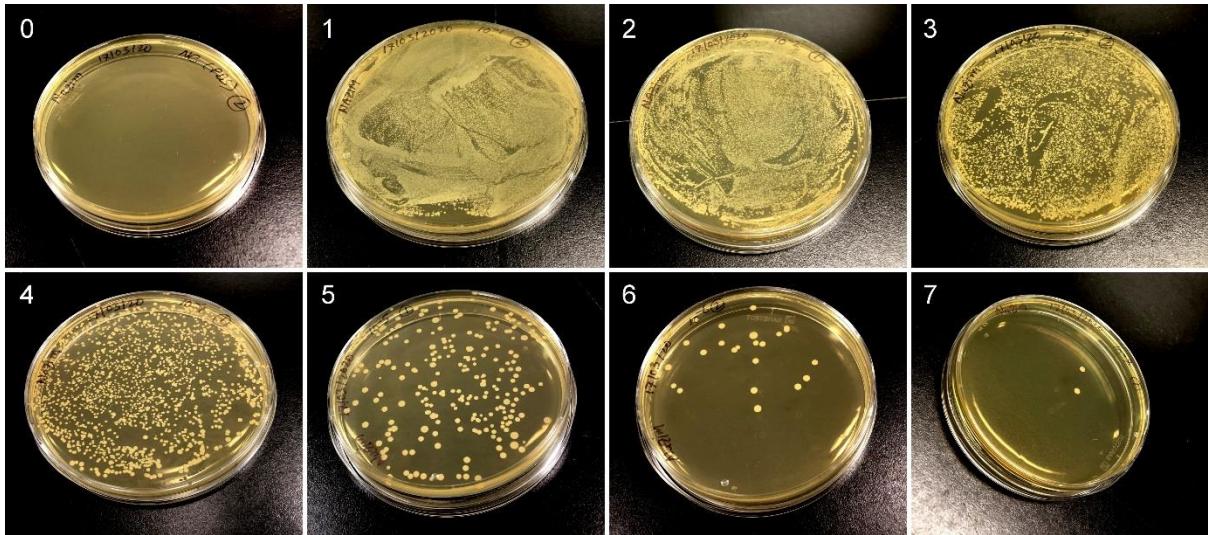


Figure 5.13: Bacteria controls on Tryptic Soy Agar (TSA) media.

(0) Negative control: Phosphate buffered saline; and (1-7) Positive control: *Staphylococcus epidermidis* in serial dilution. Images were taken after incubation for 48 hours at 37° C.

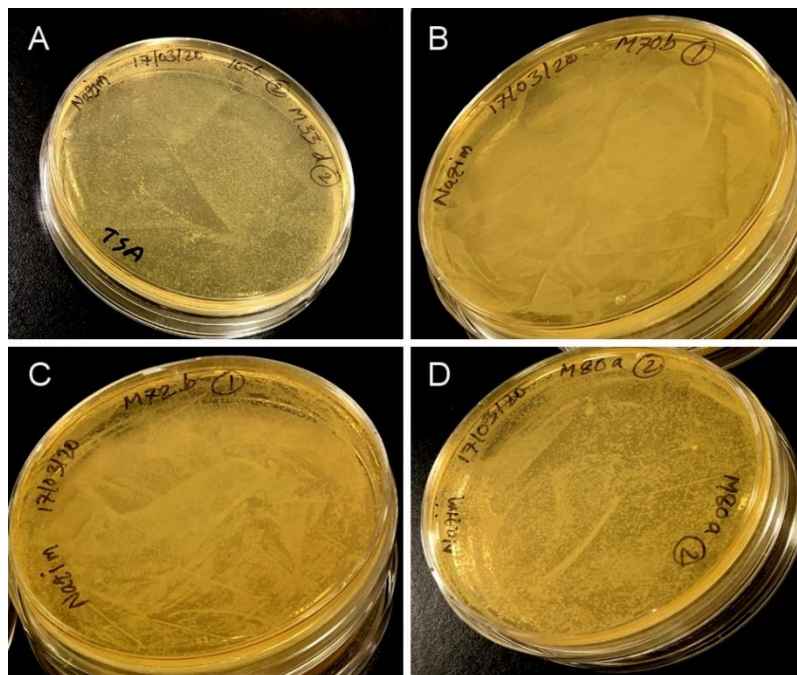


Figure 5.14: Detection of bacterial contamination in PLGA nanoparticles.

(A) Formulation NPs-C6; (B) Formulation NPs-drug-C6; (C) Formulation NPs-C6-TF; and (D) Formulation NPs-drug-C6-TF. Formulation composition can be found in Table 5.10. Images were taken after incubation of nanoparticles-spread TSA plate for 48 hours at 37° C.

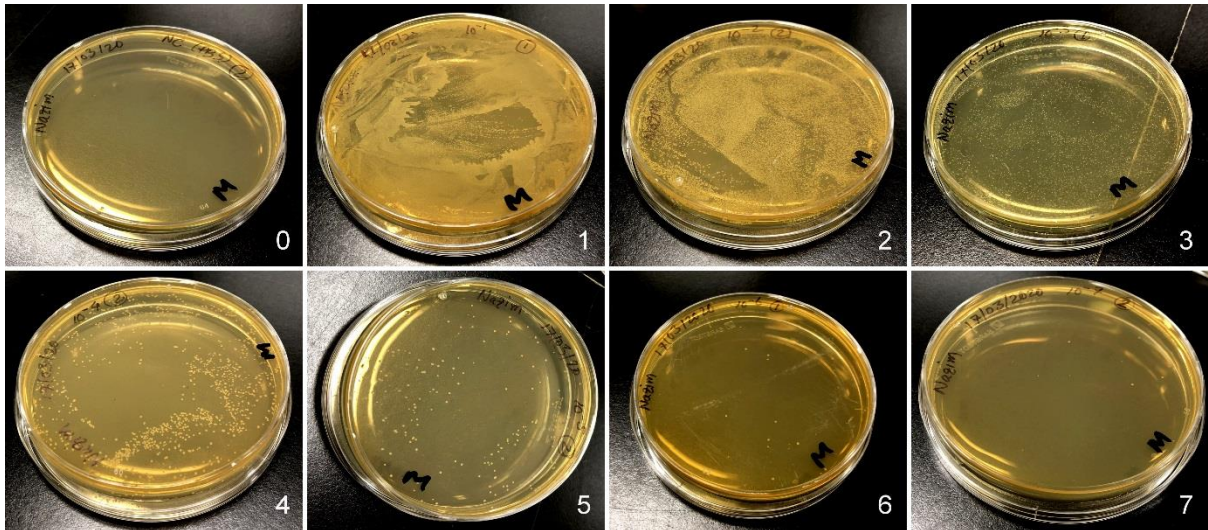


Figure 5.15: Yeast controls on Malt Agar media. (0) Negative control (phosphate buffered saline); and (1-7) Positive control (*Saccharomyces cerevisiae* in serial dilution). Images were taken after incubation for 48 hours at 25° C.

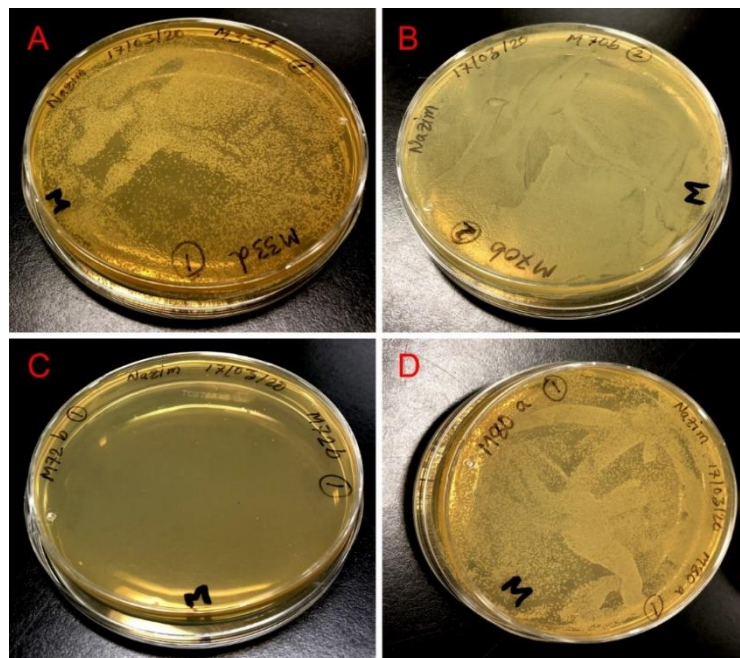


Figure 5.16: Detection of yeast contamination in PLGA nanoparticles. (A) Formulation NPs-C6; (B) Formulation NPs-drug-C6; (C) Formulation NPs-C6-TF; and (D) Formulation NPs-drug-C6-TF. Formulation composition can be found in Table 5.10. Images were taken after incubation of nanoparticles-spread Malt Agar plate for 48 hours at 25° C.

Polymeric nanoparticles can be prepared by both organic and synthetic polymers. Organic polymers, such as starches, carboxymethylcellulose, and pectins are prone to microbial depolymerization by specific extracellular proteins, such as amylases, cellulase, and pectinase respectively. However, synthetic polymers, such as PLGA are extremely resistant to microbial attack. PLGA nanoparticles are often stabilised by surfactants. Anionic surfactants are normally stable because of the slightly basic pH of the formulations. On the contrary, non-ionic surfactants are readily metabolised by microorganisms, although increased chain lengths and branching reduces the degree of attack. Cationic surfactants are used as preservatives and antiseptic; these are slowly degraded.

PLGA nanoparticles are modified by polyethylene glycol (PEG). Low molecular weight of PEG is readily degraded by sequential oxidation of the hydrocarbon chain, whereas high molecular weight is rather more uncontrollable. Lipophilic materials are extensively attacked (supported by high solubility of oxygen in many oils) when dispersed in aqueous phase, such as oil-in-water emulsions.

Preservatives and disinfectants are metabolised by many gram-negative bacteria, such as *Pseudomonas* spp. (they metabolise parabens, used as preservative, in eye drop and cause serious eye infection). Therefore, care should be taken during the selection of preservative to be used in pharmaceutical formulations.

PLGA is a heat and moisture sensitive polymer. Therefore, terminal sterilization of PLGA nanoparticles with gamma irradiation is preferred for aseptic production. It is both economic and convenient. Gamma irradiation offers advantages of low chemical reactivity with measurable residues. A study found that gamma irradiation did not have any effect on particle size, zeta potential, and encapsulation efficiency of freeze-dried PLGA nanoparticles containing hydroxypropyl- β -cyclodextrin (HP β CD) as a cryoprotectant (Parra *et al.*, 2015).

In short, PLGA nanoparticles can be contaminated by bacteria (including mycoplasma and endotoxin), viruses, and yeast during production or handling. This contamination interferes the outcome of both *in vitro* and *in vivo* biological investigation of the test nanoparticles. However, this study only determined bacteria and yeast contamination in nanoparticles qualitatively. Therefore, this study would avoid using stored nanoparticles, rather it would use freshly prepared nanoparticles for cytotoxicity and cellular uptake studies in the following chapter.

5.4. Conclusion

Current chapter optimised selected formulation F21 (from Chapter 4) by exploring further process and formulation parameters. Then it developed targeted nanoparticles with transferrin. Subsequently, it evaluated the storage stability, including the detection of any microbial contamination.

While optimising microfluidic conditions, it was found that total flow rate of 12 mL/min and flow ratio of 1:1 (aqueous phase to organic phase) were the optimal conditions for smaller particle size with narrow size distribution and high encapsulation efficiency.

Similarly, in terms of physicochemical properties of nanoparticles, optimal concentrations of PLGA, PEG, TPGS, and pimozide were found to be 20 mg/mL, 5% w/w, 1.25% w/v, and 2.5% w/w, respectively. Acetonitrile-methanol solvent system produced significantly smallest particles with higher drug encapsulation efficiency than other solvent(s)-based nanoparticles. Finally, it was found that nanoparticles collected by dialysis technique had significantly smaller particle size, however with lower encapsulation efficiency compared to centrifugation technique.

Optimised nanoparticles were adsorbed with transferrin. Transferrin adsorption was confirmed both qualitatively and quantitatively. Storage stability study suggested that nanoparticles remained stable up to 16 weeks when stored at 4°C. However, particles were found to be agglomerated when they were stored at room temperature.

PLGA nanoparticles is susceptible for microbial growth once in suspension form, although nanoparticles were found to be stable at 4°C temperature. This study detected bacterial and yeast growth in most of the formulations tested. This warrants the need of sterilisation of the formulations before *in vitro* and *in vivo* investigation. Freeze-drying could reduce the microbial growth. Freshly prepared nanoparticles could also minimise microbial interference in the results. As proposed, this study would evaluate the targeted nanoparticles in glioblastoma cell lines in the following chapter.

Chapter 6

Cytotoxicity and Cellular Uptake Studies of Targeted Nanoparticles in Glioblastoma Cell Lines

Chapter 6. Cytotoxicity and Cellular Uptake Studies of Targeted Nanoparticles in Glioblastoma Cell Lines

As previous chapter achieved an optimised and targeted formulation, this chapter therefore describes the evaluation of this formulation on human glioblastoma cell lines.

6.1. Introduction

All types of nanoparticles (such as, PLGA nanoparticles) must overcome cell membrane to get entry inside the cell. Cell membrane separates a cell's interior from the outside environment, acting as a biological barrier. Based on characteristics of this membrane, different cellular entry routes have been proposed (Figure 6.1). Two major categories of this route are endocytosis and direct cytoplasmic delivery.

Endocytosis generates small membrane vesicles (60 to 120 nm) that transport various molecules from the plasma membrane into the cytoplasm (Kaksonen and Roux, 2018). Endocytosis is further divided into two subcategories- phagocytosis and pinocytosis. Figure 6.2 illustrates mechanisms of different endocytosis processes.

Phagocytosis is performed by the immune cells, such as macrophages, dendritic cells, neutrophils, and B lymphocytes. The principal role of phagocytosis is to remove any foreign particles from the body. Therefore, nanoparticles, as unknown materials to the immune cells, are subject to phagocytosis, by physically binding to the immune cell surface receptors. Recognition and clearance of nanoparticles are mediated by opsonisation, which is a process of adsorption of serum proteins (such as, immunoglobulins) onto the surface of nanoparticles.

Pinocytosis is further subdivided into four distinct cellular uptake routes, namely (1) clathrin dependent endocytosis, (2) caveolae-dependent endocytosis, (3) clathrin and caveolae independent endocytosis, and (4) micropinocytosis. Clathrin-dependent endocytosis involves clustering and binding of nanoparticles' surface ligands to the corresponding cell surface receptors, such as transferrin receptors and epidermal growth factor receptors. Another receptor specific nanoparticle uptake route is caveolae-dependent endocytosis, which relies on caveolin-coated plasma membrane vesicles known as caveolae. Caveolae are flask shaped vesicles with diameter of 50-100 nm. Intracellular destinations of this route are Golgi apparatus and endoplasmic reticulum.

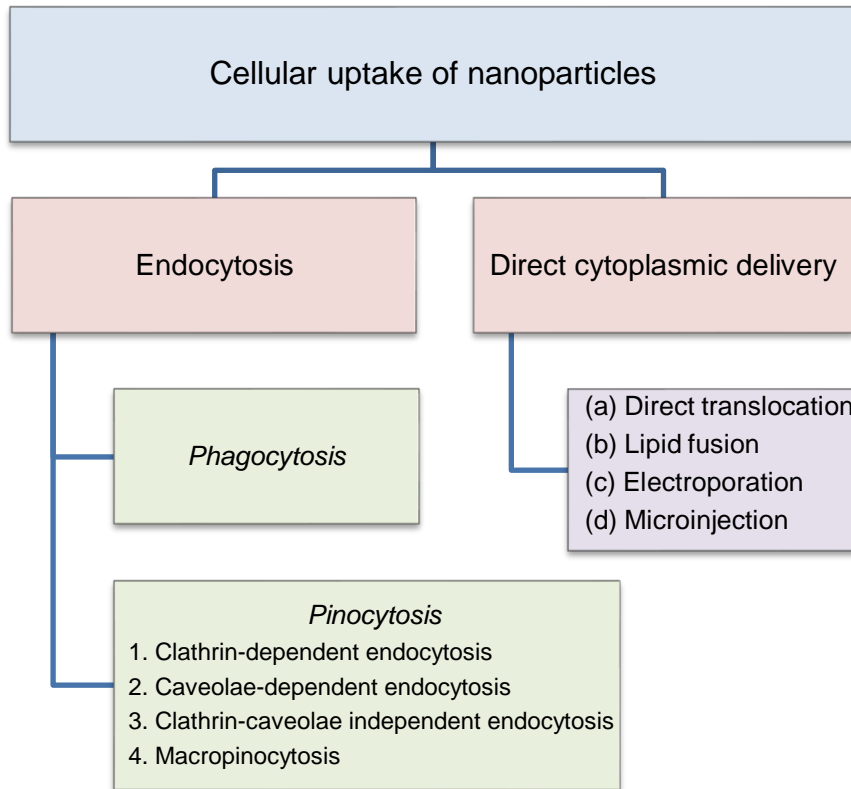


Figure 6.1: Classification of cellular uptake pathways for nanoparticles.

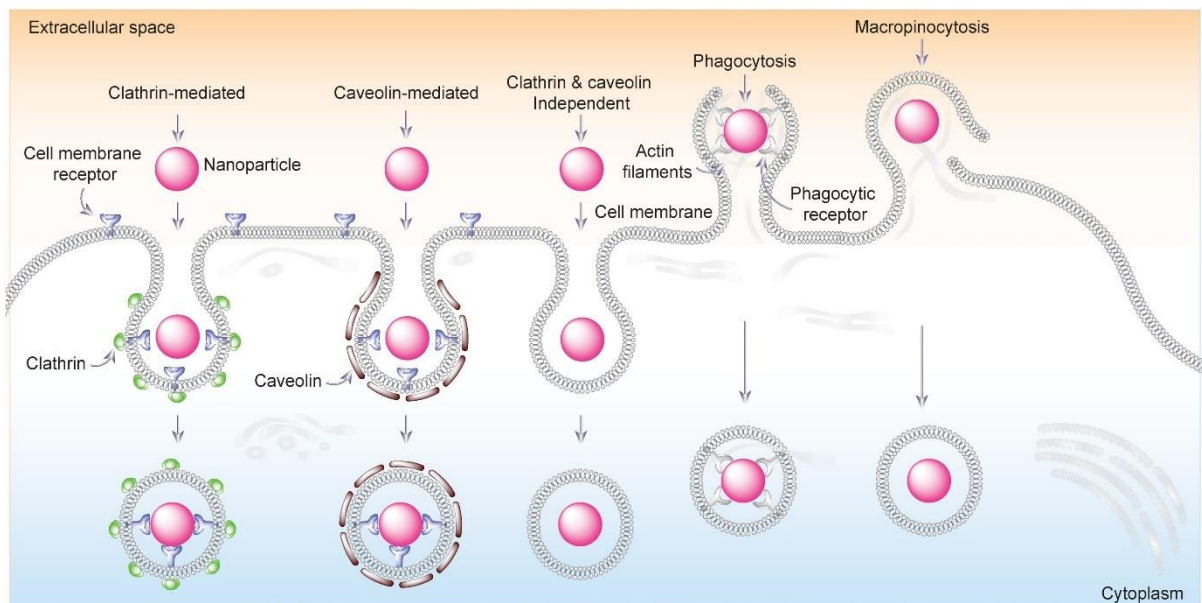


Figure 6.2: Schematic diagram showing different mechanisms of endocytosis.
Adapted from Augustine et al. (2020).

Sometimes nanoparticles can penetrate the cell without relying on clathrin or caveolae-dependent pathways. Rather, as suggested, it involves lipid rafts that are cholesterol and sphingolipid-rich domains found in plasma membrane. Unlike other routes, macropinocytosis involves non-specific cellular uptake mechanism. In this pathway, nanoparticles are trapped within the vesicle structure known as macropinosomes, which are approximately 500 to 1500 nm in size (Donahue, Acar and Wilhelm, 2019).

On the other hand, direct cytoplasmic delivery is the direct entry of nanoparticles into cytoplasm through biochemical or physical means. This route has further four distinct mechanisms, namely (a) direct translocation, (b) lipid fusion, (c) electroporation, and (c) microinjection (Figure 6.1).

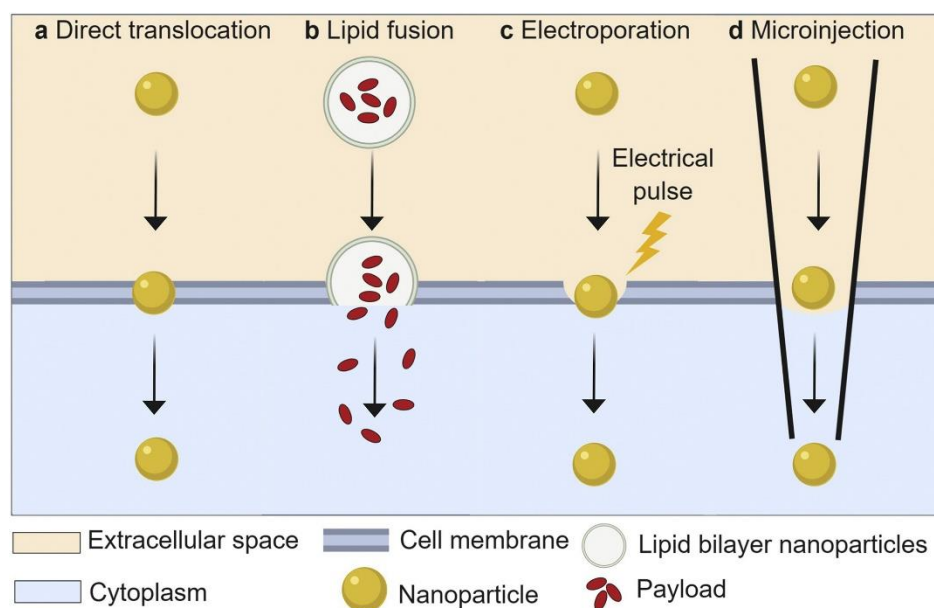


Figure 6.3: Schematic diagram of direct cytoplasmic delivery pathways for nanoparticles.
Adapted from Donahue, Acar and Wilhelm (2019).

Cytoplasmic entry by direct translocation involves disruption of cell plasma membrane after engaging with lipid bilayer, thus avoiding endosomal entrapment and energy dependent transport mechanism (Figure 6.3a). Very small particle size (<10 nm) with appropriate surface chemistry is subject to direct translocation. For example, gold nanoparticles with a size of approximately 2-4 nm and zwitterionic surface chemistry can directly diffuse through the plasma membrane of HeLa cells *in vitro* (Jiang *et al.*, 2015).

Cytoplasmic entry by lipid fusion involves fusion of lipid bilayer-coated nanoparticles and cell's plasma membrane, resulting in direct delivery of encapsulated contents into the cytoplasm (Figure 6.3b).

Nanoparticles can disrupt cell's plasma membrane by applying electrical pulses. This process is termed as electroporation (Figure 6.3c). In this technique, upon fine tuning of the electrical pulse (voltage and time), a pore is generated in the cell membrane to help nanoparticles reach the cytoplasm, by not interfering cell viability.

Microinjection process involves direct injection of nanoparticles into the cytoplasm with the help of a sophisticated microinjector (Figure 6.3d). The throughput of this technique is limited as cells need to be injected individually. Nevertheless, it can be useful tool to achieve nanotoxicological information.

Drug delivery to the brain is always challenging as blood-brain barrier (BBB) firmly regulates the passage of toxic substances from blood to the brain. It is the major obstacle for drug delivery systems to overcome for treating CNS disorders (Rempe *et al.*, 2014; Banks, 2016). BBB is composed of brain capillary endothelial cells, which line the microvessels of the brain. A typical structure of BBB is illustrated in Figure 6.4. These endothelial cells are supported by pericytes and astrocyte end-feet, both contributing to the tightness of the BBB. Paracellular transport is vastly hindered due to the tight junction protein complexes that include claudin and occludin. These junctions are further tightened by the cell's actin cytoskeleton and adapter proteins, namely cingulin and zonula occlude proteins (Johnsen *et al.*, 2019).

Nevertheless, certain essential molecules are transported through the brain capillary endothelial cells by several means namely entry by immune cells, transport protein-mediated influx (such as, glucose by glucose transporter 1), paracellular pathway, adsorptive transcytosis, passive diffusion (such as, CO₂ and O₂), lipophilic pathway, and receptor-mediated transcytosis. Figure 6.5 illustrates the transport mechanisms at the BBB. Briefly, immune cells, such as leukocytes can migrate through the endothelial cells once warranted for any immune response to the brain. The brain capillary endothelial cells express some transport proteins (such as, glucose transporter 1) that mediate the influx of nutrients (such as, glucose). Small hydrophilic molecules are transported via cell-cell junctions known as paracellular transport. Adsorptive transcytosis involves electrostatic interaction between negatively charged cell membrane and any positively charged molecule (such as, albumin), subsequently transporting the cationised molecules across the cells. On the other hand, hydrophobic molecules can readily enter the cells. However, there is a chance that p-glycoprotein could pump out the hydrophobic molecules by an efflux mechanism. Finally,

plasma proteins (such as, transferrin) can bind to the endothelial cell surface receptors (such as, transferrin receptor) to initiate their (plasma protein-receptor complex) transport across the cell. This process is called receptor-mediated transcytosis.

For nanoparticles, a promising approach that can bypass the BBB is to target transferrin receptors (TFR) expressed in brain capillary endothelial cells. Most importantly, TFR are overexpressed in brain tumour cells. Therefore, in line with the general aim of the study, the receptor-mediated transcytosis and receptor-mediated endocytosis, as already discussed in previous section are the focuses of this investigation. More specifically, this study developed transferrin coated nanoparticles to enhance their entry into the cytoplasm via transferrin receptor-mediate endocytosis.

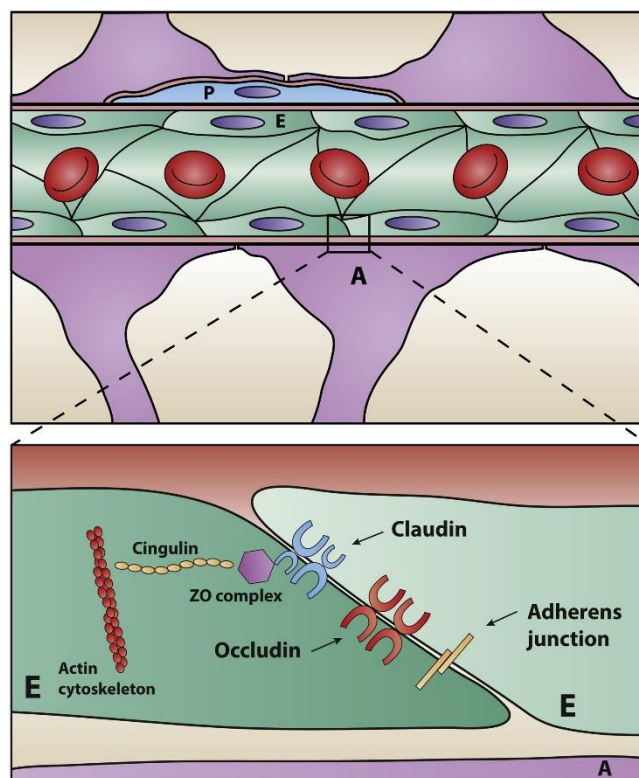


Figure 6.4: A typical structure of blood-brain barrier.
Adapted from Johnsen et al. (2019). P, pericytes; E, endothelial cells; A, astrocyte end-feet.

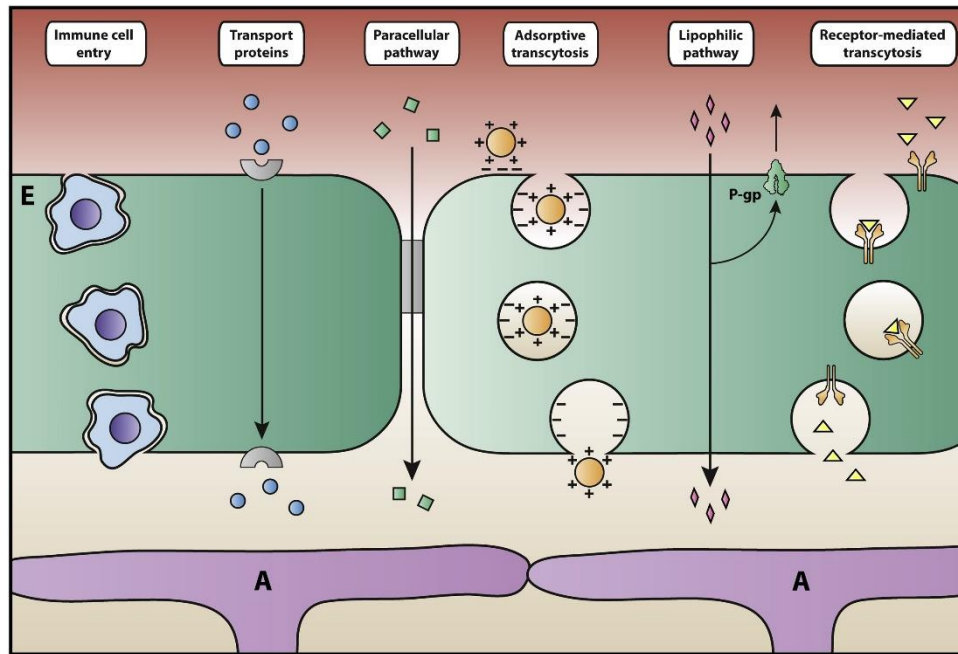


Figure 6.5: Schematic diagram of transport mechanisms at blood-brain barrier.
Adapted from Johnsen et al. (2019).

Transferrin (TF) is a monomeric glycoprotein (~80 kDa) and it is one of the most abundant (25-50 μM) plasma proteins present in normal human blood plasma. It is synthesised in both liver and central nervous system (in the oligodendrocytes and choroid plexus epithelial cells). Structurally, TF is composed of single polypeptide chain with two equal sized domains, namely N and C terminal domains. Each domain contains an iron-binding site with high affinity. Therefore, each transferrin molecule can carry two iron molecules and transport it inside the cells.

Iron is an essential element for a vast number of proteins. It is required in basic cellular process, such as oxygen transport, enzyme reactions, oxidation reaction, reduction reaction, and in cell division. Outside the cell, iron is always bound to transferrin as ferric form (Fe^{3+}), which is a non-toxic oxidative form. Inside the cell, it remains as ferrous form (Fe^{2+}), which could be toxic once allowed to occur redox reaction (Fenton reaction) with hydrogen peroxide to generate free radicals. This only happens where iron is present in excess. However, when in balance, unused Fe^{2+} inside the cell gets oxidized by iron storage protein known as ferritin. Thus, ferritin prevents Fe^{2+} from initiating unwanted redox reaction, subsequently preventing from generating reactive oxygen species and free radicals.

It is already known that TF transports iron inside the cell via transferrin receptors (TFR)-mediated endocytosis. Human TFR are transmembrane glycoprotein composed of two identical subunits of 90 kDa, which are linked by disulphide bonds. There are two types of

TFR, namely TFR1 and TFR2. In general, TFR1 is ubiquitously expressed high affinity receptor for transferrin. In contrast, expression of TFR2 is restricted to certain types of cells and its affinity for transferrin is lower compared to TFR1.

The interaction between TFR1 and TF is pH dependent. As demonstrated in Figure 6.6, extracellularly, at pH 7.4, TFR1 binds with holo-TF and internalised via clathrin-mediated endocytosis. Two ferric iron containing TF is known as holo-TF, while iron deficient TF is called apo-TF. Interestingly, at low pH in the endosome, ferric iron is dissociated from holo-TF and converted to ferrous iron, apo-TF-TFR1 complex is then transported back into the cell surface, where apo-TF is released into the bloodstream to be re-used. The iron storage protein known as ferritin is also another ligand for TFR1.

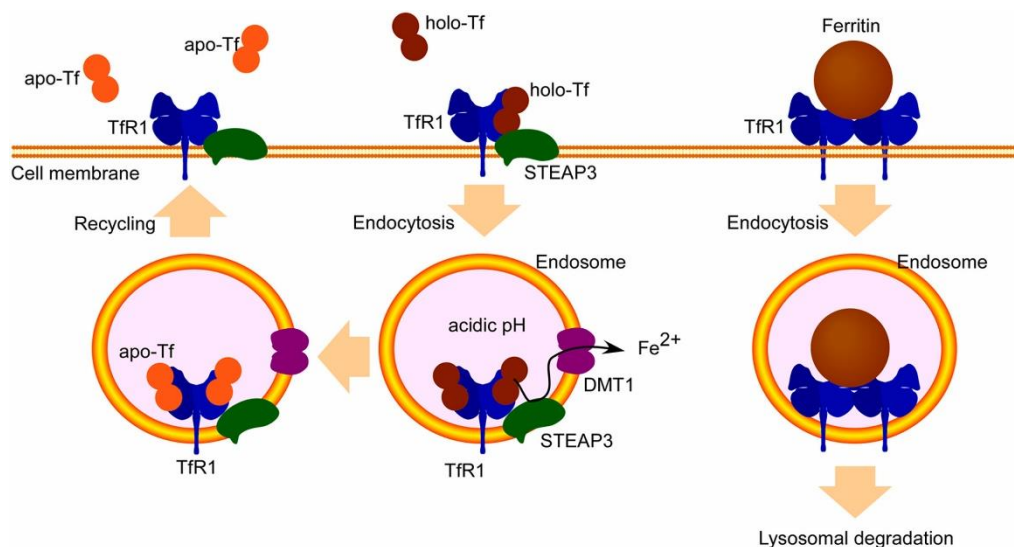


Figure 6.6: Schematic diagram of transferrin receptor 1-mediated endocytosis of holo-transferrin and ferritin, and recycle of apo-transferrin.
Adapted from Kawabata (2019).

Another receptor for TF known as TFR2 was first named and reported by Kawabata *et al.* (1999). Primarily, the structure of TFR2 is similar to TFR1. However, it has two sub types, namely TFR2- α and TFR2- β . Expression of TFR2- α was reported to be expressed selectively in hepatocytes and erythroid precursor cells, while TFR2- β was found in variety cells at low level. The binding TFR2 with holo-transferrin is also pH dependent. Furthermore, TFR2 facilitates iron delivery to the mitochondria with the aid of a functional mitochondria targeting motif existing in the intracellular domain of TFR2- α . This mechanism is illustrated in Figure 6.7, as proposed by Kawabata (2019). Briefly, holo-TF-TFR2 complex is transported

to the lysosome from endosome. Mitochondria targeting motif present in TFR2- α drives holo-TF-TFR2 complex toward a mitochondrion to physically interact with it. After interaction, iron is exported from lysosome by mucolipin and imported in the mitochondrial inner membrane by mitoferrin.

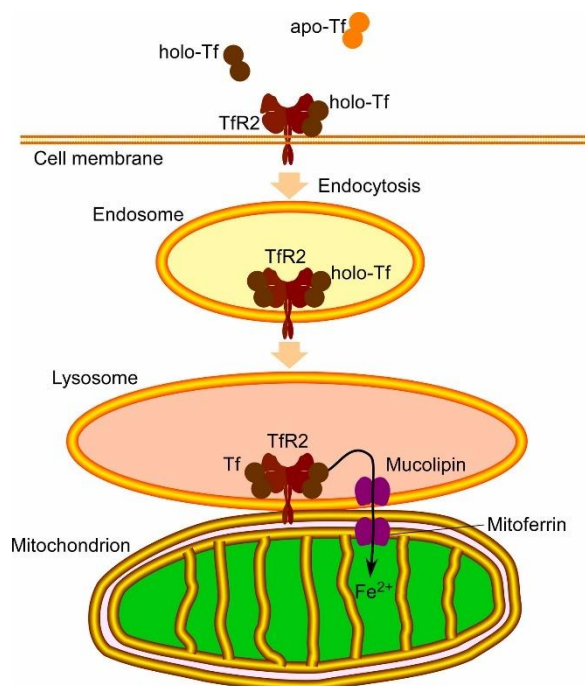


Figure 6.7: Schematic diagram of transferrin receptor 2-mediated endocytosis and hypothetical iron transport to the mitochondria.

Adapted from Kawabata (2019).

In short, mitochondria require the highest level of iron, as it is the centre of cellular respiration and the main site of oxidative phosphorylation. Furthermore, mitochondria consume iron to synthesise heme, a precursor to haemoglobin that is necessary to bind oxygen in the bloodstream. Therefore, it is understood that TF-TFR system plays a pivotal role cell survival and regeneration. Drug delivery systems are being developed targeting TFR system to transport the therapeutic molecule inside the cells. Glioblastoma cells express high level of transferrin receptors due to the high level of iron demand for uncontrolled proliferation. Based on this fact, this chapter aims to transport pimozi-encapsulated PLGA nanoparticles via TFR-mediated endocytosis, and subsequently provide evidence that pimozi could be repurposed for glioblastoma chemotherapy.

6.2. Aim and Objectives

Aim

- a) To evaluate the cytotoxic effect of pimozone-encapsulated PLGA nanoparticles (optimised and targeted formulation) in glioblastoma cell lines.

Specific objectives

- i. To confirm the expression of selected receptor proteins (5HT₇, USP1, TFR1, and TFR2,) on different glioblastoma cell lines (E2, G7, R24, and GLG).
- ii. To confirm cytotoxic effect of native pimozone by cell proliferation assay.
- iii. To investigate cytotoxicity and cellular uptake of pimozone-encapsulated nanoparticles with and without targeting ligand transferrin.

6.3. Results and Discussions

6.3.1. Expression of potential receptor proteins

Generally, cancer cells overexpress some receptor proteins during their uncontrolled cell proliferation. Similarly, human glioblastoma cells overexpress certain receptor proteins that could be selectively targeted to inhibit the cell growth.

Western blot analysis was carried out to investigate the expression of potential receptor proteins on four human glioblastoma cell lines, namely E2, G7, R24, and GLG (refer Section 2.2.4.2). This technique employed SDS-PAGE (sodium dodecyl sulfate - polyacrylamide gel electrophoresis) that separated receptor proteins, such as serotonin receptor-7 (5HT₇), ubiquitin specific protease-1 (USP1), and transferrin receptors (TFR1 and TFR2) based on their molecular weights, followed by probing them with corresponding antibodies, and subsequently detecting the protein bands by chemiluminescence method, as summarised in Figure 6.8. Glyceraldehyde 3-phosphate dehydrogenase (GAPDH) was used as a loading control. Stable and ubiquitous expression of GAPDH on all four cell lines indicates that equivalent amount of protein was loaded in different lanes of the blot (Figure 6.8).

Serotonin (5-hydroxytryptamine, abbreviated as 5-HT) is a neurotransmitter that is recognised by a family of seven serotonin receptors. Each receptor is structurally and functionally different. Among them serotonin receptor-7 (5-HT₇) was found to be stimulating glioblastoma growth (Kast, 2010).

Current study observed that 5-HT₇ receptors were expressed on all four glioblastoma cell lines (Figure 6.8). This indicates that selective 5-HT₇ receptor ligands could be potential therapeutic strategy for glioblastoma therapy. This finding is consistent with a study that concluded that human glioblastoma cell lines (U-373 MG, U-138 MG, U-87 MG, T98G, H4, DBTRG-05MG, CCFSTTG1) expressed functional 5-HT₇ receptors and three splice variants of corresponding mRNA (Mahé *et al.*, 2004).

Ubiquitination is a common reversible posttranslational modification process. A group of enzymes known as deubiquitinates (DUBs) perform on ubiquitinated substrates to catalyse the removal of ubiquitin moieties. Ubiquitin-specific protease 1 (USP1) is one of the most well characterised DUBs. It plays an important role in the regulation of DNA repair processes. Deregulation of USP1 was found to be linked in certain types of cancer

This study also found that USP1 was expressed predominantly in GLG cell lines compared to R24 (Figure 6.8). However, the expression was absent in both E2 and G7 cell lines. certain types of human cancer, suggesting that USP1 could represent a valid target in

cancer therapy. A study found that USP1 was highly expressed on human glioma tissue and this expression correlated with poor survival (Lee *et al.*, 2016).

Both transferrin receptor proteins (TFR1 and TFR2) were found to be expressed on three cell lines, except GLG. (Figure 6.8). Darker band width of TFR1 on E2 cell line indicates that it was overexpressed.

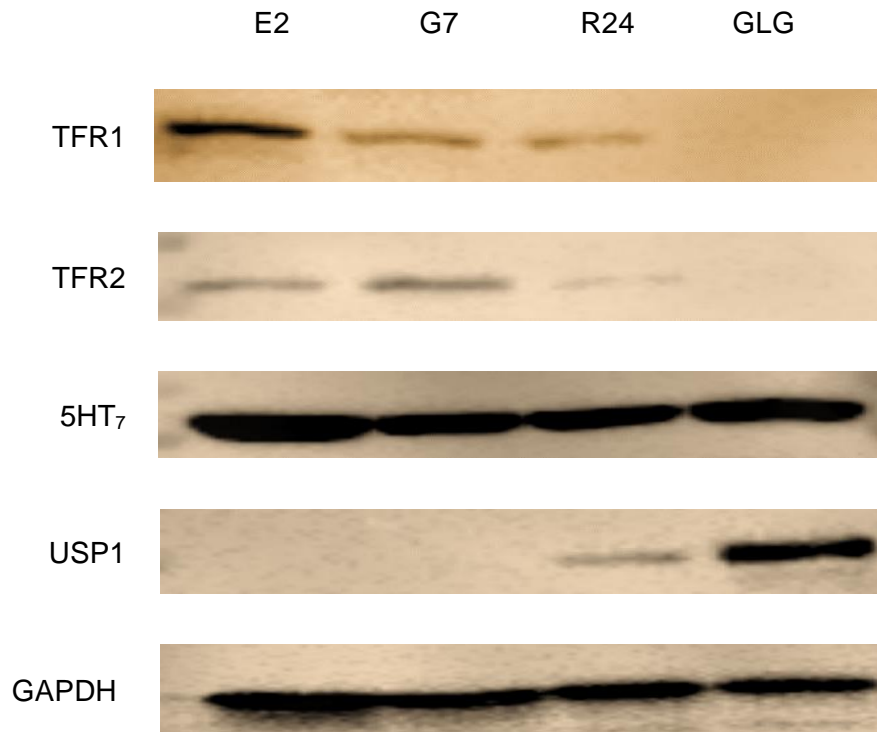


Figure 6.8: Western blot analysis of receptor proteins expressions in glioblastoma cell lines. Cell lysates were prepared from untreated glioblastoma cell lines (E2, G7, R24, and GLG) cultured for 7 days, and subjected to Western blotting with respective antibodies. TFR, transferrin receptor; 5HT₇, serotonin receptor; and USP1, ubiquitin specific protease 1. GAPDH (glyceraldehyde 3-phosphate dehydrogenase) was used as a positive control.

Transferrin receptors (TFR), as already discussed in Section 6.1, are the cell surface membrane proteins that regulate cellular iron uptake by attaching TF-iron complex via clathrin-mediated endocytosis. TFR is expressed in capillary endothelial cells in the brain. This expression was found to be linked with the cell growth. Most importantly, increased number of TFR was found to be expressed in the neoplastic brain tissue compared to the normal brain tissue (Recht *et al.*, 1990). Authors observed that there was a much higher reactivity in tumour tissue for anti-TFR.

It is already known that there are two types of TFR, namely TFR1 and TFR2. Calzolari *et al.* (2007) screened a large set of cancer cell lines, including glioblastoma, for the detection of TFR1 and TFR2 expression by Western blotting. Authors observed that the expression of TFR2 was frequent in colon cancer, glioblastoma, ovarian cancer, and lymphoma cell lines. On the other hand, the expression of TFR1 was omnipresent. Interestingly, authors noticed that the level of expression of TFR2 was inversely proportional to TFR1. In other words, cancer cell lines expressing TFR2, express TFR1 at a low level. This is consistent with E2 glioblastoma cell line of the current study, where the expression intensity of TFR1 was higher than TFR2 (Figure 6.8). A quantitative analysis of expression could further evaluate the correlation between these two receptors in E2 cells along with G7 and R24.

Later study provided further evidence that TFR2 was overexpressed on glioblastoma cell lines (Calzolari *et al.*, 2010). Furthermore, authors reported that TFR2 was absent on the normal endothelial cells of the brain. These findings suggested that the induction of TFR2 in glioma cells might provide a growth advantage. Accordingly, authors noticed that TFR2 activation induced a rapid and distinct extracellular signal regulated kinase (ERK 1 and 2) phosphorylation, contributing to the cell proliferation. As ERKs are constitutively activated in glioma cells, their level of activation is believed to be responsible for poor prognosis of glioblastoma. Authors concluded that TFR2 was a neoantigen for astrocytoma, thus attracting development of new targeted therapies.

In summary, Western blot analysis provided evidence that both transferrin receptors (TFR1 and TFR2) were expressed on three human glioblastoma cell lines out of four, although their expression intensity differed. Therefore, glioblastoma can be targeted by transferrin-coated nanoparticles carrying pimozone. Furthermore, it also proved that 5-HT₇ and USP1, which are responsible for glioblastoma growth, were expressed on glioblastoma cell lines. Early research found that pimozone could selectively bind to these receptors and inhibit them. Following experiments would evaluate this effect.

6.3.2. Cytotoxicity and cellular uptake of nanoparticles

Cytotoxicity is the detrimental effects on living cells by any substance or environmental changes. The detrimental effects could be either compromise of metabolic activity, inhibition of cell growth or cell death. The mechanisms of cell death are known as autophagy, apoptosis, and necrosis. Autophagic cell death involves a specialised process where cells get digested by cells. Apoptosis is more controlled mechanism of cell death. On the other hand, necrosis is a catastrophic cell death.

Cell proliferation, for both cancer and normal cells, is the crucial mechanism for tissue development and regeneration. Therefore, proliferation assays are necessary to determine cytotoxic effect of any drug molecule.

Cytotoxicity of pure pimozone was investigated on E2 cell line. Cell proliferation was monitored by analysing the occupied area (% confluence) of live cells images over time with and without pimozone treatment. As cells grow with time, the confluence increases, occupying more area in the microplate well. When cells stop growing due to an external effect, such as a cytotoxic drug, the confluence would remain same or decrease since the integrity of cell membrane would be damaged, leading to less occupied area by insoluble fragments of dead cells.

Initially, four concentrations of native pimozone (0.1, 1, 5, and 10 μM) dissolved in DMSO were selected to evaluate the cytotoxicity on glioblastoma cells. According to the phase object confluence data, it was observed that cells stopped growing once treated with pimozone at concentrations of 5 and 10 μM (Figure 6.9). However, no effect was noticed at concentrations of 0.1 and 1 μM . Notably, the cytotoxic effect was absent in DMSO treated cells (Figure 6.9). These results were validated by assessing cell morphology from the phase contrast images taken from each well. Representative phase contrast images of pimozone untreated and treated (5 μM) are compared in Figure 6.11. For better visualisation of intracellular uptake of pimozone, fluorescent dye (coumarin-6) treated cells are also presented in Figure 6.11.

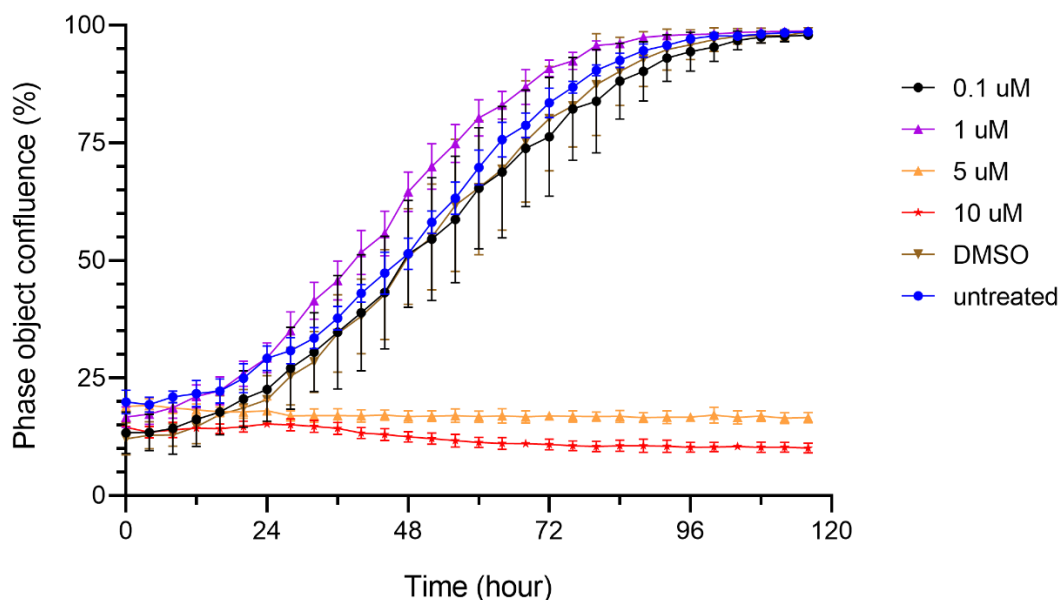


Figure 6.9: Effect of different pimozide concentrations on glioblastoma cells proliferation. E2 cells with or without pimozide treatment were incubated for 120 hours. Phase contrast images of live cells were used to produce data that represent mean confluence (%) \pm SD (n=6). Dimethyl sulfoxide (DMSO) treated and untreated cells were used as controls.

However, the cellular uptake and the mechanism of action of pure pimozide to arrest glioblastoma cell proliferation is not extensively explored. Several mechanisms have been proposed.

Pimozide is a selective serotonin receptor-7 (5-HT₇) antagonist. 5-HT₇ is highly expressed in glioblastoma. Pimozide has the highest affinity for the 5-HT₇ receptor among all first-generation antipsychotics, with a K_i value, which is a drug affinity at the receptor, of 0.5 nM (Roth *et al.*, 1994; Kast, 2010). It was reported that extracellular regulated kinase 1/2 (ERK 1/2) was activated (phosphorylated) via activation of 5-HT₇ receptor in microglia (Mahé *et al.*, 2004). Later, it was found that 5-HT₇ receptor agonism resulted in increased ERK 1/2 activation, increased interleukin-6 (IL-6) synthesis, increased signal transducer and activator of transcription-3 (STAT-3) activation, increased vascular endothelial growth factor, and increased resistance to apoptosis (Kast, 2010). In brief these all leads to growth of glioblastoma cancer cells. Thus, pimozide as a potent 5-HT₇ receptor blocker could inhibit the growth of glioblastoma by interfering with the 5-HT₇-receptor associated pathways (Figure 6.12).

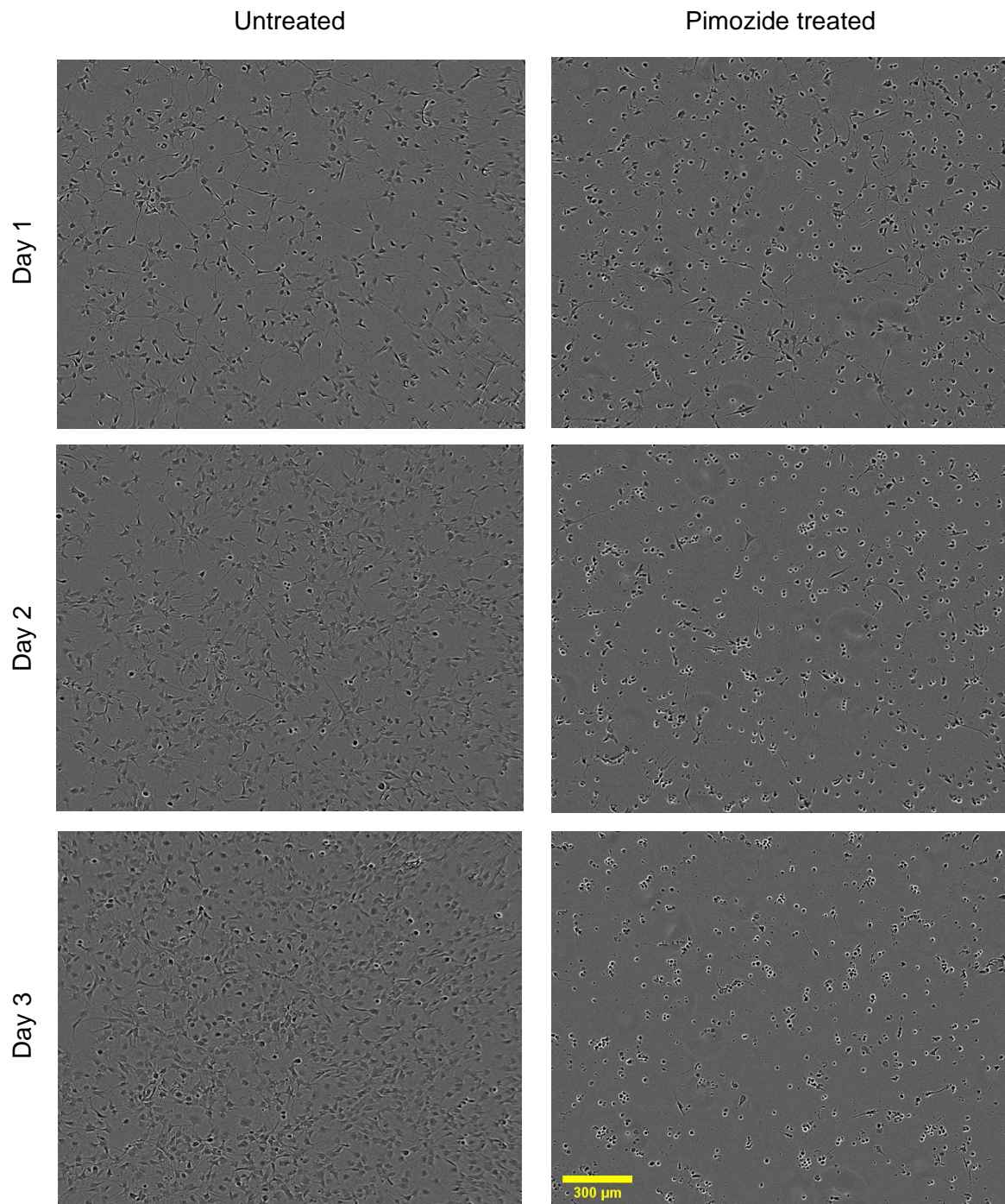


Figure 6.10: Representative phase contrast images of glioblastoma cells proliferation with and without pure pimozide treatment.

E2 cells were incubated for 120 hours after treating with pimozide (5 μM). Images were taken in every 4 hours during the incubation. Dimethyl sulfoxide (DMSO) was used as a control. Scale bar indicates 300 μm . Representative images are presented up to 72 hours for demonstration purpose only.

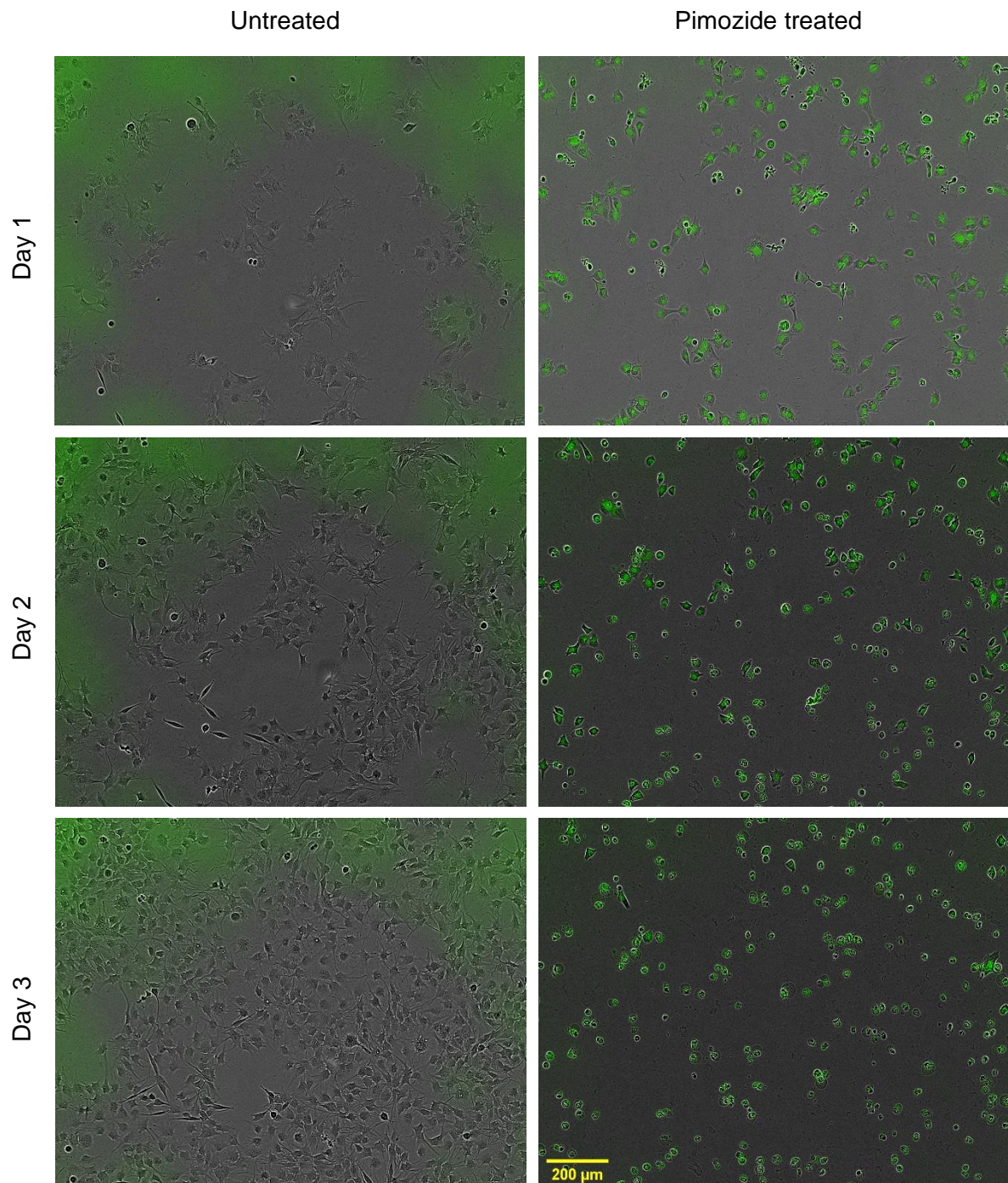


Figure 6.11: Representative phase contrast images of glioblastoma cells after pure pimozide treatment with fluorescent dye.

E2 cells were incubated for 120 hours after treating with pimozide (5 μM) with fluorescent dye (coumarin-6). Images were taken in every 4 hours during the incubation. Dimethyl sulfoxide (DMSO) was used as a control. Scale bar indicates 200 μm . Representative images are presented up to 72 hours for demonstration purpose only.

Glioblastoma stem cell maintenance and radioresistance are inhibited by targeted blocking ubiquitination-specific protease 1 (USP1) which is highly expressed in human glioma tissues (Lee *et al.*, 2016). USP1 promoted inhibiting DNA-binding protein 1 (ID1) and checkpoint kinase 1 (CHEK1) stability, leading to stem cell maintenance and radio resistance of the glioblastoma cells. As pimozide is a pharmacological inhibitor of USP1, authors reported that pimozide concentration of 7.5 μM was effective to kill all the glioblastoma cells in 3 days. Authors explained that pimozide inhibited cell survival and growth, and increased sensitivity of glioblastoma cells to radiation treatment, while sparing the normal neural progenitors (Lee *et al.*, 2016).

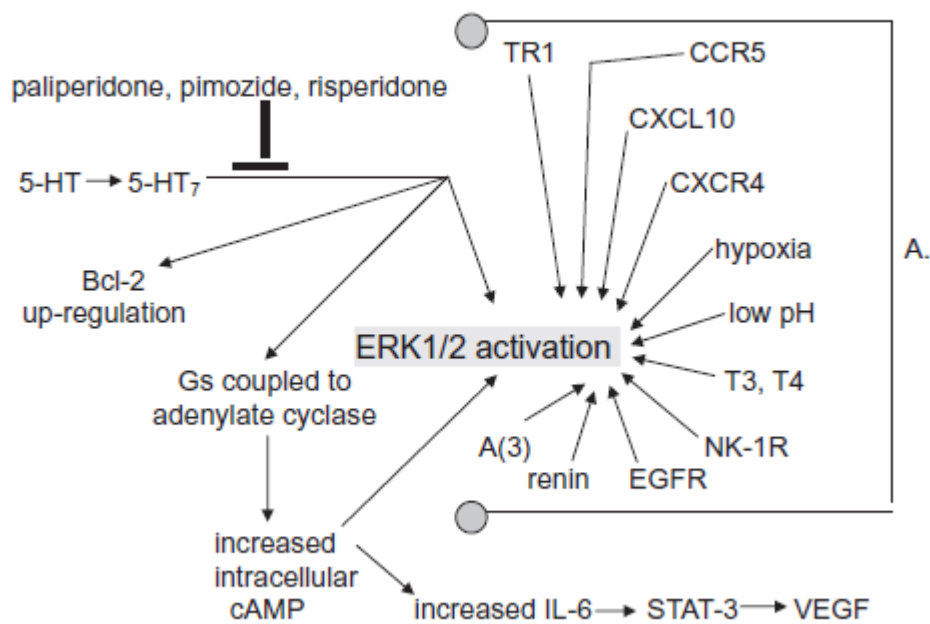


Figure 6.12: Putative representation of serotonin receptor-7 antagonism and subsequent inhibition mechanism of glioblastoma proliferation.

Adapted from (Kast, 2010). Beside serotonin receptor pathway, there are other routes that induce ERK 1/2 activation, as described in text (A).

Autophagy is a self-degradative process of cellular components, promoting cell survival in response to nutrient stress (Glick, Barth and Macleod, 2010). However, excess autophagy is harmful for cells and that could be a potential anticancer action once the autophagic cascade is strongly triggered by any drug or agent (Levy, Towers and Thorburn, 2017). Arguably, autophagy can be targeted for both stimulation and inhibition because the role of autophagy in controlling tumour immune responses is unclear. Therefore, Levy and colleagues suggested to better understand the biology and then apply that knowledge in well-designed clinical trials (Levy, Towers and Thorburn, 2017).

A study, for the first time, showed that 15 μM pimozide induced autophagic cell death in glioblastoma cell lines, namely MZ-54, LN-229 and U343 GOS-3 (Svenja *et al.*, 2018). This was because pimozide was a potent inhibitor of low voltage-gated T-type calcium channels. Arguably, inhibition of calcium channel is associated with autophagy regulation.

Over 50% of GBM tumours overexpress both epidermal growth factor receptor (EGFR) and the variant EGFRvIII simultaneously, conferring a poor prognosis. Both growth factor receptors cooperate to advance tumour progression and invasion, somewhat activating STAT signalling pathway. Pimozide inhibits STAT5 phosphorylation, cell migration and survival, when treated EGFRvIII-expressing GBM cells (Roos *et al.*, 2018).

As already discussed in chapter 1 that pimozide exerts its antipsychotic effect by blocking dopamine (D2) receptor, a recent study showed that the dopamine D2 receptor-signalling pathway might be linked to the spheroid formation in GBM cells. Authors observed that pimozide decreased the spheroid formation at a selective concentration of 0.1 μM (Weissenrieder *et al.*, 2020), suggesting another pathway for glioblastoma inhibition.

Current study already concluded that 5 μM was the minimum effective concentration of free pimozide to inhibit the complete proliferation of glioblastoma cells, however, concentrations more than 1 μM and less than 5 μM still remained unexplored in this study. Following experiment would investigate the cytotoxicity of pimozide-encapsulated nanoparticles. Furthermore, it would evaluate whether transferrin receptor targeted nanoparticles could block the glioblastoma cell growth with greater extent compared to non-targeted nanoparticles.

At first, cytotoxicity of drug-free substances, namely empty nanoparticles (NPs), distilled water (dispersion phase of nanoparticles), coumarine-6 (fluorescent dye), and TF (targeting ligand) was evaluated by comparing the cell proliferation profile of corresponding substance treated cells with untreated cells. Figure 6.13 shows that cell proliferation was not affected after treatment with empty PLGA nanoparticles, distilled water, dye, and transferrin. These

results were supported by phase contrast images of treated and untreated glioblastoma cells. Figure 6.14 shows representative images of empty nanoparticles treated cells, where it can be observed that cells proliferation was not halted. This confirmed that drug-free individual substance (at an equivalent concentration in treating formulation) was well tolerable by glioblastoma cells, which also indicated that TF-coated nanoparticles would not induce any intolerance to the glioblastoma cells. A study also reported that drug-free PLGA-TF nanoparticles did not show any cytotoxicity to human pancreatic cancer cells (Frasco *et al.*, 2015).

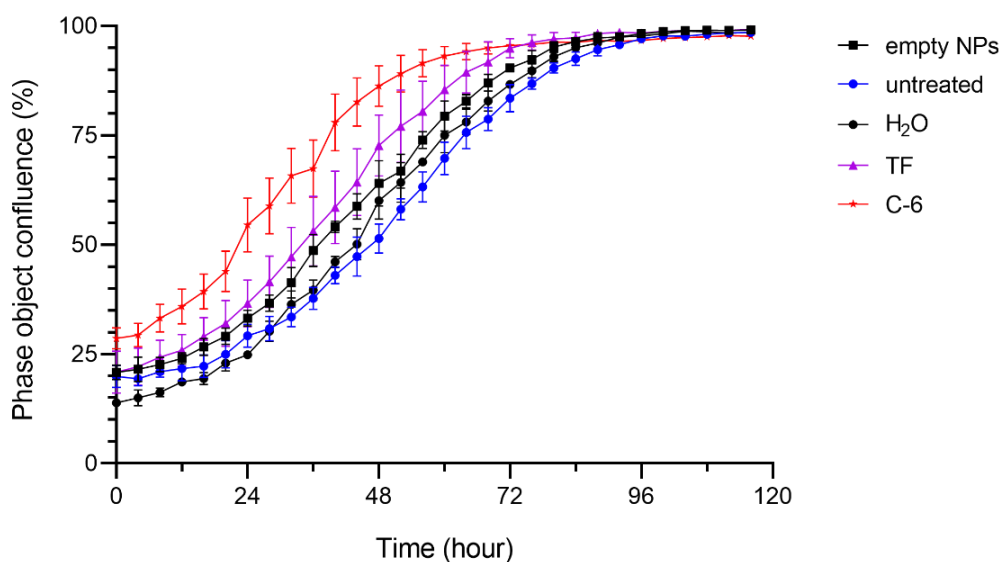


Figure 6.13: Effect of drug free-substances on glioblastoma cells proliferation.

E2 cells with or without of treatment of water (H₂O), transferrin (TF), empty nanoparticles (NPs), and fluorescent dye (C-6) were incubated for 120 hours. Phase contrast images of live cells were used to produce data that represent mean confluence (%) \pm SD (n=6).

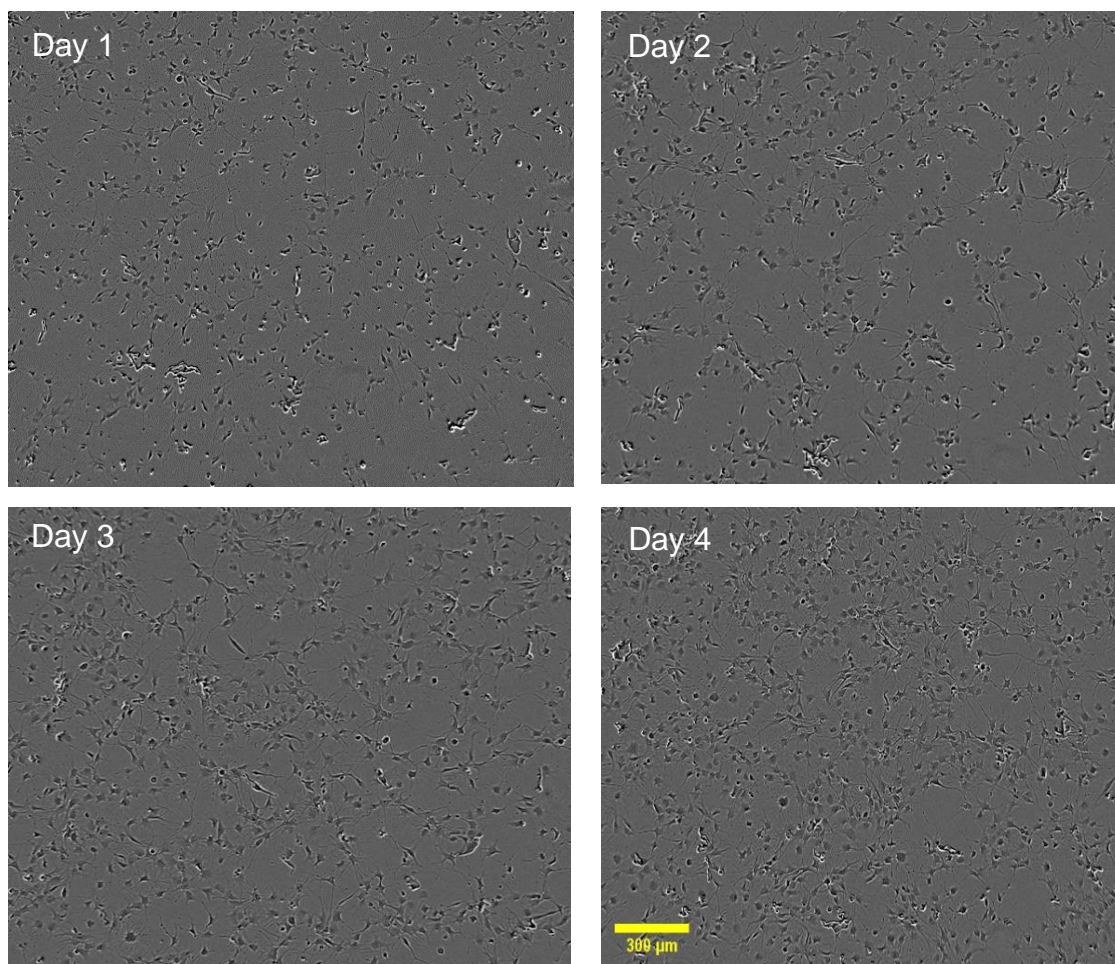


Figure 6.14: Representative phase contrast images of E2 cells after treating with empty PLGA nanoparticles.

E2 cells were incubated for 120 hours after treating with targeted and non-targeted nanoparticles. Images were taken in every 4 hours during the incubation. Scale bar indicates 300 μm .

Accordingly, E2 cells were treated with nanoparticles carrying equivalent 5 μM concentration of pimozone, calculated from the drug encapsulation efficiency. However, it was found that this treatment was unable to inhibit the cell proliferation completely (Figure 6.15). It could be explained by the sustained release of pimozone out of the PLGA nanoparticles. It was possible that pimozone released within 5 days in the glioblastoma cell line was less than its minimum effective concentration. Therefore, the dose needed to be increased. Frasco *et al.* (2015) explained that the layer of transferrin on the surface of PLGA nanoparticles could obstruct water permeation that led to lower diffusion rate of the drug (bortezomib).

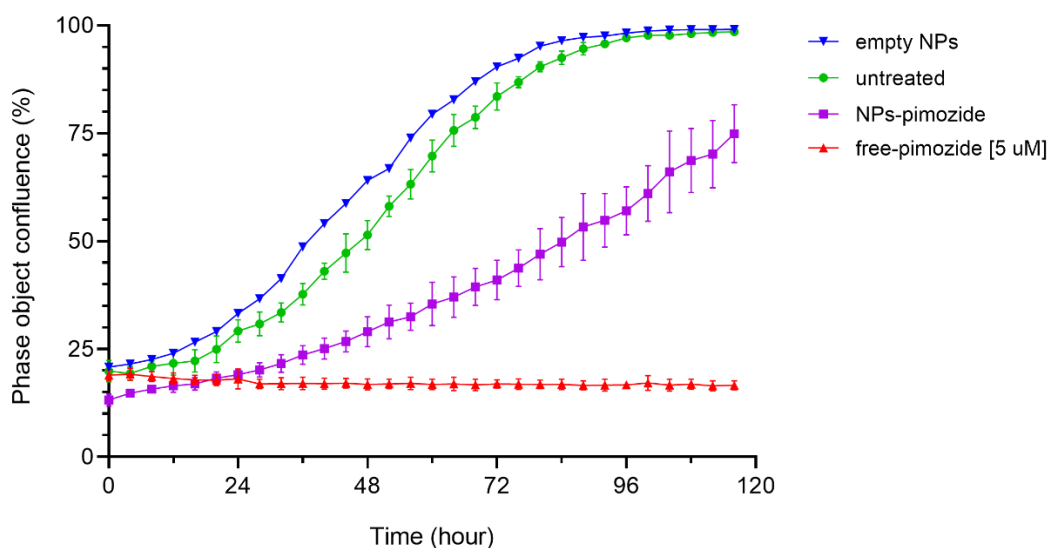


Figure 6.15: Cytotoxic effect pimozide-loaded PLGA nanoparticles on glioblastoma cells. E2 cells were incubated for 120 hours after treating with 5 μM free-pimozide, and 5 μM pimozide-encapsulated (equivalent amount based on EE calculations) nanoparticles (NPs). Cell proliferation assay used phase contrast images of live cells to produce data that represent mean confluence (%) \pm SD ($n=6$). Empty NPs were drug-free PLGA NPs.

Based on the pimozide release profile, the treatment dose of pimozide was increased to 10 μM . Cell proliferation assay showed that 10 μM pimozide-encapsulated nanoparticles effectively inhibited the cell growth, although not as same extent as free (pure) pimozide (Figure 6.16). This indicates that at dose of 10 μM pimozide must have released minimum effective concentration of pimozide, which could be 5 μM or slightly less than 5 μM . Finally, TFR targeted nanoparticles was found to be significantly more effective at inhibiting growth of glioblastoma cells compared to non-targeted nanoparticles (Figure 6.16). These findings were supported by phase contrast images of treated glioblastoma cells (Figure 6.17). For better visualisation of intracellular uptake of nanoparticles, cells treated with fluorescent dye (coumarin-6)-loaded nanoparticles are also presented in Figure 6.18.

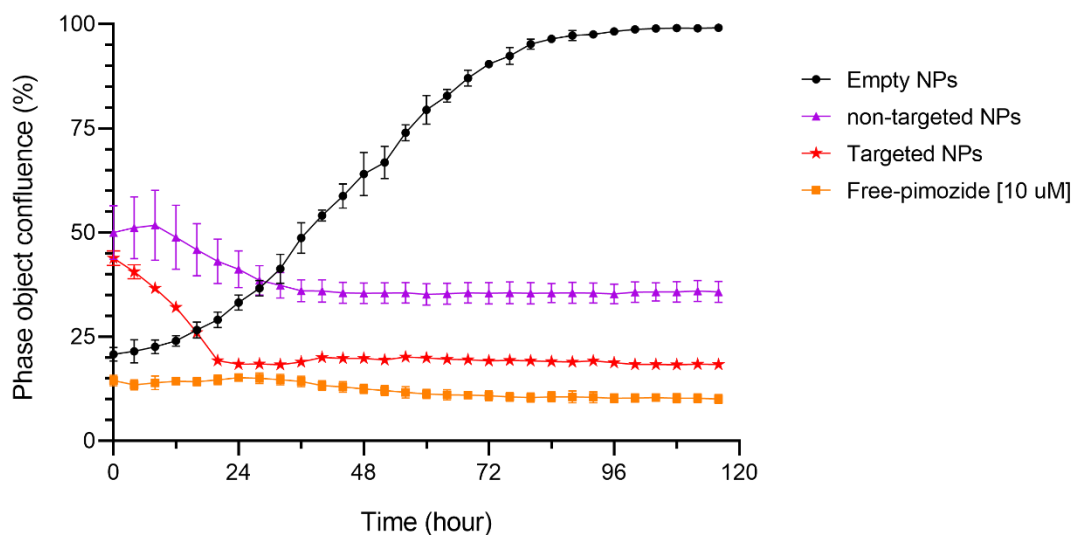


Figure 6.16: Cytotoxic effect of targeted PLGA nanoparticles on glioblastoma cells.

*E2 cells were incubated for 120 hours after treating with empty nanoparticles (NPs), and 10 μ M pimozide-encapsulated (equivalent amount based on EE calculations) targeted and non-targeted NPs. Cell proliferation assay used phase contrast images of live cells to produce data that represent mean confluence (%) \pm SD ($n=6$). Mean confluence (%) of each time point between targeted and non-targeted nanoparticles was statistically significant (** $p < 0.001$, one-way ANOVA).*

Thus, intracellular uptake of fluorescence dye (coumarin-6)-loaded nanoparticles was confirmed qualitatively using phase contrast images. However, further analysis (such as, flow cytometry) is required to assess nanoparticles uptake quantitatively.

Intracellular uptake mechanism of nanoparticles was believed to be TFR-mediated endocytosis, as already discussed in Section 6.1. However, non-targeted nanoparticles also showed cytotoxicity, although not as same extent as targeted nanoparticles (Figure 6.16). It could be due the degradation of PLGA matrix extracellularly releasing pimozide, which was then transported into cytoplasm by passive diffusion and exerted its effect via antagonism mechanisms that already discussed earlier.

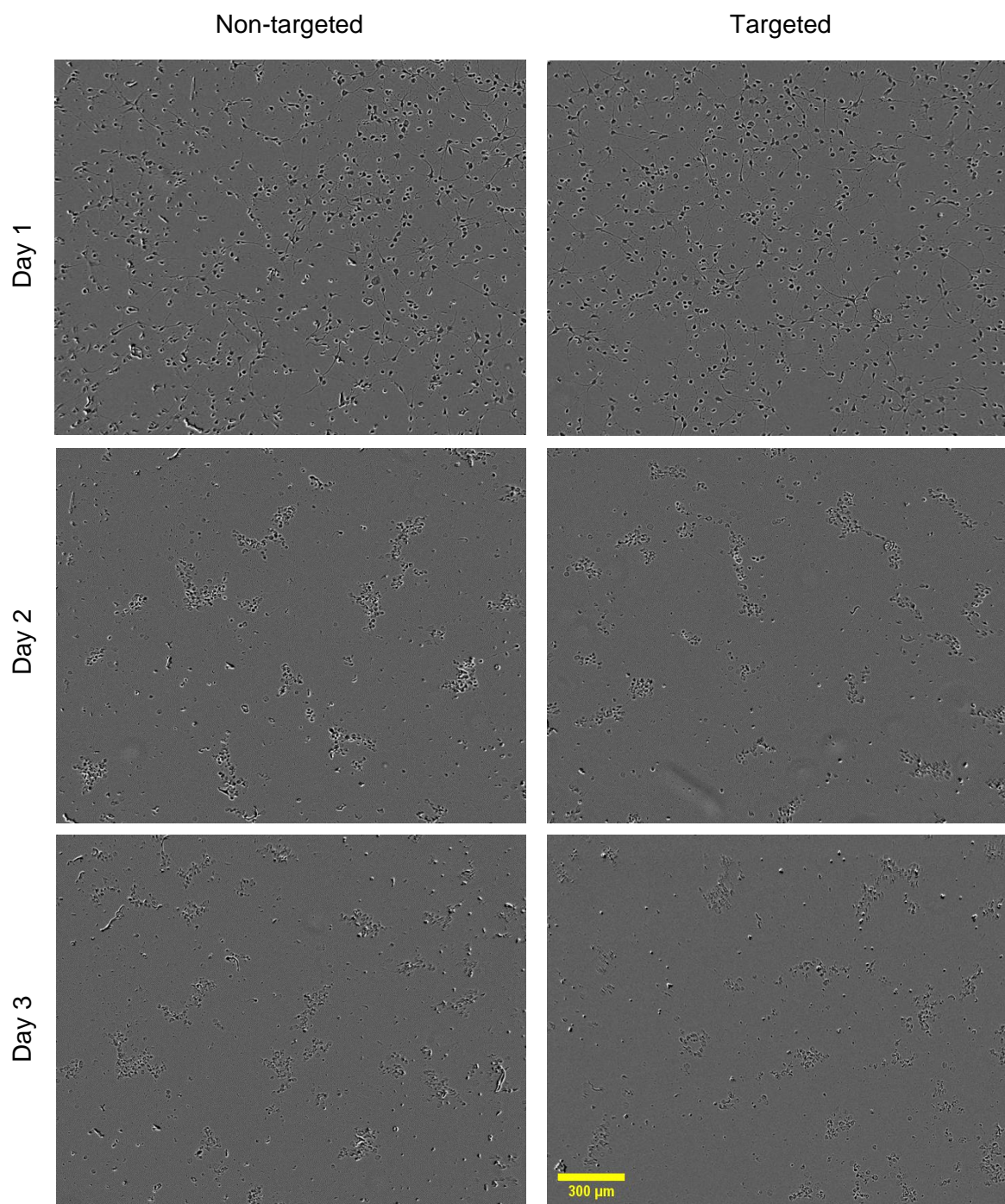


Figure 6.17: Representative phase contrast images of E2 cells after treating with targeted and non-targeted nanoparticles.

E2 cells were incubated for 120 hours after treating with targeted and non-targeted nanoparticles. Images were taken in every 4 hours during the incubation. Scale bar indicates 300 μm .

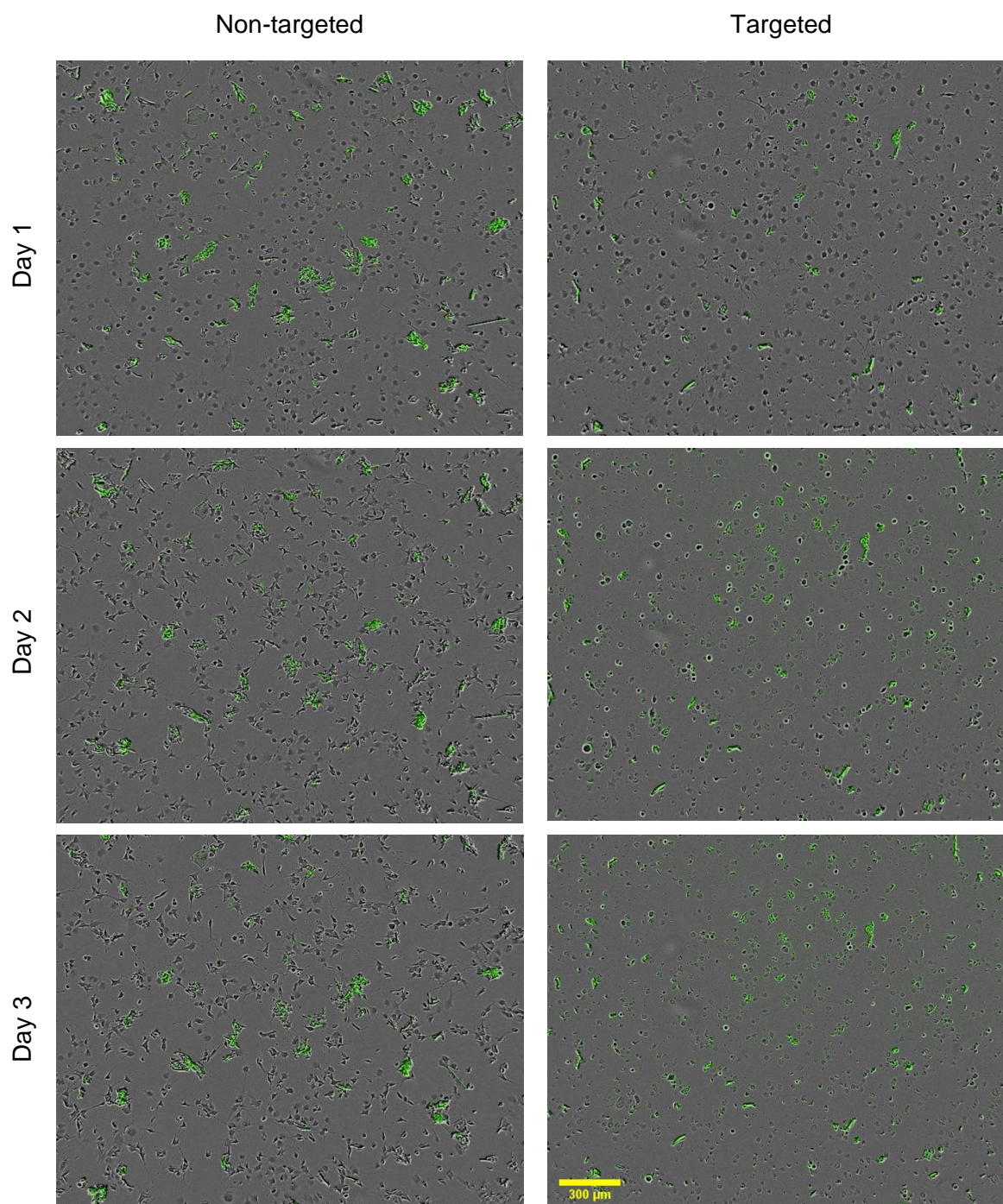


Figure 6.18: Representative phase contrast images of E2 cells after treating with fluorescent dye-loaded targeted and non-targeted PLGA nanoparticles. E2 cells were incubated for 120 hours after treating with targeted and non-targeted nanoparticles loaded with fluorescent dye (coumarin-6). Images were taken in every 4 hours during the incubation. Scale bar indicates 300 μm .

Several studies reported transferrin receptor targeted PLGA nanoparticles for glioblastoma, as mentioned in chapter 1 (Table 1.10). However, these developed nanoparticles were loaded with different drug molecules. For example, Zhang *et al.* (2019) developed PLGA-PEG-TF nanoparticles loaded with doxorubicin and tetrahydrocurcumin. Authors found enhanced cytotoxicity of targeted nanoparticles in rat C6 glioma cell line compared to non-targeted nanoparticles, supporting the results of the current study. Authors explained this was due to the selective affinity of TF towards TFR, which aided nanoparticles to be transported inside the cells by receptor mediated endocytosis. Again, this supports the hypothesis of the current study. An earlier study also observed similar results on rat C6 glioma cells, with doxorubicin loaded PGLA-PEG-TF nanoparticles (Liu *et al.*, 2013).

Another study developed magnetic silica PLGA-TF nanoparticles loaded with paclitaxel and doxorubicin (Cui *et al.*, 2013). Both *in vitro* and *in vivo* results showed that targeted nanoparticles had higher cytotoxicity compared to no-targeted nanoparticles. Authors explained this by increased cellular uptake of nanoparticles due to selective interaction of TF with TFR, also enhanced by magnetic field. In case of drug-free PLGA nanoparticles, similar trend has been reported. Chang *et al.* (2012) developed PLGA-TF nanoparticles and found increased cellular uptake compared to PLGA nanoparticles. Authors suggested that two cellular uptake pathways, namely caveolae- and clathrin-mediated endocytosis, were involved in transporting nanoparticles inside the cells.

Differently, Ramalho *et al.* (2018) developed TFR targeted PLGA nanoparticles loaded with temozolomide. Authors used OX26 type monoclonal antibody to functionalise PLGA nanoparticles targeting TFR on glioblastoma cells. It was found that cytotoxic effect of temozolomide was enhanced due to the selective antibody-TFR interaction.

In summary, this study took the advantage of nanomedicine in functionalising and targeting the transferrin receptor that overexpressed on glioblastoma cells. Although this was a limited study, nevertheless, it was evident that pimozide-encapsulated PLGA nanoparticles (as developed and optimised in earlier chapters) could effectively inhibit glioblastoma cells at a dose dependent manner. This finding suggests that the antipsychotic drug pimozide could be repurposed for glioblastoma chemotherapy in the form of PLGA nanoparticles.

6.4. Conclusion

This chapter investigated the expression of potential targeted receptor proteins on human glioblastoma cell lines. It further evaluated cellular uptake and cytotoxicity of developed nanoparticles (optimised formulation of F21) on glioblastoma cells.

Although pimozide is used to treat schizophrenia and Tourette syndrome, it is also an anticancer agent, as reported by many studies. Interestingly it is a selective 5-HT₇ antagonist, and USP1 inhibitor. Western blot analysis showed that 5-HT₇ and USP1 were expressed on glioblastoma cell lines. Therefore, pimozide becomes a potential candidate to be repurposed for glioblastoma therapy. However, it has affinity to other receptors of normal cells and induces adverse effect. That warrants a delivery system that can carry pimozide into the brain and selectively target glioblastoma cells only. However, unlike native pimozide (which crosses BBB by lipophilic pathway), delivery system faces tightly regulated BBB, which is impossible to be crossed.

Interestingly, brain capillary endothelial cells lining BBB express transferrin receptors (TFR) that selectively bind with plasma transferrin (TF) carrying iron. TFR-TF complex is then transported across the brain capillary endothelial cells via receptor mediated endocytosis mechanism. Based on this theory, this study developed TF-coated PLGA nanoparticles aiming to avoid BBB blockage.

Notably, studies reported that glioblastoma cells overexpressed TFR. This study also confirmed the expression of two types of TFR on the glioblastoma cell lines by Western blot analysis. Both TFR1 and TFR2 were expressed on most of the cell lines (in 3 out of 4). In particular, TFR1 was expressed most on E2 cell line. Therefore, it was hypothesised that TF-coated PLGA nanoparticles would be internalised more efficiently. Hence, targeted nanoparticles would be more cytotoxic compared to non-targeted nanoparticles.

In line with this hypothesis, this study found that native pimozide was cytotoxic at a minimum concentration of 5 μ M on cell line E2. However, same pimozide concentration (equivalent to 5 μ M) within PLGA nanoparticles did not effectively show any cytotoxicity. Instead, 10 μ M pimozide-encapsulated nanoparticles effectively inhibited the cell growth. Most importantly, this inhibition was significantly enhanced once treated with TFR targeted nanoparticles, proving the hypothesis.

In brief, this study has provided evidence that antipsychotic drug pimozide is a potential glioblastoma chemotherapeutic agent, and it could be repurposed in form of nanoparticles.

Chapter 7

General Conclusions and Future Directions

Chapter 7. General Conclusions and Future Directions

7.1. General Conclusions

Human race is being constantly challenged by the diseases. Therefore, the search for new therapeutics or developing existing ones is never ending. Recently, nanomedicines are making outstanding progress in delivering new or existing therapeutics in targeted sites, especially to the cancer cells, thus increasing efficacy of the drugs as well as reducing potential side effects.

Glioblastoma is a fast-growing deadly brain cancer. It is currently being treated by surgery (if possible) and radiotherapy, followed by chemotherapy. However, glioblastoma is still completely untreatable due to its heterogenous and resistive behaviour. Therefore, new interventions are always warranted. This study chose an antipsychotic agent, pimozide, which was found as a potential inhibitor of glioblastoma cell growth (also, inhibitor of other cancer cell growth) in several studies. However, pimozide has not been used clinically for glioblastoma. It could be due to its antipsychotic effect and some extrapyramidal adverse effect at the same time. Therefore, this study took the initiative to explore PLGA nanoparticles (as carrier system of pimozide) and tune their physicochemical properties to make them targeted delivery systems, aiming to repurpose pimozide for targeted glioblastoma chemotherapy.

Formulations were prepared by changing several process and formulation parameters, and subsequently characterised based on particle size, polydispersity index (PDI), surface charge, morphology, drug encapsulation efficiency (EE), and *in vitro* drug release and storage stability. This study evaluated each parameter independently, while keeping others constant, with the aim of achieving an optimised formulation.

An ultra-high-performance liquid chromatography (UHPLC) method was developed and validated to determine pimozide in the nanoparticles. Methanol was found to be an appropriate solvent of analyte over dichloromethane (DCM), since DCM produced distorted and unnecessary peaks in the chromatogram leading to poor resolution. A solid-liquid extraction method was optimised for pimozide. It was found that acetonitrile-methanol (1:5) system extracted maximum pimozide than other solvent systems used. Further, interaction between filter material and pimozide was confirmed as negligible. Finally, the method was validated by confirming specificity, linearity, accuracy, precision, limit of detection, limit of quantification, and robustness, according to the ICH guidelines.

During the preparation of nanoparticles, investigated process parameters involved preparation methods, and some intermediate steps and conditions. Firstly, both preparation methods, namely single emulsion-solvent evaporation (SE) and microfluidics showed opportunities for tuning physicochemical properties of nanoparticles. It was found that particles produced in microfluidic method were significantly smaller than SE method. Presumably, that led pimozone to release faster from nanoparticles produced by microfluidics since smaller particles had more surface area than larger particles. In addition, significantly higher encapsulation efficiency was found in nanoparticles produced by MF method compared to SE method. Secondly, freeze-drying was found to affect particle size of PVA and tween stabilised PLGA nanoparticles. Thirdly, it was found that nanoparticles collected by dialysis technique were significantly smaller, however with low drug encapsulation efficiency compared to centrifugation technique. Finally, optimal microfluidic conditions were achieved at a total flow rate of 12 mL/min and flow ratio of 1:1 (aqueous phase to organic phase) since significantly smaller particle size with narrow size distribution and high encapsulation efficiency were observed in these conditions.

This study also investigated many formulation parameters to achieve optimised formulation. Type of PLGA was found to affect physicochemical properties of nanoparticles. High molecular weight of PLGA (30-60 kDa) led to produce significantly larger particle than that of low molecular weight (24-38 kDa). Acid terminated nanoparticles were significantly smaller than its counterpart ester terminated nanoparticles. In addition, drug encapsulation efficiency seemed to be significantly higher in acid terminated nanoparticles. In terms of pimozone release, significantly slower release was noticed in acid terminated nanoparticles.

Surfactants were also found to be manipulating the physicochemical properties of PLGA nanoparticles. Of all surfactants used in this study, TPGS was observed to produce significantly smaller particles with narrow size distribution. Most importantly, TPGS was found to avoid aggregation of nanoparticles after freeze-drying since particle size remained almost unaltered after freeze-drying. Furthermore, TPGS stabilised nanoparticles released pimozone quick manner (almost 100% by 120 hours) than other surfactants stabilised nanoparticles.

Polyethylene glycol was used to modify the surface of the nanoparticle. However, PEGylation was found to increase particle size. In addition, particles size became significantly larger with high molecular weight of PEG. In addition, anionic nature of the PLGA nanoparticles was found to be reduced significantly due to the PEGylation as expected.

As part of the formulation parameters, this study also evaluated different concentrations of drug molecule (pimozide) and excipients (PLGA, PEG, and TPGS). Based on the physicochemical properties of nanoparticles, optimal concentrations of PLGA, PEG, TPGS, and pimozide were achieved at 20 mg/mL, 5% w/w, 1.25% w/v, and 2.5% w/w, respectively.

Finally, the type of organic solvent used in preparation of nanoparticles was also found to affect the properties of PLGA nanoparticles. Acetonitrile-methanol (4:1) solvent system produced significantly smallest particles with higher drug encapsulation efficiency than that of other solvents (DMSO and acetonitrile-DMSO) used as organic phase during the preparation of nanoparticles.

Active targeted nanoparticles were prepared by physical adsorption of transferrin on optimised PLGA nanoparticles. Transferrin adsorption was confirmed both qualitatively by particle size analysis and quantitatively by BCA protein assay method. Storage study suggested that nanoparticles remained stable up to 16 weeks when stored at 4°C. However, particles were found to be agglomerated when they were stored at room temperature. Furthermore, PLGA nanoparticles was susceptible for microbial growth once in suspension form. Growth of bacteria and yeast was detected in most of the stored formulations tested. This warrants the need of sterilisation of our formulations before *in vitro* and *in vivo* investigation. However, current study used freshly prepared nanoparticles to minimise the contamination.

Pimozide is a selective 5-HT₇ antagonist, and USP1 inhibitor. 5-HT₇ and USP1 are linked to glioblastoma cell growth and proliferation. Western blot analysis showed that 5-HT₇ and USP1 were expressed on glioblastoma cell lines. Therefore, pimozide becomes a potential candidate to be repurposed for glioblastoma therapy. However, it has affinity to other receptors of normal cells and induces adverse effect. That warrants a delivery system that can carry pimozide into the brain and selectively target glioblastoma cells only. However, unlike native pimozide, delivery system would have to avoid tightly regulated blood-brain barrier (BBB), which is impossible to be crossed.

Interestingly, brain capillary endothelial cells lining BBB express transferrin receptors (TFR) that selectively bind with plasma transferrin (TF) carrying iron. TFR-TF complex is then transported across the brain capillary endothelial cells via receptor mediated endocytosis mechanism. Based on this theory, this study developed TF-coated PLGA nanoparticles aiming to avoid BBB blockage. Many studies reported that glioblastoma cells also overexpressed TFR. This study confirmed the expression of two types of TFR on the glioblastoma cell lines by Western blot analysis. Both TFR1 and TFR2 were expressed on most of the cell lines (in 3 out of 4). In particular, TFR1 was expressed most on E2 cell line.

In line with this hypothesis of the study, it was found that pure pimozone was cytotoxic at a minimum concentration of 5 μM on cell line E2. However, same pimozone concentration (equivalent to 5 μM) within PLGA nanoparticles did not effectively show any cytotoxicity. Instead, 10 μM pimozone-encapsulated nanoparticles effectively inhibited the glioblastoma cell growth. Most importantly, this inhibition was significantly enhanced once treated with TFR targeted nanoparticles, proving the hypothesis of the study.

In short, this study has provided evidence that antipsychotic drug pimozone is a potential glioblastoma chemotherapeutic agent, and it could be repurposed in the form of nanoparticles.

7.2. Future Directions

Based on the findings in Western blot analysis and cell proliferation assay, *in vivo* investigations are strongly recommended for the current novel formulation. At the same time, more extensive *in vitro* studies are suggested:

- Cytotoxicity could be evaluated on glioblastoma cell lines G7 and R24 since both expressed transferrin receptors TFR1 and TFR2 (Figure 6.8).
- Cytotoxicity on normal glial cells could also be studied to estimate the potential side effects.
- Expression of transferrin receptors (TFR) on glioblastoma cell lines should be quantified and compared with expression of TFR in normal glial cells. This comparison would confirm the overexpression of transferrin receptors, including the degree of overexpression.
- A follow-up Western blot analysis could be performed after cell treatments to determine any downregulation of the targeted transferrin receptors, 5-HT₇ and USP1.

Any currently marketed drug molecule used for glioblastoma therapy, such as temozolomide, could be co-encapsulated with pimozone in targeted PLGA nanoparticles with the aim of synergistic effect.

In terms of formulation and characterisation, following studies are recommended for improvements:

- Nanoparticles have wide range of drug encapsulation efficiency (EE). The dominant factor that affects EE is composition of PLGA, such as lactide and glycolide ratio. Pimozide encapsulation efficiency could be improved by using different ratio of lactide and glycolide in PLGA. Pimozide EE could also be improved by investigating more flow rates and flow rate ratio of aqueous and organic phases in microfluidic method.
- Nanoparticles could be developed by using PLGA-PEG block-co-polymer.
- Freeze-dried nanoparticles with or without cryoprotectants could be studied to evaluate the difference in terms of physicochemical properties.
- A Design of Experiments (DoE) tool could be used to investigate multiple variables affecting the formulations, rather than using one factor at a time (OFAT) approach that was exercised in this study.
- PLGA nanoparticles could be studied for microbial contamination after using a sterilisation procedure, such as gamma-irradiation.
- Current ultra-high-performance liquid chromatography (UHPLC) method could be further developed to analyse all the excipients, such as PLGA, PEG, fluorescent dye, and transferrin at the same time. A solid phase extraction method, which is more efficient than solid/liquid extraction, could be used to separate pimozide from other excipients prior to UHPLC analysis.
- Trace amount of residual solvent present in the freeze-dried nanoparticles could be investigated by simple headspace gas chromatography (GC) analysis.

Furthermore, this study recommends evaluating this novel formulation on breast cancer cell lines, as pure pimozide was also reported to be a novel chemotherapeutic for breast cancer (Dakir *et al.*, 2018). Expression (or overexpression) of both transferrin and folate receptors in breast cancer cell lines could be studied. If required, based on the expression of receptor proteins, this novel formulation could be further functionalised with folic acid to target overexpressed folic acid receptors in breast cancer cell lines.

In fact, current formulation strategies could be used to develop nanomedicines targeting any cancer (or any other disease) with a variety of therapeutic agents, such as small molecules, proteins, DNA, and RNA.

Chapter 8

References

References

- Abdelkader, D.H. *et al.* (2018) 'Effect of process variables on formulation, in-vitro characterisation and subcutaneous delivery of insulin PLGA nanoparticles: An optimisation study', *Journal of Drug Delivery Science and Technology*, 43, pp. 160–171. doi:10.1016/j.jddst.2017.10.004.
- Abrego, G. *et al.* (2014) 'Design of Nanosuspensions and Freeze-Dried PLGA Nanoparticles as a Novel Approach for Ophthalmic Delivery of Pranoprofen', *Journal of Pharmaceutical Sciences*, 103(10), pp. 3153–3164. doi:10.1002/jps.24101.
- Acharya, S. and Sahoo, S.K. (2011) 'PLGA nanoparticles containing various anticancer agents and tumour delivery by EPR effect', *Advanced Drug Delivery Reviews*, 63(3), pp. 170–183. doi:10.1016/j.addr.2010.10.008.
- Ahn, H.K. *et al.* (2014) 'A phase II trial of Cremophor EL-free paclitaxel (Genexol-PM) and gemcitabine in patients with advanced non-small cell lung cancer', *Cancer Chemotherapy and Pharmacology*, 74(2), pp. 277–282. doi:10.1007/s00280-014-2498-5.
- Akbarzadeh, A. *et al.* (2013) 'Liposome: classification, preparation, and applications', *Nanoscale Research Letters*, 8(1), p. 102. doi:10.1186/1556-276X-8-102.
- Alamein, A.M.A.A., Hussien, L.A.E.A. and Mohamed, E.H. (2015) 'Univariate spectrophotometry and multivariate calibration: Stability-indicating analytical tools for the quantification of pimozone in bulk and pharmaceutical dosage form', *Bulletin of Faculty of Pharmacy, Cairo University*, 53(2), pp. 173–183. doi:10.1016/j.bfopcu.2015.10.003.
- Alix-Panabières, C. and Pantel, K. (2016) 'Clinical Applications of Circulating Tumor Cells and Circulating Tumor DNA as Liquid Biopsy', *Cancer Discovery*, 6(5), pp. 479–491. doi:10.1158/2159-8290.CD-15-1483.
- Alshamsan, A. (2014) 'Nanoprecipitation is more efficient than emulsion solvent evaporation method to encapsulate cucurbitacin I in PLGA nanoparticles', *Saudi Pharmaceutical Journal*, 22(3), pp. 219–222. doi:10.1016/j.jsps.2013.12.002.
- An, Q. *et al.* (2020) 'Repurposed drug candidates for antituberculosis therapy', *European Journal of Medicinal Chemistry*, 192, p. 112175. doi:10.1016/j.ejmech.2020.112175.
- Ananta, J.S., Paulmurugan, R. and Massoud, T.F. (2016) 'Temozolomide-loaded PLGA nanoparticles to treat glioblastoma cells: a biophysical and cell culture evaluation', *Neurological Research*, 38(1), pp. 51–59. doi:10.1080/01616412.2015.1133025.
- Andtbacka, R.H.I. *et al.* (2015) 'Talinogene Laherparepvec Improves Durable Response Rate in Patients With Advanced Melanoma', *Journal of Clinical Oncology: Official Journal of the American Society of Clinical Oncology*, 33(25), pp. 2780–2788. doi:10.1200/JCO.2014.58.3377.
- Aparicio-Blanco, J. *et al.* (2020) 'Glioblastoma chemotherapeutic agents used in the clinical setting and in clinical trials: Nanomedicine approaches to improve their efficacy', *International Journal of Pharmaceutics*, 581, p. 119283. doi:10.1016/j.ijpharm.2020.119283.

- Augustine, R. *et al.* (2020) 'Cellular uptake and retention of nanoparticles: Insights on particle properties and interaction with cellular components', *Materials Today Communications*, 25, p. 101692. doi:10.1016/j.mtcomm.2020.101692.
- Awouters, F.H.L. and Lewi, P.J. (2007) 'Forty years of antipsychotic Drug research--from haloperidol to paliperidone--with Dr. Paul Janssen', *Arzneimittel-Forschung*, 57(10), pp. 625–632. doi:10.1055/s-0031-1296660.
- Bacanli, M. *et al.* (2021) 'Evaluation of cytotoxic and genotoxic effects of paclitaxel-loaded PLGA nanoparticles in neuroblastoma cells', *Food and Chemical Toxicology*, 154, p. 112323. doi:10.1016/j.fct.2021.112323.
- Badea, N. *et al.* (2020) 'Systems based on carbon nanotubes with potential in cancer therapy', *Materials Chemistry and Physics*, 241, p. 122435. doi:10.1016/j.matchemphys.2019.122435.
- Baeyens, W. (1977) 'Determination of pimozide in oral preparations by spectrofluorometry', *Talanta*, 24(9), pp. 579–581. doi:10.1016/0039-9140(77)80053-2.
- Bainor, A. *et al.* (2011) 'Bicinchoninic acid (BCA) assay in low volume', *Analytical Biochemistry*, 410(2), pp. 310–312. doi:10.1016/j.ab.2010.11.015.
- Banks, W.A. (2016) 'From blood-brain barrier to blood-brain interface: new opportunities for CNS drug delivery', *Nature Reviews. Drug Discovery*, 15(4), pp. 275–292. doi:10.1038/nrd.2015.21.
- Barenholz, Y. (Chezy) (2012) 'Doxil® — The first FDA-approved nano-drug: Lessons learned', *Journal of Controlled Release*, 160(2), pp. 117–134. doi:10.1016/j.jconrel.2012.03.020.
- Bastiancich, C. *et al.* (2017) 'Injectable nanomedicine hydrogel for local chemotherapy of glioblastoma after surgical resection', *Journal of Controlled Release*, 264, pp. 45–54. doi:10.1016/j.jconrel.2017.08.019.
- Bertolesi, G.E. *et al.* (2002) 'The Ca(2+) channel antagonists mibefradil and pimozide inhibit cell growth via different cytotoxic mechanisms', *Molecular Pharmacology*, 62(2), pp. 210–219. doi:10.1124/mol.62.2.210.
- Bhandari, R. *et al.* (2019) 'Development of a new, sensitive, and robust analytical and bio-analytical RP-HPLC method for in-vitro and in-vivo quantification of naringenin in polymeric nanocarriers', *Journal of Analytical Science and Technology*, 10(1), p. 11. doi:10.1186/s40543-019-0169-1.
- Bhatia, S.N. and Ingber, D.E. (2014) 'Microfluidic organs-on-chips', *Nature Biotechnology*, 32(8), pp. 760–772. doi:10.1038/nbt.2989.
- Bhowmik, A. *et al.* (2017) 'Anti-SSTR2 peptide based targeted delivery of potent PLGA encapsulated 3,3'-diindolylmethane nanoparticles through blood brain barrier prevents glioma progression', *Oncotarget*, 8(39), pp. 65339–65358. doi:10.18632/oncotarget.18689.
- Bidkar, A.P., Sanpui, P. and Ghosh, S.S. (2020) 'Transferrin-Conjugated Red Blood Cell Membrane-Coated Poly(lactic-co-glycolic acid) Nanoparticles for the Delivery of Doxorubicin and Methylene Blue', *ACS Applied Nano Materials*, 3(4), pp. 3807–3819. doi:10.1021/acsnm.0c00502.

Brain Tumour Research (2020) *Glioblastoma multiforme - Brain Tumour Research*. Available at: <https://www.braintumourresearch.org/info-support/types-of-brain-tumour/glioblastoma-multiforme> (Accessed: 1 June 2020).

Byrne, J.D., Betancourt, T. and Brannon-Peppas, L. (2008) 'Active targeting schemes for nanoparticle systems in cancer therapeutics', *Advanced Drug Delivery Reviews*, 60(15), pp. 1615–1626. doi:10.1016/j.addr.2008.08.005.

Cai, N. *et al.* (2017) 'The STAT3 inhibitor pimoziide impedes cell proliferation and induces ROS generation in human osteosarcoma by suppressing catalase expression', *American Journal of Translational Research*, 9(8), pp. 3853–3866.

Calzolari, A. *et al.* (2007) 'Transferrin receptor 2 is frequently expressed in human cancer cell lines', *Blood Cells, Molecules, and Diseases*, 39(1), pp. 82–91. doi:10.1016/j.bcmd.2007.02.003.

Calzolari, A. *et al.* (2010) 'Transferrin Receptor 2 Is Frequently and Highly Expressed in Glioblastomas', *Translational Oncology*, 3(2), pp. 123–134. doi:10.1593/tlo.09274.

Cancer Research UK (2017a) *Treatment for cancer | Cancer in general | Cancer Research UK, Cancer Research UK*. Available at: <https://about-cancer.cancerresearchuk.org/about-cancer/cancer-in-general/treatment> (Accessed: 9 June 2020).

Cancer Research UK (2017b) *What is chemotherapy? | Cancer in general | Cancer Research UK, Cancer Research UK*. Available at: <https://www.cancerresearchuk.org/about-cancer/cancer-in-general/treatment/chemotherapy/what-chemotherapy-is> (Accessed: 7 June 2020).

Cancer Research UK (2018) *What is radiotherapy? | Cancer treatment | Cancer Research UK, Cancer Research UK*. Available at: <https://www.cancerresearchuk.org/about-cancer/cancer-in-general/treatment/radiotherapy/about> (Accessed: 7 June 2020).

Cancer Research UK (2019) *What are brain tumours? | Brain tumours | Cancer Research UK, Cancer Research UK*. Available at: https://www.cancerresearchuk.org/about-cancer/brain-tumours/about?_ga=2.22177529.398170308.1591030282-804919862.1591030282 (Accessed: 1 June 2020).

Cancer Research UK (2020) *Types of brain tumours | Cancer Research UK, Cancer Research UK*. Available at: <https://www.cancerresearchuk.org/about-cancer/brain-tumours/types> (Accessed: 6 June 2020).

Cancer Research UK (2021) *Cancer growth blockers | Targeted cancer drugs | Cancer Research UK, Cancer Research UK*. Available at: <https://www.cancerresearchuk.org/about-cancer/cancer-in-general/treatment/targeted-cancer-drugs/types/cancer-growth-blockers> (Accessed: 23 September 2021).

Carlson, M. and Thompson, R.D. (2000) 'Analyte loss due to membrane filter adsorption as determined by high-performance liquid chromatography', *Journal of Chromatographic Science*, 38(2), pp. 77–83. doi:10.1093/chromsci/38.2.77.

Chang, J. *et al.* (2009) 'Characterization of endocytosis of transferrin-coated PLGA nanoparticles by the blood–brain barrier', *International Journal of Pharmaceutics*, 379(2), pp. 285–292. doi:10.1016/j.ijpharm.2009.04.035.

Chang, J. *et al.* (2012) 'Transferrin adsorption onto PLGA nanoparticles governs their interaction with biological systems from blood circulation to brain cancer cells', *Pharmaceutical Research*, 29(6), pp. 1495–1505. doi:10.1007/s11095-011-0624-1.

Chen, D. *et al.* (2012) 'Rapid discovery of potent siRNA-containing lipid nanoparticles enabled by controlled microfluidic formulation', *Journal of the American Chemical Society*, 134(16), pp. 6948–6951. doi:10.1021/ja301621z.

Chen, J.-J. *et al.* (2017) 'The neuroleptic drug pimozide inhibits stem-like cell maintenance and tumorigenicity in hepatocellular carcinoma', *Oncotarget*, 8(11), pp. 17593–17609. doi:10.18632/oncotarget.4307.

Chen, S. *et al.* (2019) 'Recent advances in non-ionic surfactant vesicles (niosomes): Fabrication, characterization, pharmaceutical and cosmetic applications', *European Journal of Pharmaceutics and Biopharmaceutics*, 144, pp. 18–39. doi:10.1016/j.ejpb.2019.08.015.

Chen, Y. *et al.* (2020) 'Repurposing of antipsychotics perphenazine for the treatment of endometrial cancer', *Bioorganic & Medicinal Chemistry Letters*, 30(14), p. 127239. doi:10.1016/j.bmcl.2020.127239.

Cheng, J. *et al.* (2007) 'Formulation of Functionalized PLGA-PEG Nanoparticles for In Vivo Targeted Drug Delivery', *Biomaterials*, 28(5), pp. 869–876. doi:10.1016/j.biomaterials.2006.09.047.

Cheng, Y. and Ji, Y. (2019) 'RGD-modified polymer and liposome nanovehicles: Recent research progress for drug delivery in cancer therapeutics', *European Journal of Pharmaceutical Sciences*, 128, pp. 8–17. doi:10.1016/j.ejps.2018.11.023.

Chirasani, S.R. *et al.* (2008) 'Transferrin-receptor-mediated iron accumulation controls proliferation and glutamate release in glioma cells', *Journal of Molecular Medicine*, 87(2), p. 153. doi:10.1007/s00109-008-0414-3.

Chiu, D.T. *et al.* (2017) 'Small but Perfectly Formed? Successes, Challenges, and Opportunities for Microfluidics in the Chemical and Biological Sciences', *Chem*, 2(2), pp. 201–223. doi:10.1016/j.chempr.2017.01.009.

Cho, E.J. *et al.* (2013) 'Nanoparticle characterization: state of the art, challenges, and emerging technologies', *Molecular Pharmaceutics*, 10(6), pp. 2093–2110. doi:10.1021/mp300697h.

Choi, Y.H. and Han, H.-K. (2018) 'Nanomedicines: current status and future perspectives in aspect of drug delivery and pharmacokinetics', *Journal of Pharmaceutical Investigation*, 48(1), pp. 43–60. doi:10.1007/s40005-017-0370-4.

Colvin, C.L. and Tankanow, R.M. (1985) 'Pimozide: use in Tourette's syndrome', *Drug Intelligence & Clinical Pharmacy*, 19(6), pp. 421–424. doi:10.1177/106002808501900602.

Coors, E.A. *et al.* (2005) 'Polysorbate 80 in medical products and nonimmunologic anaphylactoid reactions', *Annals of Allergy, Asthma & Immunology*, 95(6), pp. 593–599. doi:10.1016/S1081-1206(10)61024-1.

Cortés-Ríos, J. *et al.* (2020) 'Protein quantification by bicinchoninic acid (BCA) assay follows complex kinetics and can be performed at short incubation times', *Analytical Biochemistry*, 608, p. 113904. doi:10.1016/j.ab.2020.113904.

Cui, Y. *et al.* (2013) 'Transferrin-conjugated magnetic silica PLGA nanoparticles loaded with doxorubicin and paclitaxel for brain glioma treatment', *Biomaterials*, 34(33), pp. 8511–8520. doi:10.1016/j.biomaterials.2013.07.075.

Cui, Y. *et al.* (2016) 'Dual-Targeting Magnetic PLGA Nanoparticles for Codelivery of Paclitaxel and Curcumin for Brain Tumor Therapy', *ACS Applied Materials & Interfaces*, 8(47), pp. 32159–32169. doi:10.1021/acsami.6b10175.

Cui, Y. *et al.* (2020) 'Dual-Target Peptide-Modified Erythrocyte Membrane-Enveloped PLGA Nanoparticles for the Treatment of Glioma', *Frontiers in Oncology*, 10. doi:10.3389/fonc.2020.563938.

Dakir, E.-H. *et al.* (2018) 'The anti-psychotic drug pimozide is a novel chemotherapeutic for breast cancer', *Oncotarget*, 9(79), pp. 34889–34910. doi:10.18632/oncotarget.26175.

Deb, P.K. *et al.* (2019) 'Chapter 16 - Protein/Peptide Drug Delivery Systems: Practical Considerations in Pharmaceutical Product Development', in Tekade, R.K. (ed.) *Basic Fundamentals of Drug Delivery*. Academic Press (Advances in Pharmaceutical Product Development and Research), pp. 651–684. doi:10.1016/B978-0-12-817909-3.00016-9.

Destá, Z. *et al.* (1998) 'Identification and characterization of human cytochrome P450 isoforms interacting with pimozide', *The Journal of Pharmacology and Experimental Therapeutics*, 285(2), pp. 428–437.

Domínguez-Ríos, R. *et al.* (2019) 'Cisplatin-loaded PLGA nanoparticles for HER2 targeted ovarian cancer therapy', *Colloids and Surfaces B: Biointerfaces*, 178, pp. 199–207. doi:10.1016/j.colsurfb.2019.03.011.

Donahue, N.D., Acar, H. and Wilhelm, S. (2019) 'Concepts of nanoparticle cellular uptake, intracellular trafficking, and kinetics in nanomedicine', *Advanced Drug Delivery Reviews*, 143, pp. 68–96. doi:10.1016/j.addr.2019.04.008.

Dong, Y. *et al.* (2017) 'Identification of antipsychotic drug fluspirilene as a potential anti-glioma stem cell drug', *Oncotarget*, 8(67), pp. 111728–111741. doi:10.18632/oncotarget.22904.

Dutta, B., Barick, K.C. and Hassan, P.A. (2021) 'Recent advances in active targeting of nanomaterials for anticancer drug delivery', *Advances in Colloid and Interface Science*, 296, p. 102509. doi:10.1016/j.cis.2021.102509.

Duwa, R. *et al.* (2020) 'Cetuximab conjugated temozolomide-loaded poly (lactic-co-glycolic acid) nanoparticles for targeted nanomedicine in EGFR overexpressing cancer cells', *Journal of Drug Delivery Science and Technology*, 60, p. 101928. doi:10.1016/j.jddst.2020.101928.

Ebrahimzadeh, H. *et al.* (2013) 'Determination of haloperidol in biological samples using molecular imprinted polymer nanoparticles followed by HPLC-DAD detection', *International Journal of Pharmaceutics*, 453(2), pp. 601–609. doi:10.1016/j.ijpharm.2013.05.054.

El-Hammadi, M.M. *et al.* (2017) 'Folic acid-decorated and PEGylated PLGA nanoparticles for improving the antitumour activity of 5-fluorouracil', *International Journal of Pharmaceutics*, 516(1), pp. 61–70. doi:10.1016/j.ijpharm.2016.11.012.

Elkordy, A.A. (ed.) (2013) *Applications of Calorimetry in a Wide Context: Differential Scanning Calorimetry, Isothermal Titration Calorimetry and Microcalorimetry*. IntechOpen.

- Elmaci, I. and Altinoz, M.A. (2018) 'Targeting the cellular schizophrenia. Likely employment of the antipsychotic agent pimozide in treatment of refractory cancers and glioblastoma', *Critical Reviews in Oncology/Hematology*, 128, pp. 96–109. doi:10.1016/j.critrevonc.2018.06.004.
- Escalona-Rayó, O. *et al.* (2019) 'Rapamycin-loaded polysorbate 80-coated PLGA nanoparticles: Optimization of formulation variables and in vitro anti-glioma assessment', *Journal of Drug Delivery Science and Technology*, 52, pp. 488–499. doi:10.1016/j.jddst.2019.05.026.
- Esim, O. *et al.* (2020) 'Influence of emulsifiers on the formation and in vitro anticancer activity of epirubicin loaded PLGA nanoparticles', *Journal of Drug Delivery Science and Technology*, 60, p. 102027. doi:10.1016/j.jddst.2020.102027.
- Fako, V. *et al.* (2016) 'Inhibition of wnt/ β -catenin Signaling in Hepatocellular Carcinoma by an Antipsychotic Drug Pimozide', *International Journal of Biological Sciences*, 12(7), pp. 768–775. doi:10.7150/ijbs.14718.
- Fonte, P. *et al.* (2015) 'Co-encapsulation of lyoprotectants improves the stability of protein-loaded PLGA nanoparticles upon lyophilization', *International Journal of Pharmaceutics*, 496(2), pp. 850–862. doi:10.1016/j.ijpharm.2015.10.032.
- Fonte, P. *et al.* (2016) 'Annealing as a tool for the optimization of lyophilization and ensuring of the stability of protein-loaded PLGA nanoparticles', *International Journal of Pharmaceutics*, 503(1), pp. 163–173. doi:10.1016/j.ijpharm.2016.03.011.
- Fraikin, J.-L. *et al.* (2011) 'A high-throughput label-free nanoparticle analyser', *Nature Nanotechnology*, 6(5), pp. 308–313. doi:10.1038/nnano.2011.24.
- Franks, F. (1998) 'Freeze-drying of bioproducts: putting principles into practice', *European Journal of Pharmaceutics and Biopharmaceutics*, 45(3), pp. 221–229. doi:10.1016/S0939-6411(98)00004-6.
- Frasco, M.F. *et al.* (2015) 'Transferrin surface-modified PLGA nanoparticles-mediated delivery of a proteasome inhibitor to human pancreatic cancer cells', *Journal of Biomedical Materials Research Part A*, 103(4), pp. 1476–1484. doi:10.1002/jbm.a.35286.
- Furman, C. *et al.* (2017) 'Development and validation of a reversed-phase HPLC method for the quantification of paclitaxel in different PLGA nanocarriers', *Electrophoresis*, 38(19), pp. 2536–2541. doi:10.1002/elps.201600552.
- Ganipineni, L.P., Danhier, F. and Pr eat, V. (2018) 'Drug delivery challenges and future of chemotherapeutic nanomedicine for glioblastoma treatment', *Journal of Controlled Release*, 281, pp. 42–57. doi:10.1016/j.jconrel.2018.05.008.
- Gelosa, P. *et al.* (2020) 'Drug repurposing in cardiovascular diseases: Opportunity or hopeless dream?', *Biochemical Pharmacology*, 177, p. 113894. doi:10.1016/j.bcp.2020.113894.
- Girotra, P., Singh, S.K. and Kumar, G. (2016) 'Development of zolmitriptan loaded PLGA/poloxamer nanoparticles for migraine using quality by design approach', *International Journal of Biological Macromolecules*, 85, pp. 92–101. doi:10.1016/j.ijbiomac.2015.12.069.
- Glick, D., Barth, S. and Macleod, K.F. (2010) 'Autophagy: cellular and molecular mechanisms', *The Journal of pathology*, 221(1), pp. 3–12. doi:10.1002/path.2697.

- Goldstein, J.I. *et al.* (2017) *Scanning Electron Microscopy and X-Ray Microanalysis*. 4th ed. 2018 edition. New York, NY: Springer.
- Gonzalez-Angulo, A.M. and Meric-Bernstam, F. (2010) 'Metformin: A Therapeutic Opportunity in Breast Cancer', *Clinical Cancer Research*, 16(6), pp. 1695–1700. doi:10.1158/1078-0432.CCR-09-1805.
- Gorgannezhad, L. *et al.* (2018) 'Circulating tumor DNA and liquid biopsy: opportunities, challenges, and recent advances in detection technologies', *Lab on a Chip*, 18(8), pp. 1174–1196. doi:10.1039/C8LC00100F.
- Gorog, S. (1995) *Ultraviolet-Visible Spectrophotometry in Pharmaceutical Analysis*. 1st edition. Boca Raton, Fla: CRC Press.
- Gould, R.J. *et al.* (1983) 'Antischizophrenic drugs of the diphenylbutylpiperidine type act as calcium channel antagonists', *Proceedings of the National Academy of Sciences of the United States of America*, 80(16), pp. 5122–5125. doi:10.1073/pnas.80.16.5122.
- Govindaraju, K. *et al.* (2020) 'Unveiling the anticancer and antimycobacterial potentials of bioengineered gold nanoparticles', *Process Biochemistry*, 96, pp. 213–219. doi:10.1016/j.procbio.2020.06.016.
- Graves, R.A. *et al.* (2004) 'Effect of different ratios of high and low molecular weight PLGA blend on the characteristics of pentamidine microcapsules', *International Journal of Pharmaceutics*, 270(1), pp. 251–262. doi:10.1016/j.ijpharm.2003.10.019.
- Guo, J. *et al.* (2011) 'Aptamer-functionalized PEG-PLGA nanoparticles for enhanced anti-glioma drug delivery', *Biomaterials*, 32(31), pp. 8010–8020. doi:10.1016/j.biomaterials.2011.07.004.
- Guo, Y. *et al.* (2013) 'The applications of Vitamin E TPGS in drug delivery', *European Journal of Pharmaceutical Sciences*, 49(2), pp. 175–186. doi:10.1016/j.ejps.2013.02.006.
- Haggag, Y. *et al.* (2016) 'Preparation and in vivo evaluation of insulin-loaded biodegradable nanoparticles prepared from diblock copolymers of PLGA and PEG', *International Journal of Pharmaceutics*, 499(1), pp. 236–246. doi:10.1016/j.ijpharm.2015.12.063.
- Haggag, Y.A. *et al.* (2017) 'Nano-encapsulation of a novel anti-Ran-GTPase peptide for blockade of regulator of chromosome condensation 1 (RCC1) function in MDA-MB-231 breast cancer cells', *International Journal of Pharmaceutics*, 521(1), pp. 40–53. doi:10.1016/j.ijpharm.2017.02.006.
- Haggag, Y.A. *et al.* (2018) 'Polymeric nano-encapsulation of 5-fluorouracil enhances anti-cancer activity and ameliorates side effects in solid Ehrlich Carcinoma-bearing mice', *Biomedicine & Pharmacotherapy*, 105, pp. 215–224. doi:10.1016/j.biopha.2018.05.124.
- Haggag, Y.A. *et al.* (2019) 'Novel Ran-RCC1 Inhibitory Peptide-Loaded Nanoparticles Have Anti-Cancer Efficacy In Vitro and In Vivo', *Cancers*, 11(2). doi:10.3390/cancers11020222.
- Han, G. *et al.* (2015) 'AMPK/mTOR-mediated inhibition of survivin partly contributes to metformin-induced apoptosis in human gastric cancer cell', *Cancer Biology & Therapy*, 16(1), pp. 77–87. doi:10.4161/15384047.2014.987021.
- Hanahan, D. and Weinberg, R.A. (2011) 'Hallmarks of Cancer: The Next Generation', *Cell*, 144(5), pp. 646–674. doi:10.1016/j.cell.2011.02.013.

Hashemi, M. *et al.* (2021) 'Mitoxantrone-Loaded PLGA Nanoparticles for Increased Sensitivity of Glioblastoma Cancer Cell to TRAIL-Induced Apoptosis', *Journal of Pharmaceutical Innovation* [Preprint]. doi:10.1007/s12247-021-09551-8.

van der Helm, M.W. *et al.* (2016) 'Microfluidic organ-on-chip technology for blood-brain barrier research', *Tissue Barriers*, 4(1), p. e1142493. doi:10.1080/21688370.2016.1142493.

Herland, A. *et al.* (2016) 'Distinct Contributions of Astrocytes and Pericytes to Neuroinflammation Identified in a 3D Human Blood-Brain Barrier on a Chip', *PLOS ONE*, 11(3), p. e0150360. doi:10.1371/journal.pone.0150360.

Hoda, M. *et al.* (2016) 'Anti-proliferative and apoptosis-triggering potential of disulfiram and disulfiram-loaded polysorbate 80-stabilized PLGA nanoparticles on hepatocellular carcinoma Hep3B cell line', *Nanomedicine: Nanotechnology, Biology and Medicine*, 12(6), pp. 1641–1650. doi:10.1016/j.nano.2016.02.013.

Hoff, D.D.V. *et al.* (2016) 'Phase I Study of PSMA-Targeted Docetaxel-Containing Nanoparticle BIND-014 in Patients with Advanced Solid Tumors', *Clinical Cancer Research*, 22(13), pp. 3157–3163. doi:10.1158/1078-0432.CCR-15-2548.

Holzer, M. *et al.* (2009) 'Physico-chemical characterisation of PLGA nanoparticles after freeze-drying and storage', *European Journal of Pharmaceutics and Biopharmaceutics*, 72(2), pp. 428–437. doi:10.1016/j.ejpb.2009.02.002.

Hrkach, J. *et al.* (2012) 'Preclinical Development and Clinical Translation of a PSMA-Targeted Docetaxel Nanoparticle with a Differentiated Pharmacological Profile', *Science Translational Medicine*, 4(128), pp. 128ra39-128ra39. doi:10.1126/scitranslmed.3003651.

Huang, J. *et al.* (2018) 'Repurposing psychiatric drugs as anti-cancer agents', *Cancer Letters*, 419, pp. 257–265. doi:10.1016/j.canlet.2018.01.058.

IARC (2020) *Cancer Tomorrow*. Available at: <https://gco.iarc.fr/tomorrow/home> (Accessed: 17 September 2021).

ICH (2005) *Validation of Analytical Procedures: Text and Methodology, Quality Guidelines*. Available at: <https://www.ich.org/page/quality-guidelines> (Accessed: 10 May 2021).

Jandaghi, P. *et al.* (2016) 'Expression of DRD2 Is Increased in Human Pancreatic Ductal Adenocarcinoma and Inhibitors Slow Tumor Growth in Mice', *Gastroenterology*, 151(6), pp. 1218–1231. doi:10.1053/j.gastro.2016.08.040.

Jia, H. *et al.* (2018) 'The enhanced antitumour response of pimozone combined with the IDO inhibitor L-MT in melanoma', *International Journal of Oncology*, 53(3), pp. 949–960. doi:10.3892/ijo.2018.4473.

Jiang, Y. *et al.* (2015) 'The Interplay of Size and Surface Functionality on the Cellular Uptake of Sub-10 nm Gold Nanoparticles', *ACS Nano*, 9(10), pp. 9986–9993. doi:10.1021/acs.nano.5b03521.

Johnsen, K.B. *et al.* (2019) 'Targeting the transferrin receptor for brain drug delivery', *Progress in Neurobiology*, 181, p. 101665. doi:10.1016/j.pneurobio.2019.101665.

Kabra, P., Nargund, L.V.G. and Murthy, M.S. (2014) 'RP-HPLC METHOD FOR ESTIMATION OF AN ANTIPSYCHOTIC DRUG - PIMOZIDE', *Asian Journal of Pharmaceutical and Clinical Research*, pp. 49–51.

- Kaksonen, M. and Roux, A. (2018) 'Mechanisms of clathrin-mediated endocytosis', *Nature Reviews Molecular Cell Biology*, 19(5), pp. 313–326. doi:10.1038/nrm.2017.132.
- Karnik, R. *et al.* (2008) 'Microfluidic Platform for Controlled Synthesis of Polymeric Nanoparticles', *Nano Letters*, 8(9), pp. 2906–2912. doi:10.1021/nl801736q.
- Kast, R.E. (2010) 'Glioblastoma chemotherapy adjunct via potent serotonin receptor-7 inhibition using currently marketed high-affinity antipsychotic medicines', *British Journal of Pharmacology*, 161(3), pp. 481–487. doi:10.1111/j.1476-5381.2010.00923.x.
- Kawabata, H. *et al.* (1999) 'Molecular Cloning of Transferrin Receptor 2: A NEW MEMBER OF THE TRANSFERRIN RECEPTOR-LIKE FAMILY*', *Journal of Biological Chemistry*, 274(30), pp. 20826–20832. doi:10.1074/jbc.274.30.20826.
- Kawabata, H. (2019) 'Transferrin and transferrin receptors update', *Free Radical Biology and Medicine*, 133, pp. 46–54. doi:10.1016/j.freeradbiomed.2018.06.037.
- Kayl, A.E. and Meyers, C.A. (2006) 'Side-effects of chemotherapy and quality of life in ovarian and breast cancer patients', *Current Opinion in Obstetrics and Gynecology*, 18(1), pp. 24–28. doi:10.1097/01.gco.0000192996.20040.24.
- Kelani, K. *et al.* (1997) 'Spectrophotometric Determination of Some n-Donating Drugs Using DDQ', *Analytical Letters*, 30(10), pp. 1843–1860. doi:10.1080/00032719708001702.
- Kerbusch, T. *et al.* (1997) 'Sensitive assay for pimozone in human plasma using high-performance liquid chromatography with fluorescence detection: application to pharmacokinetic studies', *Journal of Chromatography. B, Biomedical Sciences and Applications*, 694(1), pp. 163–168. doi:10.1016/s0378-4347(97)00152-7.
- Khoei, S. and Yaghoobian, M. (2017) 'Chapter 6 - Niosomes: a novel approach in modern drug delivery systems', in Andronesco, E. and Grumezescu, A.M. (eds) *Nanostructures for Drug Delivery*. Elsevier (Micro and Nano Technologies), pp. 207–237. doi:10.1016/B978-0-323-46143-6.00006-3.
- Kiel, M.J. *et al.* (2014) 'Integrated genomic sequencing reveals mutational landscape of T-cell prolymphocytic leukemia', *Blood*, 124(9), pp. 1460–1472. doi:10.1182/blood-2014-03-559542.
- Kim, T.-Y. *et al.* (2004) 'Phase I and pharmacokinetic study of Genexol-PM, a cremophor-free, polymeric micelle-formulated paclitaxel, in patients with advanced malignancies', *Clinical Cancer Research: An Official Journal of the American Association for Cancer Research*, 10(11), pp. 3708–3716. doi:10.1158/1078-0432.CCR-03-0655.
- Kirtonia, A. *et al.* (2020) 'Repurposing of drugs: An attractive pharmacological strategy for cancer therapeutics', *Seminars in Cancer Biology* [Preprint]. doi:10.1016/j.semcan.2020.04.006.
- Kohno, M. *et al.* (2020) 'The effect of PLGA molecular weight differences on risperidone release from microspheres', *International Journal of Pharmaceutics*, 582, p. 119339. doi:10.1016/j.ijpharm.2020.119339.
- Kongsamut, S. *et al.* (2002) 'A comparison of the receptor binding and HERG channel affinities for a series of antipsychotic drugs', *European Journal of Pharmacology*, 450(1), pp. 37–41. doi:10.1016/s0014-2999(02)02074-5.

- Kozak, D. *et al.* (2012) 'Simultaneous Size and ζ -Potential Measurements of Individual Nanoparticles in Dispersion Using Size-Tunable Pore Sensors', *ACS Nano*, 6(8), pp. 6990–6997. doi:10.1021/nn3020322.
- Kumar, R. (2019) 'Chapter 8 - Lipid-Based Nanoparticles for Drug-Delivery Systems', in Mohapatra, S.S. *et al.* (eds) *Nanocarriers for Drug Delivery*. Elsevier (Micro and Nano Technologies), pp. 249–284. doi:10.1016/B978-0-12-814033-8.00008-4.
- Kurzawa, M., Kowalczyk-Marzec, A. and Szlyk, E. (2004) 'Conductometric and spectrophotometric determination of haloperidol, droperidol and pimozide', 49, pp. 91–99.
- Lababidi, N. *et al.* (2019) 'Microfluidics as tool to prepare size-tunable PLGA nanoparticles with high curcumin encapsulation for efficient mucus penetration', *Beilstein Journal of Nanotechnology*, 10(1), pp. 2280–2293. doi:10.3762/bjnano.10.220.
- Lee, B.K., Yun, Y. and Park, K. (2016) 'PLA micro- and nano-particles', *Advanced Drug Delivery Reviews*, 107, pp. 176–191. doi:10.1016/j.addr.2016.05.020.
- Lee, J.-K. *et al.* (2016) 'USP1 targeting impedes GBM growth by inhibiting stem cell maintenance and radioresistance', *Neuro-Oncology*, 18(1), pp. 37–47. doi:10.1093/neuonc/nov091.
- Lee, J.N., Park, C. and Whitesides, G.M. (2003) 'Solvent Compatibility of Poly(dimethylsiloxane)-Based Microfluidic Devices', *Analytical Chemistry*, 75(23), pp. 6544–6554. doi:10.1021/ac0346712.
- Levy, J.M.M., Towers, C.G. and Thorburn, A. (2017) 'Targeting autophagy in cancer', *Nature Reviews. Cancer*, 17(9), pp. 528–542. doi:10.1038/nrc.2017.53.
- Li, X. *et al.* (2021) 'Novel insights on the encapsulation mechanism of PLGA terminal groups on ropivacaine', *European Journal of Pharmaceutics and Biopharmaceutics*, 160, pp. 143–151. doi:10.1016/j.ejpb.2021.01.015.
- Li, Y. *et al.* (2018) 'Mechanisms of enhanced antiglioma efficacy of polysorbate 80-modified paclitaxel-loaded PLGA nanoparticles by focused ultrasound', *Journal of Cellular and Molecular Medicine*, 22(9), pp. 4171–4182. doi:10.1111/jcmm.13695.
- Liu, G.D. *et al.* (2013) 'PEG-PLGA Nanoparticle Modified by Transferrin Loading Doxorubicin: In Vitro and In Vivo Studies for Glioma', *Advanced Materials Research*, 750–752, pp. 1643–1650. doi:10.4028/www.scientific.net/AMR.750-752.1643.
- Logan, F.A. *et al.* (1982) 'Pimozide: adverse reaction and prolonged half-life', *The British Journal of Psychiatry: The Journal of Mental Science*, 140, pp. 433–434. doi:10.1192/bjp.140.4.433.
- Lohita, M. *et al.* (2014) 'UV spectrophotometric determination of pimozide in bulk and tablet dosage forms', 2(9). Available at: https://www.wjpsonline.org/view_issue.php?title=UV-spectrophotometric-determination-of-pimozide-in-bulk-and-tablet-dosage-forms (Accessed: 16 July 2020).
- Luiz, M.T. *et al.* (2019) 'In vitro evaluation of folate-modified PLGA nanoparticles containing paclitaxel for ovarian cancer therapy', *Materials Science and Engineering: C*, 105, p. 110038. doi:10.1016/j.msec.2019.110038.

Luo, L. *et al.* (2021) 'Drug repurposing against coronavirus disease 2019 (COVID-19): A review', *Journal of Pharmaceutical Analysis* [Preprint]. doi:10.1016/j.jpha.2021.09.001.

Lynch, K.B., Chen, A. and Liu, S. (2018) 'Miniaturized high-performance liquid chromatography instrumentation', *Talanta*, 177, pp. 94–103. doi:10.1016/j.talanta.2017.09.016.

Ma, A. *et al.* (2019) 'USP1 inhibition destabilizes KPNA2 and suppresses breast cancer metastasis', *Oncogene*, 38(13), pp. 2405–2419. doi:10.1038/s41388-018-0590-8.

Madani, F. *et al.* (2020) 'Paclitaxel/methotrexate co-loaded PLGA nanoparticles in glioblastoma treatment: Formulation development and in vitro antitumor activity evaluation', *Life Sciences*, 256, p. 117943. doi:10.1016/j.lfs.2020.117943.

Maeki, M. *et al.* (2015) 'A strategy for synthesis of lipid nanoparticles using microfluidic devices with a mixer structure', *RSC Advances*, 5(57), pp. 46181–46185. doi:10.1039/C5RA04690D.

Maeki, M. *et al.* (2017) 'Understanding the formation mechanism of lipid nanoparticles in microfluidic devices with chaotic micromixers', *PLOS ONE*, 12(11), p. e0187962. doi:10.1371/journal.pone.0187962.

Mahé, C. *et al.* (2004) 'Functional expression of the serotonin 5-HT₇ receptor in human glioblastoma cell lines', *British Journal of Pharmacology*, 143(3), pp. 404–410. doi:10.1038/sj.bjp.0705936.

Maksimenko, O. *et al.* (2019) 'Doxorubicin-loaded PLGA nanoparticles for the chemotherapy of glioblastoma: Towards the pharmaceutical development', *International Journal of Pharmaceutics*, 572, p. 118733. doi:10.1016/j.ijpharm.2019.118733.

Malinovskaya, Y. *et al.* (2017) 'Delivery of doxorubicin-loaded PLGA nanoparticles into U87 human glioblastoma cells', *International Journal of Pharmaceutics*, 524(1), pp. 77–90. doi:10.1016/j.ijpharm.2017.03.049.

Mathew, A. *et al.* (2012) 'Curcumin Loaded-PLGA Nanoparticles Conjugated with Tet-1 Peptide for Potential Use in Alzheimer's Disease', *PLOS ONE*, 7(3), p. e32616. doi:10.1371/journal.pone.0032616.

McCall, R.L. and Sirianni, R.W. (2013) 'PLGA Nanoparticles Formed by Single- or Double-emulsion with Vitamin E-TPGS', *Journal of Visualized Experiments: JoVE* [Preprint], (82). doi:10.3791/51015.

McCreadie, R.G. *et al.* (1979) 'Plasma pimozide profiles in chronic schizophrenics.', *British Journal of Clinical Pharmacology*, 7(5), pp. 533–534.

MedlinePlus (2017) *Pimozide*, *MedlinePlus*. Available at: <https://medlineplus.gov/druginfo/meds/a686018.html> (Accessed: 21 May 2020).

Mercorelli, B., Palù, G. and Loregian, A. (2018) 'Drug Repurposing for Viral Infectious Diseases: How Far Are We?', *Trends in Microbiology*, 26(10), pp. 865–876. doi:10.1016/j.tim.2018.04.004.

Meyer, V.R. (2010) *Practical High-Performance Liquid Chromatography*. 5th edn. Wes Sussex, UK: Wiley-Blackwell.

- Michiels, M., Hendriks, R. and Heykants, J. (1982) '[39] Radioimmunoassay of pimozone', in *Methods in Enzymology*. Academic Press (Immunochemical Techniques Part D: Selected Immunoassays), pp. 542–551. doi:10.1016/0076-6879(82)84041-X.
- Miller, R. (2016) 'Emulsifiers: Types and Uses', in Caballero, B., Finglas, P.M., and Toldrá, F. (eds) *Encyclopedia of Food and Health*. Oxford: Academic Press, pp. 498–502. doi:10.1016/B978-0-12-384947-2.00249-X.
- Mitra, A. *et al.* (2010) 'Nano-optofluidic Detection of Single Viruses and Nanoparticles', *ACS Nano*, 4(3), pp. 1305–1312. doi:10.1021/nn901889v.
- Mittal, G. *et al.* (2007) 'Estradiol loaded PLGA nanoparticles for oral administration: Effect of polymer molecular weight and copolymer composition on release behavior in vitro and in vivo', *Journal of Controlled Release*, 119(1), pp. 77–85. doi:10.1016/j.jconrel.2007.01.016.
- Mohanty, S.K. *et al.* (2017) 'STAT3 and STAT5A are potential therapeutic targets in castration-resistant prostate cancer', *Oncotarget*, 8(49), pp. 85997–86010. doi:10.18632/oncotarget.20844.
- Molassiotis, A. *et al.* (2005) 'Use of complementary and alternative medicine in cancer patients: a European survey', *Annals of Oncology*, 16(4), pp. 655–663. doi:10.1093/annonc/mdi110.
- Monge, M. *et al.* (2020) 'Functionalized PLGA nanoparticles prepared by nano-emulsion templating interact selectively with proteins involved in the transport through the blood-brain barrier', *European Journal of Pharmaceutics and Biopharmaceutics*, 156, pp. 155–164. doi:10.1016/j.ejpb.2020.09.003.
- Monsuez, J.-J. *et al.* (2010) 'Cardiac side-effects of cancer chemotherapy', *International Journal of Cardiology*, 144(1), pp. 3–15. doi:10.1016/j.ijcard.2010.03.003.
- Morais, A.R. do V. *et al.* (2016) 'Freeze-drying of emulsified systems: A review', *International Journal of Pharmaceutics*, 503(1), pp. 102–114. doi:10.1016/j.ijpharm.2016.02.047.
- Mothi, M. and Sampson, S. (2013) 'Pimozone for schizophrenia or related psychoses', *The Cochrane Database of Systematic Reviews*, (11), p. CD001949. doi:10.1002/14651858.CD001949.pub3.
- Mu, L. and Feng, S.S. (2003) 'A novel controlled release formulation for the anticancer drug paclitaxel (Taxol®): PLGA nanoparticles containing vitamin E TPGS', *Journal of Controlled Release*, 86(1), pp. 33–48. doi:10.1016/S0168-3659(02)00320-6.
- Murakami, H. *et al.* (1997) 'Influence of the degrees of hydrolyzation and polymerization of poly(vinylalcohol) on the preparation and properties of poly(dl-lactide-co-glycolide) nanoparticle', *International Journal of Pharmaceutics*, 149(1), pp. 43–49. doi:10.1016/S0378-5173(96)04854-5.
- Mylonaki, I. *et al.* (2018) 'Imaging the porous structure in the core of degrading PLGA microparticles: The effect of molecular weight', *Journal of Controlled Release*, 286, pp. 231–239. doi:10.1016/j.jconrel.2018.07.044.
- Nance, E. *et al.* (2014a) 'Brain-Penetrating Nanoparticles Improve Paclitaxel Efficacy in Malignant Glioma Following Local Administration', *ACS Nano*, 8(10), pp. 10655–10664. doi:10.1021/nn504210g.

Nance, E. *et al.* (2014b) 'Brain-penetrating nanoparticles improve paclitaxel efficacy in malignant glioma following local administration', *ACS nano*, 8(10), pp. 10655–10664. doi:10.1021/nn504210g.

National Cancer Institute (2017a) *Types of Cancer Treatment*, National Cancer Institute. Available at: <https://www.cancer.gov/about-cancer/treatment/types> (Accessed: 1 May 2020).

National Cancer Institute (2017b) *Types of Cancer Treatment - National Cancer Institute*, National Cancer Institute. Available at: <https://www.cancer.gov/about-cancer/treatment/types> (Accessed: 9 June 2020).

Nelson, B. (2018) 'A fluid future for liquid biopsies', *Cancer Cytopathology*, 126(12), pp. 963–964. doi:10.1002/cncy.22087.

Nelson, E.A. *et al.* (2007) 'Pimozide Inhibits STAT5 Signaling in Chronic Myelogenous Leukemia and Reduces the Viability of Both Imatinib Sensitive and Imatinib Resistant Cells.', *Blood*, 110(11), pp. 2953–2953.

Nelson, E.A. *et al.* (2011) 'The STAT5 inhibitor pimozide decreases survival of chronic myelogenous leukemia cells resistant to kinase inhibitors', *Blood*, 117(12), pp. 3421–3429. doi:10.1182/blood-2009-11-255232.

Nelson, E.A. *et al.* (2012) 'The STAT5 Inhibitor Pimozide Displays Efficacy in Models of Acute Myelogenous Leukemia Driven by FLT3 Mutations', *Genes & Cancer*, 3(7–8), pp. 503–511. doi:10.1177/1947601912466555.

Nguyen, P.V. *et al.* (2021) 'Nanomedicines functionalized with anti-EGFR ligands for active targeting in cancer therapy: Biological strategy, design and quality control', *International Journal of Pharmaceutics*, 605, p. 120795. doi:10.1016/j.ijpharm.2021.120795.

NICE (2020) *Pimozide*, National Institute for Health and Care Excellence. NICE. Available at: <https://bnf.nice.org.uk/drug/pimozide.html> (Accessed: 21 May 2020).

Norouzi, M. *et al.* (2020) 'Clinical applications of nanomedicine in cancer therapy', *Drug Discovery Today*, 25(1), pp. 107–125. doi:10.1016/j.drudis.2019.09.017.

Ojanperä, I. *et al.* (1991) 'Combined Use of Normal and Reversed Phase Thin Layer Chromatography in the Screening for Basic and Quaternary Drugs', *Journal of Liquid Chromatography*, 14(8), pp. 1435–1446. doi:10.1080/01483919108049625.

Operti, M.C. *et al.* (2021) 'PLGA-based nanomedicines manufacturing: Technologies overview and challenges in industrial scale-up', *International Journal of Pharmaceutics*, 605, p. 120807. doi:10.1016/j.ijpharm.2021.120807.

Özkan, S.A., Özkan, Y. and Şentürk, Z. (2002) 'Electrooxidation of pimozide and its differential pulse voltammetric and HPLC–EC determination', *Analytica Chimica Acta*, 453(2), pp. 221–229. doi:10.1016/S0003-2670(01)01412-X.

Panchapakesan, U. and Pollock, C. (2018) 'Drug repurposing in kidney disease', *Kidney International*, 94(1), pp. 40–48. doi:10.1016/j.kint.2017.12.026.

Pande, M. and Bhaskarwar, A.N. (2016) *Nanoparticles: Preparation and Characterization*. 1st edn. New York: Momentum Press.

Paranjpe, M.D., Taubes, A. and Sirota, M. (2019) 'Insights into Computational Drug Repurposing for Neurodegenerative Disease', *Trends in Pharmacological Sciences*, 40(8), pp. 565–576. doi:10.1016/j.tips.2019.06.003.

Parra, A. *et al.* (2015) 'Design and elaboration of freeze-dried PLGA nanoparticles for the transcorneal permeation of carprofen: Ocular anti-inflammatory applications', *Colloids and Surfaces B: Biointerfaces*, 136, pp. 935–943. doi:10.1016/j.colsurfb.2015.10.026.

Pedersen–Bjergaard, S., Gammelgaard, B. and Halvorsen, T.G. (2019) *Introduction to Pharmaceutical Analytical Chemistry*. 2 edition. Hoboken, NJ: Wiley.

Pereverzeva, E. *et al.* (2019) 'Toxicological study of doxorubicin-loaded PLGA nanoparticles for the treatment of glioblastoma', *International Journal of Pharmaceutics*, 554, pp. 161–178. doi:10.1016/j.ijpharm.2018.11.014.

Plummer, M. *et al.* (2016) 'Global burden of cancers attributable to infections in 2012: a synthetic analysis', *The Lancet. Global Health*, 4(9), pp. e609-616. doi:10.1016/S2214-109X(16)30143-7.

Pluym, A. (1979) 'TLC differentiation of butyrophenone and diphenylbutylpiperidine compounds from phenothiazine derivatives', *Journal of Pharmaceutical Sciences*, 68(8), pp. 1050–1052. doi:10.1002/jps.2600680834.

Polte, J. *et al.* (2010) 'Nucleation and Growth of Gold Nanoparticles Studied via in situ Small Angle X-ray Scattering at Millisecond Time Resolution', *ACS Nano*, 4(2), pp. 1076–1082. doi:10.1021/nn901499c.

Potter, T.M. *et al.* (2015) *Assay Cascade Protocols, Detection of microbial contamination, Nanotechnology Characterization Laboratory*. Available at: <https://ncl.cancer.gov/resources/assay-cascade-protocols> (Accessed: 3 April 2020).

Pourasghar, M. *et al.* (2019) 'Development of a fast and precise method for simultaneous quantification of the PLGA monomers lactic and glycolic acid by HPLC', *Journal of Pharmaceutical Analysis*, 9(2), pp. 100–107. doi:10.1016/j.jpha.2019.01.004.

Precision NanoSystem (2021) *NxGen - A Disruptive Technology Enabling Transformative Medicine*. Available at: <https://www.precisionnanosystems.com/platform-technologies/product-comparison/nxgen> (Accessed: 19 September 2021).

Pringsheim, T. and Marras, C. (2009) 'Pimozide for tics in Tourette's syndrome', *The Cochrane Database of Systematic Reviews*, (2), p. CD006996. doi:10.1002/14651858.CD006996.pub2.

PubChem, D. (2021) *Pimozide*. Available at: <https://pubchem.ncbi.nlm.nih.gov/compound/16362> (Accessed: 1 October 2021).

PubChem Database (2020) *Pimozide, National Center for Biotechnology Information*. Available at: <https://pubchem.ncbi.nlm.nih.gov/compound/16362> (Accessed: 21 May 2020).

PubChem Database (2021) *Polyvinyl alcohol*. Available at: <https://pubchem.ncbi.nlm.nih.gov/compound/11199> (Accessed: 20 July 2021).

Punde, N.S., Kapade, V.G. and Srivastava, A.K. (2018) 'Electrocatalytic behavior of copper ferrite decorated carbon nanofibers towards oxidative determination of antipsychotic drug

Pimozide', *Journal of Electroanalytical Chemistry*, 825, pp. 87–96. doi:10.1016/j.jelechem.2018.08.015.

Pushpakom, S. *et al.* (2019) 'Drug repurposing: progress, challenges and recommendations', *Nature Reviews Drug Discovery*, 18(1), pp. 41–58. doi:10.1038/nrd.2018.168.

Raj, S. *et al.* (2021) 'Specific targeting cancer cells with nanoparticles and drug delivery in cancer therapy', *Seminars in Cancer Biology*, 69, pp. 166–177. doi:10.1016/j.semcancer.2019.11.002.

Ramalho, M.J. *et al.* (2018) 'Receptor-mediated PLGA nanoparticles for glioblastoma multiforme treatment', *International Journal of Pharmaceutics*, 545(1), pp. 84–92. doi:10.1016/j.ijpharm.2018.04.062.

Recht, L. *et al.* (1990) 'Transferrin receptor in normal and neoplastic brain tissue: implications for brain-tumor immunotherapy', *Journal of Neurosurgery*, 72(6), pp. 941–945. doi:10.3171/jns.1990.72.6.0941.

Regeur, L. *et al.* (1986) 'Clinical features and long-term treatment with pimozide in 65 patients with Gilles de la Tourette's syndrome.', *Journal of Neurology, Neurosurgery, and Psychiatry*, 49(7), pp. 791–795.

Reimer, L. and Kohl, H. (2008) *Transmission Electron Microscopy: Physics of Image Formation*: 36. 5th ed. 2008 edition. New York, NY: Springer.

Rempe, R. *et al.* (2014) 'Strategies to overcome the barrier: use of nanoparticles as carriers and modulators of barrier properties', *Cell and Tissue Research*, 355(3), pp. 717–726. doi:10.1007/s00441-014-1819-7.

Ren, Y. *et al.* (2018) 'Pimozide suppresses colorectal cancer via inhibition of Wnt/ β -catenin signaling pathway', *Life Sciences*, 209, pp. 267–273. doi:10.1016/j.lfs.2018.08.027.

Rivera-Hernández, G. *et al.* (2021) 'Polyvinyl alcohol based-drug delivery systems for cancer treatment', *International Journal of Pharmaceutics*, 600, p. 120478. doi:10.1016/j.ijpharm.2021.120478.

Robertson, M.M. *et al.* (2017) 'Gilles de la Tourette syndrome', *Nature Reviews Disease Primers*, 3(1), pp. 1–20. doi:10.1038/nrdp.2016.97.

Robin, B. *et al.* (2021) 'Tuning morphology of Pickering emulsions stabilised by biodegradable PLGA nanoparticles: How PLGA characteristics influence emulsion properties', *Journal of Colloid and Interface Science*, 595, pp. 202–211. doi:10.1016/j.jcis.2021.03.061.

Roces, C.B., Christensen, D. and Perrie, Y. (2020) 'Translating the fabrication of protein-loaded poly(lactic-co-glycolic acid) nanoparticles from bench to scale-independent production using microfluidics', *Drug Delivery and Translational Research*, 10(3), pp. 582–593. doi:10.1007/s13346-019-00699-y.

Rondanin, R. *et al.* (2017) 'Effects of Pimozide Derivatives on pSTAT5 in K562 Cells', *ChemMedChem*, 12(15), pp. 1183–1190. doi:10.1002/cmdc.201700234.

Roos, A. *et al.* (2018) 'EGFRvIII-Stat5 Signaling Enhances Glioblastoma Cell Migration and Survival', *Molecular cancer research: MCR*, 16(7), pp. 1185–1195. doi:10.1158/1541-7786.MCR-18-0125.

Roth, B.L. *et al.* (1994) 'Binding of typical and atypical antipsychotic agents to 5-hydroxytryptamine-6 and 5-hydroxytryptamine-7 receptors', *The Journal of Pharmacology and Experimental Therapeutics*, 268(3), pp. 1403–1410.

Sachdeva, R. *et al.* (2019) 'ID1 Is Critical for Tumorigenesis and Regulates Chemoresistance in Glioblastoma', *Cancer Research*, 79(16), pp. 4057–4071. doi:10.1158/0008-5472.CAN-18-1357.

Sahin, A. *et al.* (2017) 'Using PVA and TPGS as combined emulsifier in nanoprecipitation method improves characteristics and anticancer activity of ibuprofen loaded PLGA nanoparticles', *Die Pharmazie*, 72(9), pp. 525–528. doi:10.1691/ph.2017.7015.

Sallee, F.R. *et al.* (1987) 'Pharmacokinetics of pimozide in adults and children with Tourette's syndrome', *Journal of Clinical Pharmacology*, 27(10), pp. 776–781. doi:10.1002/j.1552-4604.1987.tb02995.x.

Senapati, S. *et al.* (2018) 'Controlled drug delivery vehicles for cancer treatment and their performance', *Signal Transduction and Targeted Therapy*, 3(1), pp. 1–19. doi:10.1038/s41392-017-0004-3.

Sharma, N., Madan, P. and Lin, S. (2016) 'Effect of process and formulation variables on the preparation of parenteral paclitaxel-loaded biodegradable polymeric nanoparticles: A co-surfactant study', *Asian Journal of Pharmaceutical Sciences*, 11(3), pp. 404–416. doi:10.1016/j.ajps.2015.09.004.

Shaw, V., Srivastava, S. and Srivastava, S.K. (2019) 'Repurposing antipsychotics of the diphenylbutylpiperidine class for cancer therapy', *Seminars in Cancer Biology* [Preprint]. doi:10.1016/j.semcancer.2019.10.007.

Shi, X.-N. *et al.* (2015) 'In Silico Identification and In Vitro and In Vivo Validation of Anti-Psychotic Drug Fluspirilene as a Potential CDK2 Inhibitor and a Candidate Anti-Cancer Drug', *PLOS ONE*, 10(7), p. e0132072. doi:10.1371/journal.pone.0132072.

Shkodra-Pula, B. *et al.* (2019) 'Effect of surfactant on the size and stability of PLGA nanoparticles encapsulating a protein kinase C inhibitor', *International Journal of Pharmaceutics*, 566, pp. 756–764. doi:10.1016/j.ijpharm.2019.05.072.

Shubhra, Q.T.H. *et al.* (2014) 'Surface modification of HSA containing magnetic PLGA nanoparticles by poloxamer to decrease plasma protein adsorption', *Colloids and Surfaces B: Biointerfaces*, 122, pp. 529–536. doi:10.1016/j.colsurfb.2014.07.025.

Silva, A.T.C.R. *et al.* (2015) 'Synthesis, Characterization, and Study of PLGA Copolymer in Vitro Degradation', *Journal of Biomaterials and Nanobiotechnology*, 6(1), pp. 8–19. doi:10.4236/jbmb.2015.61002.

Simpson, H.M. *et al.* (2018) 'STAT5 inhibition induces TRAIL/DR4 dependent apoptosis in peripheral T-cell lymphoma', *Oncotarget*, 9(24), pp. 16792–16806. doi:10.18632/oncotarget.24698.

Sleire, L. *et al.* (2017) 'Drug repurposing in cancer', *Pharmacological Research*, 124, pp. 74–91. doi:10.1016/j.phrs.2017.07.013.

Smith, B.C. (2011) *Fundamentals of Fourier Transform Infrared Spectroscopy*. 2nd edition. CRC Press.

Smyj, R., Wang, X.-P. and Han, F. (2012) 'Chapter 7 - Pimozide', in Brittain, H.G. (ed.) *Profiles of Drug Substances, Excipients and Related Methodology*. Academic Press, pp. 287–311. doi:10.1016/B978-0-12-397220-0.00007-6.

Soetaert, F. *et al.* (2020) 'Cancer therapy with iron oxide nanoparticles: Agents of thermal and immune therapies', *Advanced Drug Delivery Reviews* [Preprint]. doi:10.1016/j.addr.2020.06.025.

Stauffer, E., Dolan, J.A. and Newman, R. (2008) 'CHAPTER 8 - Gas Chromatography and Gas Chromatography—Mass Spectrometry', in Stauffer, E., Dolan, J.A., and Newman, R. (eds) *Fire Debris Analysis*. Burlington: Academic Press, pp. 235–293. doi:10.1016/B978-012663971-1.50012-9.

Stoll, D.R. and Mack, A.E. (2019) *Effects of Sample Diluent on Analyte Recovery in Reversed-Phase and HILIC Separations, Chromatography Online*. Available at: <https://www.chromatographyonline.com/view/mind-diluent-effects-sample-diluent-analyte-recovery-reversed-phase-and-hilic-separations> (Accessed: 5 May 2021).

Strobl, J.S. *et al.* (1990) 'Inhibition of human breast cancer cell proliferation in tissue culture by the neuroleptic agents pimozide and thioridazine', *Cancer Research*, 50(17), pp. 5399–5405.

Strobl, J.S. *et al.* (1998) 'The cell death response to gamma-radiation in MCF-7 cells is enhanced by a neuroleptic drug, pimozide', *Breast Cancer Research and Treatment*, 51(1), pp. 83–95. doi:10.1023/a:1006046604062.

Strobl, J.S. and Peterson, V.A. (1992) 'Tamoxifen-resistant human breast cancer cell growth: inhibition by thioridazine, pimozide and the calmodulin antagonist, W-13', *The Journal of Pharmacology and Experimental Therapeutics*, 263(1), pp. 186–193.

Stroock, A.D. *et al.* (2002) 'Chaotic mixer for microchannels', *Science (New York, N.Y.)*, 295(5555), pp. 647–651. doi:10.1126/science.1066238.

Sufi, S.A. *et al.* (2020) 'Enhanced drug retention, sustained release, and anti-cancer potential of curcumin and indole-curcumin analog-loaded polysorbate 80-stabilized PLGA nanoparticles in colon cancer cell line SW480', *International Journal of Pharmaceutics*, 588, p. 119738. doi:10.1016/j.ijpharm.2020.119738.

Suk, J.S. *et al.* (2016) 'PEGylation as a strategy for improving nanoparticle-based drug and gene delivery', *Advanced Drug Delivery Reviews*, 99, pp. 28–51. doi:10.1016/j.addr.2015.09.012.

Svenja, Z. *et al.* (2018) *Loperamide, Pimozide, and STF-62247 Trigger Autophagy-Dependent Cell Death in Glioblastoma Cells, Cell death & disease*. Cell Death Dis. doi:10.1038/s41419-018-1003-1.

Swider, E. *et al.* (2018) 'Customizing poly(lactic-co-glycolic acid) particles for biomedical applications', *Acta Biomaterialia*, 73, pp. 38–51. doi:10.1016/j.actbio.2018.04.006.

Torchilin, V.P. (2010) 'Passive and Active Drug Targeting: Drug Delivery to Tumors as an Example', in Schäfer-Korting, M. (ed.) *Drug Delivery*. Berlin, Heidelberg: Springer (Handbook of Experimental Pharmacology), pp. 3–53. doi:10.1007/978-3-642-00477-3_1.

- Tran, S. *et al.* (2017) 'Cancer nanomedicine: a review of recent success in drug delivery', *Clinical and Translational Medicine*, 6(1), p. 44. doi:10.1186/s40169-017-0175-0.
- Trenkensschuh, E. and Friess, W. (2021) 'Freeze-drying of nanoparticles: How to overcome colloidal instability by formulation and process optimization', *European Journal of Pharmaceutics and Biopharmaceutics*, 165, pp. 345–360. doi:10.1016/j.ejpb.2021.05.024.
- Valencia, P.M. *et al.* (2010) 'Single-step assembly of homogenous lipid-polymeric and lipid-quantum dot nanoparticles enabled by microfluidic rapid mixing', *ACS nano*, 4(3), pp. 1671–1679. doi:10.1021/nn901433u.
- Vasita, R. and Katti, D.S. (2012) 'Structural and functional characterization of proteins adsorbed on hydrophilized polylactide-co-glycolide microfibers', *International Journal of Nanomedicine*, 7, pp. 61–71. doi:10.2147/IJN.S26453.
- Vengala, P., Dintakurthi, S. and Subrahmanyam, C.V.S. (2013) 'Lactose coated ceramic nanoparticles for oral drug delivery', *Journal of Pharmacy Research*, 7(6), pp. 540–545. doi:10.1016/j.jopr.2013.06.015.
- Venugopal, V. *et al.* (2018) 'Anti-EGFR anchored paclitaxel loaded PLGA nanoparticles for the treatment of triple negative breast cancer. In-vitro and in-vivo anticancer activities', *PLoS ONE*, 13(11), p. e0206109. doi:10.1371/journal.pone.0206109.
- Vitha, M.F. (2017) *Chromatography: Principles and Instrumentation*. New Jersey, USA: Wiley.
- Vu, H.T.H. *et al.* (2019) 'Utilization of Microfluidics for the Preparation of Polymeric Nanoparticles for the Antioxidant Rutin: A Comparison with Bulk Production', *Pharmaceutical Nanotechnology*, 7(6), pp. 469–483. doi:10.2174/2211738507666191019141049.
- Vyas, D., Patel, M. and Wairkar, S. (2021) 'Strategies for active tumor targeting-an update', *European Journal of Pharmacology*, p. 174512. doi:10.1016/j.ejphar.2021.174512.
- Webb, C. *et al.* (2020) 'Using microfluidics for scalable manufacturing of nanomedicines from bench to GMP: A case study using protein-loaded liposomes', *International Journal of Pharmaceutics*, 582, p. 119266. doi:10.1016/j.ijpharm.2020.119266.
- Weissenrieder, J.S. *et al.* (2020) 'The Dopamine D2 Receptor Contributes to the Spheroid Formation Behavior of U87 Glioblastoma Cells', *Pharmacology*, 105(1–2), pp. 19–27. doi:10.1159/000502562.
- WHO (2021) *Cancer, Cancer*. Available at: <https://www.who.int/news-room/fact-sheets/detail/cancer> (Accessed: 16 September 2021).
- Wicki, A. *et al.* (2015) 'Nanomedicine in cancer therapy: Challenges, opportunities, and clinical applications', *Journal of Controlled Release*, 200, pp. 138–157. doi:10.1016/j.jconrel.2014.12.030.
- Wiklund, E.D. *et al.* (2010) 'Cytotoxic effects of antipsychotic drugs implicate cholesterol homeostasis as a novel chemotherapeutic target', *International Journal of Cancer*, 126(1), pp. 28–40. doi:10.1002/ijc.24813.
- Wilkinson, S. *et al.* (2008) 'The use of complementary therapy by men with prostate cancer in the UK', *European Journal of Cancer Care*, 17(5), pp. 492–499. doi:10.1111/j.1365-2354.2007.00904.x.

- Williams, M.S., Longmuir, K.J. and Yager, P. (2008) 'A practical guide to the staggered herringbone mixer', *Lab on a Chip*, 8(7), pp. 1121–1129. doi:10.1039/B802562B.
- Xie, H. and Smith, J.W. (2010) 'Fabrication of PLGA nanoparticles with a fluidic nanoprecipitation system', *Journal of Nanobiotechnology*, 8(1), p. 18. doi:10.1186/1477-3155-8-18.
- Xu, J. *et al.* (2017) 'Controllable Microfluidic Production of Drug-Loaded PLGA Nanoparticles Using Partially Water-Miscible Mixed Solvent Microdroplets as a Precursor', *Scientific Reports*, 7(1), pp. 1–12. doi:10.1038/s41598-017-05184-5.
- Xu, Q.A. (2013) *Ultra-High Performance Liquid Chromatography and Its Applications*. 1 edition. New Jersey, USA: Wiley.
- Xue, Q. *et al.* (2020) 'Penfluridol: An antipsychotic agent suppresses lung cancer cell growth and metastasis by inducing G0/G1 arrest and apoptosis', *Biomedicine & Pharmacotherapy*, 121, p. 109598. doi:10.1016/j.biopha.2019.109598.
- Yan, M. *et al.* (2010) 'Quantitative determination of pimozide in human plasma by liquid chromatography-mass spectrometry and its application in a bioequivalence study', *Journal of Pharmaceutical and Biomedical Analysis*, 51(5), pp. 1161–1164. doi:10.1016/j.jpba.2009.11.015.
- Yang, C.-E. *et al.* (2019) 'The antipsychotic chlorpromazine suppresses YAP signaling, stemness properties, and drug resistance in breast cancer cells', *Chemico-Biological Interactions*, 302, pp. 28–35. doi:10.1016/j.cbi.2019.01.033.
- Yang, R. (2018) *Analytical Methods for Polymer Characterization*. 1st edition. Boca Raton: CRC Press.
- Yesenia Hernández-Giottonini, K. *et al.* (2020) 'PLGA nanoparticle preparations by emulsification and nanoprecipitation techniques: effects of formulation parameters', *RSC Advances*, 10(8), pp. 4218–4231. doi:10.1039/C9RA10857B.
- Yusuf, M. *et al.* (2021) 'Brain targeted Polysorbate-80 coated PLGA thymoquinone nanoparticles for the treatment of Alzheimer's disease, with biomechanistic insights', *Journal of Drug Delivery Science and Technology*, 61, p. 102214. doi:10.1016/j.jddst.2020.102214.
- Zemrak, W.R. and Kenna, G.A. (2008) 'Association of antipsychotic and antidepressant drugs with Q-T interval prolongation', *American journal of health-system pharmacy: AJHP: official journal of the American Society of Health-System Pharmacists*, 65(11), pp. 1029–1038. doi:10.2146/ajhp070279.
- Zhang, X. *et al.* (2019) 'Multifunctional Polyethylene Glycol (PEG)-Poly (Lactic-Co-Glycolic Acid) (PLGA)-Based Nanoparticles Loading Doxorubicin and Tetrahydrocurcumin for Combined Chemoradiotherapy of Glioma', *Medical Science Monitor: International Medical Journal of Experimental and Clinical Research*, 25, pp. 9737–9751. doi:10.12659/MSM.918899.
- Zhang, Z. *et al.* (2020) 'Overcoming cancer therapeutic bottleneck by drug repurposing', *Signal Transduction and Targeted Therapy*, 5(1), pp. 1–25. doi:10.1038/s41392-020-00213-8.
- Zhigaltsev, I.V. *et al.* (2012) 'Bottom-up design and synthesis of limit size lipid nanoparticle systems with aqueous and triglyceride cores using millisecond microfluidic mixing',

Langmuir: the ACS journal of surfaces and colloids, 28(7), pp. 3633–3640. doi:10.1021/la204833h.

Zhou, W. *et al.* (2016) 'The antipsychotic drug pimozide inhibits cell growth in prostate cancer through suppression of STAT3 activation', *International Journal of Oncology*, 48(1), pp. 322–328. doi:10.3892/ijo.2015.3229.

Zhu, H. *et al.* (2014) 'Co-delivery of chemotherapeutic drugs with vitamin E TPGS by porous PLGA nanoparticles for enhanced chemotherapy against multi-drug resistance', *Biomaterials*, 35(7), pp. 2391–2400. doi:10.1016/j.biomaterials.2013.11.086.

Chapter 9

Appendices

Appendices

Appendix 1: Preparation of surfactant solutions

Surfactant solution	Preparation workflow
Poly vinyl alcohol (1.25 % w/v)	12.5 grams of PVA was weighed and transferred to a beaker with 800 mL of hot water followed by magnetic stirring on a hot plate (at 80°C) overnight. The solution was made up 1 litre with additional distilled water in a volumetric flask after filtration.
Polysorbate 80 (1.25% w/v)	12.5 grams of polysorbate 80 was dissolved in 1 litre of distilled water upon stirring, followed by filtration.
Poloxamer 188 (1.25% w/v)	Similar procedure as polysorbate 80. However, total volume was 100 mL.
TPGS (0.5, 1.25, and 2% w/v)	At first, 2% w/v TPGS was prepared by dissolving 2 grams of TPGS in 100 mL of distilled water upon magnetic stirring, followed by filtration. Required dilutions were made to prepare concentrations of 1.25, and 0.5% (w/v).

Appendix 2: DLS data (Representative)

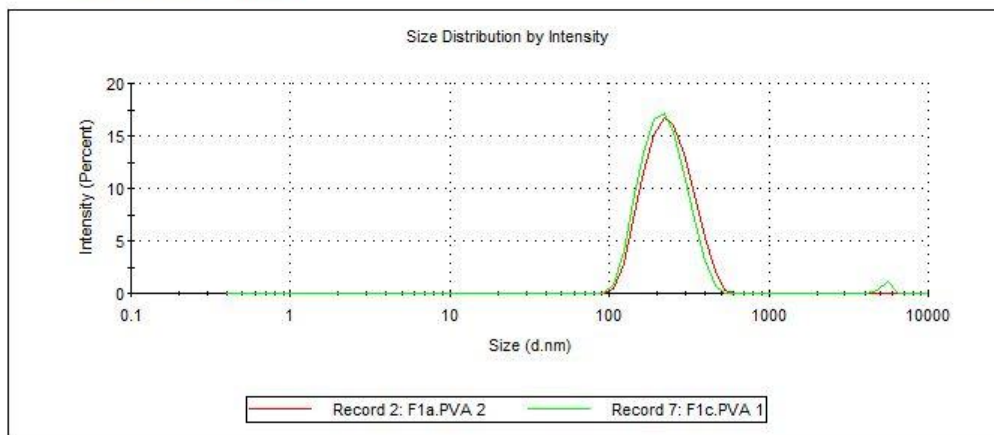
Particle size and PDI measurement of formulation F1

Sample Name: F1a.PVA 2
SOP Name: mansettings.nano
File Name: SE.AT.PLGA.2.5pmz
Record Number: 2
Material Rf: 1.47
Material Absorbtion: 0.000
Dispersant Name: Water
Dispersant Rf: 1.330
Viscosity (cP): 0.8872
Measurement Date and Time: 23 July 2018 11:20:12

Temperature (°C): 25.0
Count Rate (kcps): 462.0
Cell Description: Disposable sizing cuvette
Duration Used (s): 60
Measurement Position (mm): 4.65
Attenuator: 7

	Size (d.nm):	% Intensity:	St Dev (d.nm):
Z-Average (d.nm): 219.7	Peak 1: 242.9	100.0	78.80
Pdi: 0.093	Peak 2: 0.000	0.0	0.000
Intercept: 0.929	Peak 3: 0.000	0.0	0.000

Result quality : **Good**



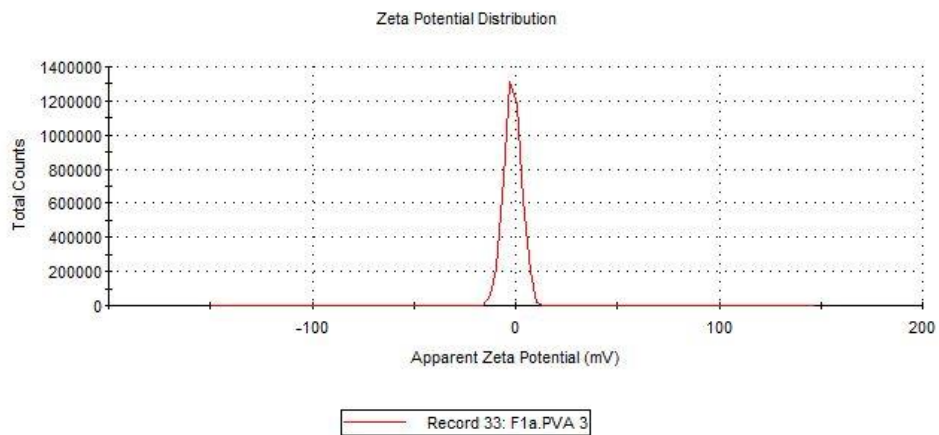
Zeta potential measurement of formulation F1

Sample Name: F1a.PVA3
SOP Name: mansettings.nano
File Name: SE.AT.PLGA.2.5pmz
Record Number: 33
Date and Time: 23 July 2018 14:49:16
Dispersant Name: Water
Dispersant RI: 1.330
Viscosity (cP): 0.8872
Dispersant Dielectric Constant: 78.5

Temperature (°C): 25.0
Count Rate (kcps): 206.7
Cell Description: Clear disposable zeta cell
Zeta Runs: 44
Measurement Position (mm): 2.00
Attenuator: 4

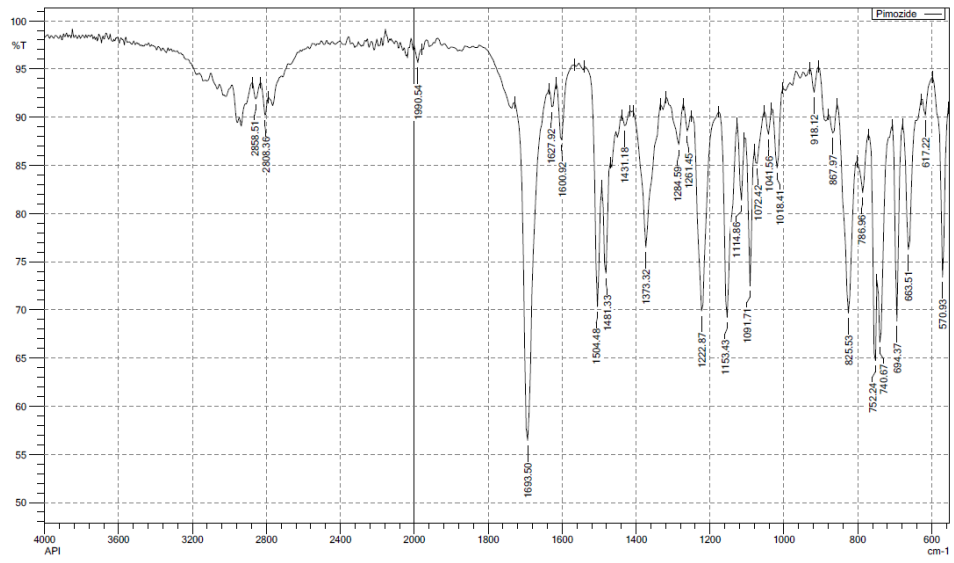
	Mean (mV)	Area (%)	St Dev (mV)
Zeta Potential (mV): -1.47	Peak 1: -1.47	100.0	4.20
Zeta Deviation (mV): 4.20	Peak 2: 0.00	0.0	0.00
Conductivity (mS/cm): 1.09	Peak 3: 0.00	0.0	0.00

Result quality : Good

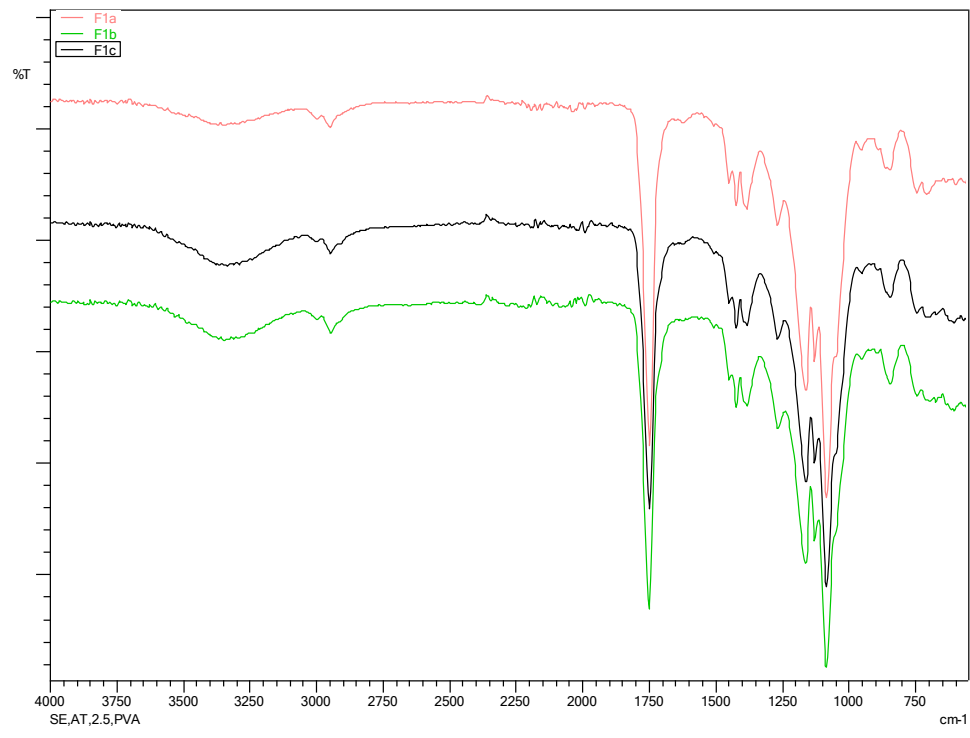


Appendix 3: FTIR spectra (Representative)

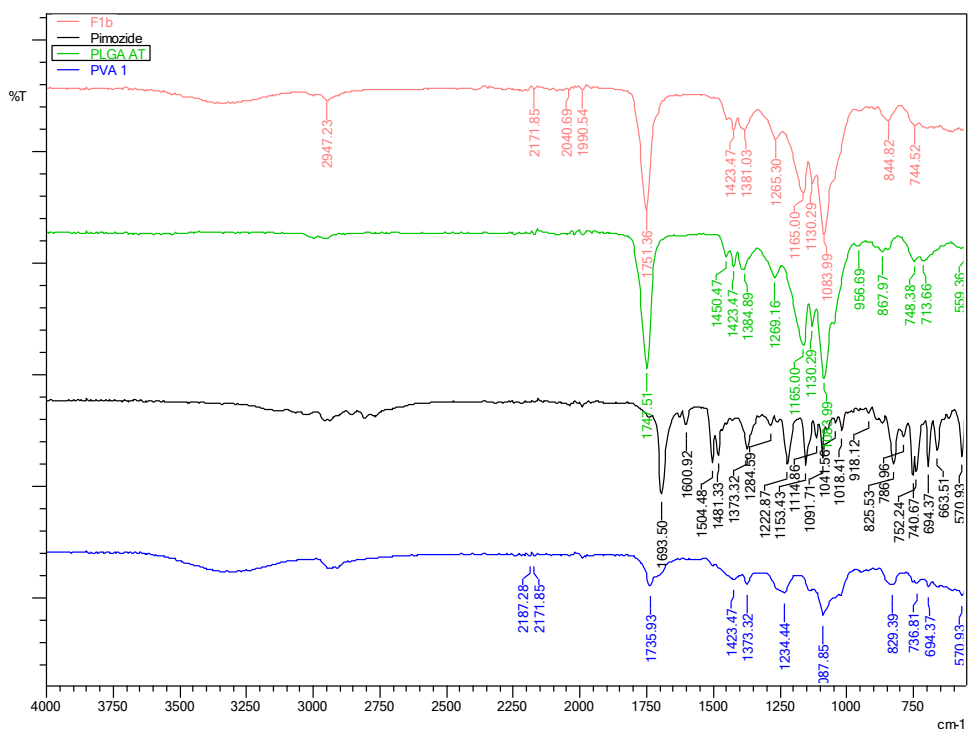
(a) FTIR spectrum of pure pimozide



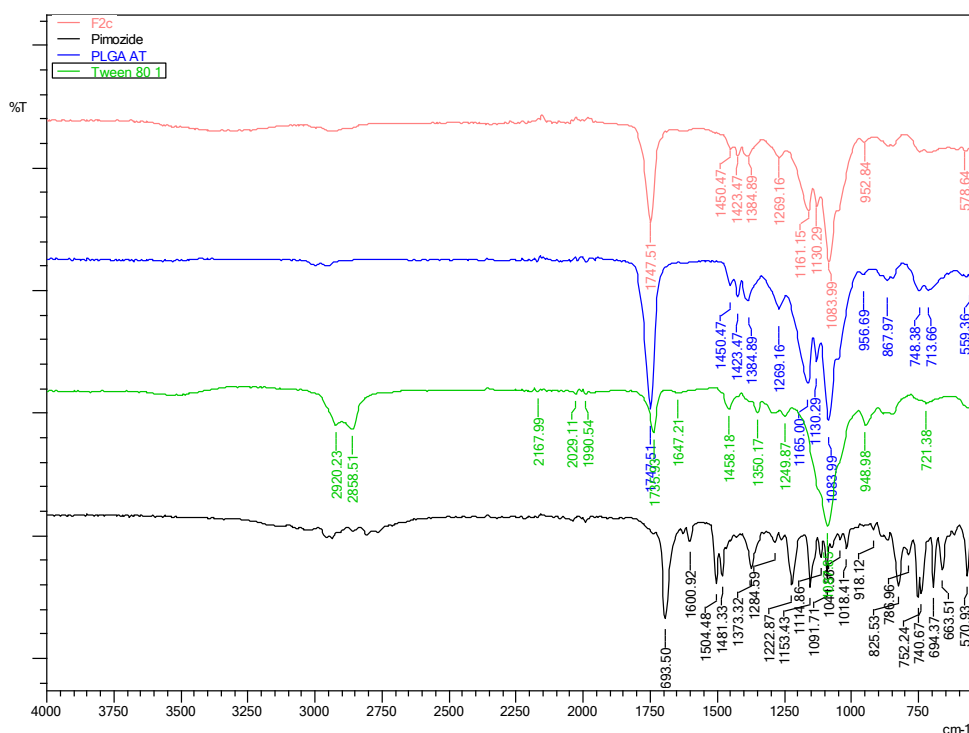
(b) FTIR spectra of formulation F1 (three independent replicates)



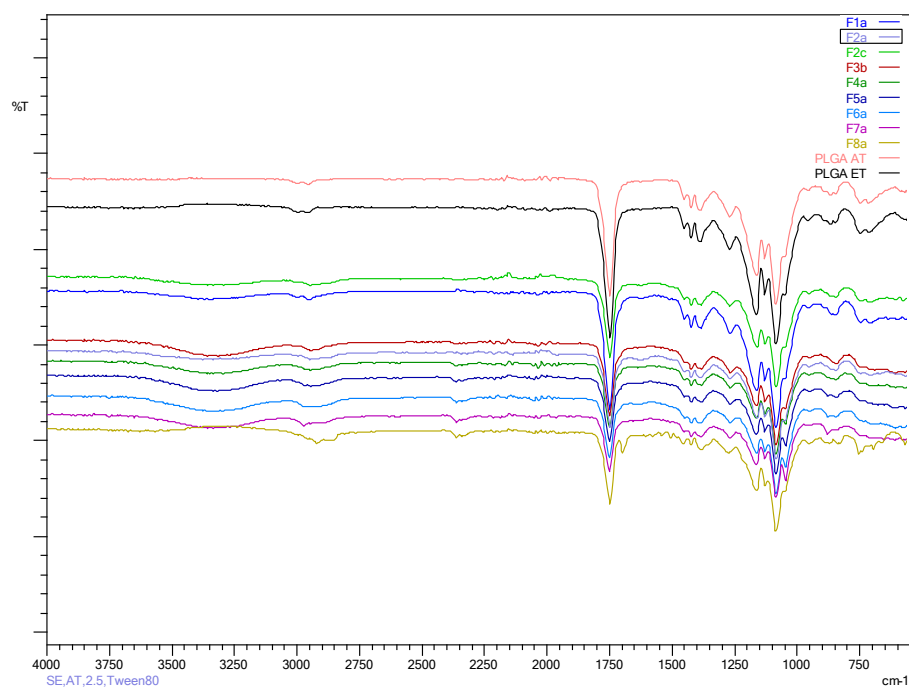
(c) Overlay of FTIR spectra of formulation F1 and comprising materials



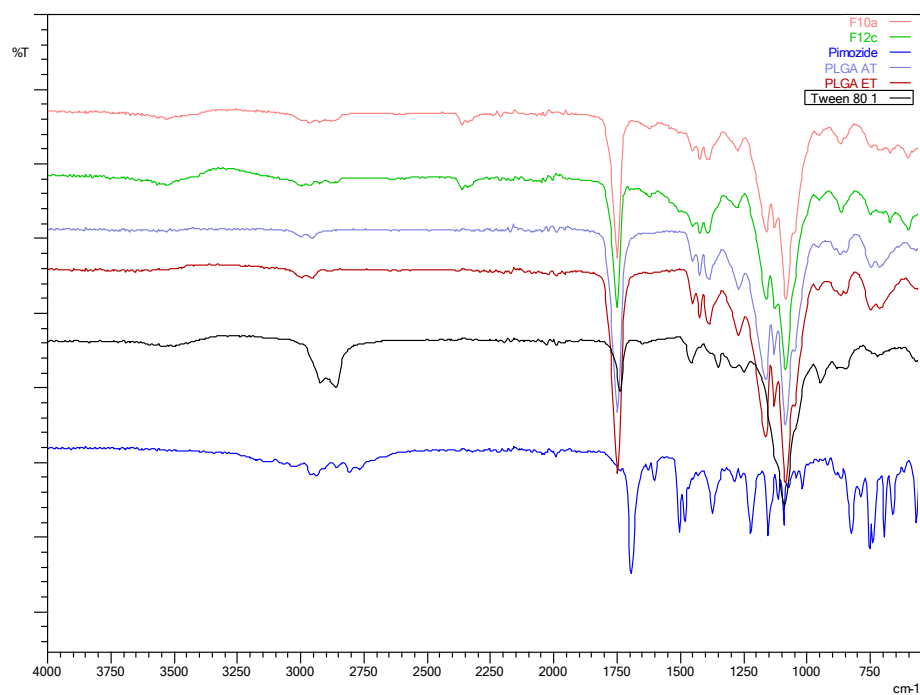
(d) Overlay of FTIR spectra of formulation F2 and comprising materials



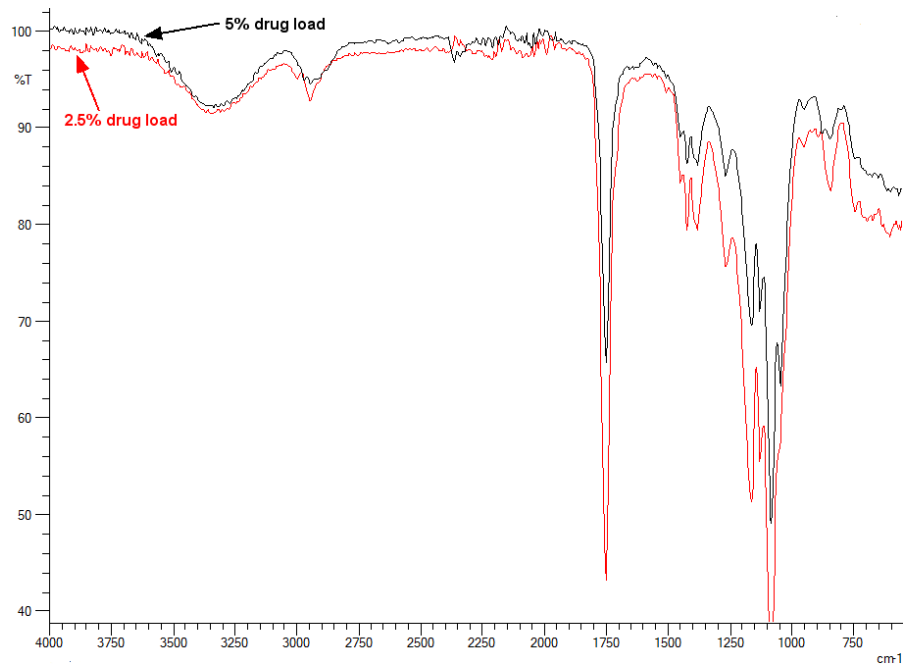
(e) Overlay of FTIR spectra of all formulations prepared by SE method



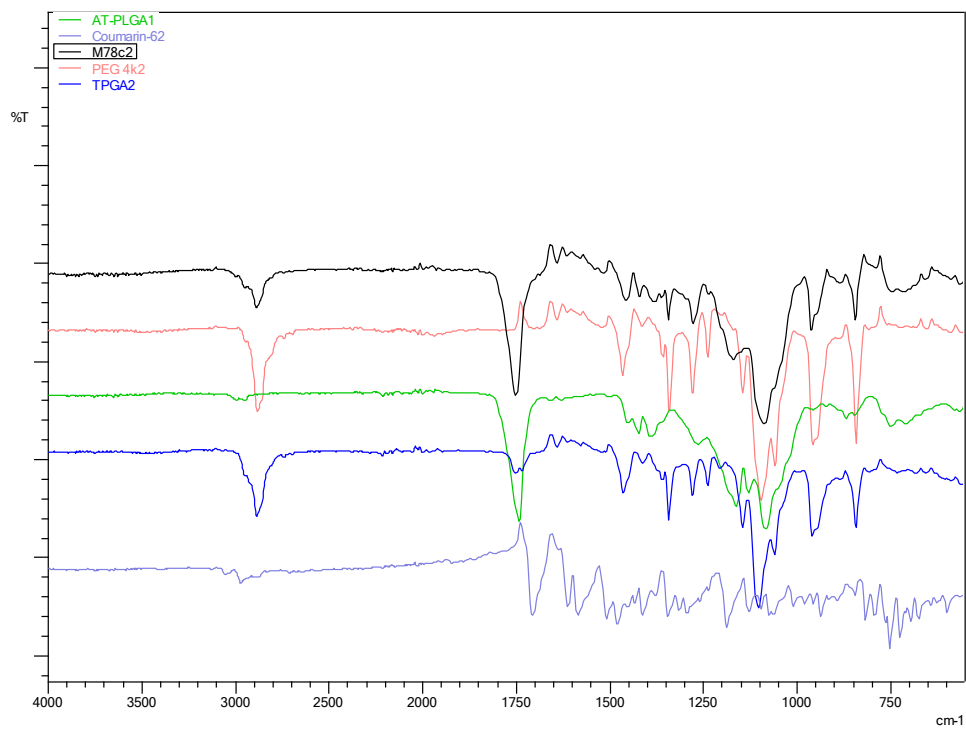
(f) Overlay of FTIR spectra of formulations F10 and F12 prepared by MF method



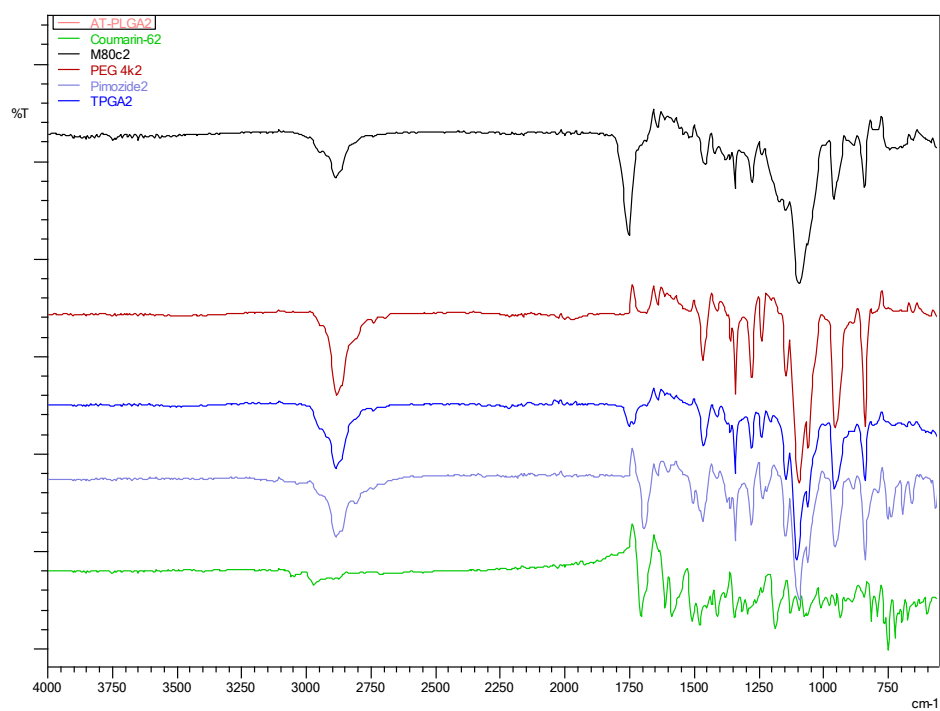
(g) Overlay of FTIR spectrum of two different concentrations of pimozone loaded nanoparticles



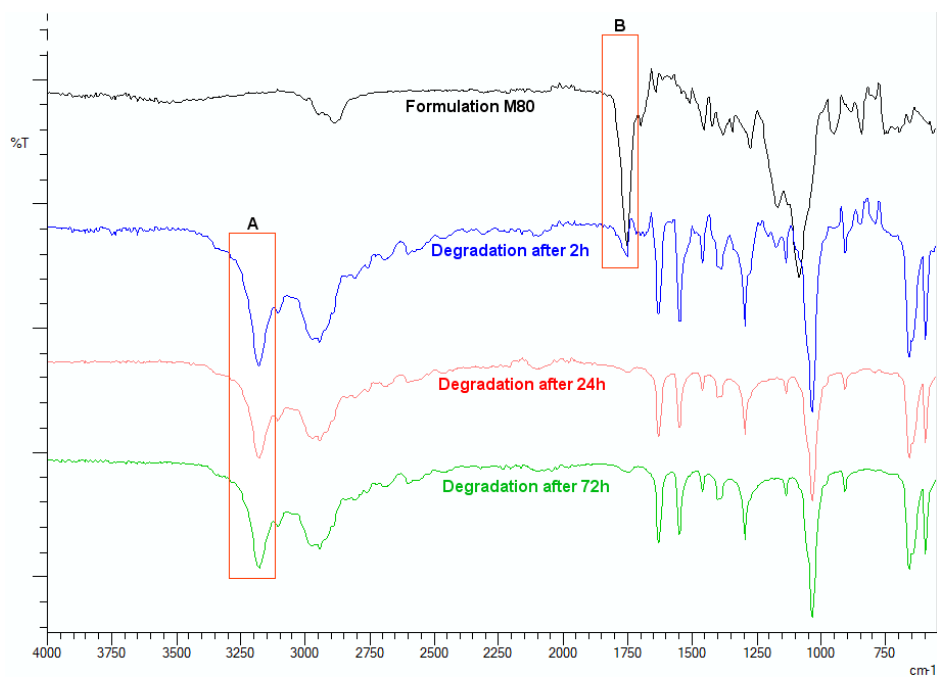
(h) Overlay of FTIR spectra of formulation NPs-C6 and comprising materials



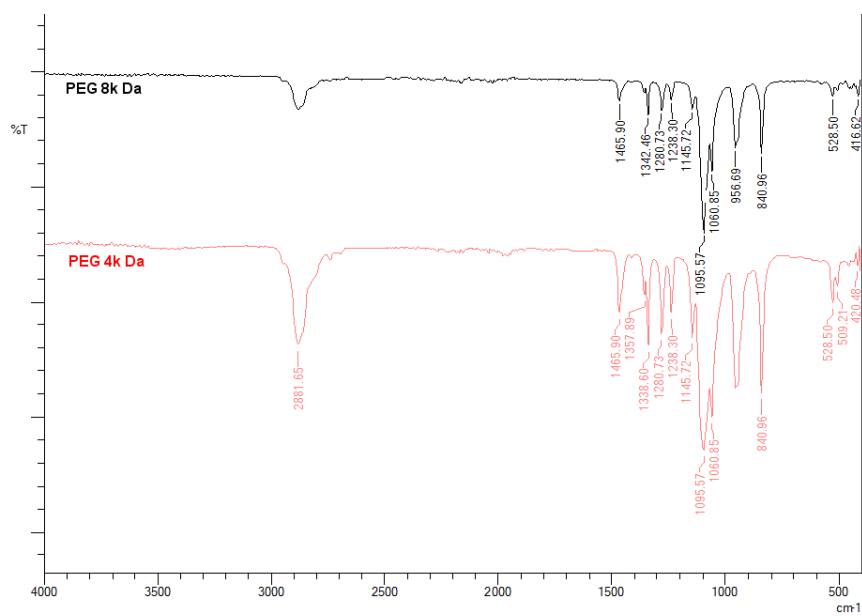
(i) Overlay of FTIR spectra of formulation NPs-drug-C6 and comprising material



(j) FTIR spectra of drug release profile of formulation NPs-drug-C6

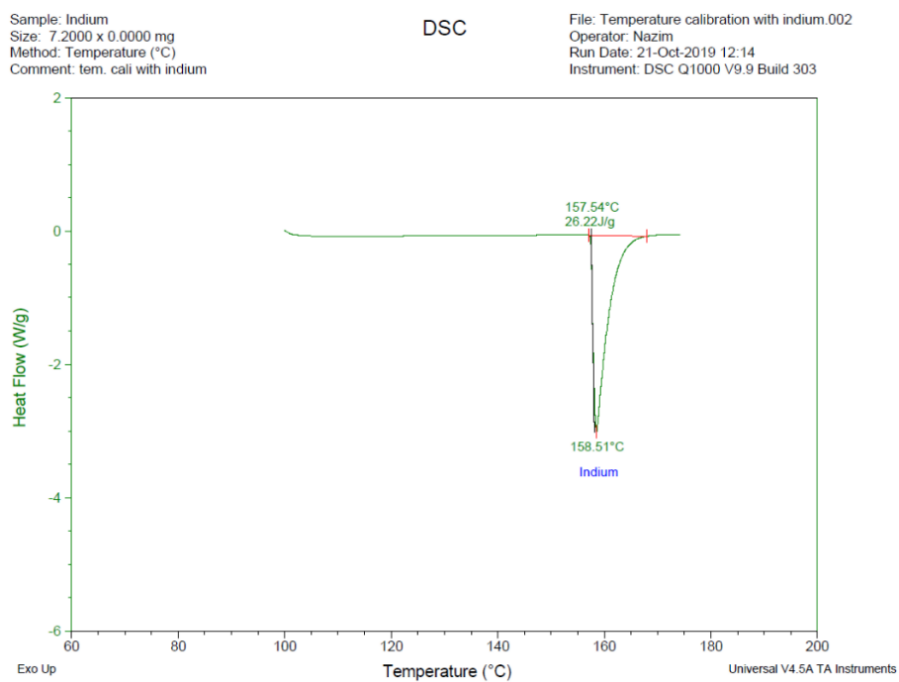


(k) Comparative FTIR spectra of PEG 4 kDa and 8 kDa.

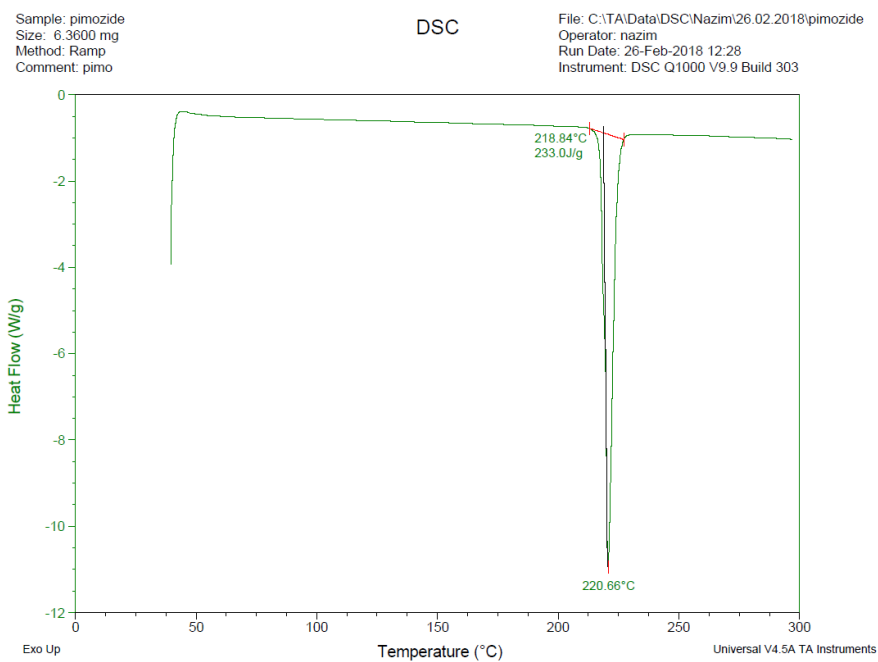


Appendix 4: DSC thermograms (Representative)

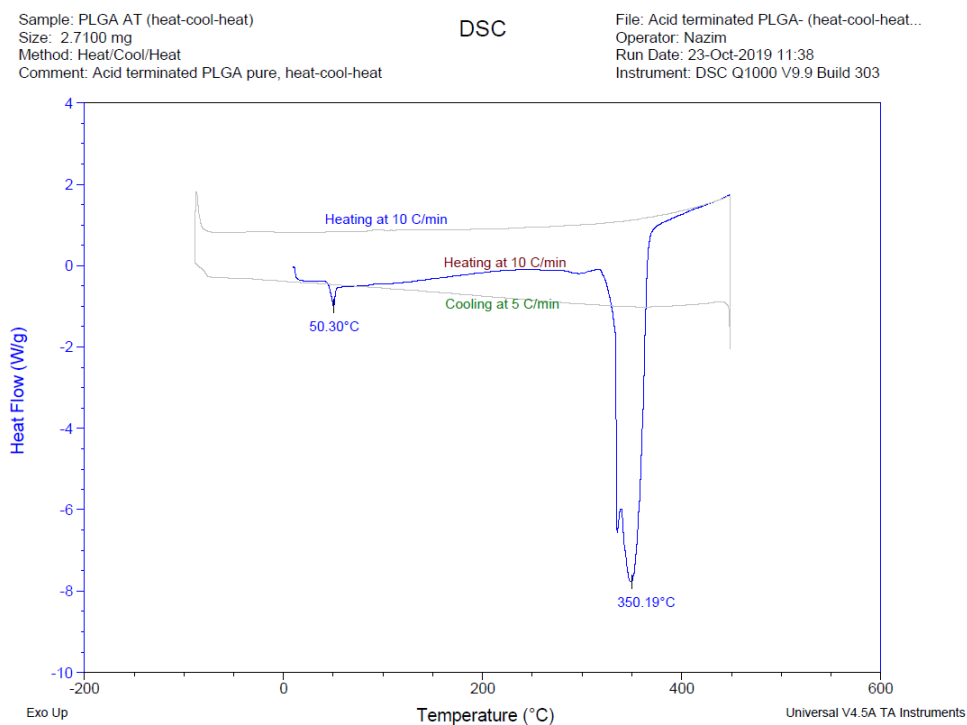
(a) DSC calibration thermogram of indium



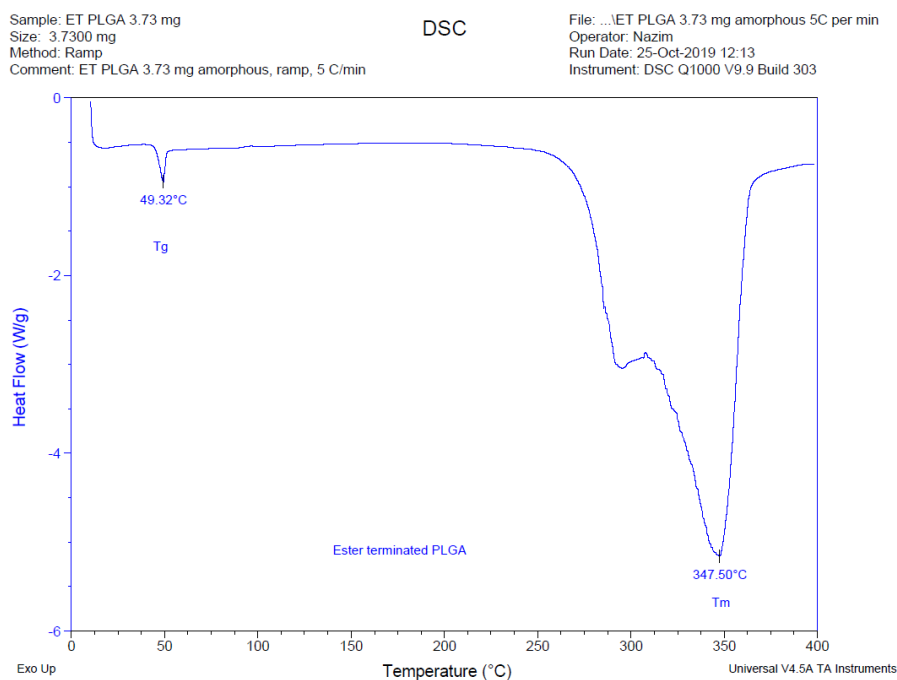
(b) DSC thermogram of pure pimozide



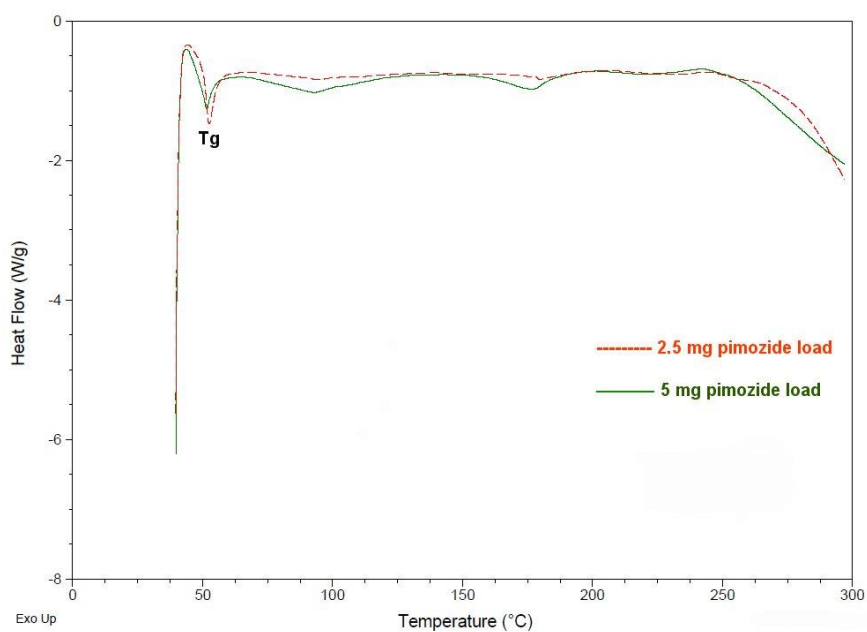
(c) DSC thermogram of pure AT-PLGA (Mw: 24-38 kDa)



(d) DSC thermogram of pure ET-PLGA (Mw: 24-38 kDa)



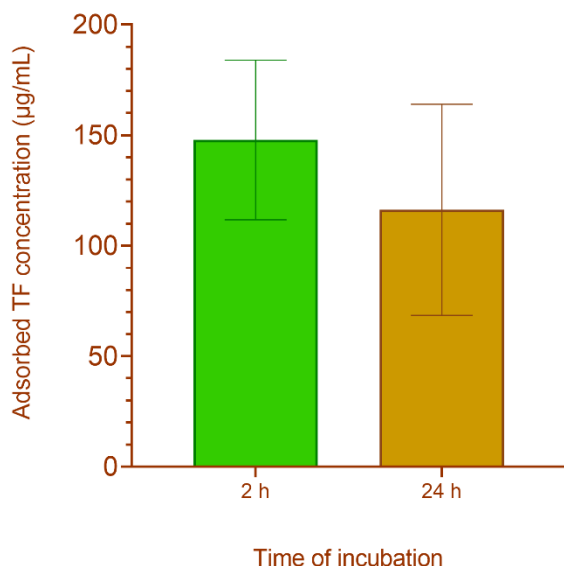
(e) Overlay of DSC thermograms of two different concentrations of pimozone-loaded nanoparticles



Appendix 5: Drug encapsulation efficiency in different techniques

Formulation code	Encapsulation efficiency (EE) (%)	
	UV-Vis spectroscopy	UHPLC
F1	72 ± 8.4	72 ± 7.8
F2	39 ± 15	34 ± 12
F3	40 ± 1.9	47 ± 0.1
F4	34 ± 9.3	35 ± 8.5
F9	72 ± 8.5	80 ± 6.7
F10	88 ± 2.8	74 ± 4.5
F11	83 ± 2.3	71 ± 4.3
F12	43 ± 9.3	51 ± 3.8

Appendix 6: Optimisation of transferring adsorption



Appendix 7: Preparation of microbial growth media

Preparation of Tryptic Soy Agar

40 grams of dehydrated Tryptic Soy Agar (TSA) media were suspended in 1 litre of purified filtered water. Sterilization was performed at 121°C for 15 minutes followed by cooling to 45-50°C. Prior to dispensing into sterile Petri dishes followed by incubation in refrigerator, the suspension media was mixed gently.

Preparation of Malt Agar

20 grams of malt extract and 20 grams of agar were suspended in 1 litre of purified filtered water. Sterilization was performed at 121°C for 15 minutes followed by cooling to 45-50°C. Prior to dispensing into sterile Petri dishes followed by incubation in refrigerator, the suspension media was mixed gently.

Appendix 8: Different preparations for Western blot analysis

Name	Preparation workflow
Tris-buffered saline (TBS)	To make 1 litre of TBS stock (10X) solution 24 grams of Tris Base (Tris-hydroxymethyl-methylamine) and 88 grams of NaCl were dissolved in distilled water, followed by adjusting pH to 7.6 with 12 N HCl.
Tris-buffered saline Tween (TBST)	0.025% v/v Tween was added to TBS (1X) solution to make TBST solution.
Tris-glycine saline (TGS)	To prepare 1 litre of TGS (10X) stock buffer, 30 grams of Tris Base, 144 grams of glycine and 10 grams of SDS (1%) were dissolved in distilled water upon magnetic stirring (recorded pH 8.3).
SDS lysis buffer	1% v/v SDS and 50 mM Tris buffer were mixed to make SDS lysis buffer (100 mL).
Loading buffer	3 mL of SDS (20%), 3.75 mL Tris buffer (1 M) at pH 6.8, 4.5 mL of glycerol and 150 μ L 2-mercaptoethanol were mixed, followed by addition of required volume of distilled water to make up 15 mL. Loading buffer was stored at 4 ⁰ C.
Inhibitor mixer	1 mL of inhibitor mixer was prepared by adding 50 μ L of protease phosphatase cocktail inhibitor (PPCI) to 950 μ L of SDS lysis buffer.

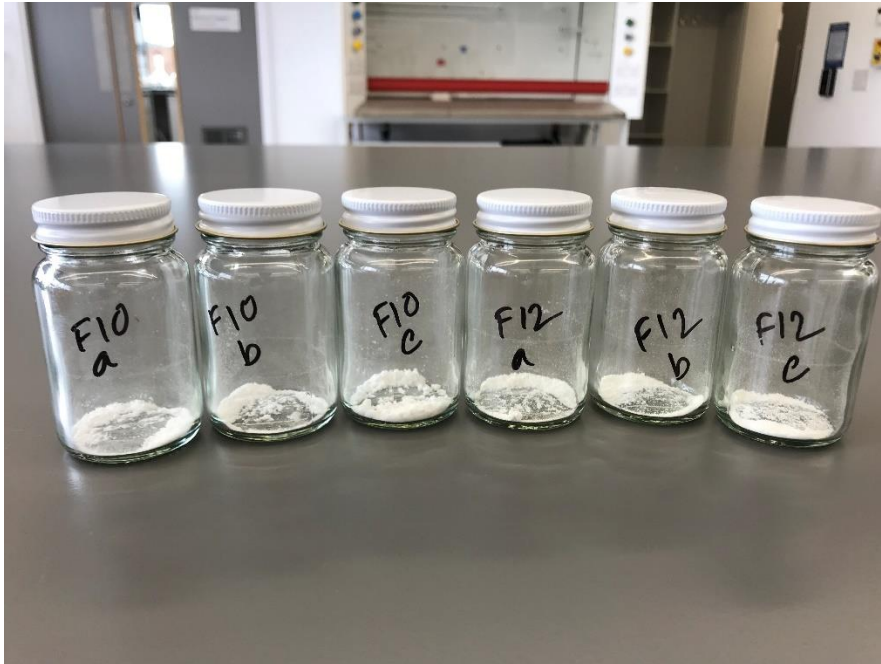
Appendix 9: Statistical analysis (Representative)

Statistical difference of particle size between two preparation methods

1	Table Analyzed	Size (SE vs MF) paired
2		
3	Column B	Microfluidic
4	vs.	vs.
5	Column A	Single emulsion
6		
7	Paired t test	
8	P value	.007
9	P value summary	**
10	Significantly different (P < 0.05)?	Yes
11	One- or two-tailed P value?	Two-tailed
12	t, df	t=3.771, df=7
13	Number of pairs	8
14		
15	How big is the difference?	
16	Mean of differences (B - A)	-92.75
17	SD of differences	69.57
18	SEM of differences	24.60
19	95% confidence interval	-150.9 to -34.59
20	R squared (partial eta squared)	0.6701
21		
22	How effective was the pairing?	
23	Correlation coefficient (r)	-0.6722
24	P value (one tailed)	.034
25	P value summary	*
26	Was the pairing significantly effective?	Yes

Appendix 10: Freeze-dried nanoparticles (Representative)

Digital photo of freeze-dried nanoparticles (Formulation F10 and F12)



Appendix 10: Author's Research Engagements and Background

Conferences

- Attended 'The great north pharmacy research conference' on 21st July 2017 at Science Complex, City Campus, University of Sunderland.
- Presented a poster entitling 'Repurposing pimozide for the treatment of glioblastoma by developing biodegradable polymeric nanoparticles' at Postgraduate Research Student Conference, University of Sunderland held on 28th June 2018.
- Participated on the poster presentations at Great North Pharmacy Research Collaborative Conference in Association with Pharmacy Management, Newcastle held on 6th July 2018. The poster entitling 'Preparation and characterization of pimozide loaded biodegradable nanoparticles as delivery systems for anticancer activity'.
- Attended Academy of Pharmaceutical Sciences (APS) conference in Glasgow held on 7th September 2018 and presented a poster entitling 'Fabrication and physicochemical characterization of novel pimozide loaded PLGA nanoparticles.
- Presented a poster entitling 'Preparation and characterization of pimozide loaded poly lactic-co-glycolic acid (PLGA) nanoparticles for glioblastoma targeted delivery' at American Association of Pharmaceutical Scientists (AAPS) conference on 4th-7th November 2018. <https://tinyurl.com/AAPS2018PharmaSci360>
- Attended 'ACS on campus' seminar at Durham University on 28th November 2018.
- Presented a poster at 3rd European Conference held in Bologna, Italy on 25-26th March 2019.
- Attended 9th Chemical Nanoscience Symposium Newcastle held on 4th April 2019 at Newcastle University.
- Attended a seminar on 'Pfizer analytical R&D (plant in Kent)' held on 8th May 2019 at University of Sunderland.
- Attended 'The ChromSoc Annual Spring Symposium' held on 9th May 2019 at Stadium of Light, Sunderland.
- Attended and presented a poster entitling 'Repurposing antipsychotic drug pimozide for anticancer activity by developing polymeric nanoparticulate delivery systems' at CRS Annual Meeting and Exposition 2019 held on 21st - 24th July 2019 in Valencia, Spain. <https://tinyurl.com/CRS2019NazimUddin>
- Attended and presented two posters entitling 'A comparative study of physicochemical properties of pimozide nanoparticles based on preparation methods' and 'Surface modification of pimozide nanoparticles: preparation and

characterization' at 10th APS International PharmSci Conference held on 11th-13th September 2019 at University of Greenwich, London.

- Attended and presented a poster entitling 'Effect of surfactant and surface coating materials on the physicochemical properties of pimozone nanoparticles' at 2019 AAPS PharmSci360 annual meeting held on 3rd-6th November 2019 in San Antonio, Texas, USA. <https://tinyurl.com/AAPS2019>
- Presented (virtually) a poster titling 'Development of Pimozone-Loaded PLGA Nanoparticles Targeting Glioblastoma' in the 2021 AAPS PharSci360 annual meeting on 17th-20th October 2021, Philadelphia, PA, USA.

Publications

- Faheem, A.M., Elkordy, A.A. and Uddin, N. (2019) 'Fabrication and physicochemical characterisation of novel pimozone loaded PLGA nanoparticles', British Journal of Pharmacy, 4(1). doi: <https://doi.org/10.5920/bjpharm.615>.
- Uddin, M.N., Elkordy, A.A. and Faheem, A.M. (2022) 'Effect of process and formulation parameters in developing pimozone-loaded PLGA nanoparticles by microfluidic method', On-going manuscript preparation for the Journal of Pharmaceutical Sciences.
- Uddin, M.N., Elkordy, A.A., Lough, J.W. and Faheem, A.M. (2022) 'Development and validation of an ultra-high-performance liquid chromatography (UHPLC) method to analyse pimozone in PLGA nanoparticles', On-going manuscript preparation for the Journal of Chromatography A.
- Uddin, M.N., Elkordy, A.A. and Faheem, A.M. (2022) 'Repurposing pimozone by developing transferrin receptor targeted PLGA nanoparticles for glioblastoma chemotherapy', On-going manuscript preparation for the International Journal of Pharmaceutics.

Trainings, workshops, and seminars

- Attended 'Safety and COSHH inductions' on 15th March 2017 at University of Sunderland.
- Attended 'Bio-safe training' on 10th April 2017 at University of Sunderland.
- Completed 'Prepare to teach course' on 24th and 25th October 2017 instructed by Dr. Alan Tree, University of Sunderland.
- Received training for 'speed reading approaches' at Research Friday workshop on 27th October 2017 at University of Sunderland.
- Attended 'SPSS for basic statistical analysis' workshop on 4th December 2017 at University of Sunderland.
- Attended workshop on 'Microsoft Office software for creating research report' on 6th December 2017 at University of Sunderland.
- Attended workshop on 'Presenting your research' that demonstrated how to create poster and PowerPoint presentations on 11th December 2017 at University of Sunderland.
- Attended 'SPSS in hypothesis testing' workshop on 15th December 2017 at University of Sunderland.
- Attended a seminar on 'Physical and chemical transformation in optically trapped aerosol droplets: drug delivery, cloud formation and microreactions' presented by Dr. Tom Carruthers, Newcastle University on 7th February 2018.
- Attended 'Bio-safety training' on 17th May 2018 at University of Sunderland.
- Attended workshop entitled 'Create your own free WordPress website to raise your research profile or display pictures of your artwork' on 26th June 2018 at University of Sunderland.
- Attended 'IncuCyte[®] Zoom' training for live cell analysis held on 20th June 2019 at University of Sunderland.
- Attended a seminar on 'The gateway to helping change patients' lives through the pharmaceutical industry' presented by Pfizer's employees.
- Attended a seminar on 'Strategies for improved pharmaceutical sample preparation' presented by Astra Zeneca's employee.
- Attended a seminar on 'The role of analytical chemistry in the development of pharmaceuticals' presented by AstraZeneca's employee.

Laboratory teaching

- Carried out laboratory demonstrations from March 2018 to March 2020, and October 2021 to present.
- Assisted faculty members in running team-based learning (TBL) sessions.
- Achieved the status of Associate Fellow of the Higher Education Academy (AFHEA) on 17th December 2019 (reference: PR178068).

Educational background

- MSc. in Drug Discovery and Development (2016).
- BSc. in Pharmacy (2013).